**A FLASH VAPORIZATION SYSTEM FOR
DETONATION OF HYDROCARBON FUELS
IN A PULSE DETONATION ENGINE**

DISSERTATION

Kelly Colin Tucker, Major, USAF

AFIT/DS/ENY/05-03

**DEPARTMENT OF THE AIR FORCE
AIR UNIVERSITY**

AIR FORCE INSTITUTE OF TECHNOLOGY

Wright-Patterson Air Force Base, Ohio

AFIT/DS/ENY/05-03

A FLASH VAPORIZATION SYSTEM FOR
DETONATION OF HYDROCARBON FUELS
IN A PULSE DETONATION ENGINE

DISSERTATION

Presented to the Faculty

Graduate School of Engineering and Management

Air Force Institute of Technology

Air University

Air Education and Training Command

In Partial Fulfillment of the Requirements for the

Degree of Doctor of Philosophy

Kelly Colin Tucker, B.S., M.S.
Major, USAF

June 2005

AFIT/DS/ENY/05-03

A FLASH VAPORIZATION SYSTEM FOR
DETONATION OF HYDROCARBON FUELS
IN A PULSE DETONATION ENGINE

Kelly Colin Tucker, B.S., M.S.
Major, USAF

Approved:

Date

_____
Paul I. King (Chairman)

_____
Ralph A. Anthenien (Member)

_____
Glen P. Perram (Member)

_____
Frederick R. Schauer (Member)

_____
Won B. Roh (Dean's Representative)

Accepted:

_____
Robert A. Calico, Jr.   Date
Dean, Graduate School of Engineering and Management

iii

Acknowledgements

Table of Contents

List of Figures

List of Tables

List of Symbols

Acronyms

AFIT   Air Force Institute of Technology
AFRL   Air Force Research Laboratory
CEA   calculation of complex chemical equilibrium code
CJ   Chapman-Jouguet
DDT   deflagration-to-detonation transition
EXCST   extended corresponding states model
ERC   extendable research code
ff   PDE thrust tube fill fraction (%)
FLTP   Constant enthalpy temperature and pressure flash command
FN   fuel nozzle flow number or flow coefficient
FVS   flash vapor system
GC   gas chromatograph
HE   high explosive
PDE   pulse detonation engine
NIST   National Institute of Standards and Technology
OH   hydroxyl radical
ON   octane number
PMT   photo multiplier tube
PR-EOS   Peng-Robinson equation of state
R-K   Runge-Kutta
RTV   room temperature vulcanizing
SMD   Sauter mean diameter
TCD   thermal conductivity detector
TTL   transistor to transistor logic
ZND   Zeldovich, von Neumann, and Döring wave theory

Symbols

a   speed of sound in a gas (ft/s or m/s)
A   Arrhenius rate constant
A_{exit} exit area (m^2)
B   Spaulding transfer number (dimensionless)
d_0 initial fuel droplet diameter (m)
D   diffusivity (m^2/sec)
E   activation energy (kJ)
F   thrust (lbf, N)
γ ratio of specific heats (dimensionless)
h   enthalpy (J/kg)
λ detonation cell 2D height or width but not length (mm)
$\dot{m}$ mass flow rate (lbm/s, kg/s)
MW   molecular weight (gm/mole)
P   pressure (atm, psi, Pa)

Symbols (continued)

φ	equivalence ratio (dimensionless)
R	specific gas constant (J/kg/K)
$R_{universal}$	universal gas constant (8.313 J/gm/K)
σ	standard deviation (units of data analyzed)
ρ_{liquid}	liquid density of fuel (lbm/ft^3, kg/m^3)
ρ_{gas}	vapor density of fuel at surface of a droplet (lbm/ft^3, kg/m^3)
T	Temperature (°F, K)
τ	ignition time (seconds)
t_e	evaporation time
$T_{critical}$	critical temperature of the fuel (K)
$P_{critical}$	critical pressure of the fuel (kPa)

Units

°C	Celsius
cm	centimeter
°F	Fahrenheit
fps	frames per second
ft	foot
gm	gram
Hz	frequency (cycles/second)
in	inch
J	Joule
K	Kelvin
kg	kilogram
kW	kilowatt
lbm	pound mass
m	meter
mm	millimeter (10^{-3} m)
μm	micron (10^{-6} m)
nm	nanometer (10^{-9} m)
psi	pound per square inch
Pa	Pascal
ppm	parts per million
sec	second

AFIT/DS/ENY/05-03

Abstract

Current research by both the US Air Force and Navy is concentrating on obtaining detonations in a pulse detonation engine (PDE) with low vapor pressure, kerosene based jet fuels. These fuels, however, have a low vapor pressure and the performance of a liquid hydrocarbon fueled PDE is significantly hindered by the presence of fuel droplets. A high pressure, fuel flash vaporization system (FVS) has been designed and built to reduce and eliminate the time required to evaporate the fuel droplets. Four fuels are tested: n-heptane, isooctane, aviation gasoline, and JP-8. The fuels vary in volatility and octane number and present a clear picture on the benefits of flash vaporization. Results show the FVS quickly provided a detonable mixture for all of the fuels tested without coking or clogging the fuel lines. Combustion results validated the model used to predict the fuel and air temperatures required to achieve gaseous mixtures with each fuel. The most significant achievement of the research was the detonation of flash vaporized JP-8 and air. The results show that the flash vaporized JP-8 used 20 percent less fuel to ignite the fuel air mixture twice as fast (8 ms from 16 ms) when compared to the unheated JP-8 combustion data. Likewise, the FVS has been validated as a reliable method to create the droplet free mixtures required for liquid hydrocarbon fueled PDEs.

A FLASH VAPORIZATION SYSTEM FOR DETONATION
OF HYDROCARBON FUELS IN A PULSE DETONATION ENGINE

I. Introduction

Detonation phenomena was neither observed nor documented until the late 1800s.[1] Soon it was understood that the detonation wave released the energy stored within the fuel and air mixture at a rate tens of thousands of times faster than a deflagration wave.[2] To apply this rapid energy release for propulsion was obviously desirable, but the ability to generate repetitive detonations within a reasonable length (~1 m) was difficult and no suitable method was found. In the 1930s, German engineers were able to generate thrust using pulsing propulsion with the pulsejet.

Although the pulsejet was unsuccessful in generating a detonation during the pulsing cycle, the confined deflagrations still produced reasonable propulsive power at a low cost and with a relatively simple design. The pulsejet was used in World War II on the first cruise missile, the German V-1 Buzz Bomb. The engine used low-octane gasoline and operated at roughly 40 Hz. The fuel was injected directly behind the intake valves and mixed with air prior to ignition with a spark plug. The pulsejet required sufficient ram air pressure to operate, and a catapult system was needed to accelerate the vehicle to sufficient speed and inlet pressure for the engine to run effectively.[3] After WWII, interest in the turbojet engine overcame the pulsejet, and only recently did significant interest arise again in the potential for a pulse detonation engine. The primary interest is due the projected low cost, light weight, simplicity and potential for high efficiency expected by the engine.

The United States Air Force and Navy are currently funding research[4, 5] to mature the Pulse Detonation Engine (PDE) for operational use. High cycle efficiency, simplicity, low cost, and the potential for a large flight Mach number (0-5) operation make the PDE an attractive propulsion system. While many debate the actual cycle efficiency,[2, 6, 7, 8] the consensus opinion states that the PDE cycle holds great promise to exceed the performance of the Brayton cycle used in jet engines. Generating detonations for propulsion applications requires a homogeneous and droplet free fuel and air mixture as well as a detonation initiation mechanism to make the PDE thrust sufficiently high to be practical.[2]

The PDE derives thrust through the repetitive development of a detonation wave in a tube. The engine produces thrust when the detonation wave raises the pressure inside the thrust tube and expels the resulting products from the tube at high speeds. Since combustion energy does not have to drive a turbine as in the Brayton cycle, the PDE cycle also results in a high thermal efficiency over most flight conditions.[6] The thrust can be scaled by increasing the number of thrust tubes and by increasing the frequency each tube is fired. If scaled properly, a PDE could replace or augment current propulsion systems.

Currently, three primary research areas must be addressed to make the PDE a viable propulsion system. The first is to transition the PDE from gaseous fuels to readily available liquid fuels such as aviation gasoline and jet fuel. The second is to reduce the time required to ignite and detonate a fuel and air mixture. The third and final area is to reduce the time required to fill the long slender thrust tube with a detonable mixture and at a high static pressure.

These areas of research are currently being addressed using both experimental and computational techniques. The majority of experimental work uses gaseous fuel such as hydrogen, and often with an oxidizer such as gaseous oxygen. The primary benefit of the H_2/O_2 mixture is that very little energy $(1.5\,mJ)$[9] is required to directly initiate a detonation. Recent efforts[4] have successfully transitioned the oxidizer from oxygen to air. With the change of oxidizer, the detonation initiation energy rises six orders of magnitude to $4.3\,KJ$,[9] and now either an oxygen enriched pre-detonator or an obstacle based transition process is required to generate the detonation. A more thorough review of current pulse detonation engine research can be found elsewhere.[2, 10]

Prior to this work, deflagration waves have not been routinely transitioned into detonation waves with a jet fuel such as the Air Force's JP-8 and air because of the narrow equivalence ratio detonability limits, the inability to quickly evaporate and mix the fuel prior to combustion, and unsatisfactory fuel injection schemes. Currently, the ability to achieve detonations with ambient temperature liquid hydrocarbon fuels requires the fuel injection system to consistently supply a well-dispersed, sub-five-micron spray field to the detonation chamber.[11] Current turbine engine pressure atomization nozzles are incapable of producing this size of droplets. To further reduce the droplet size, the air is heated to speed up the droplet evaporation to achieve the small size to facilitate the ignition and detonation processes. A flash vaporization system (FVS) could be used to accomplish this more quickly.

Frank Whittle, the British inventor of the gas turbine engine, attempted the earliest documented FVS. Whittle used a heated fuel system in his early gas turbine engine combustor in an effort to better atomize the fuel prior to combustion.

3

Unfortunately, poor control of the fuel flow rates and clogged fuel lines caused by both thermal oxidation and endothermic reactions prevented the success of this FVS.[12] These two sets of reactions are the primary reason FVSs have not been widely implemented or successful.

Research[13] has shown that removing the dissolved oxygen in the fuel, due to contamination with air, can prevent the thermal oxidation problems. Current technologies do not have the capability to practically deoxygenate the fuel on board an aircraft, nor is bubbling nitrogen through the several tons of fuel carried by commercial and military aviation feasible. Systems to more easily deoxygenate fuel are under development, but the size and cost of the device will limit use on smaller or life limited air vehicles. For cruise missiles, the fuel could be deoxygenated prior to storage in the missile.

To address the problem of endothermic reactions, the controlling factors are temperature and the time the fuel stays at elevated temperatures. At temperatures as low as 400 °C, measurable endothermic reactions can occur within minutes and the rates increase with increase temperatures. Not all endothermic reactions are bad. Controlling the types of reactions that occur by placing additives in the fuel or catalyst coatings on the fuel system walls have shown promise in reducing the particulate formation that clogs the fuel lines. These topics will be discussed further at the end of Chapter II.

Very little research had been performed using FVSs until hydrocarbon fueled supersonic combustion ramjets (scramjets) were actively pursued. In a scramjet, combustion reactants must mix and combust while traveling at supersonic speeds. These speeds force the combustion to be completed within milliseconds to keep the combustor length reasonable. Like the pulse detonation engine, much of the research has been

accomplished using gaseous fuels in an effort to negate the additional time required for evaporation and mixing when using liquid fuels. One such research project[14] used flash vaporized Jet-A, which is similar to JP-8, in a scramjet combustor study. The fuel was flash vaporized at temperatures up to 610 K and saw primary fuel utilization efficiencies in the range of 80 - 100%. These efficiencies were significantly higher than the 30 - 60% recorded with unheated fuel injection with the same geometry and test conditions. Fuel utilization efficiency, or combustion efficiency, is a measure of how much chemical energy was released through combustion relative to the total energy stored in the fuel injected into the scramjet combustor.

Motivation

The integration of liquid fuels into a PDE is important because all flight vehicles are volume limited, and both gaseous and cryogenic fuels require more rigorous and heavier storage and handling requirements. The low vapor pressure kerosene based jet fuels used by the Air Force and Navy are safer and have a higher energy density than high vapor pressure aviation gasoline. The low vapor pressure of JP-8 inhibits evaporation of the fuel and lessens the likelihood of an accidental spill forming a combustible mixture. Unfortunately, the low vapor pressure also inhibits the formation of a mixture capable of transitioning and sustaining a detonation wave. The unsteady nature of the PDE requires that the combustion processes of ignition and detonation occur in the shortest time possible to allow high frequency (and high time-averaged thrust) operation. In a high pressure fuel injection system without flash vaporization, a high performance pressure atomizing nozzle can supply fuel at droplet sizes ranging from 25 to 70

microns.[15] The unheated droplets rely on heat and mass transfer to evaporate and mix with the air prior to combustion. The droplet lifetimes are longer than the combustion timescales of the PDE. Without sufficient time to evaporate all of the droplets, a portion of the fuel remains in liquid form. Since ignition and combustion occur in the gaseous phase, some of the initial ignition energy is spent evaporating nearby droplets. This reduces the maximum temperature and slows the ignition. The FVS heats the liquid fuel to a temperature above the boiling point at the final mixture pressure. At the temperatures required to flash vaporize the fuel, however, any oxygen dissolved in the fuel will begin to react and produce carbon deposits causing significant problems within the fuel system. The heated fuel system requires that the dissolved oxygen in the fuel be completely removed to operate effectively. Because of the challenges posed, this research developed a FVS to create a suitable droplet-free JP-8 and air mixture to achieve the combustion performance required for a practical liquid fueled PDE.

Approach

The ultimate goal of this research is to initiate a JP-8 and air detonation within a working PDE using an automotive spark ignition system and a Schelkin-like spiral with no oxygen enhancement or pre-detonator. To accomplish this goal, a liquid fueled FVS is designed and integrated into a working gaseous fueled PDE. The FVS works by heating high pressure (3.5 MPa) liquid fuel to a temperature that, when injected into lower pressure (200 kPa) air, flashes and maintains the fuel in vapor form.

This research tested three high vapor pressure fuels and one low vapor pressure fuel; n-heptane (n-C_7H_{16}), isooctane (i-C_8H_{18}), aviation gasoline, and JP-8, respectively.

A liquid vapor equilibrium computer model is used to predict what fuel and air conditions are required to create a suitable mixture that will resist condensation. The model uses a single component (1-specie) high vapor pressure n-heptane or isooctane with air to predict the liquid vapor composition for a given set of test conditions. The JP-8 is a multi-component hydrocarbon fuel, and a JP-8 surrogate (10-species) model is developed to predict the optimal fuel and air operating conditions to achieve a droplet free envelope. JP-8 presents the biggest challenge in generating a suitable vaporized mixture capable of ignition and transitioning to a detonation.

The four fuels tested in this research represent a wide range of octane numbers (0-100). N-heptane and isooctane represent the two fuels for which the automotive octane number combustion standard is derived. It is hypothesized that the octane number may prove to be a useful correlation to predict the difficulty in generating detonations in a particular fuel for which the octane number is known.

A successful FVS must produce a fuel and air mixture capable of igniting and transitioning to a detonation. This must occur within the fixed geometry of the thrust tube with a Schelkin-like spiral and be valid for a range of equivalence ratios for each fuel. For this to work, several areas needed to be studied and understood. First, this research determined the effects of the fuel injection temperature on the ignition times and on the combustion wave speed. It is hypothesized that if the ignition times vary with the fuel injection temperature, then it is proposed that the fuel trapped in the droplets is effectively unusable for ignition and the mixture will behave as if it were more lean (fuel starved) during the ignition process. The hypothesis is supported by the understanding that the fuel droplet evaporation time of a low vapor pressure fuel such as dodecane or

JP-8 is longer than the chemical reaction (including ignition) time scales.[16] To properly capture the droplet effects experimentally, a range of equivalence ratios are used to determine the ignition times for both high and low vapor pressure hydrocarbon fuels. When droplets are present, the expected ignition-time curve is shifted higher (richer) in equivalence ratio. Second, this research produced a FVS that generated a fuel and air mixture with sufficiently high quality that the experimental results agreed well with the ignition and detonation trends published in the literature concerning the affect of equivalence ratio. Separate from the combustion performance of the FVS are the methods employed to prepare the fuel to be heated to the temperatures required to reach flash vaporization. Lastly, this research engineered an FVS that provided fuel at sufficiently high temperatures without experiencing the thermal oxidation and endothermic reactions that caused particulate formation and damaged prior FVS efforts.

Organization

This initial chapter has served to lay the framework of the problem and the justification for the development of a flash vaporization system in a pulse detonation engine. Chapter II provides the necessary background to better understand the specific pulse detonation engine combustion environment, the challenges of transitioning to a detonation in mixtures with and without liquid droplets, and the difficulties encountered when heating fuel to temperatures from ambient to over 800 K. The facilities, hardware, and instrumentation used on the PDE and the FVS are described in Chapter III. Chapter IV is an overview of the software routines designed to extract the pertinent combustion data as well as the error analysis of the data acquisition equipment. The fuel flash

vaporization system is presented in detail in Chapter V. The discussion includes the predicted operational envelope required to achieve fully gaseous mixtures as well as the specific fuel temperatures needed to flash vaporize. The combustion results are presented and discussed in Chapter VI and include ignition times, the deflagration-to-detonation transition times, and detonation wave speeds. The performance of the heated fuel system is also given. Chapter VII presents the conclusions and provides the overall impact of the work on the PDE community. Propositions of future efforts designed to build off of this research and the implications of future success are also discussed.

II. Background

The main goal of this research is to design and build a fuel flash vaporization system to quickly create mixtures with liquid hydrocarbon fuels that can be detonated. For this system to be successful, the times required to ignite and to detonate a mixture must be quantified and ideally reduced by flash vaporizing the fuel during the mixing process. This chapter will explain what mixture properties are required during ignition and what mixture characteristics are needed for a detonation to form. Ignition and detonation events are explained in detail and include the effects of fuel droplets on combustion performance. The effect of fuel vapor pressure on combustion performance is also addressed.

Flammability and Ignition Limits

Combustion in a pulse detonation engine occurs in a premixed fuel and air composition. The fuel and air mixture fills the length of a PDE thrust tube, and combustion is initiated at the closed end of the tube. After ignition, a combustion wave forms, travels through the mixture, and exits the open end of the tube. A fuel and air mixture cannot always sustain combustion and is dependent on the temperature, the pressure, and the relative amounts of fuel and air. Depending on the previously mentioned properties, the mixture is characterized as behaving as either explosive or slow reacting. The explosive mixture can immediately sustain combustion throughout. A slow reacting mixture has few, if any, reactions taking place, and the reactions that do take place lose sufficient energy to the surroundings at a faster rate than the heat released. The reactions may continue slowly but thermal run away never occurs. The flammability

limits are used to define where the flame will propagate or self support. Figure 2.1 shows the flammability limits for an n-heptane and air mixture at various temperatures and equivalence ratios at 1 atm. The equivalence ratio (φ) is given by the following relationship:

$$\phi = \frac{\left(\dfrac{fuel}{air}\right)_{ACTUAL}}{\left(\dfrac{fuel}{air}\right)_{STOICH}} \qquad (2.1)$$

where *fuel* and *air* can be defined by mass, mol/volume, partial pressure, or mole fraction in the mixture. Stoichiometric (φ = 1) is defined as the ratio of fuel and air such that the fuel and oxygen are completely consumed producing only H_2O and CO_2 during the reaction. If the ratio is less than stoichiometric (φ < 1) then the mixture is fuel lean, and if the mixture is greater than stoichiometric (φ > 1) then the mixture is fuel rich
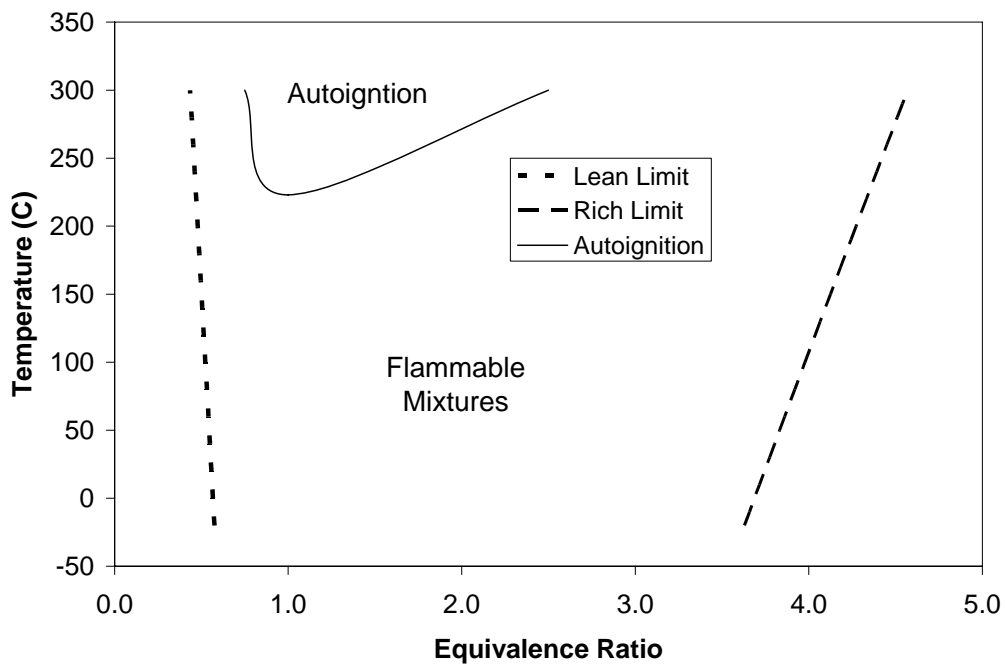
Figure 2.1 Flammability limits for an n-C_7H_{16} and air mixture at 1 atm. Data from Ref. 17.

The ignition delay time is defined as the time between the deposit of ignition energy and the resulting onset of a rapid reaction. The initial energy deposit initiates chemical reactions through a heat rise and radical production. The total ignition time can be broken into a combination of induction time and chemical time. The induction time is the time needed to form the critical concentration of radicals that are sufficient to initiate the reactions that lead to ignition. The chemical time is defined as proportional to the inverse of reaction rate and relates to the time required for the reactants to achieve ignition. For a forced ignition system such as the spark used in this research, an ionized plasma is created in the gap between the center electrode and the ground. This plasma is the source for the critical pool of radicals and occurs at the instant the energy is deposited making the induction time zero. The chemical time then becomes the determining factor for an ignition indicator to be observed.

The ignition limits are a subset of the flammability limits and are based on the critical amount of reactants and a finite ignition energy. The ignition limits are defined at an upper and lower equivalence ratio where the abrupt rise in minimum ignition energy occurs.[18] The flammability limits differ from the ignition limits in that it is defined as where combustion can be sustained after ignition has already been established, potentially under different conditions. The experimentally determined minimum ignition energy varies with equivalence ratio as shown in Fig. 2.2. The minimums for n-pentane and n-heptane occur at equivalence ratios of 1.3 and 1.8, respectively. The minimum ignition energy, $Q'_{\min}$, can be related to the laminar wave speed, S_L, as

$$Q'_{\min} \approx \frac{\lambda^3 T_O^2 (T_F - T_O)}{S_L^3 P^2 C_P^2}$$

(2.2)

where λ is the thermal conductivity, T_O is the initial temperature, T_F is the flame temperature, P is the pressure, and Cp is the heat capacity of the mixture.[1]
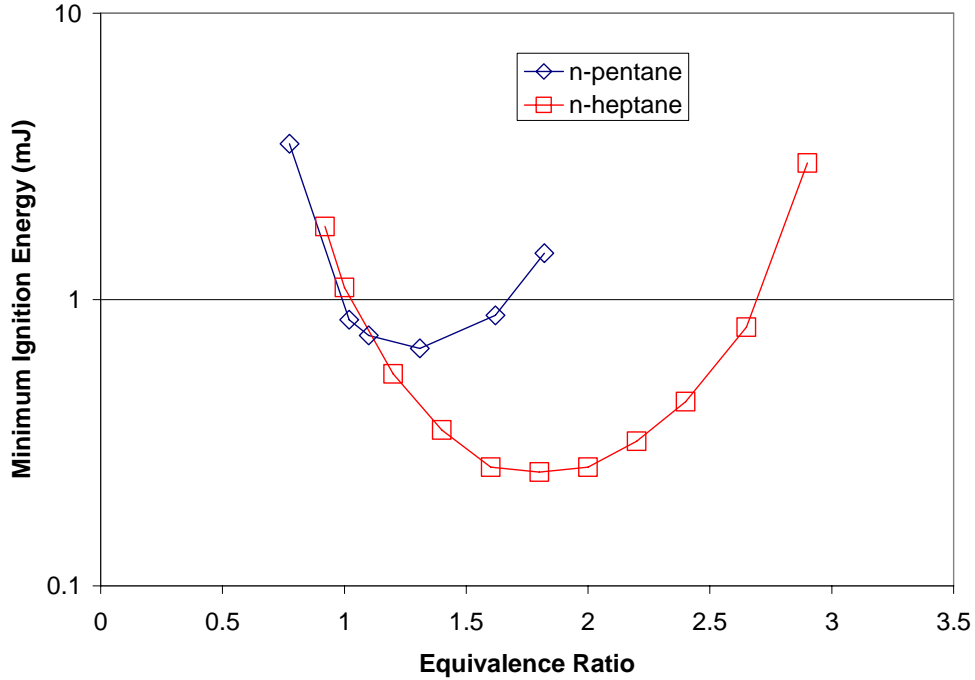
Figure 2.2 Minimum spark ignition energy for n-C_5H_{12} with air and n-C_7H_{16} with air at 1 atm and 25 °C. Data from Ref. 19.

The laminar wave speed, S_L, in a premixed fuel and air mixture is dependent on the reaction rate and the rate heat diffuses into the reactants. The laminar wave speed can be described approximately as

$$S_L \approx \sqrt{\frac{\alpha RR}{\rho}} \qquad (2.3)$$

where α is the diffusivity, ρ is the density, and RR is the reaction rate. The minimum ignition times can be related to the maximum kinetic reaction rate and to the minimum ignition energy through the laminar flame speed as presented in Eqn. 2.2 and Eqn. 2.3. The maximum flame temperature and wave speed for most hydrocarbon-air systems peaks at an equivalence ratio slightly above stoichiometric.[1] As will be shown in the

results chapter, the ignition times follow the same trends as the minimum ignition energy and the observed minimums occur near the equivalence ratios slightly (0.3 ~ 0.4) above stoichiometric.

For a fuel and air mixture with suspended droplets, the total ignition time now includes a droplet evaporation time in addition to the chemical time discussed previously. As will be shown in Chapter V, the longer of the two times for ambient temperature hydrocarbon fuels is the droplet evaporation time.[16] Ignition requires both the fuel and oxidizer to be a vapor for homogeneous chemical reactions to occur. The trends in Fig. 2.3 show that larger fuel droplets require a larger minimum ignition energy. The absolute values of the minimum ignition energy depend on the residence time between droplet injection and the ignition energy deposit. The trends are useful in showing that droplet size should be minimized to limit the potential effect on ignition time.
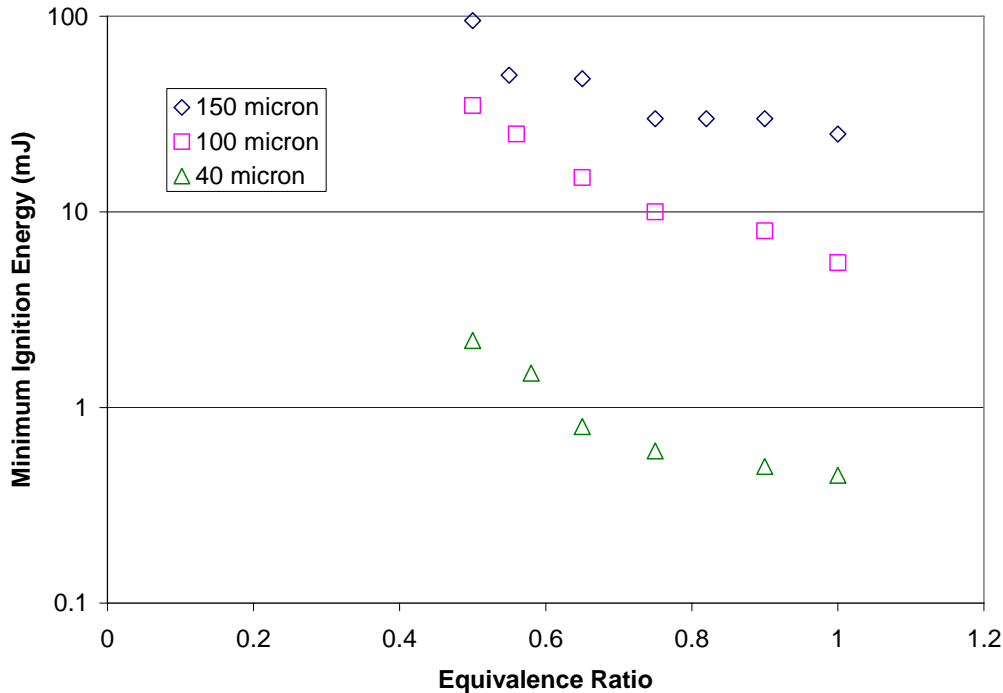
Figure 2.3 Minimum ignition energies for quiescent heavy fuel oil with air for three Sauter mean diameter droplet sizes. P = 100 kPa and T = 290 K. Data from Ref. 12 as adapted from Ref. 20.

To achieve the shortest chemical ignition times possible, the state variables that influence the combustion of hydrocarbon and air mixtures should be considered. Using global reaction theory, the chemical time can be correlated to the thermo-physical properties of reactant concentration, pressure, and temperature. The primary assumption is that the complex reactions are adequately modeled in a single reaction, though in reality, only the trends are predicted. Using the Arrhenius rate expression from chemical kinetics, chemical time can be defined as proportional to the inverse of the reaction rate, RR, as given by

$$\tau \approx \frac{1}{RR} = AP^{-n}\varphi^{-m}\exp\left(\frac{E}{RT_{mix}}\right) \tag{2.4}$$

where A, n, and m are experimentally[12] determined constants, φ is the equivalence ratio of the mixture, and T_{mix} is the mixture temperature. The values of the superscripts in Eqn. 2.4 are found in the literature[21] ranging from n equal to 0.5 to 2.5, and with m equal to between 0.17 and 0.75. The variables (P, T, and φ) are valid only within a defined region of the flammability limits of the mixture.

Droplet Characterization

To understand the droplet effect on the combustion parameters considered in this work, droplet nomenclature must be defined. Droplets generated by a pressure atomization nozzle are characterized by mean drop size, drop size distribution, spray pattern, and spray cone angle. The definition of mean diameter varies depending on its intended use. The Sauter Mean Diameter (SMD) is used to describe a characteristic droplet with a volume to surface ratio that is equal to that of the spray as a whole.[22]

The volume mean diameter D_{30} which is defined for a discrete distribution as

$$D_{30} = \sqrt[3]{\frac{\sum N_i \delta_i^3}{\sum N_i}}$$

(2.5)

where N_i is the number of droplets of diameter δ_i. The volume mean diameter is the average droplet volume of the spray. The surface mean diameter is the area or surface of the droplets with a surface area equal to the mean surface area and is given by

$$D_{20} = \sqrt{\frac{\sum N_i \delta_i^2}{\sum N_i}}$$

(2.6)

where N_i is the number of droplets, and δ_i is the average diameter of the size range. The SMD is defined as the volume to surface mean diameter and is given by

$$SMD = D_{32} = \frac{D_{30}^3}{D_{20}^2}$$

(2.7)

and is the diameter of an equivalent droplet with a ratio of volume to surface area equal to that of the entire spray.

Deflagration and Detonation Defined

Once ignition has been established in a premixed gas, two types of combustion waves may ensue: deflagration or detonation. A deflagration is defined as a combustion wave traveling at a subsonic speed relative to the unburned gas, sustained by the chemical reactions. If a combustible mixture in a long duct is ignited at the open end, a

deflagration wave will form and attain a steady velocity on the order of centimeters per second to meters per second. If the same combustible mixture is ignited at the closed end of a tube, a deflagration will form and travel into the unburned reactants upstream as before. The confined gases behind the wave, however, raise the pressure and accelerate the combustion wave and may potentially lead to a detonation with a velocity on the order of kilometers per second. A detonation is defined as a combustion wave that travels at supersonic speeds relative to the unburned gas and is driven and sustained by the chemical reactions and the shock preceding it respectively.[1, 23] The transition from a deflagration to a detonation is known as the deflagration-to-detonation transition (DDT) process and is described in more detail later.

Detonation Initiation in a Long Tube without Obstacles

As related to this research, the DDT process begins when an explosive fuel air mixture in the closed end of a PDE thrust tube is ignited. The mixture is assumed homogenous and quiescent. The initial deflagration releases sufficient heat that the mixture temperature increases. Because of the confinement and temperature increase, the pressure rises and causes compression waves form and propagate upstream at the speed of sound. The compression waves raise the temperature of the unburned reactants ahead of the flame. The increase in the temperature results in the increase of the local speed of sound, and assuming the mixture behaves as a perfect gas, follows the relationship shown in Eqn. 2.8,

$$a = \sqrt{\gamma R T} \tag{2.8}$$

where a is the speed of sound in m/sec, γ is the dimensionless ratio of specific heats, R is the specific gas constant of the mixture in m^2/sec^2/K, and T is the temperature in Kelvin.

As more of the mixture combusts, the subsequent compression waves travel faster through the now preheated reactants and begin to coalesce. A second effect of the increase in temperature and pressure of the reactants is the subsequent increase in the reaction rate of the mixture and therefore the flame speed. At some point, the coalescing compression waves become strong and fast enough to form a shock wave. The shock wave travels through the initially at rest unburned reactants, but the gas behind the shock travels at a velocity relative to the strength of the shock. As the shock accelerates, the unburned mixture between the shock and the flame front transitions from laminar to turbulent flow. The turbulence increases the mixing of the burning and unburned gases, enhances the heat release, and further accelerates the compression waves. While this is occurring, the strengthening shock wave moving into the quiescent region raises the temperature of the unburned gas above the auto ignition point ahead of the flame front. The shock is now initiating the combustion process and the reaction zone (flame front) behind the shock continuously feeds compression waves to sustain the shock front. A detonation is now said to have formed and becomes the primary mode of combustion. The detonation flame travels much faster (10^3 m/sec) in the highly compressed and preheated gases compared to the deflagration (10^{-2} m/sec) that began the process.[1] The detonation wave achieves a steady state velocity based on the heat release of the combusting mixture.

The DDT process described in the previous paragraph supplies the basic thermodynamic drivers in the transition process. Many of the specific features observed

during the process were left out. Using a sketch (Fig. 2.4) of Schlieren photographs taken of the DDT process, the following commentary is given.[23]

1. Compression waves form ahead of an accelerating laminar flame, and the waves coalesce into a shock. The gases behind the shock transition to turbulent flow, tripping a turbulent flame brush upstream of the laminar flame (Fig 2.4a).

2. Inside the turbulent reaction, an explosion within an explosion forms transverse waves. An overdriven detonation wave travels into the unburned reactants and a sonic retonation wave travels back through the products (Fig. 2.4 b).

3. A spherical shock develops and the shock front, retonation wave, and reaction zone interact and form a steady detonation wave (Fig. 2.4c).
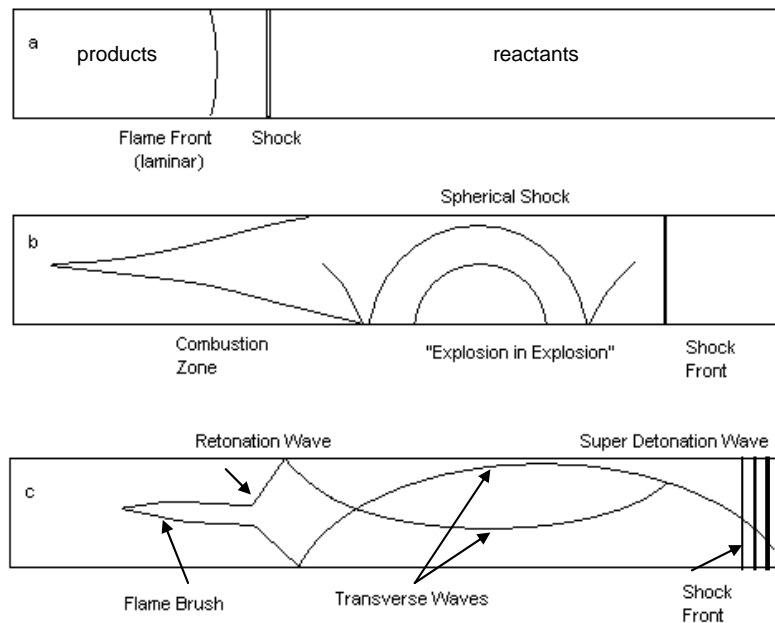
Figure 2.4 Key physical structures during a detonation transition.[23]

Detonation Transition with Obstacles

The deflagration-to-detonation transition distance can be reduced by using an obstacle such as a Schelkin spiral within the thrust tube. Many researchers[4, 24, 25, 26] have found that internal structures with differing geometries, including confinement, can increase the speed (and shorten the distance) at which a deflagration wave transitions into

a detonation wave. A Schelkin spiral (Fig. 2.5) placed in the closed end of a PDE thrust tube is one such obstacle. The compression waves that form from the deflagration in the closed end of the tube interact with and form hot spots along the surface of the spiral. These hot spots encourage the explosion within an explosion described in the previous section.[27] Each subsequent explosion enhances the flame-shock interaction through the increased pressure and heat release. Researchers[24] have found that a three dimensional helical rotation of the flame produces bow shaped shocks that propagate upstream and reflect off the walls to enhance the DDT process. Results show that H_2 and air detonations can be repeatedly generated within 20 to 40 cm (8 to 16 in) of spiral whereas, without an obstacle, it could take upwards of 2 to 3 m (6-9 ft) to transition.[4] Once a detonation has formed, the wave speed will settle to a single velocity dictated by the mixture properties as described in the theoretical detonation performance section.
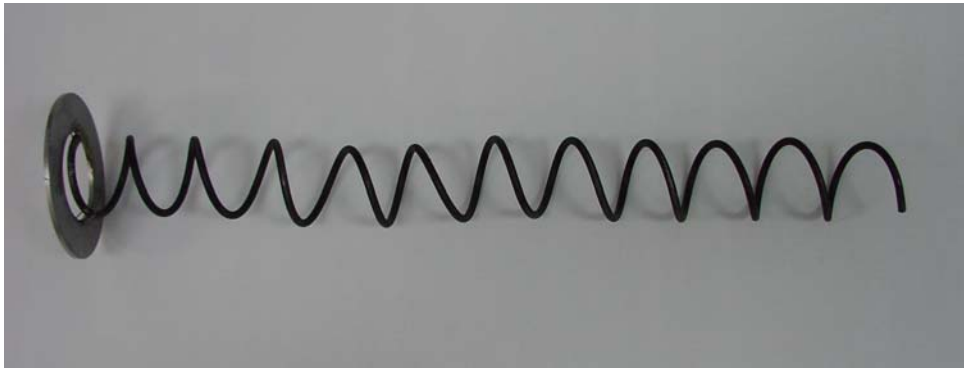
Figure 2.5 Schelkin spiral with retaining disk.

Pre-Detonators and Detonation Branching

As will be discussed later in this chapter, detonations, with gaseous oxygen as the oxidizer, can be directly initiated with little to no transition length. These directly initiated detonations can be propagated into a less sensitive, harder to detonate mixture such as a hydrocarbon fuel with air as the oxidizer. Several researchers[11, 28] have used this

pre-detonator method with oxygen enriched air to create a viable detonation in a much shorter distance (~17 cm). An obstacle transitioned n-heptane and air mixture will take up to 1 m to transition to a detonation. The use of a pre-detonator is not desirable, however, because a separate supply of oxygen must be carried on a volume limited aircraft or missile.

In lieu of using the oxygen enriched pre-detonator, a similar performance gain can be achieved by branching established detonations from one tube to another and has been shown to greatly reduce the ignition and DDT times. During the branching process (Fig. 2.6), a detonation is formed using an obstacle based method in a PDE thrust tube. The detonation is then channeled through a fuel and air mixture located in a curved crossover pipe and directed into the closed end of a receiver PDE thrust tube. As currently used, the detonation fails upon entering the receiver tube and instead becomes a high energy and high pressure ignition mechanism to begin the DDT process in the second tube. The results of previous branched detonation efforts[29, 30, 31, 32] show a reduction in the combined spark initiated ignition and DDT times by 85% (from 8 ms to 1.2 ms) for a stoichiometric n-C_7H_{16} and air mixture.
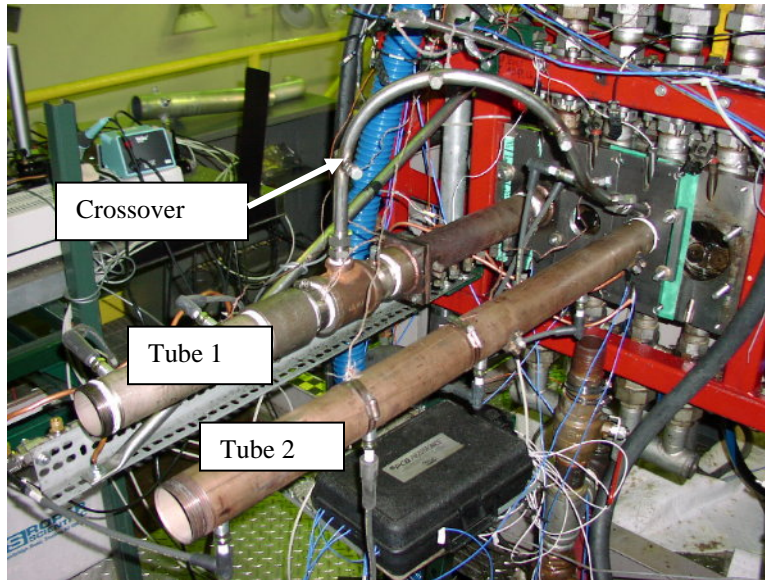
Figure 2.6 Branched detonation setup. Detonation wave travels from the middle of tube 1 to the closed end of tube 2.

Theoretical Detonation Performance

The combustion performance of a PDE depends primarily on whether or not a detonation occurs within the thrust tube for a given cycle. A detonation is considered to have occurred if the combustion wave speed is at or near (within ± 10%) the upper Chapman-Jouguet (CJ) point. The CJ point is based on the Hugoniot curve, which relates continuity, energy, momentum, and the perfect gas law for a one dimensional, steady, planar detonation wave.[33] The CJ point denotes the conditions of complete energy conversion from the chemical energy stored in the fuel to thermal energy. It can be shown that the CJ velocity occurs at the point of minimum entropy[1] and is the equilibrium point for the steady combustion process. Detonations are considered overdriven or super detonations when the wave speed exceeds the Chapman-Jouguet wave speed for that mixture at the given conditions. Overdriven detonations often occur during the DDT process, though at a sufficient distance past the transition point, the detonation will

22

eventually settle to the steady state velocity defined as the CJ velocity. Experimental data for a spark initiated heptane and air mixture is shown in Fig. 2.7 with a theoretical CJ velocity[34] of 1794 m/s. The top of the Fig. 2.7 represents the PDE thrust tube with a Schelkin spiral (sloped lines) filling the first meter and instrumented with seven ion sensors along the length of the tube. Combustion begins on the left (closed end) of the tube, and the combustion wave accelerates until crossing and exceeding the CJ velocity at 1 meter. The velocity slows at the next set of sensors to a value roughly 10% over the theoretical CJ value. The data shows a large variation (± 400 m/s) during the DDT and super detonation regions; however, the data collapses neatly into a tightly confined spread (± 65 m/s) when achieving the steady state condition at 1.15 m.
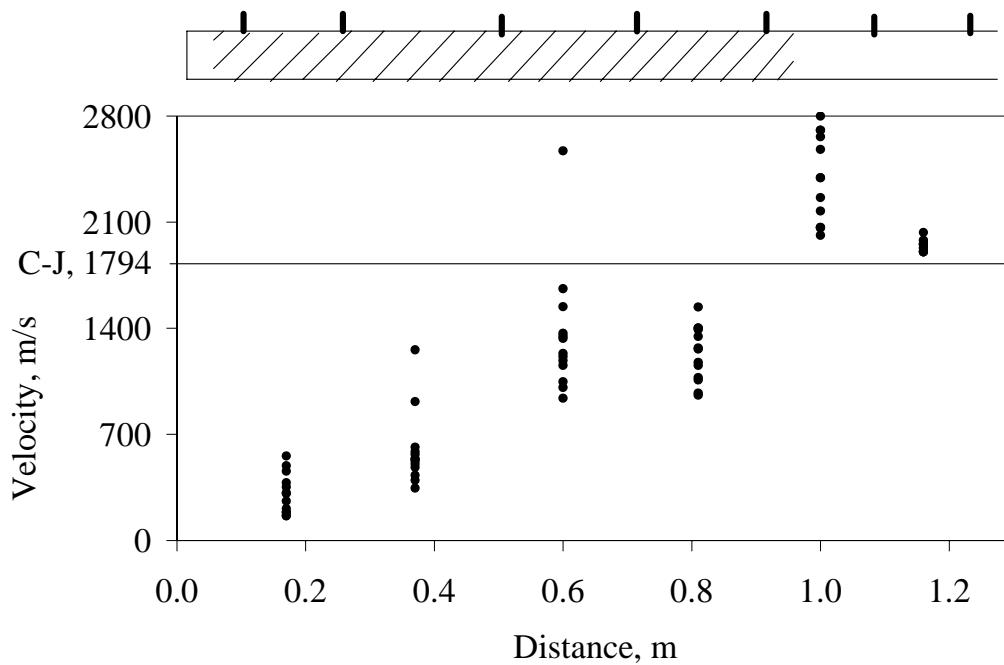
Figure 2.7 Average combustion wave speeds along the length of a PDE thrust tube. Hatched line at the top represents a Schelkin spiral and tick mark represent wave speed sensors for a n-C_7H_{16} and air mixture at an equivalence ratio of one. Used with permission from Ref. 32.

Detonation Cell Size

Once a detonation has developed, the self sustaining detonation wave contains structures that repeat while traversing through the reactive mixture. These features can be captured experimentally using an axial histogram called a smoke foil. The smoke foil uses deposited soot or carbon on the inside of a detonation tube to capture the shape created at the intersection of the incident shock and the reflected shock at the mach stem shock. This high temperature feature is called the triple point (Fig. 2.8). The result is a fish scale like pattern shown in Fig. 2.9 and denotes the cellular structure of the propagating wave as found on a smoke foil. The individual Mach stems combine to form the two dimensional detonation wave front traveling down the tube. The cell structure is three dimensional; though two dimensional effects dominate in slender narrow tubes and three dimensional effects are more influential with wider tubes or tubes with larger diameters.[35] The cell size is normally denoted by the symbol λ and is a measure of the height of a cell.[1] As will be discussed later, the cell size has been found to be related to the amount of energy required to initiate a detonation.
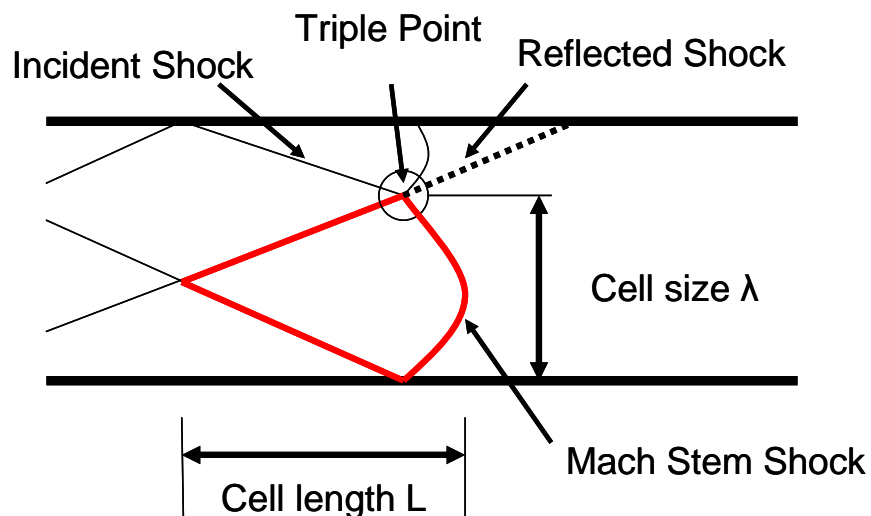
Figure 2.8 Detonation cell structure for a 2D wave running to the right.
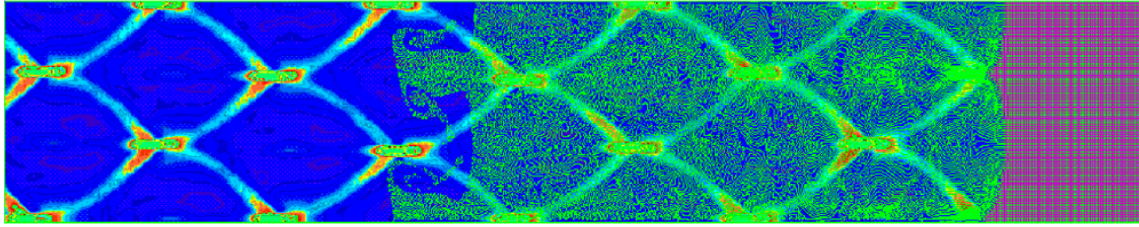
Figure 2.9 CFD Smoke foil for H_2 and air mixture. Used with permission from Ref. 36.

Direct Detonation Initiation Energy

The experimentally determined energy required to directly initiate a hydrocarbon fuel and air detonation is on the order of 1 MJ (Fig. 2.10) and is not available from modern automotive electrical ignition systems which provide 100 mJ pulses.[37] The relative magnitude of these initiation energies, however, does provide insight into the difficulty to transition to a detonation with the obstacle method described previously.
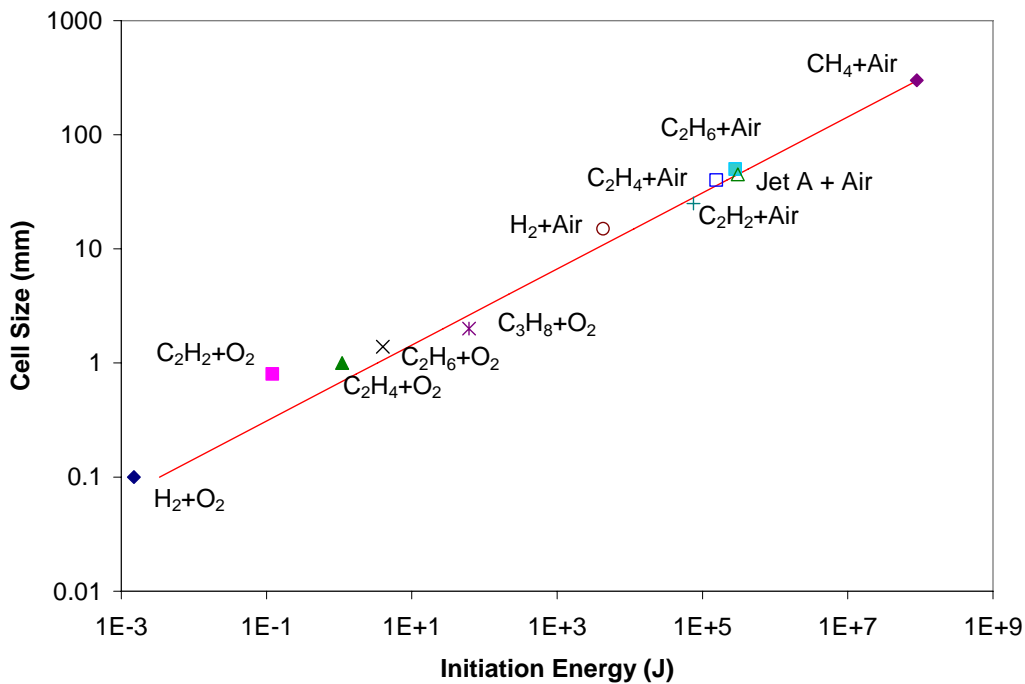
Figure 2.10 Cell size (λ) versus initiation energy at $\varphi=1$. Data from Refs. 9, 21, and 39.

The best fit line of the data in Fig. 2.10 which correlates the amount of energy to directly initiate a detonation ($E_{initiation}$) to detonation cell size (λ) in mm with either oxygen or air as the oxidizer is given by

$$E_{initiation} = 3.375\lambda^3 \text{ (Joules)} \qquad (2.9)$$

It should be noted that this correlation will only hold for an equivalence ratio of one. The initiation energy drops by the cube of the cell size. Also, when pure oxygen is the oxidizer, several orders of magnitude less initiation energy is required than with air.

Oxidizer and Stoichiometry Effects on Detonations

The cell size increases with the dilution of nitrogen in the mixture as seen in Fig. 2.11. The cell size increases by two orders of magnitude (1 to 100 mm) through the addition of nitrogen to an n-C_7H_{16} (n-heptane) mixture until the equivalent air mixture is obtained at 80% dilution. The addition of 80% N_2 diluent has increased the required detonation energy by over 1MJ.
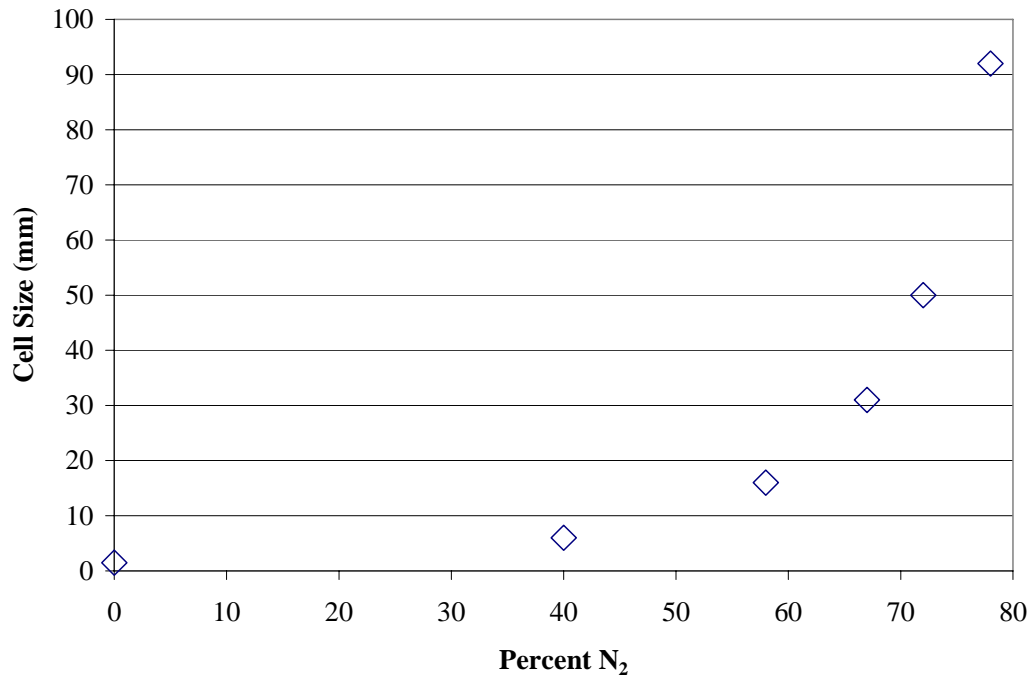
Figure 2.11 N-C$_7$H$_{16}$ and O$_2$ detonation cell size (λ) with diluent N$_2$. Data from Ref. 9.

The energy release from a stoichiometric hydrocarbon fuel and air mixture is on the order of 43MJ/kg,[40] but with some fuels at off stoichiometric conditions, there will not be enough energy to create and support a shock of sufficient strength to generate a detonation. The transition energy is provided by the combustion heat release, but a transition process must be in place to develop the detonation from a deflagration since the energy cannot be released quickly enough to initiate the detonation directly.

A near stoichiometric mixture requires the least amount of energy to directly initiate a detonation. Aside from the C$_2$H$_2$ (acetylene) mixture with air, most of the fuels shown in Fig. 2.12 have a minimum cell size at or near an equivalence ratio of one. Initial pressure is also important in determining the cell size of a detonation in a specific mixture. In Fig. 2.13, the cell size decreases with an increase initial pressure.
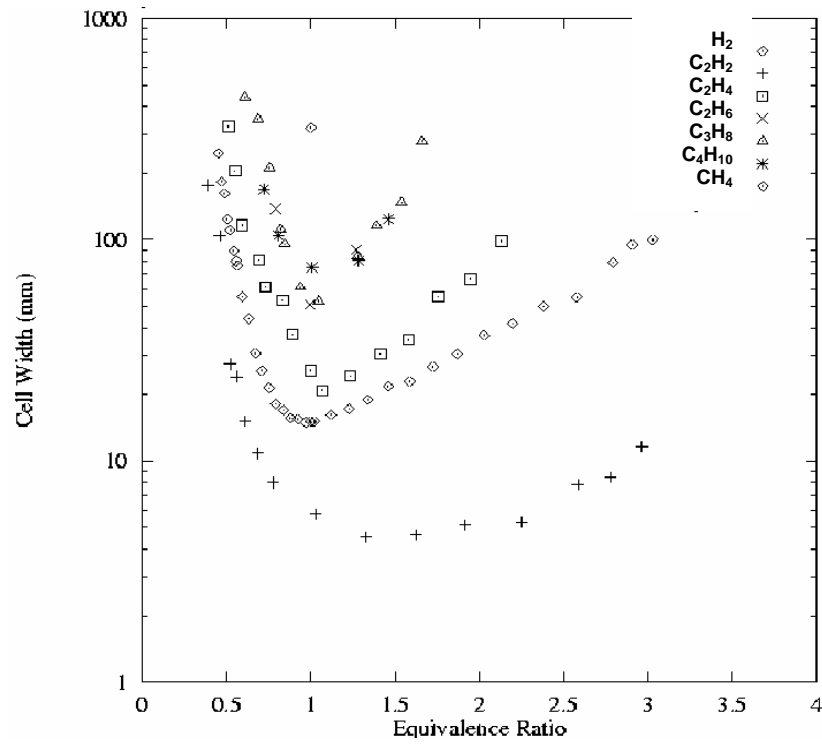
Figure 2.12 Cell size (λ) versus equivalence ratio for various fuels with air. Data from Ref. 39 as adapted from Ref. 9and used with permission.
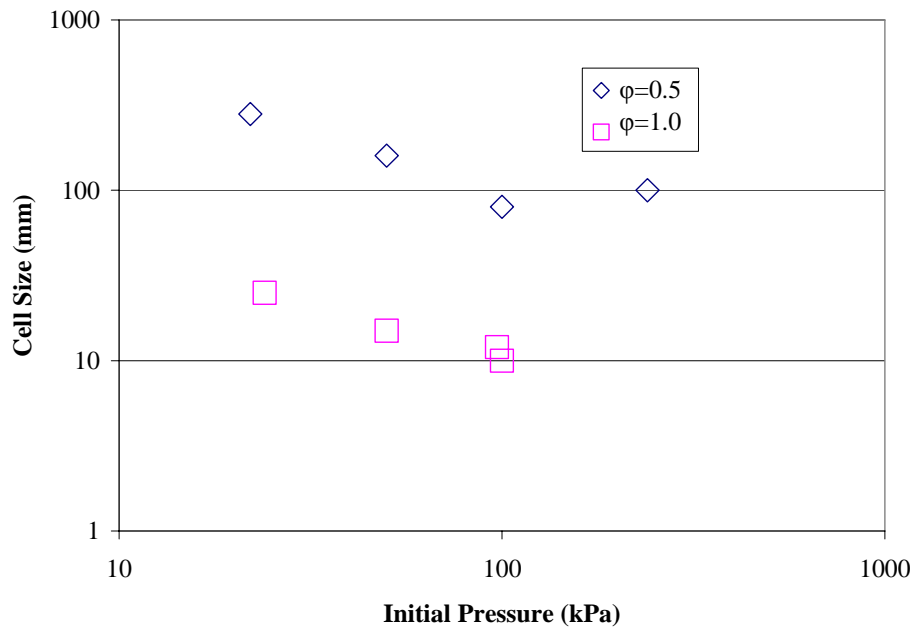
Figure 2.13 Cell size (λ) versus initial pressure for H_2 and air at two equivalence ratios. Data from Ref. 9.

Droplet Effects on Detonations

The local stoichiometry effects on heat release rates require the fuel and air to be well mixed to DDT. The detonation limits are much narrower than the flammability limits for a given fuel and oxidizer mixture (Table 2.1). The presence of droplets affects the homogeneity of the mixture and as a result, the detonability of the mixture. The minimum detonation initiation energy requirement for two phase (liquid and vapor) fuel-air sprays increases with droplet diameter, and the detonability limits of the fuel and air are widened by reducing the droplet size and increasing the fuel temperature.[28]

Table 2.1 Comparison of deflagration and detonation limits. Data from Ref. 1.

	Lean (vol %)		Rich (vol %)	
	Deflagration	Detonation	Deflagration	Detonation
H_2 - O_2	4	15	94	90
H_2 - air	4	18	74	59
C_3H_8-O_2	2	3	55	37

The unheated fuels in Table 2.2 reflect the difficulty in generating detonations with large fuel droplets suspended in the mixture even with the robust high explosive initiation method and pre-detonators.

Table 2.2 Detonation limits for liquid sprays in air in tubes using high explosive (HE) drivers and pre-detonators. JP-10 data from Ref. 11, all other data from Ref. 41.

Fuel	Formula	Droplet size (μm)	Lean Limit φ_L	Rich Limit φ_R	Initiation method
n-heptane	n-C_7H_{16}	~10	0.65	1.6	HE driver
n-heptane	n-C_7H_{16}	~700	no det	no det	HE driver
kerosene	$C_{11.6}H_{23.2}$	~780	no det	no det	HE driver
n-decane	n-$C_{10}H_{22}$	~400	no det	no det	$2H_2/O_2$ pre-detonator
JP-10	$C_{10}H_{16}$	~3	1.5	1.5	JP-10/O_2 pre-detonator

Previous researchers[11] noted that to achieve a detonation with a low vapor pressure fuel (JP-10) and air required at least 70% of the fuel to be in vapor form, and the fuel droplets to have a Sauter Mean Diameter (SMD) of 3 µm or smaller. The data in Fig. 2.14 is for finely atomized but unheated JP-10 into a vitiated air supply. The detonation was initiated with a JP-10 and O_2 pre-detonator. The air was heated using a vitiation process where hydrogen is injected and combusted with air prior to the fuel injection. Make up oxygen is injected near the liquid fuel injection point to replenish the oxygen used during heating. The published test conditions were at a global equivalence ratio of 1.5. The difficulty of achieving detonations at the aforementioned conditions was probably caused by poor mixing and liquid droplets. As will be shown in Chapter VI, under similar test conditions, detonations can be achieved at lower equivalence ratios with unheated fuel but will behave as a locally lean, globally rich mixture.
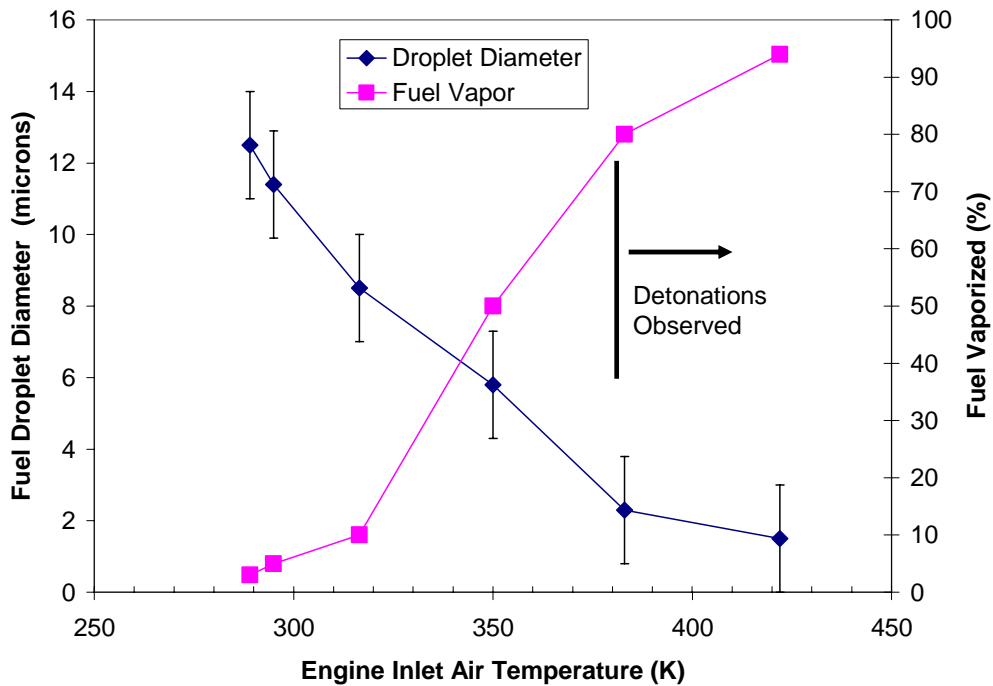
Figure 2.14 Air temperature effect on droplet diameter (SMD) and equivalent fuel vapor for JP-10 and air at an equivalence ratio of 1.5. Data from Ref. 11.

It is important to understand the combustion mechanisms within a steady state detonation wave to properly address the effect of the droplets. The one dimensional theory of the structure of a detonation wave was proposed independently by Zeldovich, von Neumann, and Döring (ZND).[42] They stated that the detonation wave can be considered as a shock wave driven by and coupled with a trailing combustion wave (Fig. 2.15). The shock raises the temperature of the unburned fuel air mixture above the auto ignition point. After some chemical time, which is denoted by the length of the induction zone, the fuel and oxidizer components begin to react quickly (reaction zone) and release enough energy to drive the shock wave preceding it.

For most hydrocarbon and air mixtures the CJ wave speed is roughly 1800 meters per second or Mach 5.3 relative to the unburned gases. The burned gases follow the detonation wave at a speed less the sonic velocity (~ 992 m/s) of the burned gases. The burned gas velocity is therefore considerably less than the detonation wave speed. A thorough discussion of the methods to calculate these velocities can be found elsewhere.[1, 23, 34] The overall thickness of the detonation wave is on the order of one centimeter, and the resulting timescale for the detonation wave to heat the mixture and release the full enthalpy of combustion is less than 6 microseconds.
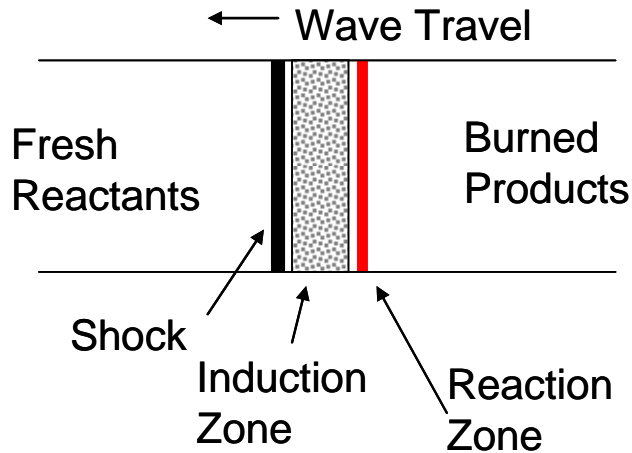
Figure 2.15 ZND model for gaseous fuel and air 1D detonation.

High vapor pressure fuels such as aviation gasoline and heptane are more readily evaporated and do not have the strong droplet size sensitivity (Fig 2.16). Previous work[43] has shown that for high vapor pressure fuel droplets, the shock wave would adequately shatter and evaporate the heptane droplets up to sizes on the order of 400 μm, leading to high vapor pressure fuel detonation characteristics which are similar to that of a gas phase detonation. Similar behavior has been observed with low vapor pressure fuel with droplets on the order of 3 microns.
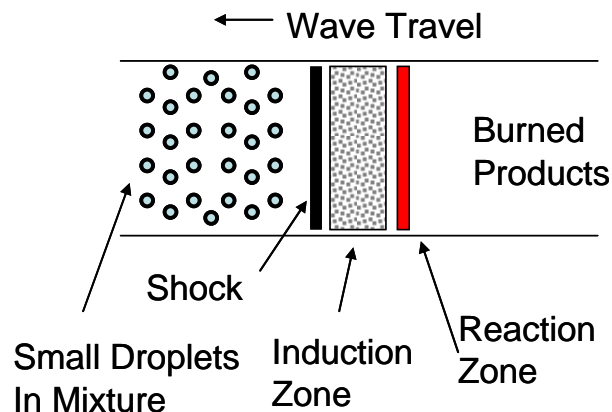
Figure 2.16 ZND model for high vapor pressure fuel and air mixture 1D detonation with droplets.

Now consider a detonation wave propagating through the two-phase mixture with low vapor pressure fuel droplets of varying size with features shown in Fig. 2.17. The induction zone must now include the droplet evaporation time as well as the previously mentioned chemical time. The detonation wave fails because an insufficient amount of fuel vapor is present in the mixture to sustain the detonation.[11] The droplets are in effect not small enough to be completely shattered by the shock or be vaporized by the subsequent high temperature, and thus not able to achieve the results of the high vapor fuels. This agrees well with other[44, 45, 46] two phase low vapor pressure fuel mixtures studies. The detonation wave survival depends on the droplet breakup and subsequent combustion in the reaction zone behind the shock. The burning droplets could not release energy fast enough to sustain the detonation wave.
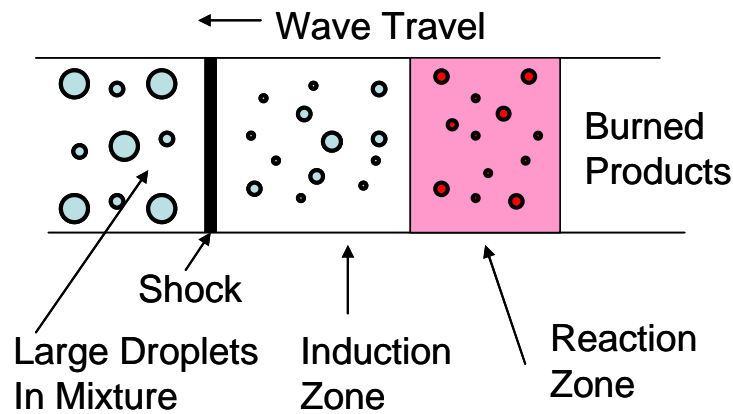
Figure 2.17 ZND model for low vapor pressure fuel and air mixture 1D detonation with droplets.

The droplet effects on the combustion performance with low vapor pressure fuels, such as n-decane and kerosene, led to measured detonation wave speeds that were 23.5% lower than the theoretical CJ detonation velocities for the global equivalence ratio.[46] The reaction zones were long and were governed by the shock generated breakup and long

33

evaporation times of the liquid droplets. The high vapor pressure fuel heptane, however, was able to attain detonation wave speeds very close to the expected CJ speeds (3.3%) and there was little difference between completely evaporated and partially evaporated fuels with high vapor pressure liquid droplet experiments. The low vapor pressure droplet results showed an increase in length of the induction and reaction zones on the order of 4 cm or four times the gaseous or small droplet induction zone.[44] Relating this increase to an equivalent increase in the overall cell size, the droplets have increased the required initiation energy by 4 cubed or 64 times (Eqn 2.9). For detonation of JP-8, a low vapor pressure fuel, the droplets must be nearly evaporated to eliminate these effects or a detonation will not be achievable.

Octane Number Defined

Of the four fuels tested, both isooctane and n-heptane are used to define the octane rating of automotive fuels (Table 2.3). Since the detonation is driven by the compression heating by the preceding shock, the relationship to octane number (ON) may provide insight to the detonability of the fuel. It has been proposed[47] that a variability in ON in a PDE could be used to increase or decrease the sensitivity of generating detonations. In a spark initiated automobile engine, knock refers to the noise emitted when the fuel and air mixture inside the engine ignites prematurely due to compression heating instead of the desired combustion initiated by the spark. The compression heating of the unburned mixture from the advancing piston can auto ignite the fuel and air mixture prior to the spark initiation (Fig. 2.18). The premature ignition event releases the

stored chemical energy in the fuel at a rate between 5 and 25 times faster than the spark initiated rate.[48]

Table 2.3 Octane numbers and auto ignition temperatures (AIT) at 1 atm.

Fuel	Octane Number[49, 50]	AIT [17] (C)
n-heptane	0	223
isooctane	100	423
av gas	100	440
JP-8	15~25	228~242
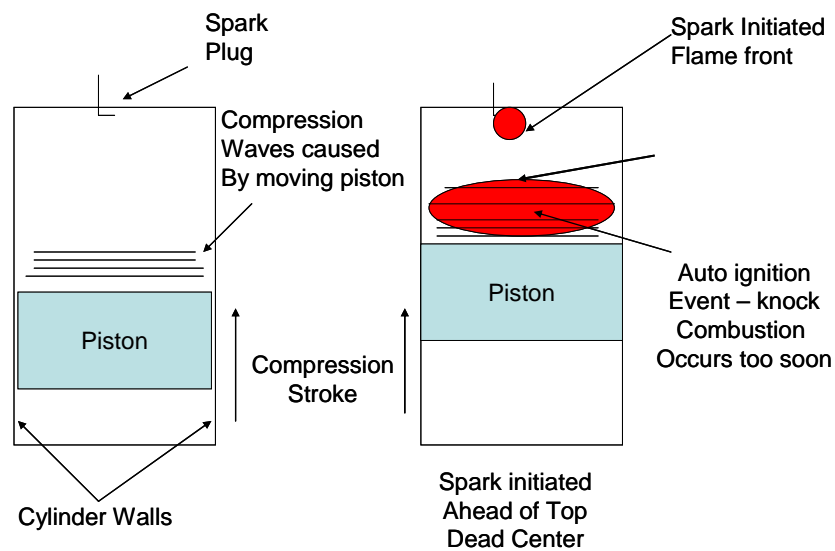
Figure 2.18 Automotive knock event in an internal combustion engine.[51]

The fuel ON relates the resistance to knock relative to a mixture of isooctane and n-heptane. The higher the octane number, the more resistant the fuel is to exhibit the previously described knock phenomena. Two methods are commonly used to determine the fuel octane number. The Research Method[52] tests fuels at representative low speed city driving conditions, and the Motor Method[53] tests fuels at representative high speed highway driving. The resulting research octane number and motor octane number are

35

used to determine an antiknock index. The historical standard ASTM Specification D 439 is used for determining the antiknock index by simply averaging the two numbers.[50]

Reduced ignition times have been reported with lower octane number fuels.[54] The experimental work here will attempt to correlate both the ignition and detonation times with octane number for a pulse detonation engine.

Static and Dynamic Heating of Fuel

The success of the flash vaporization system relies on the ability to repeatedly heat the fuel to high temperatures without thermal fuel degradation which can damage the fuel system. Dissolved oxygen within the fuel, due to contamination with air, can chemically react with the fuel at elevated temperatures.[55, 56] Table 2.4 gives the maximum amount of dissolved air in JP-8 at equilibrium as a function of temperature and pressure.

Table 2.4 Molar fraction of dissolved air in JP-8 with temperature and pressure. Data from Ref. 57.

Pressure (bar)	23.8 °C	200 °C
10.34	0.0139	0.015
20.69	0.0289	0.0312
48.28	0.0707	0.0733
103.45	0.1512	0.154

The reactions between the fuel and the dissolved oxygen are termed thermal-oxidative and occur at fuel temperatures between 393 K and 533 K. The products from these reactions cause carbon particulates[56] and carbonaceous deposits on metal surfaces in fuel systems.[55] The amount of deposits varies linearly with the amount of dissolved oxygen in the fuel[58] and increases with fuel temperature.[56] The insoluble particulates can clog the small openings on fuel spray nozzles, and the deposits on the walls can reduce

heat transfer properties of the tube and increase the pressure drop through the fuel system. The fuel thermal stability can be increased to 755 K by reducing the oxygen content to less than 1 part per million (ppm). At this contamination level, the reactions with the dissolved oxygen are considered negligible.[55, 56] The second problem is endothermic reactions which can also produce particulates and clog fuel lines. The time the fuel spends at the higher temperatures will dictate the amount of cracking (endothermic) reactions that take place. Research[59] has been performed to determine the effect of time on the heating of static n-dodecane (n-$C_{12}H_{26}$). Dodecane was used as a representative jet fuel and was thermally stressed at temperatures of 400 °C and 450 °C. In these tests, the sample fuel was deoxygenated with N_2 to minimize the presence of dissolved O_2 prior to heating so that no thermal oxidative reactions should occur. The fuel samples were then pressurized at 6.9 MPa and placed in a preheated sand bath at the test temperature for the desired time, and then cold quenched and analyzed using a gas chromatograph. The results of these tests are shown in Fig. 2.19 where the fuel, n-dodecane (n-$C_{12}H_{26}$), was statically heated and continuously sampled to determine the cracking rate. At 400 °C, the fuel takes 233 minutes to crack 20% of n-dodecane into smaller chain hydrocarbons, but at 450 °C, the fuel decomposes by 20% in only 17 minutes.
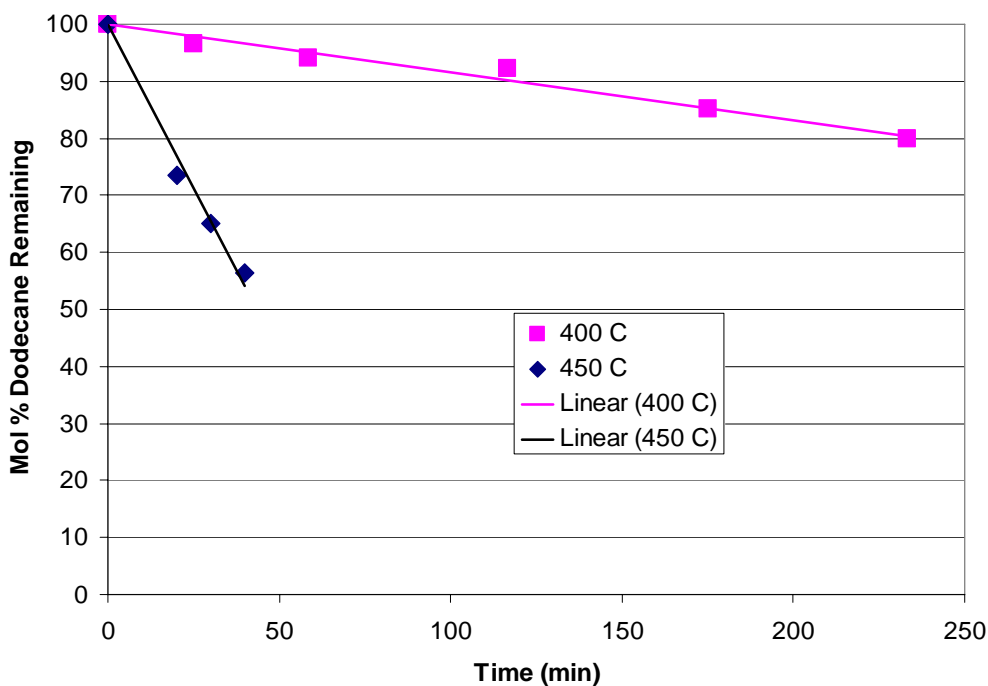
Figure 2.19 Percentage of n-$C_{12}H_{26}$ remaining during static heating after being heated under 6.9MPa of N_2. Data from Ref. 59.

For the flash vaporization system described in Chapter V, the fuel is statically heated until used; therefore, the test temperatures should not exceed 350 K to ensure that no endothermic reactions have taken place. The temperature limit should ensure that the JP-8 does not degrade during the static heating. If higher temperatures are required, then a method of heating the fuel quickly (on the order of seconds) should be used unless cracking is desired. Flowing systems, due to shorter residence times, have the ability to heat the fuel to higher temperatures before the thermal cracking of the mixture occurs. The percentage of the fuel undergoing endothermic reactions can be controlled by the flow rates at the higher temperatures. The endothermic reactions can be constrained so long as the residence time at temperature is shorter than the chemical time required to decompose the fuel. The results from a flowing heated fuel system[60] are shown in Fig. 2.20.
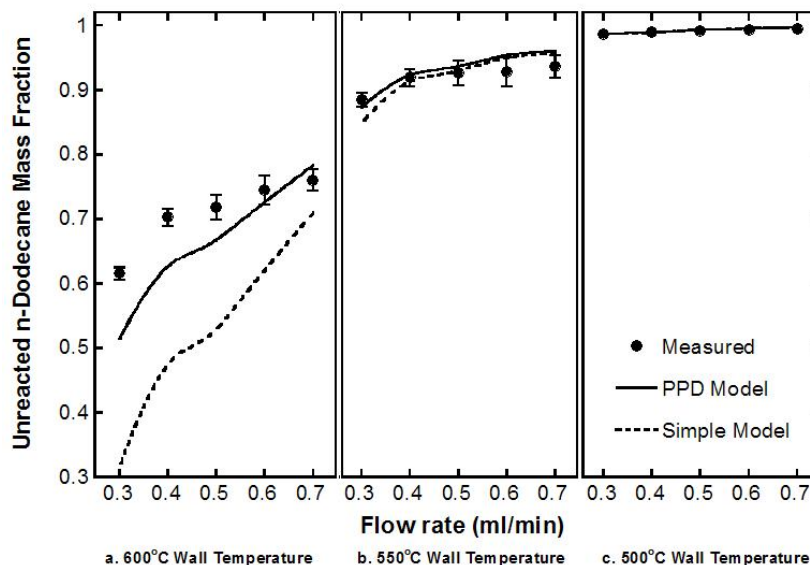
Figure 2.20 Comparison of experimental versus calculated n-$C_{12}H_{26}$ degradation for varying steady state wall temperatures and flow rates. Used with permission from Ref. 60.

During these tests, the wall temperature was held constant and the flow rate through the tubes was varied to determine the amount of cracking for n-dodecane. For the five flow rates studied, the fuel did not measurably crack at the 500 °C wall temperature. The paper60 showed that the fuel quickly reached the wall temperature and was constant except for minor temperature drops occurring due to the endothermic reactions taking place. The data shown in Fig. 2.19 also agrees well with other researchers56 efforts using deoxygenated Jet A. That data showed that Jet A can be heated near 480 °C (755 K) before significant cracking and the associated surface deposition occurs. The sizing of a heated fuel system for the required flow rates must not exceed the upper temperature limits or the particulate problems discussed previously will degrade the operation of the FVS. Off design operation will be a challenge to the designer. JP-8 is Jet A with three military specified additives, and similar performance between the two fuels is expected.

III. Facilities and Instrumentation

This research was performed in the Air Force Research Laboratory (AFRL) Pulsed Detonation Research Facility at Wright Patterson AFB, Ohio. The facility incorporates two electrically driven camshafts situated in a General Motors Quad 4 head. Four thrust tubes are attached where pistons would normally interact with the head and valves. In this work, only two steel pipe thrust tubes, each with a 5.2 cm interior diameter and 152 cm long, are fired at a frequency of 15 Hz each for an aggregate 30 Hz. The rotating cams provide a three-part cycle with equal time (120 degrees) to fill, fire, and purge the thrust tubes. The manifold pressure behind the valves is adjusted to provide the correct fill volume at the desired operating frequency. The fill volume is defined as the volume of the thrust tube when the fuel air mixture expands to atmospheric pressure at the open end of the tube.

Air Supply for the PDE

The facility setup for the AFRL PDE is shown in Fig. 3.1. Two Ingersoll-Rand PAC AIR 300 air compressors supply facility high pressure air for both the fill and purge portions of the PDE cycle. A 6.4 cubic meter reservoir receives and stores the compressed air. Downstream of the reservoir, two tubes tee off into separate fill and purge lines. Dome loaders regulate the air pressure and are used in conjunction with orifice plates to meter the required mass flow. This value is calculated and controlled by the facility computer. When making large changes in mass flow requirements, the orifice plates are manually changed. The tubes are filled when an electric motor turns the cam shafts to open the valves within the PDE head.
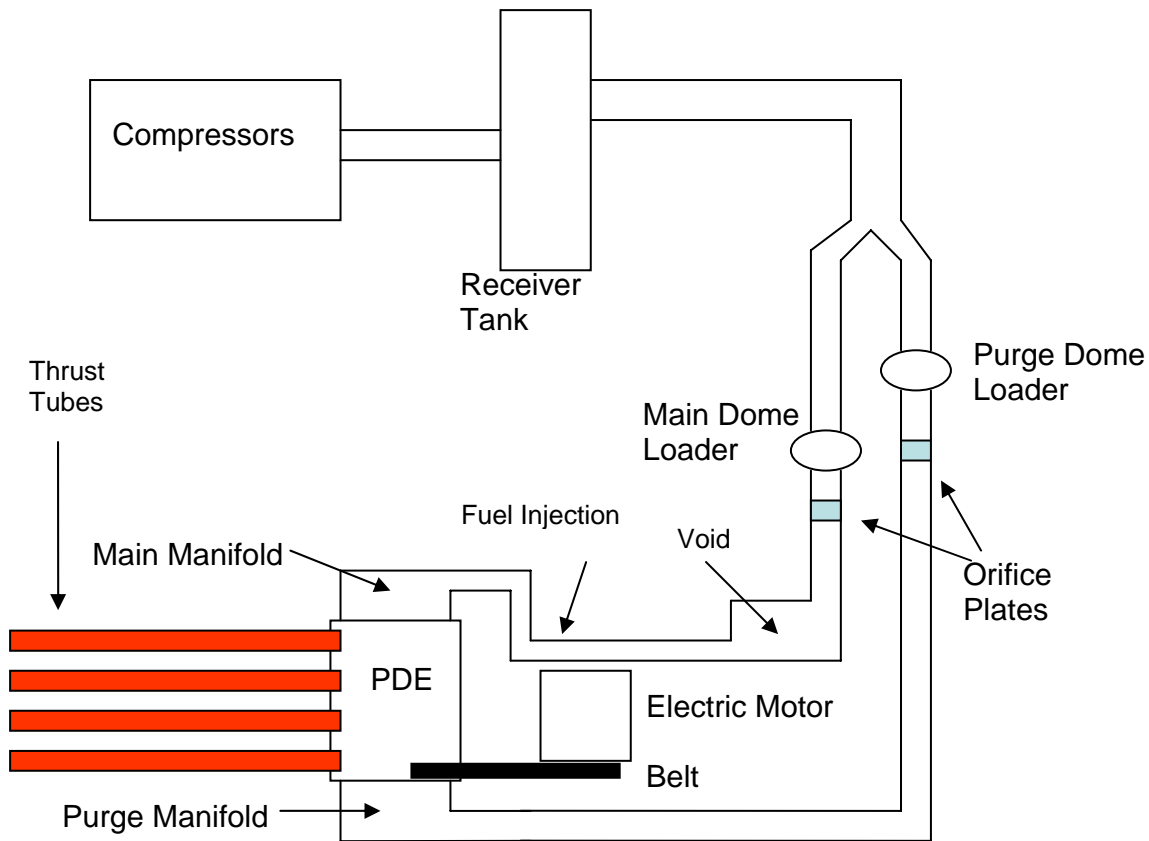
Figure 3.1 Facility air sketch

Multi-tube operation provides near continuous mass flow rates as the valves open and close for all four tubes. When less than four tubes are used, there is an increase in the unsteadiness in the air flow. Specifically, for a 30 Hz, single tube run, the air system will provide a continuous 3.59 kg per minute flow rate. Since the intake valves are only open for one-third of the cycle (0.0111 sec), the other two-thirds of the cycle (0.0222 sec), the air is being stored in the system and the air pressure rises. A problem arises in the location of the fuel injector. These fluctuations cause the air to speed up and slow down depending whether or not the thrust tubes are being filled. If the fuel is injected steadily near the valves upstream of the intake manifold, the mixture varies between fuel rich and fuel lean with the mass fluctuations. The fuel injector was placed 6.5 meters from the

intake valves where the velocity fluctuations were 20% of the values nearest the intake

valves to minimize the potential stoichiometry effects.

Air and Fuel Flow Calculations

The amount of air and fuel required for each cycle was approximated by solving

the following equations. The air mass flow required for the PDE is determined by the

total thrust tube volume the fuel and air mixture will fill at atmospheric pressure each

second.

$$\dot{V}_{total} = V_{tube} \, x Frequency$$
Required volumetric flow rate (m^3/s) where frequency is the detonation pulse rate   (3.1)

$$\dot{V}_{total} = \dot{V}_{air} + \dot{V}_{fuel}$$
Volumetric flow determined by air and fuel flow   (3.2)

$$\dot{m}_{air} = \dot{V}_{air} \frac{P_{atm}}{R_{air} T_{mix}}$$
Ideal gas relationship for air (kg/s)   (3.3)

$$\dot{m}_{fuel} = \dot{V}_{fuel} \frac{P_{atm}}{R_{fuel} T_{mix}}$$
Ideal gas relationship for gaseous fuel (kg/s)   (3.4)

$$R_{fuel} = \frac{R_{universal}}{MW_{fuel}}$$
Specific gas constant for gaseous fuel (kJ/kg/K)   (3.5)

$$T_{mix} = \frac{\dot{m}_{fuel} T_{fuel} + \dot{m}_{air} T_{air}}{\dot{m}_{fuel} + \dot{m}_{air}}$$
Mass averaged mixture temperature (K) (approx)   (3.6)

$$\frac{\dot{m}_{fuel}}{\dot{m}_{air}} = 0.065988$$
Stoichiometric ratio for n-heptane and air   (3.7)

Solving these equations simultaneously gives the required air and fuel mass flow for a given tube volume and engine firing frequency at a specific air and fuel temperature and assumes the fuel is fully gaseous during the fill process. The control computer calculates the above values using the measured manifold temperature.

Fuel Injection Locations

Two different fuel injection locations were used for the FVS testing. For the three high vapor fuels (heptane, isooctane, and aviation gasoline), a long mixing length (6.5 m) was used in conjunction with an axial mixer to provided smaller air velocity fluctuations at the fuel injectors. The quality of the flow is improved by moving the injectors far from the manifold where the strongest pressure and velocity oscillations are experienced. This problem is discussed in greater detail in Appendix B.
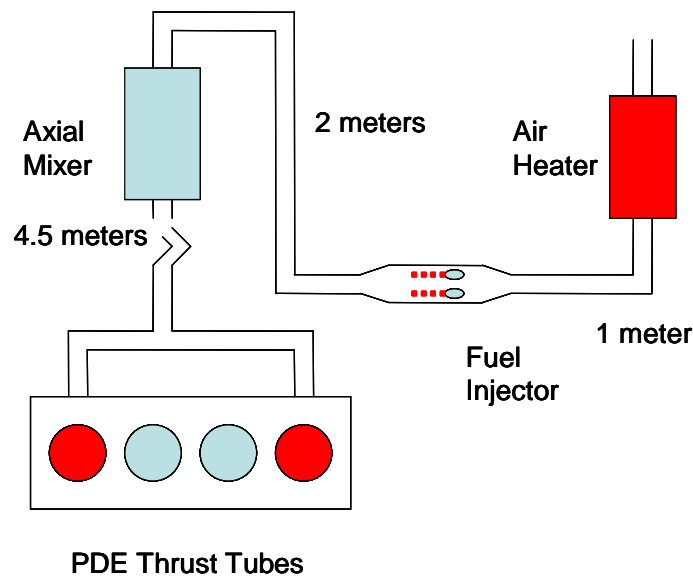
Figure 3.2 Fuel injection and air flow schematic for high vapor pressure fuels. The two outer circles represent the two tubes being used for the tests.

An axial mixer (Fig. 3.3) was added to reduce the variation in fuel to air ratio during the cycle. The length of the mixer was 0.53 m with two 0.46 m long pipes welded within the mixer body. The average velocity entering the mixer was 27.5 m/s and the total time for the air to traverse each side was 16.6 ms. The 16.6 ms residence time on each side of the mixer totals 33.3 ms and equates to a full cycle of the intake valves opening and closing (see Fig. B.3). No attempt was made to quantify the effect of the axial mixer or the pressure losses through the mixer. The combined exit area of the 19 holes on each interior pipe was larger (by 11.4%) than the entrance pipe diameter.
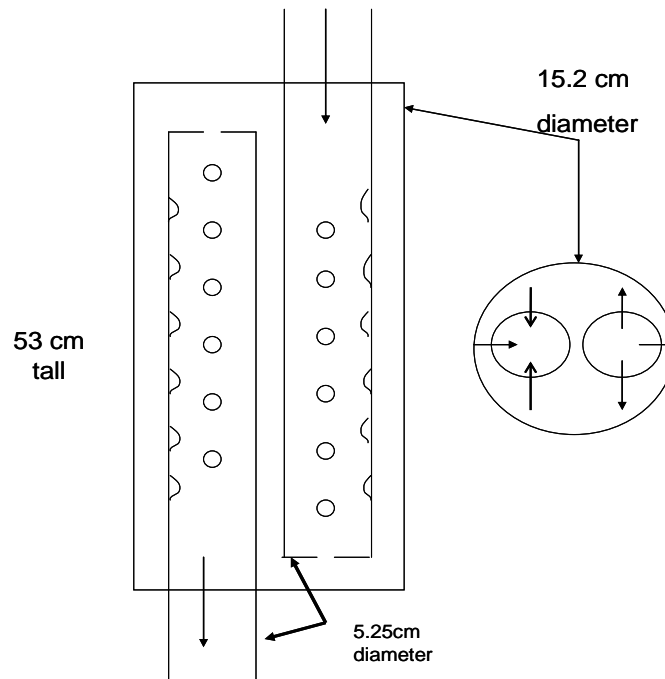
Figure 3.3 Axial mixer diagram. Fuel and air mixture enters the top and exits the bottom.

The JP-8 and air mixing length was shortened to 1.3 meters from 6.5 meters to minimize heat loss due to higher air temperature requirements and is shown in Fig. 3.4. The air temperature was increased from 311 K for the high vapor pressure fuels to a maximum of 422 K for the JP-8 setup. This shorter mixing length did cause an increase

in the velocity fluctuation at the fuel injectors (Appendix B), but allows for less heat loss. Due to safety concerns associated with potential fuel pooling, the axial mixer was not used during the JP-8 fuel injection runs.
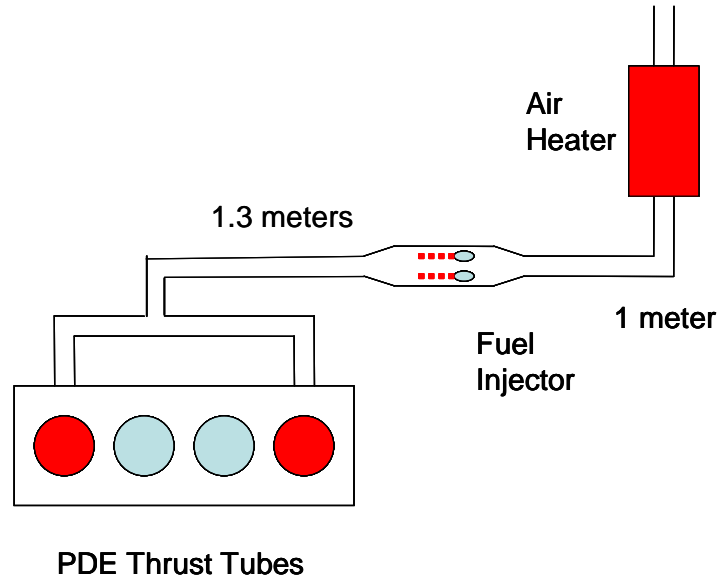
Figure 3.4 Sketch of furnace and injector setup for JP-8 fuel injection. The two outer circles represent the two tubes being used for the tests.

Flash Vaporization System Components

The following discussion describes the components that make up the fuel flash vaporization system and how the system is controlled. The fuel flow rates were controlled by varying the pressure on the nitrogen bottle regulator that feeds the hydraulic accumulators as shown in Fig. 3.5. When the desired fuel and air test conditions are reached, the pneumatically driven ball valve was opened and fuel was allowed to flow to the fuel nozzles at the injector spray bar to be mixed with the air. The now premixed fuel and air travels to the intake manifold to be valved into the two thrust tubes for combustion.
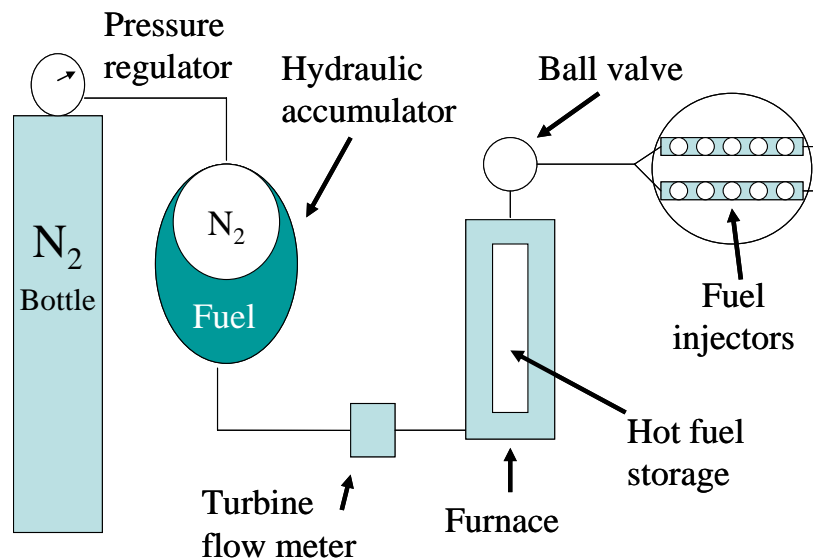
Figure 3.5 High pressure fuel system schematic.

Hydraulic Accumulators

Hydraulic accumulators are used to store the pressurized fuel and are shown in Fig. 3.6. A standard nitrogen bottle and high pressure (1200 psi) regulator supplied the high pressure gaseous nitrogen to expand the pliable bladders that exert force on the liquid fuel. Two Greer-Olaer Products, Model #30A-2.5A (2.5 gal) P/N 800730 hydraulic bladder accumulators were obtained to provide the nitrogen driven, bladder separated fuel. The bladder material was a Buna N polymer and is compatible with each fuel tested and is shown as the oval inside the accumulator in Fig. 3.5. As the fuel exits the accumulators during a test, the regulator maintains the nitrogen pressure acting on the fuel by flowing more nitrogen into the bladder to makeup the lost volume. A key benefit to this setup is the high pressure nitrogen is not absorbed by the fuel. Other studies[57] have used dissolved gases in fuels to help break up the fuel at the nozzle when the gas comes out of solution due the pressure drop during injection. The method is called an effervescent injection and was not studied in this work. During the fuel preparation, the

46

fuel was consistently saturated with nitrogen at atmospheric pressure (~1 bar), and the fuel and air manifold never dropped below 1.5 bar so the effervescent effects were negligible.

Figure 3.6 Photo of two 9.5 liter hydraulic accumulators.

Fuels

The fuels tested were purchased from a variety of chemical suppliers by the AFRL/PRTC Combustion branch. Table 3.1 describes the brand and quality of the fuels.

Table 3.1 Fuel brands and specifications.

Fuel	Brand	Quality
n-heptane	Sigma-Aldrich	>99%
isooctane	Philips	>99%
Av Gas	Philips	100 Low Lead
JP-8	Amoco	MIL-T-83133

Flow Meter

The fuel flow rates were measured by a Flow Technologies, model FT4-8AEU2-LEAT5, turbine flow meter. The meter has ball bearings and is designed for liquid operation with fluids at temperatures up to 494 K. The flow meter was positioned well

upstream of the furnace and measured only room temperature fuel with a density correction at temperatures between 275 K and 300 K. The flow meter uses an RF pickoff and the resulting signal is sent to a frequency port on a data acquisition board in the control computer. The board then counts the flow meter revolutions and the software converts those counts into a volumetric flow. Calibrations were performed on each fuel and are shown in Fig. 3.7 and were within $\pm 1\%$ of the factory specified full range calibration. The flow meter calibrations were performed using a calibrated flask and a stop watch. Recording times were on the order of one minute with timing accuracies within 1 second or $1/60^{th}$ of the volumetric flow rate.
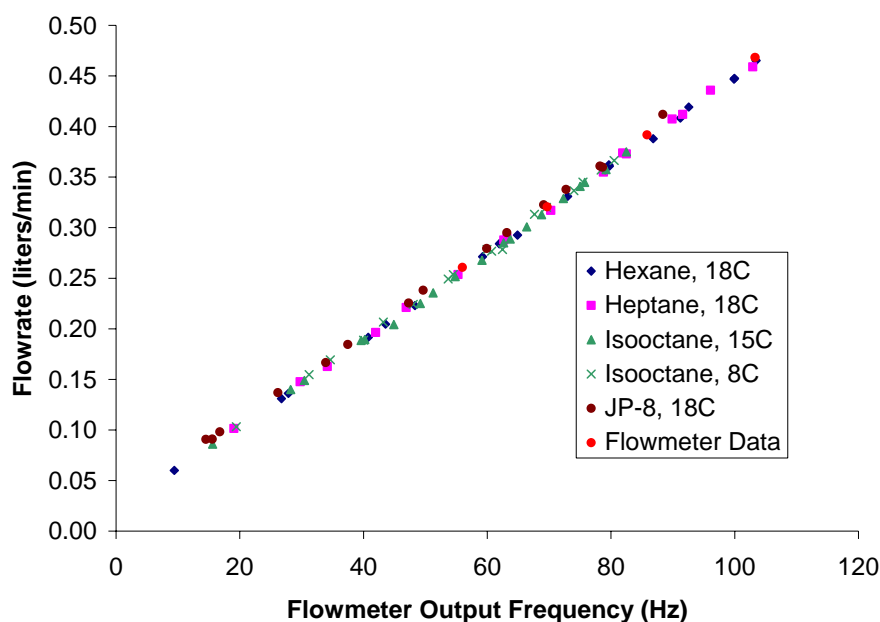
Figure 3.7 Flow meter calibration data for each fuel.

The calibration data is plotted in Fig. 3.7 with the manufacturer supplied calibration data. The desired flow meter output for control of the fuel system is a fuel mass flow rate not volumetric flow rate output by the flow meter. A thermocouple was

placed downstream of the flow meter to accurately measure the fuel temperature, and a user supplied density relationship (via SUPERTRAPP) converted the fuel volume to fuel mass.

Fuel Heater

A Lindberg, Model 55342-4, radiative furnace heated the fuel for the flash vaporization system. The furnace operates at a maximum temperature of 1473 K when supplied with 5.4 kW of power. The interior dimensions are 11.4 cm (4.5 in) diameter cylindrical space, 0.61 m (2 ft) long. Tests were performed with fuel temperatures ranging from ambient to above the critical temperature of the fuel. The range provided insight into the effects of injection temperature and the reduced ignition time relative to an unheated fuel injection system. A coiled 6.35 mm (0.25 in) diameter tube spans the length of the heater. The tube length inside the heater is 15.0 m and is wrapped around a 6.03 cm diameter, 51 cm long schedule 80 stainless steel pipe. The wrapped tubing was constructed from Silco® stainless steel and has a high temperature silicone coating applied on the interior surface. The coating retards reactions between the fuel and metal contaminants in the walls and reduces deposit formation. The 6.03 m pipe was coated with an anti-coking coating manufactured and applied by Restek Corporation. The coating thickness is on the order of hundreds of Angstroms[61] and provided a negligible decrease in fuel line and nozzle cross-sectional area.
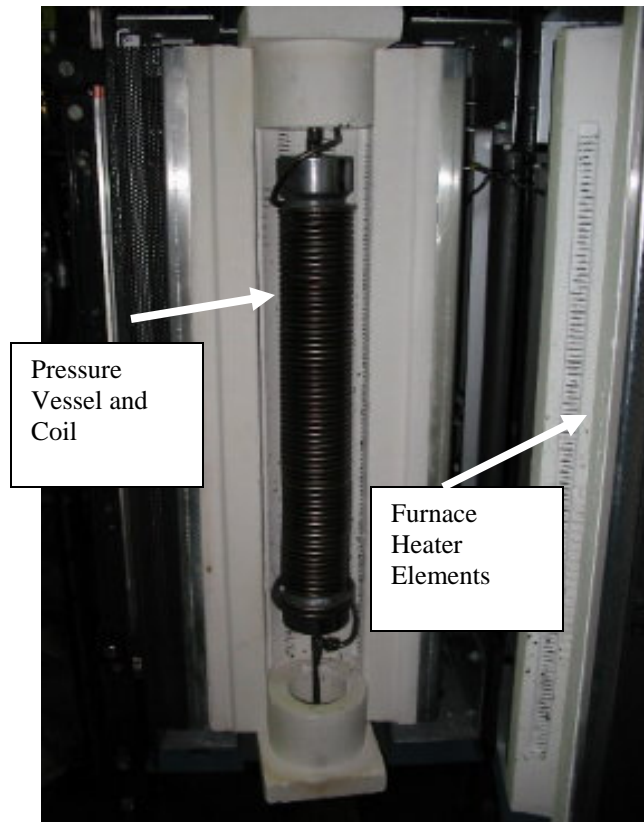
Figure 3.8 Vertically mounted Lindberg clamshell radiative furnace.
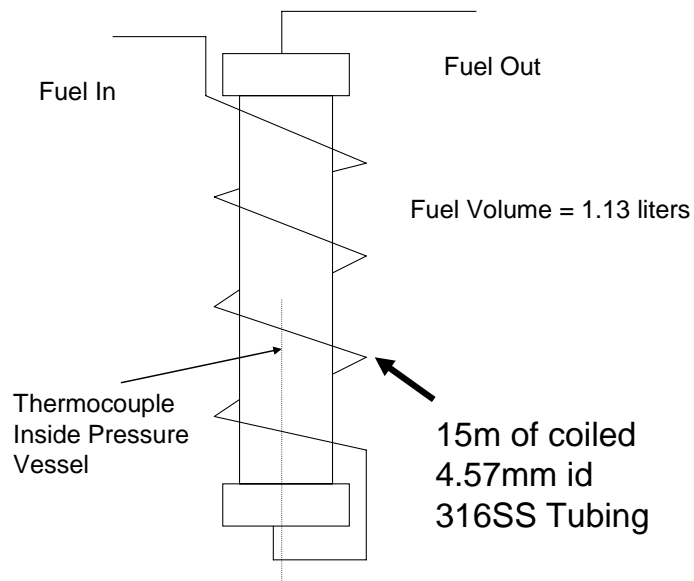
Figure 3.9 Stainless steel pressure vessel.

Active Insulation

Active insulation was an important mechanism to limit the amount of heat lost from the fuel when traveling between the furnace and the fuel injection nozzles. A flexible shaped heating element or tape heater, served to raise the temperature of the metal tubes and valves from the furnace exit to the nozzle entrance. The maximum exterior temperature attainable with the tape heater for the valve shown in Fig. 3.10 was 500 K. When fuel was heated above 500 K and flowed through the valve, the valve temperature would also rise while the fuel temperature dropped.
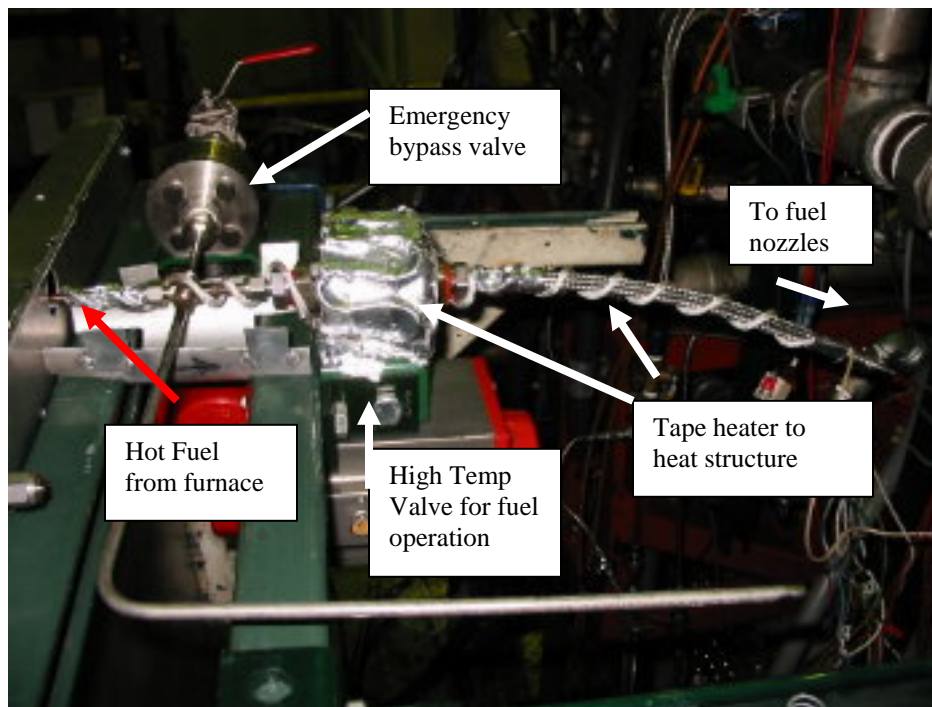
Figure 3.10 Active Insulation for components outside the furnace box without cover.

The furnace and tape heater locations were N_2 purged. This served to lean out the oxygen from the air and provided an added level of safety to prevent unwanted combustion should a fuel leak occur. The furnace and pressure vessel were completely enclosed and nitrogen was fed at a set rate controlled by a pressure regulator. As the

nitrogen leaked from the box, it was channeled through an enclosure that housed the tape

heater and insulation to the injection point on the air system.

High Temperature Ball Valve

A model 941-NPT-600-31 Bonetti, ANSI Class 600 ball valve, made of 316

stainless steel and rated to 823 K at 47.2 bar was used to turn on and off the fuel flow

during the tests. The three piece valve used graphite seals with full port, bubble tight,

fugitive emission. The valve is mounted and driven remotely with a fire safe Triac

pneumatic operator, model 2R80SRO.

Fuel Injector Setup

A dual spray bar arrangement was designed and built to provide sufficient nozzle

sizing for a variety of fuel temperatures and fuel flow rates. A total of 10 fuel nozzles

could be used at any given time with nozzle flow numbers set to match the desired flow

rate using the following relationship. The standard relationship[16] for correlating flow

coefficients with nozzle flow rates and pressures is given by

$$FN = \frac{\dot{m}}{\sqrt{\Delta P}} \qquad (3.8)$$

where $\dot{m}$ is mass flow in (lbm/hr) and ΔP is the pressure across the nozzle in (lbf/in^2).

When the fuel temperature rises, however, the fuel density drops (Fig. 3.11) and Eqn. 3.8

must be corrected for the change in density as given in Eqn. 3.9,
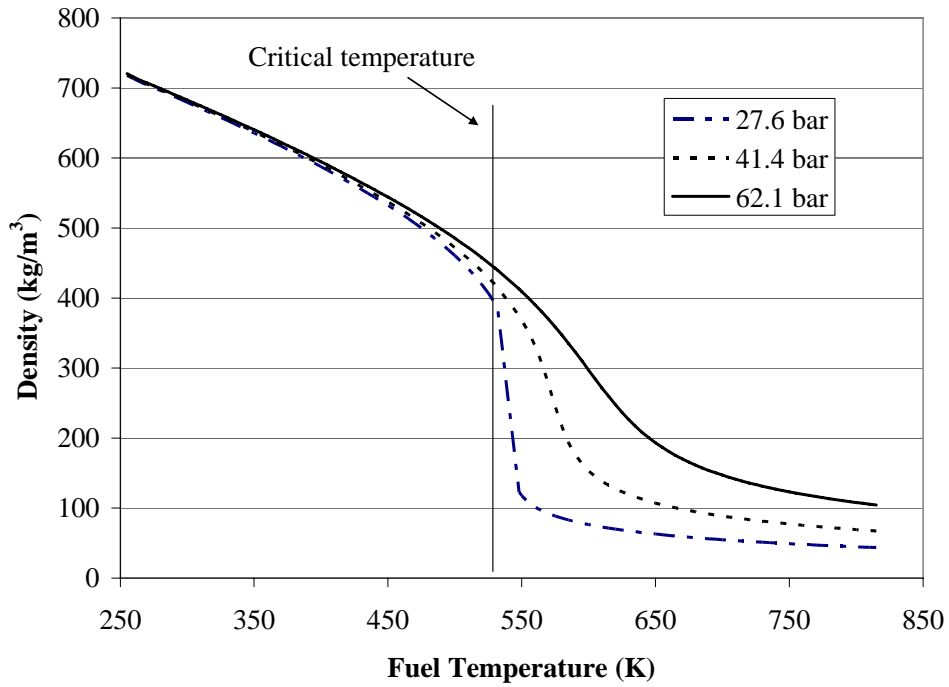
Figure 3.11 Heptane density at three pressures. The vertical line denotes the fuel critical temperature.

$$FN = \frac{\dot{m}}{\sqrt{\Delta P}} \sqrt{\frac{\rho_{CAL}}{\rho_{ACTUAL}}} \tag{3.9}$$

where ρ_{CAL} is the nozzle calibration density[16] of 48 lbm/ft^3 and ρ_{ACTUAL} is the actual density as given by Fig. 3.11 for the given temperature and pressure. The flow numbers are published by the manufacturer after being flow tested to ensure the values fall within $\pm$ 10%. Equation 3.9 was derived from the one dimensional Bernoulli's relationship and continuity and the flow number is given without units. The flow numbers are additive and allow the use of several nozzles to match the desired flow rate.

Table 3.2 Fuel Nozzle serial numbers and flow coefficients.

Fuel Nozzle		Test Pressure	Flow Limits (lbm/hr)		Spray Angle	Flow Number
P/N		psid	hi	lo	degrees	lbm/hr/(lbf/in^2)^0.5
27710	- 18	100	3.8	4.2	90	0.4
46817	- 4	100	5.3	4.7	70	0.5
59216	- 5	100	9.6	10.4	90	1
27700	- 17	100	9.6	9.9	82.5	1
27700	- 18	100	9.6	9.9	62.5	1
27710	- 8	100	16.4	15.6	75	1.6

The fuel nozzles were made by Delevan and are widely used in gas turbine engines. The nozzle has four primary pieces and includes a mesh cylinder to filter the fuel, the nozzle body, a spacer, and a retaining clip. The minimum area is shown in Fig. 3.12 as slots cut into a solid piece on the upper portion of the filter cylinder.
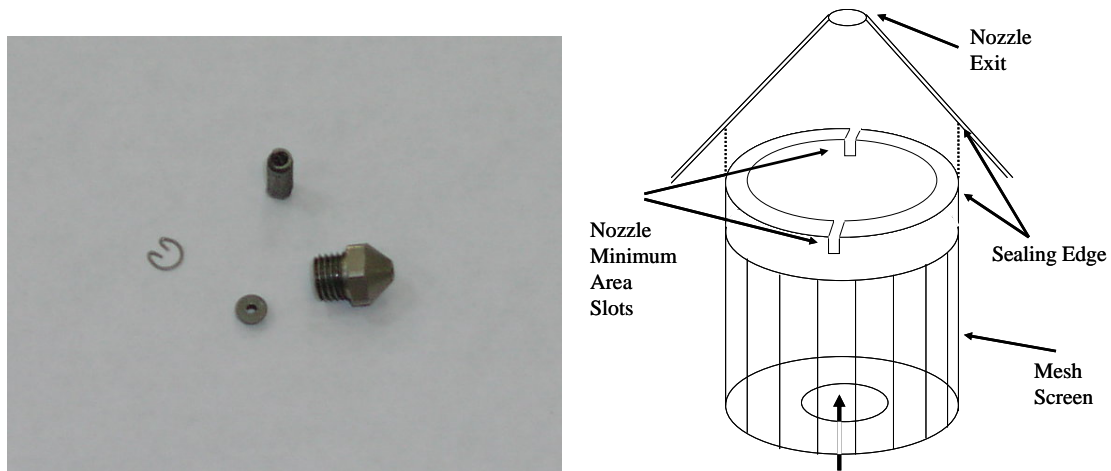
Figure 3.12 Photo and sketch of pressure atomizing nozzle components.

Several parameters within the fuel injector spray bar geometry are monitored during the testing as shown in Fig. 3.13. The injector pressure and both the fuel (T1) and injector wall (T2) temperatures are recorded during testing. The area between the spray

bars and the manifold walls (A1, A2, and A3) have equal area between them, and thus have roughly equal air flow around the injectors.
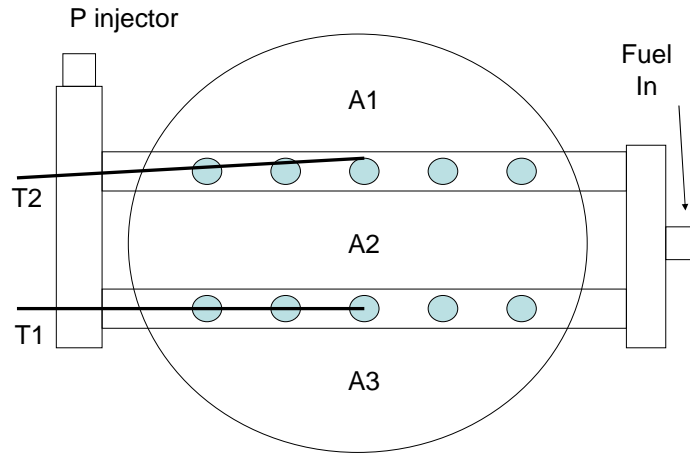
Figure 3.13 Fuel Injector Spray Bars (front view). Filled circles denote the locations of pressure atomizing fuel nozzles. Air is flowing out of the page.

Ignition System

A 12 volt DC automotive digital ignition system supplied power to the spark plug. The system provided a series of 105 – 115 milli-Joule sparks[37] into the hydrocarbon fuel air mixture via a capacitance discharge. The number of sparks per cycle was verified using a high speed camera. A 250 μsec duration pulse was noted every 1.1 ms (± 37 μsec). A total of four sparks are deposited during each ignition event at the operating frequency of 15 Hz.

Instrumentation

Measurement of the ignition, detonation, and unsteady flow phenomena described previously in Chapters II and III is now presented. Differential pressure transducers are used to measure the unsteady air flow within the PDE air system. Pressure rises associated with ignition are measured with dynamic pressure transducers and hydroxyl

radical (OH) filtered photo multiplier tubes (PMTs). The combustion wave speeds are measured using ion sensors, dynamic pressure transducers, and PMTs.

Figure 3.14 shows the physical setup of the closed end (head) of the PDE thrust tube where the ignition times were measured.
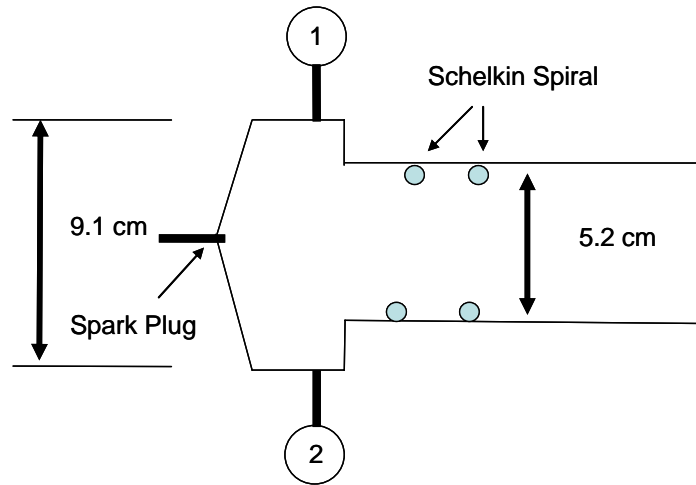
Figure 3.14 PDE Ignition Instrumentation locations.

where
1. Thermocouple for head wall temperature or PMT

2. PCB dynamic pressure transducer

The testing for all four fuels was performed with a 1.52 m long, 5.2 cm diameter tube, with a 1.22 m Schelkin like spiral as shown in Fig. 3.15. Ion sensors are located within the spiral, at the exit of the spiral, and after the spiral with locations noted in Table 3.3.

Table 3.3 Ion sensor locations on the two thrust tubes.

Tube	Sensor 1 location (m)	Sensor 2 location (m)	Sensor 3 location (m)	Tube End location (m)
One	1.122	1.271	1.439	1.511
Four	1.125	1.277	1.427	1.503
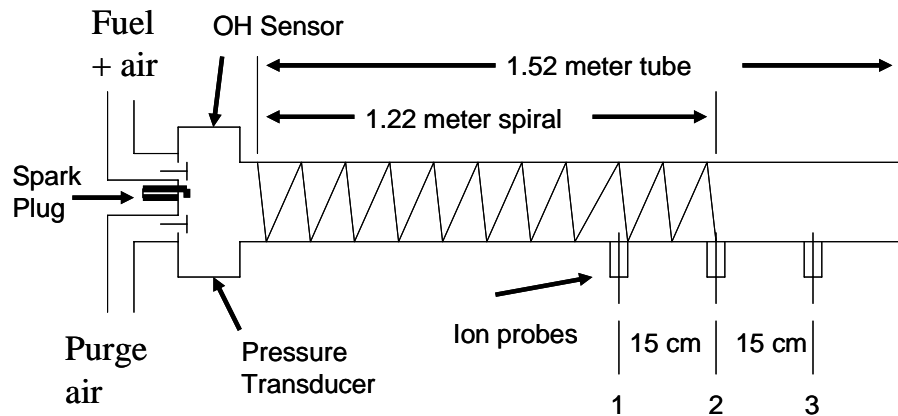
Figure 3.15 Location of instrumentation on the PDE thrust tube.

Data Acquisition Cards

A National Instruments Corporation NI PCI-6110, with 4 pseudo differential channels, 12 bit A/D with a maximum of 5 mega-samples per sec per channel was used to record the high speed combustion data.[62]   Input is 20 mV$_{DC}$ to 10 V$_{DC}$. Four of these boards are linked together and managed by an in house program called *Online Wave Speed* written by Mr. Jeff Stutrud of AFRL/PRTC.   Acceptable sensor inputs include pressure transducers, ion probes, spark timing pulses, photo diodes, OH sensors, and amplified thermocouple data.

Dynamic Pressure Transducers

A dynamic pressure transducer, the PCB Piezotronics ICP model number 102M232, rated to 345 bar in its dynamic range, is used to measure head pressure changes and determine ignition times. The transducers are covered with an ablative material that protects them from the high combustion temperatures. The cover material is a 0.5 mm thick red RTV silicone gasket that fills a slight recess between the threaded

57

casing and the center portion of the sensor. The sensor diameter is 0.56 mm inside a 0.375 inch, 24 thread count exterior. When wear on the material is noticed, the RTV is removed, and new material is applied and cut flush with a razor blade. The coating provides a consistently repeatable protective cover for the device.[63]

The transducer measures dynamic pressure using a piezoelectric material, in this case a quartz crystal, that outputs a voltage when a pressure is applied. The operating temperature range is from 219 K to 394 K. The transducer is protected from the high temperatures in the head by actively cooling the engine block where the sensor is mounted and the sensor tip is protected with the aforementioned ablative material. The ablative material does slightly dampen the response, but in comparison with results from absolute pressure transducers and other detonation wave speed measuring devices shows excellent agreement.[63] The dynamic pressure transducer is suitable for measuring dynamic events, but when a static pressure is applied the measurement voltage eventually bleeds to zero; therefore, it cannot be used to determine absolute pressures or very slow changes in pressure.[64]

Differential Pressure Transducers

An Endevco piezoresistive pressure transducer, model 8510-C, rated at 15 psig was used to measure the fluctuating intake manifold and injector pressures without fuel flow or combustion. It was also used to measure pressure on the back wall of the head of the detonation tube during the fill, fire, and purge portions of the cycle without combustion. The transducer uses a four arm Wheatstone bridge, dielectrically isolated silicone on silicone sensor, to measure changes. It has internal temperature compensation

from -18 °C to 93 °C. The sensor is powered and conditioned by an Endevco model 4428A and outputs full range to ± 5 V_{DC}.

Ion Sensors

The ion sensors (Fig. 3.16) are time of flight sensors and trigger off the conductive portion of the combustion wave where a high density of ions exists. Three sensors are placed in series along the length of a thrust tube and the detonation wave triggers each sensor denoting the time the wave reached that sensor. With the timing and spacing between the sensors known, the average wave speed between the sensors can be readily calculated. A more thorough discussion of the ion sensor performance and background is found in Appendix E.

Figure 3.16 NGK C-9E spark plug ion sensor.

Thermocouples

The FVS system was instrumented throughout with both type J (Iron-Constantan) and type T (Copper Constantan) thermocouples. The thermocouples were both 1/16th inch (1.58 mm) and 1/8th inch (3.16 mm) depending on the location and desired response. The 1/16th inch had faster response due to the reduced mass of the sensor tip. At the injector, the two thermocouples were both *special limits of error* designated and conform to meet

the ANSI MC96.1 specification (1975). The probes were 6 inches (15.2 cm) long and had grounded junctions at the tip with 304 stainless steel sheath materials.

High Speed Flow Visualization

High speed flow visualization can be accomplished using a clear polycarbonate tube and a high speed digital video camera. A Kodak, NMOS based digital camera operating at up to 40,500 frames per second (fps) was used to determine the spark rate of the ignition system. At the highest speed, the camera has a resolution of 64 x 64 pixels and increases to a resolution of 64 x 256 pixels when the speed is lowered to 18,000 fps.[24]

Photo Multiplier Tubes

An RCA, Model 1P28, all purpose photo multiplier tube (PMT) was used to capture light as a result of combustion. The PMT housing was coupled to an Ocean Optics multimode fiber optic cable.[65] The cable fiber is designed for ultra violet, visible (UV-VIS) capture with minimal attenuation (less than 0.15 db/m) in the 250 to 800 nm wavelength. The cable is 1 m long and has a 400 micron core diameter. The sensor makes line of sight measurements with a 24.8 degree cone acceptance angle at the end of the fiber.[66] A 309 nm (± 5 nm) bandwidth filter located in the PMT housing was used to capture the combustion produced hydroxyl (OH) radical emission.[66] The fiber was attached to the end of a 11.7 cm hollow tube (reducing the light acceptance cone) that was mounted into the closed end of the PDE tube where the combustion was initiated (see Fig. 3.15) and opposite the dynamic pressure transducer. The sensors were used to denote the initial time the event (ignition or detonation wave arrival) was captured by the

sensor and thus was not calibrated to determine the amount of OH present in the event. The data reduction routine mirrors the pressure transducer routine discussed in detail in the next chapter.

Gas Chromatograph

During the sparging calibration, the thermal conductivity detector (TCD) in a Hewlett Packard 5890 Series II Gas Chromatograph (GC) was used to measure oxygen dissolved in the fuel. During the deoxygenation experiment described in the next section, the sparging process is periodically stopped and a new fuel sample is fed into the GC. A very thin tube (0.25 to 0.53 mm diameter and between 15 to 100 m long) containing the mixture of interest is heated into the gas phase. The mobile or gas phase of each molecular component in the mixture takes a certain amount of time to exit the tube. As it exits the tube, the vapor passes over a filament in a circuit. The change in resistance is measured and plotted versus time. Peaks appear on the plot, and the area under the curves at different times indicates the amount of each component found in mixture based on a prior calibration. For the dissolved oxygen, the retention time is near 0.363 minute. Periodically, the tube needs to be flushed or burned off since some the heavier species do not move as fast and may corrupt the next reading.[67]

Fuel Conditioning

Preparation of the fuel was required to remove the dissolved oxygen and to prevent the thermal oxidation described earlier in Chapter II. The Ostwald coefficient (Eqn. 3.10) is used to relate the maximum volume of a gas absorbed in the fuel at varying temperatures (Fig 3.17).

$$Ostwald\ Coefficient = \frac{volume_{GAS}}{volume_{FUEL}} \tag{3.10}$$
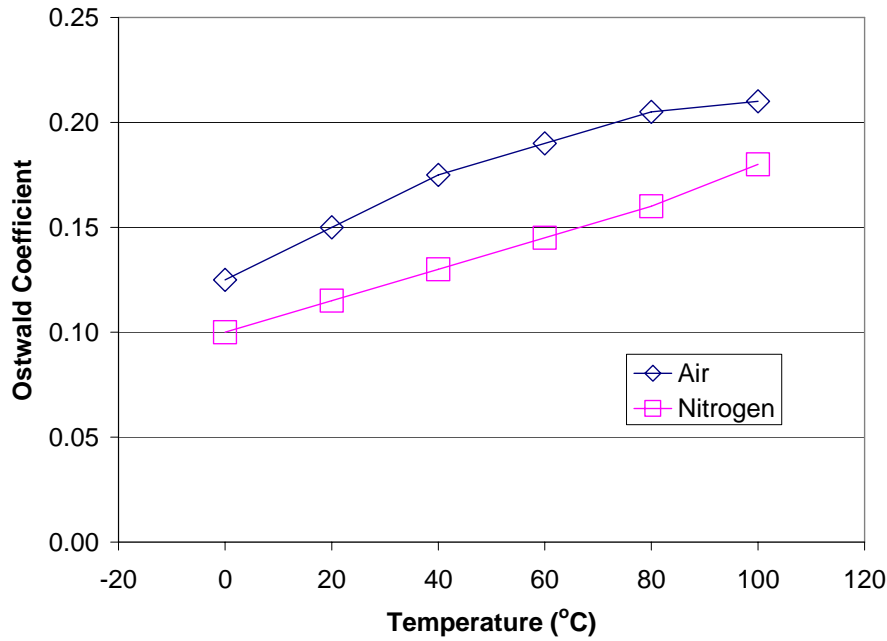
Figure 3.17 Ostwald's Coefficient for JP-8 for varying temperatures at 1 atm. Data from Ref. 40.

The Ostwald coefficient is independent of pressure; therefore, since the volume is constant, when pressure is relaxed a certain mass of the dissolved gases will come out of solution. Pressure, and thus mass, is determined through Boyle's law (Eqn. 3.11) and a corresponding states model described in Appendix C.

$$PV=constant \tag{3.11}$$

Sparging the fuel with N_2 is one way to remove the oxygen from liquid hydrocarbon fuels. During sparging, nitrogen bubbled through the fuel from a submerged wand (Fig. 3.18). The nitrogen agitates and displaces the dissolved oxygen in both the liquid fuel and in the gaseous ullage region above the fuel (Fig. 3.19).

Figure 3.18 Top view of fuel sparge tank nitrogen wand (spiral).
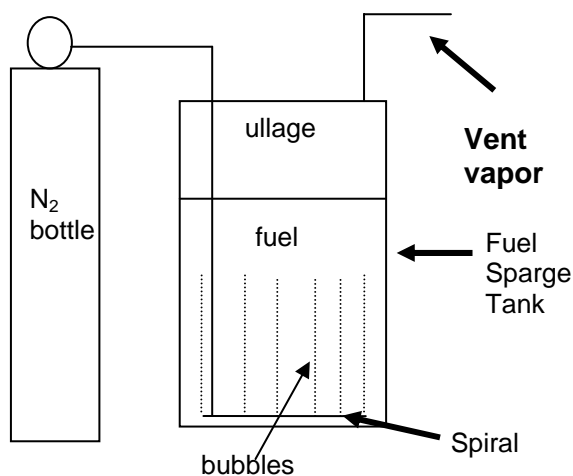
Figure 3.19 Fuel sparging setup.

The nitrogen and oxygen gases exit the fuel tank through a vent. The displaced oxygen rises to the ullage region of the tank and is eventually leaned out and replaced by the nitrogen. It was impractical to test every batch of fuel for oxygen contamination during testing; therefore, a procedure for fuel preparation was developed and validated. Tests were performed with a gas chromatograph (GC) to determine the volume of nitrogen required to fully deoxygenate the fuel. The test began with 100% air saturated fuel with a 42% ullage region. The fuel was saturated with air at 4.1 bar bubbled up from the coil (Fig. 3.17) for 5 minutes. Three baseline saturation readings were taken at the saturation condition and are presented in Table 3.4.

Table 3.4 Gas chromatograph oxygen saturation readings (average of three).

fuel	abundance
n-C_6H_{14}	3,341,314.67
i-C_8H_{18}	3,416,230.33
JP-8	2,235,593.00

The literature[68] states the baseline oxygen saturation reading corresponds to 65 to 80 ppm of oxygen by weight. Nitrogen was then bubbled through the fuel at a rate of 142 liters/hour and GC readings were taken until the oxygen level fell below 1.3% of the saturation reading.[69] The results of the sparge calibration tests are presented in Fig. 3.20.
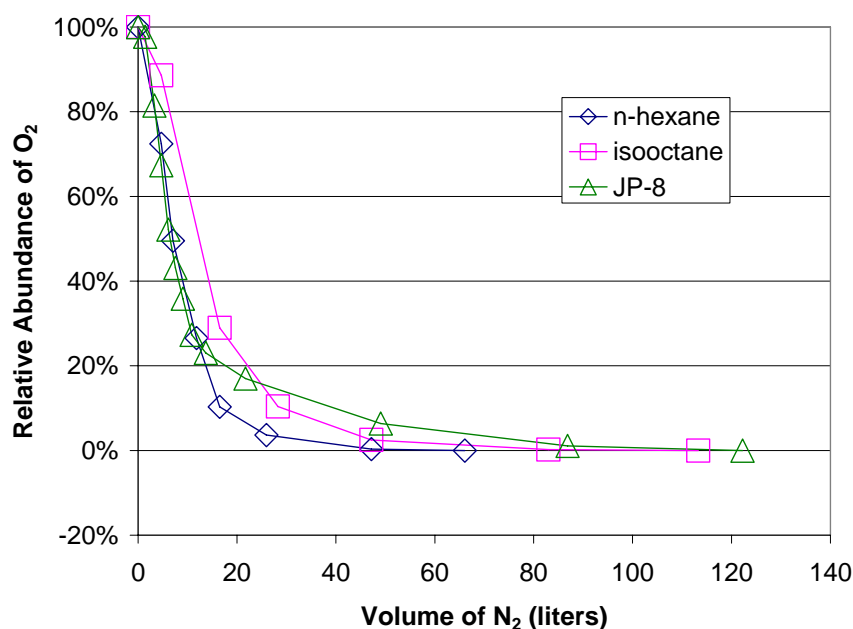
Figure 3.20 Fuel dissolved oxygen relative abundance after sparging with N_2. Data from Ref. 69.

Interestingly, when the values of relative abundance in Fig. 3.20 are plotted on a log scale (Fig. 3.21) the single component fuels, (n-C_6H_{14} and i-C_8H_{18}) both had nearly exponential behavior. The multi-component JP-8, however, had two slopes with the change occurring after 14 liters and enclosed by the circle. The change in slope likely

represents the difficulty removing the dissolved O_2 from the different constituents within the fuel.
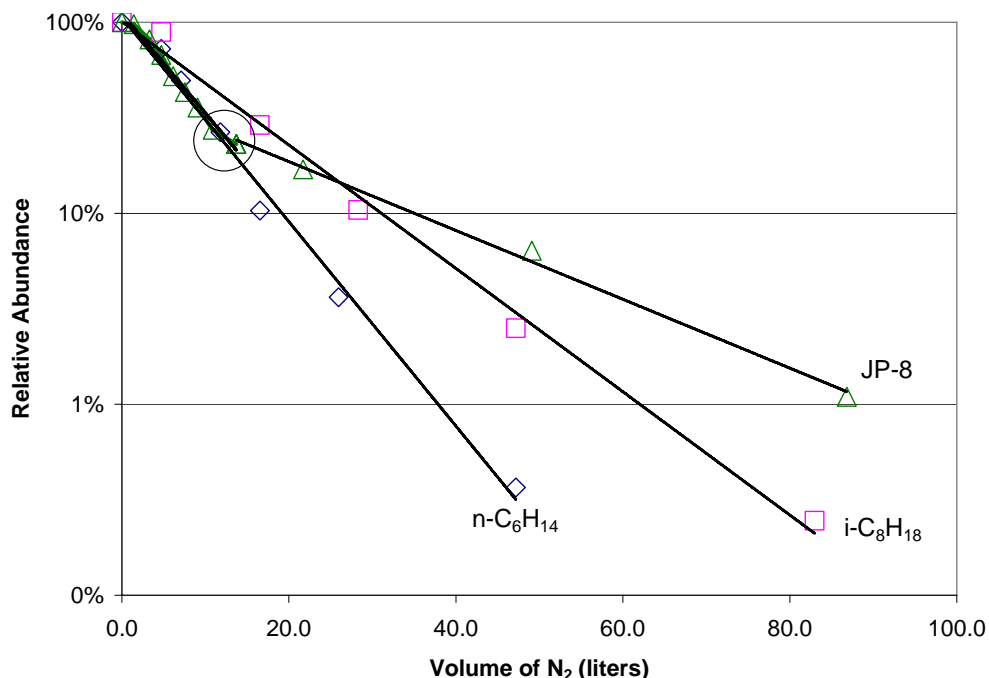
Figure 3.21 Fuel dissolved oxygen relative abundance for single and multi-component fuels with best fit lines after sparging with N_2. Circle marks the slope change for the JP-8 data.

Two of the fuels used in this work, n-heptane and aviation gasoline, were not calibrated using the GC. The Ostwald coefficient for those two fuels is similar (within 5%) to the other hydrocarbon fuels (Table 3.5), and the deoxygenation performance was expected to fall within the sparging results of the other fuels. A factor of safety of two was added to the actual volume of nitrogen sparged through the fuel to preclude any air contamination. Two different cuts of gasoline were available in the literature and are presented for comparison. Kerosene is the primary component in jet fuels, and the Ostwald coefficients values agree well between Table 3.5 (0.146) and the JP-8 (0.15) values plotted in Fig. 3.17.

Table 3.5 Ostwald coefficient for dissolved air as a function of temperature for four fuels. Data from Ref. 70.

Fuel	Temperature (K)	Pressure (kPa)	Ostwald Coefficient
n-heptane	298.15	101.325	0.245
isooctane	293.15	101.325	0.258
kerosene	273.15	101.325	0.139
kerosene	293.15	101.325	0.146
gasoline C (100 Octane)	293.15	101.325	0.261
gasoline D (100 Octane)	293.15	101.325	0.252

The first iteration of the high pressure fuel system used in this work did not use hydraulic accumulators, and instead used high pressure nitrogen acting directly on the fuel. The nitrogen pushed the fuel through the fuel nozzles and kept the fuel from changing phase while heated in the furnace. Since the pressure placed on the fuel changed during the tests (27 to 69 bar), different levels of nitrogen saturation in the fuel occurred along the fuel system lines. The nitrogen saturation variation caused large differences (~25%) between the nozzle calculated fuel flow rate and the turbine flow meter output. Some fuel systems[71] use dissolved gases to increase the atomization performance of liquid fuels. The gases are introduced into the fuel near the injection point and the result is an effervescent or barbotaged injection system. When the pressure drops through the fuel injector, the dissolved gases in the liquid fuel come out of solution and help break up the droplets. To prevent these effects, the fuel was separated from the high pressure nitrogen through the use of a bladder within a fuel accumulator described in Chapter II.

Test Procedure

Tests were performed by statically heating the fuel to the desired fuel temperature using the furnace at a power level between 15% and 20%. The low power level limited the controller set point overshoot as well as limited the maximum metal temperature within the furnace. The desired end fuel temperature was not exceeded by more than 40 °C. The mass of fuel stored within the furnace varied depending on the fuel temperature and density. At temperatures below or near supercritical, there was sufficient mass stored in the furnace for runs up to two minutes; however, at temperatures above supercritical temperature, the significant drop in fuel density provided much shorter run times. The fuel injection pressures were varied from 27 bar to 69 bar to change the fuel flow rate through the fixed area nozzles (Eqn. 3.9). The desired range of mass flow rates was set by the combined nozzle flow number of the fuel nozzles placed in the injector bank and the pressure acting on the hydraulic accumulator. Adjusting the pressure resulted in a range of equivalence ratios between 0.8 and 1.4. The airflow rate was set constant to the value required to completely fill the thrust tube at atmospheric pressure at the given manifold (premixed) temperature and was not changed with equivalence ratio during the runs.

When the fuel temperature neared the desired test point, the PDE fill and purge valves were taken to the desired test frequency. The air was then turned on and heated to the desired air entrance temperature at the intake manifold. After thermal equilibrium was achieved within the air intake system, the test could begin. Two computers were used simultaneously to take data. The computer controlling the PDE operation recorded the mechanical operation of the PDE including temperatures and pressures throughout the air

and fuel system and was recorded at 1 Hz. The test began when the spark ignition system was energized, and the high temperature ball valve (Fig. 3.10) was opened to allow fuel to flow to the fuel nozzles and mix with the air. Combustion would begin within the PDE thrust tubes, and after the fuel flow rate settled out, the engine would operate normally. High-speed combustion data was taken at two different spark delays. The high-speed data sets were taken on a separate computer at specific times annotated on the control computer to match the data with the proper test conditions and operating equivalence ratio. With the significant number of data points recorded at each spark delay, time to capture and store the data took roughly 30 seconds. After the acquisition of the second data set at a different spark delay, the high temperature ball valve was closed and the test was terminated. The pressure exerted on the fuel was then raised by 3.3 bar to increase the fuel flow rate, and the next test was started after the fuel again reached the desired temperature test point.

IV. Data Reduction and Error Analysis

Combustion Data

The data taken during this research was nominally 10 data channels at 1MHz per channel for 0.8 sec. The raw file contains roughly 8 million data points saved in binary format to a size of 13.8 Megabits. The raw *LabVIEW* data is encoded directly from the analog to digital converter as 2 byte integers. The data reduction software begins by converting the integer values back to floating point using a curve saved with the data. Next, the spark plug signal (square wave) is used to separate each PDE cycle into a separate binary data file for ease of processing. Each cycle is processed to determine ignition and DDT times, as well as combustion wave speeds.

In Fig. 4.1, the square wave represents the signal sent from the control computer to the spark ignition system to deposit the spark in the head (closed end) of the PDE thrust tube to begin the combustion process. The second trace is the dynamic pressure transducer located in the head (Fig. 3.14). The data presented below has not been filtered and represents the relative magnitudes of the sensors involved. The data rate allowed the collection of 10 to 12 usable combustion cycles per tube. These cycles were run through the data reduction software to determine the ignition times, DDT times, and the combustion wave speeds. The averages for each data set for each tube and the standard deviations between the individual cycles captured during the runs are given in the results chapter.
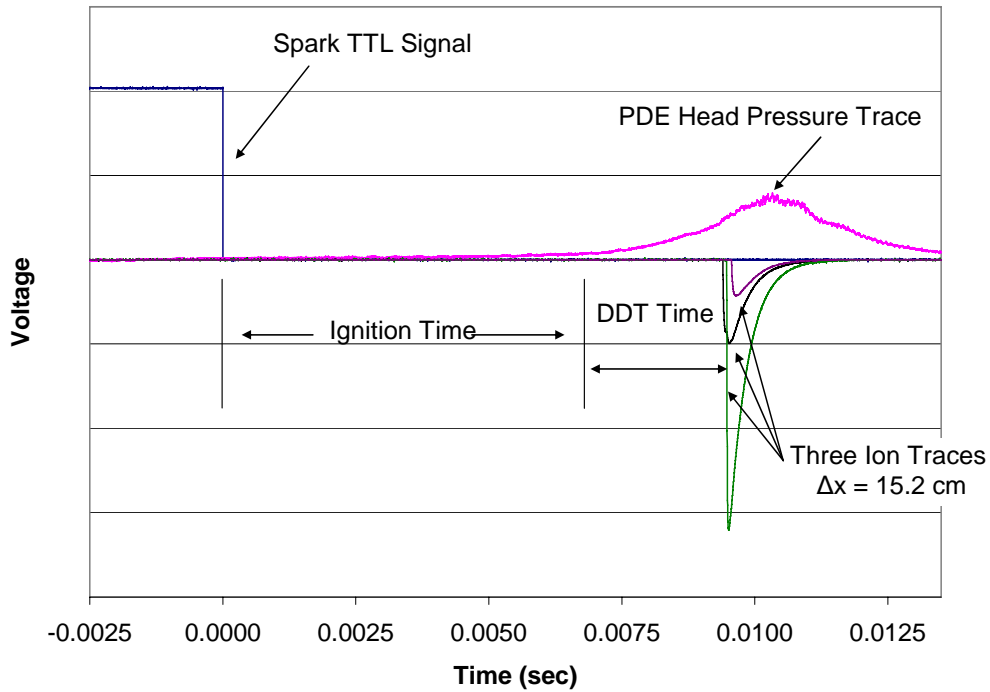
Figure 4.1 JP-8 and air pressure and ion sensor traces for one tube.

Ignition Time

Ignition time is determined from the initial pressure rise in the closed end of the head of a PDE thrust tube after the spark has been deposited in the mixture. The pressure rise is measured by a PCB dynamic pressure transducer. The data reduction process begins by filtering the pressure transducer data using a fourth-order, 401 point Savitzky-Golay digital finite-impulse response filter.[72] The filter removes high-frequency noise and suppresses the jitter in the slope calculations. The downward (right hand) side of the square wave (TTL) denotes the time the computer sent the spark command to the ignition system on the PDE. The ignition time was determined by performing a linear regression through a group of 600 points. With the data taken at 1 MHz sample rate, the 600 points relates to a 600 microsecond segment of data. During the data reduction, the code steps forward one point at a time and recalculates the slope until the desired threshold is met.

The threshold for ignition was arbitrarily set at a voltage rise rate (5 volts/sec), not a voltage value. With the 15 Hz firing frequency and without combustion occurring, the pressure waves in the closed end of the PDE thrust tube during the fire cycle fluctuated 0.2 bar due to the expansion and compression waves experienced from the dynamic filling process. These small pressure fluctuations did not cause sufficiently fast pressure rises that could be interpreted as an ignition event. As seen in Fig. 4.2, the 345 bar dynamic pressure transducer measures the pressure waves without combustion and returns a pressure rise rate (slope) that stays at or below a value of 1.5 volt/sec. At higher detonation firing frequencies, the pressure waves within the tube are stronger (Fig. A.3) and would exhibit larger slopes.
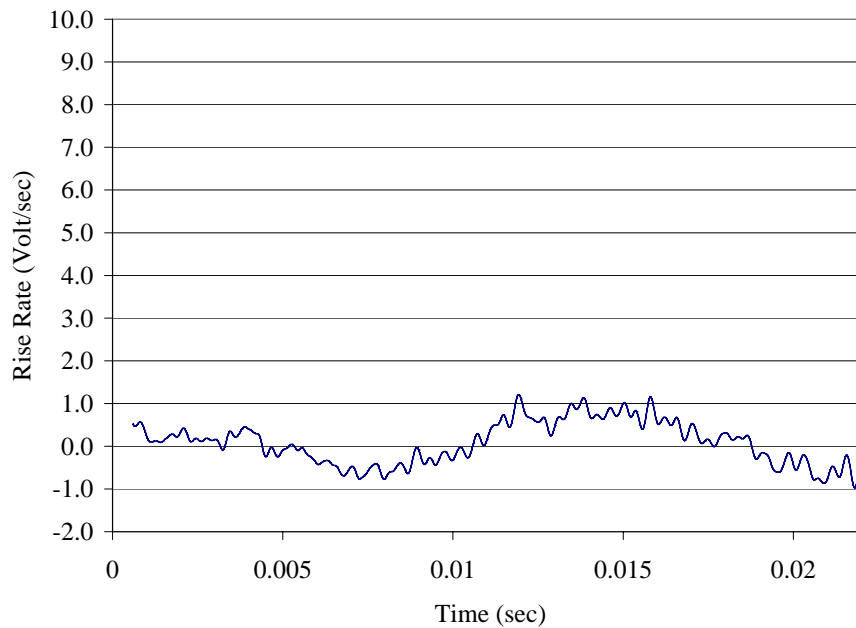
Figure 4.2 Calculated pressure rise rate without combustion.

When combustion occurs, the pressure rise rate (slope) begins increasing rapidly. The slope output for 10 pressure traces for a single tube is shown in Fig. 4.3. The data has a slope threshold of five volts/sec or roughly four times the maximum value without

combustion (Fig. 4.2). The rate change is readily apparent, and the use of this method desensitizes the data reduction to any temperature shift in the pressure transducer or variation from sensor to sensor.
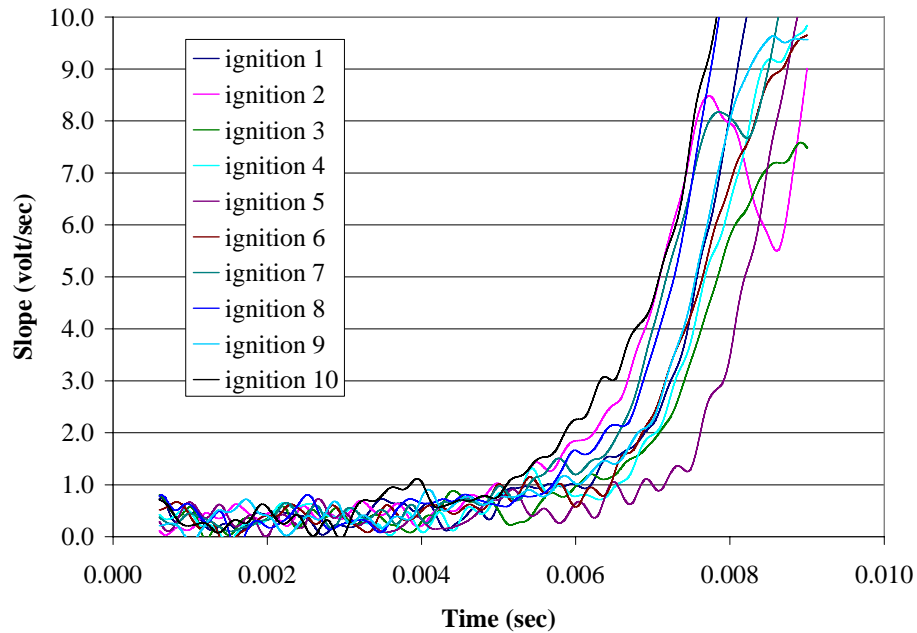
Figure 4.3 Calculated pressure rise rate with combustion to determine ignition time.

To validate the performance of the dynamic pressure transducer to measure ignition times, testing was performed with both a pressure transducer and an OH filtered photo multiplier tube (PMT). The results from the two methods are shown in Fig. 4.4. The ignition time trends between the two sensors are very similar. The pressure transducer ignition times were on the order of 10 to 15% faster than the OH sensor using the regression method described previously. The OH sensor had a reduced field of view and focused on a point slightly off from the spark plug within the head of the PDE. Soot formation on the fiber optic cable also degraded the OH sensor performance after several runs. Due to the favorable durability and response times of the pressure transducer, it was chosen as the primary sensor for ignition time determination.
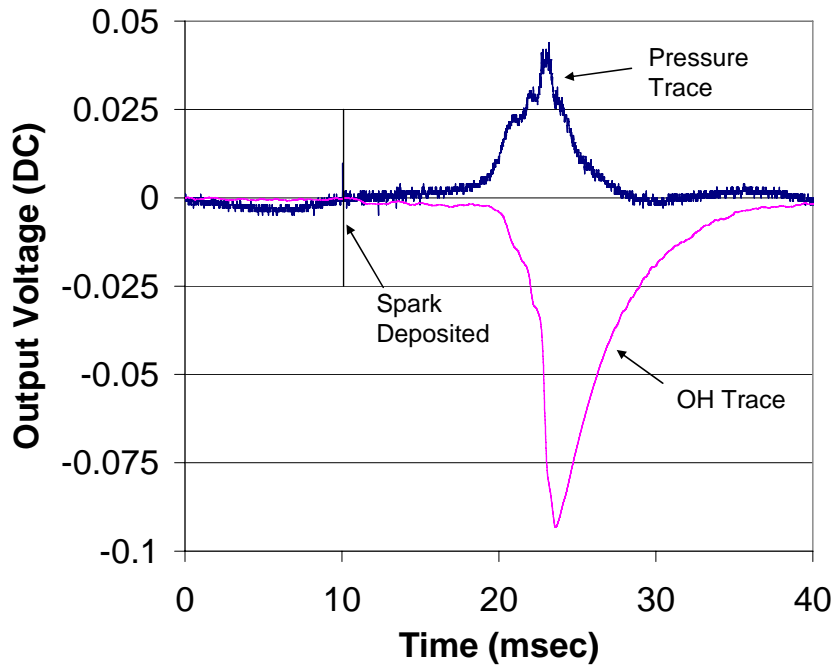
Figure 4.4 Comparison of a pressure sensor and OH sensor for an n-C_7H_{16} and air mixture at 15 Hz.[49]

Wave Speed

The combustion wave speeds are calculated by using an ion probe voltage threshold process. A drop in voltage at the ion sensor marks the time the conductive portion of the detonation wave arrived at the location in the PDE thrust tube. The algorithm finds the corner when the sensor first captures that event. The measured time is then used with the distance between the sensors to calculate an average wave speed. For each channel identified as an ion sensor, the point of measurement for the wave speed is selected using the following algorithm. First, the initial 1,000 points (1 ms) in the engine cycle are averaged for each ion probe channel to provide a baseline zero for that channel. The wave speed is then measured from the first point in the first group of at least 500 points that falls below the baseline value by the threshold amount (1.0 %) specified by the user. This effectively captures the corners of the ion signals in Fig. 4.5. The times are

73

then used with the location of the sensors to determine the average speed of the combustion wave from sensor to sensor.
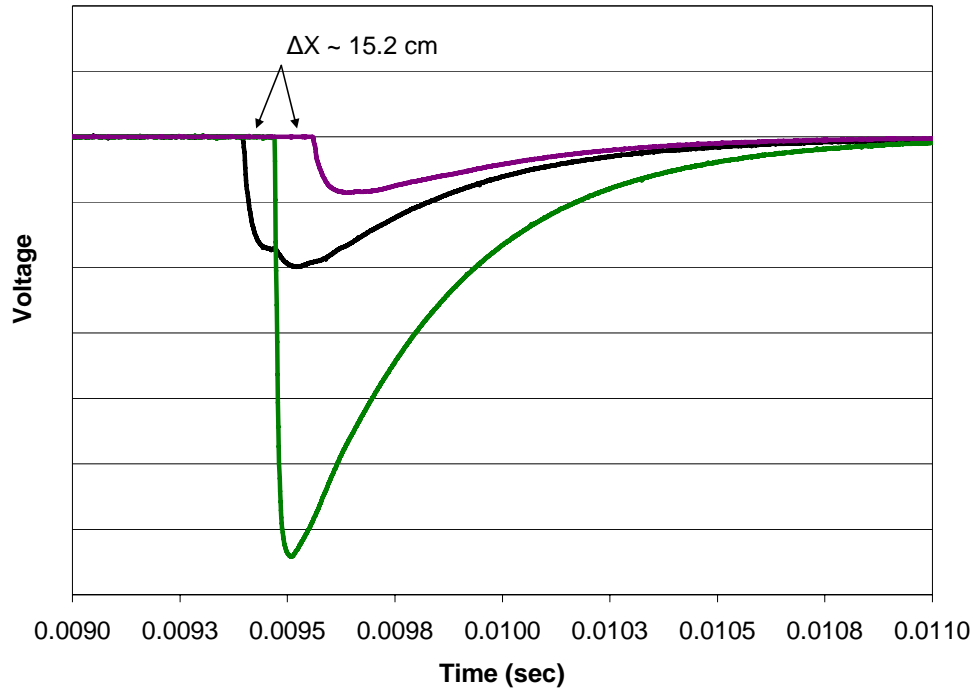
Figure 4.5 Example of three ion traces used to determine wave speeds. Corners denote wave arrival at sensor. JP-8 and air at 15 Hz.

Air System Pressure Traces

The static pressures near the injector, manifold, and PDE head were collected at 100 kHz for one second collecting 15 complete firing cycles. The pressure cycles were then averaged to determine the pressure at each location. The first and last cycles were not completely captured so only 13 cycles were used. This data was used to determine the pressures in the manifold near the valves and at the fuel injectors as well as in the PDE thrust tube without combustion and are shown in Appendix B.
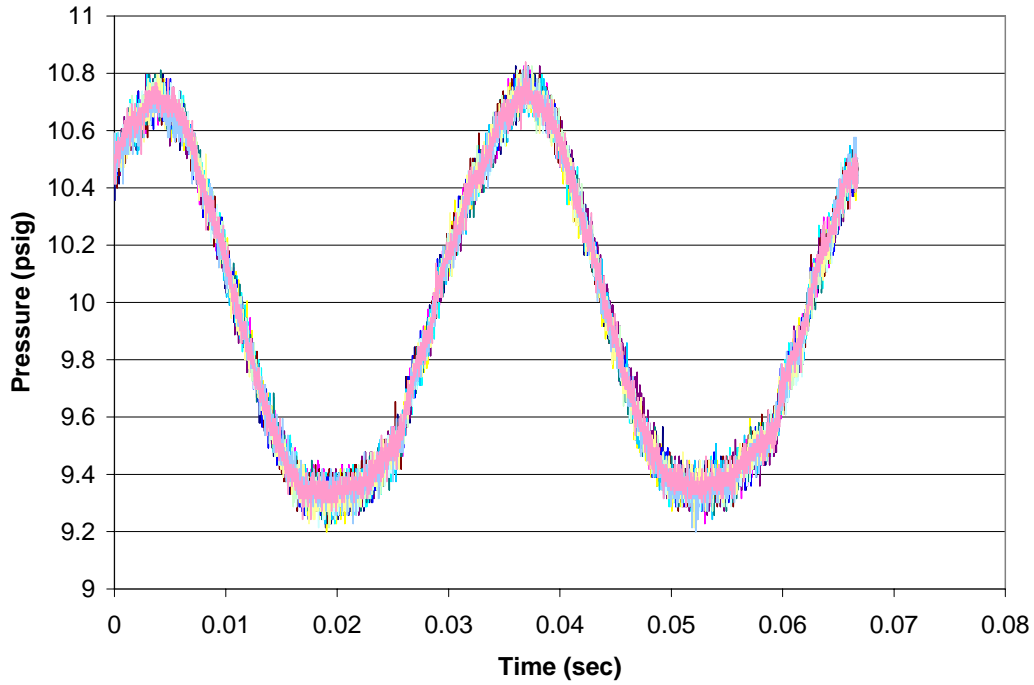
Figure 4.6 Thirteen manifold pressure traces in one data set. ($\sigma_{max} < 0.5\%$)

Standard Deviations

Since each data set is a combination of several combustion events, the standard deviation of the data set gives a quantifiable measure of how closely the values agreed from one cycle to another within the data set. The standard deviation[73] for this work was defined as

$$\sigma = \sqrt{\frac{\sum_{i=1}^{n}(x_i - \bar{x}_i)^2}{n-1}} \tag{4.1}$$

where n is the number of samples and $\bar{x}$ is the average of the sample. For all of the combustion data, the standard deviation of the average data points given for each tube are plotted.

75

Error Analysis

Regardless of the effort to insure the accuracy of any experimental measurement, inherent scatter or error will occur. The purpose of this uncertainty analysis is to accurately account for all potential errors within the experimental process performed in this work.

Time

The data acquisition recorded voltages at 1,000,000 data points per second, meaning one data point was taken every 1 μs, resulting in ± 0.5 μs of error.[62] The cumulative error for time measurements due to data acquisition limitations is ± 0.5 μs. The ion sensor response time[74] is on the order of 100 ns and is less than the data acquisition time of 1.0 μs.

Location

The sensor locations were measured to within 1.6 mm or ± 0.8 mm. The time between sensors was nominally 83 μs, therefore the location error for the ion sensors resulted in a ± 9.5 m/s in wave speed error.

Digitization

The data acquisition board allows the user to select a range of voltages to sample each channel with a resolution of 12 bits.[62] Selecting a narrow range of voltages specific to the output of the specific type of sensor results in a higher resolution to the data sampled. The voltage range for the PCB pressure transducer was ± 1 volt DC and had a

measured resolution within a 0.5 mV step. The ion sensor and TTL pulse for ignition

times were measured with a 0 to 5 volt DC window and resulted in a resolution within a

larger 2.4 mV step. The specific values of the ion sensor output and TTL pulses were not

used, but instead the changes in the output voltages were used to determine event times

(corners) in the data reduction software and thus time accuracies were more important.

Pressure

The combustion head pressure values, measured by the PCB pressure transducers,

were used only for ignition time determination. The magnitude of the values was not

specific to this work and therefore, was not presented. Since the pressure rise rate was

used to determine ignition, the responsiveness or rise time was important. The PCB

pressure transducers have a published rise time of less than 1 μs.[75] No degradation in rise

time due to the RTV coating on the transducer was measured.[63] The PDE head pressures

values without combustion were taken with the Endevco pressure transducers. The

calibration for that pressure was accurate to 0.1% and the repeatability was shown in

Fig. 4.6 with a maximum standard deviation of 0.5%.

V. Fuel Flash Vaporization System

As stated previously in Chapters I and II, the combustion performance of a liquid hydrocarbon fueled pulse detonation engine is hindered by the presence of fuel droplets and long ignition times.[48] Long ignition times limit the maximum operating frequency and the thrust achievable by a PDE thrust tube. The ignition times can be reduced by increasing the amount of fuel vapor present in the mixture. A high pressure fuel flash vaporization system was built to eliminate the evaporation time for liquid hydrocarbon fuels of varying vapor pressure. The fuels are n-heptane, isooctane, aviation gasoline, and JP-8. The following discussion describes the droplet evaporation rate for unheated fuel and the methodology of the fuel flash vaporization system.

Fuel Evaporation

Previous researchers[11, 76] have relied on heated air with unheated fuel to reach the desired state of small droplets or fully vaporized mixtures. The speed at which these mixtures reach equilibrium is driven by the heat transfer rate between the air and the droplet as well as the vapor pressure of the fuel. The ignition time is determined by evaporation rate and chemical (or induction) times, whereas evaporation is the longer of the two times for hydrocarbon fuels.[16] The evaporation time of a droplet[23] (t_e) is given by

$$t_e = \frac{\rho_{liquid} d_0^2}{8D\rho_{gas} \ln(1+B)} \tag{5.1}$$

where d_0 is the initial droplet diameter, D is diffusivity, ρ_{liquid} is the density of the liquid at the droplet temperature, ρ_{gas} is the density of the vapor at the surface, and B is the Spaulding transfer number (Table 5.1).

Table 5.1 Fuel liquid density and molecular weight. Data from Refs.16, 40, 70, 77.

Fuel	Liquid density (kg/m^3) @ T= 25 °C	Fuel molecular weight (gm/mol)
n-heptane	679	100
isooctane	690	114
Aviation Gasoline	724	108
Kerosene / Jet A	805	160 (est)

For the four fuels used in this work, fuel densities are similar in magnitude but the vapor pressures are significantly different (Table 5.2). The true vapor pressure is defined as the pressure exerted by its vapors at a specific temperature in the absence of air. The vapor pressure rises with temperature and facilitates the increased rate of evaporation of the droplets.

Table 5.2 Vapor pressures at various temperatures. Data from Refs. 40 and 79.

Temperature (°C)	Vapor Pressure (kPa)			
	isooctane	n-heptane	aviation gasoline	JP-8
20	5.2	4.7	23	0.05
50	19.6	18.9	70	1.3
60	28.6	28.0	94	2.0
80	56.9	56.9	190	4.4
100	103.6	105.6	250 (est)	8.4

Using the following method,[16] the Spaulding transfer number B_M can be calculated by

$$B_M = \frac{Y_F}{1 - Y_F} \tag{5.2}$$

and Y_F is the mass fraction of fuel at the surface which can be determined using

$$Y_F = \left[1 + (\frac{P}{P_F} - 1) \frac{M_A}{M_F} \right]^{-1} \tag{5.3}$$

where P is the ambient pressure (combined fuel vapor pressure and air partial pressure) and P_F is the fuel vapor pressure at the surface of the droplet, and M_F and M_A are the molecular weights of fuel and air, respectively.

The vapor pressure can be determined based on the temperature at the surface of the droplet (T_S) using the data in Table 5.2 or by using a modified version of the Clausius-Clapeyron equation given as

$$P_F = \exp \left[a - \frac{b}{T_S - 43} \right] \tag{5.4}$$

where a and b are constants found in Table 5.3. Since JP-8 is a combination of several hydrocarbons, the data in Table 5.2 was curve fit and valid up to 410 K.

Table 5.3 Clausius-Clapeyron equation constants for two fuels. T_{bn} is the normal boiling point of the fuel. Data from Ref 16.

Fuel	n-heptane	aviation gasoline
T_{bn} (K)	371.4	333.0
a for $T > T_{bn}$	14.2146	14.1964
a for $T < T_{bn}$	14.3896	13.7600
b for $T > T_{bn}$	3151.68 K	2777.65 K
b for $T < T_{bn}$	3209.45 K	2651.13 K

The droplet lifetimes (Table 5.4) for high vapor pressure n-heptane and low vapor pressure JP-8 give the longest droplet lifetimes for the vapor pressure class. Both the droplet and air temperatures are important to determine what the droplet surface temperature is during evaporation. If the droplet lifetime is much shorter (i.e. 10 times) than the heat transfer time, then the fuel temperature is used, but if the droplet lifetime is much longer than the heat transfer time then the air temperature should be used. As will be discussed in the results section, the manifold temperature remained roughly constant despite the enthalpy of vaporization due to the thermal mass and heat transfer from the intake manifold to the mixture after fuel injection.

The heat transfer calculations in Table 5.4 were measured for a sphere with free convection and a Nusselt number of 2.0.[38] Forced convection was ignored since the drag coefficient on a sphere becomes large (10) as the droplet Reynolds number becomes small (50) and will attain the flow velocity quickly.

Table 5.4 Evaporation lifetime for a 70 μm droplet. Highlight denotes selected time to calculate the percentage of liquid mass remaining.

Fuel	total mass flow (kg/sec)	T_{Air} (K)	T_{Fuel} (K)	manifold residence time (sec)	heat transfer time (sec)	droplet lifetime at T_{Air} (sec)	droplet lifetime at T_{Fuel} (sec)	liquid mass remaining (%)
n-C_7H_{16}	0.121	310	310	0.237	0	0.233	0.233	00.0
n-C_7H_{16}	0.121	310	390	0.237	0.031	0.233	0.027	00.0
JP-8	0.106	366	366	0.046	0	0.256	0.256	74.3
JP-8	0.098	394	300	0.046	0.026	0.114	6.036	46.1
JP-8	0.098	394	394	0.046	0	0.114	0.114	46.1
JP-8	0.090	422	410	0.047	0.009	0.067	0.081	16.5
JP-8	0.090	422	446	0.047	0.005	0.067	0.047	0.00

The manifold residence time (Table 5.4) is the time the droplet has from injection into the manifold until combustion. If the droplet lifetime is shorter than the residence time, then sufficient time has passed and the droplet can be said to have completely evaporated. If the droplet lifetime is longer than the residence time then some of the fuel mass will still be liquid and unusable for the combustion time (~15 ms) required of the PDE. The 70 μm droplet predicted lifetime data presented in Table 5.4 was chosen because it was the largest SMD measured by the manufacturer (next section). No attempt was made to determine the spray droplet sizes for the fuel injector described previously in Chapter III. The droplet lifetime prediction is presented to support the hypothesis that some liquid will remain unusable for combustion. The droplet evaporation time gives an estimation of the evaporation characteristics and takes into account the physics of the process. The percentage of liquid fuel remaining is presented in Table 5.4 and shows that for room temperature n-heptane, there is sufficient time for the fuel to completely evaporate. For room temperature JP-8 into 394 K air, over 46 percent of the fuel is still liquid, and as will be shown later in this chapter, will never reach a fully vaporized equilibrium in an adiabatic system. The goal of this research is to inject the fuel at a sufficiently high temperature using the flash vaporization system to eliminate the time required for any size droplets to evaporate.

Fuel Injection System

Delevan pressure atomizing nozzles are used to generate small droplets during the fuel injection process for both heated and unheated fuel. The combination of small droplets and high temperature fuel provides the fastest vaporization method achievable.

In Fig. 5.1, the Sauter mean diameter (defined previously in Eqn. 2.7) performance for a fuel nozzle with a flow number (FN) equal to 1.1, shows that droplets between 20 and 70 microns are normally generated for unheated liquid fuel with a pressure differential of 6.9 bar.
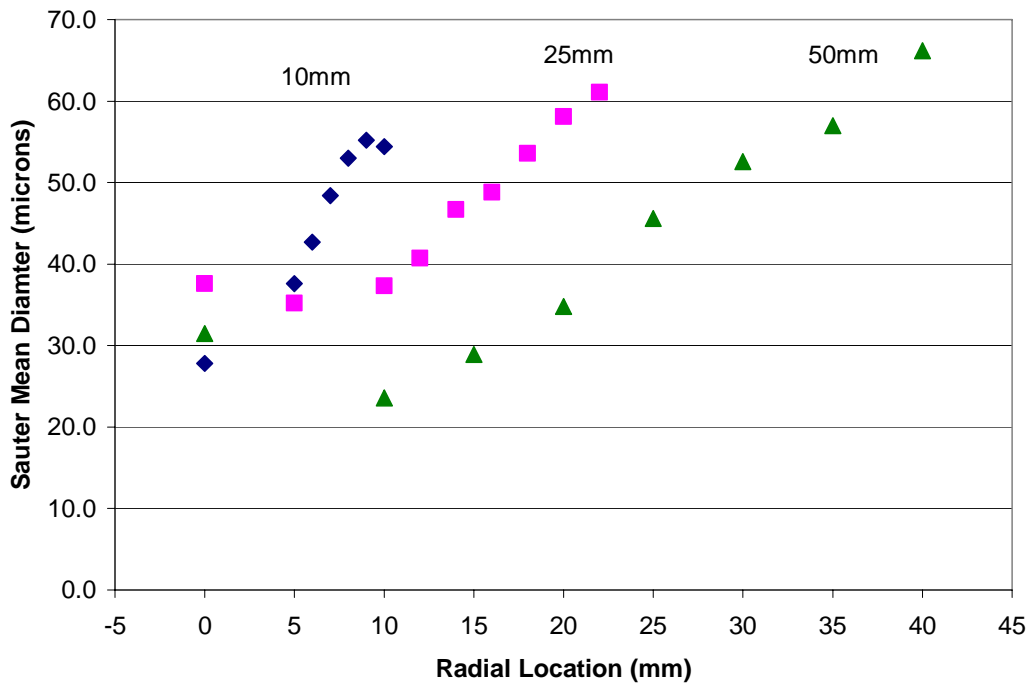
Figure 5.1 Radial Sauter mean diameter droplet size distribution for Delevan pressure atomizing nozzle at three axial locations downstream of the nozzle. Data from Ref. 15.

Tests were performed with water to determine the nozzle flow patterns at liquid injection temperatures at two temperatures into 1 bar of atmospheric pressure. In Fig. 5.2(a), water is injected at 25 °C and the resulting liquid spray is very wide with individual droplets discernible. In Fig. 5.2(b), the water temperature is 200 °C, and the resulting spray is tightly confined and has features consistent with a supersonic jet, and therefore denotes a gaseous injection. The supersonic jet drops the static temperature, however, and causes some of the vapor to condense back into the liquid visible in the photo. An important result of this test is that the water still vaporized well below the

critical temperature. This test did not completely mimic the fuel system injection because the air surrounding the jet was stagnant and did not entrain or mix with a high volume of air. When the flash vaporization system operates at or above the temperature required to ensure vaporization, the resulting mixture should reach equilibrium quickly and the fuel should not condense back into a liquid.
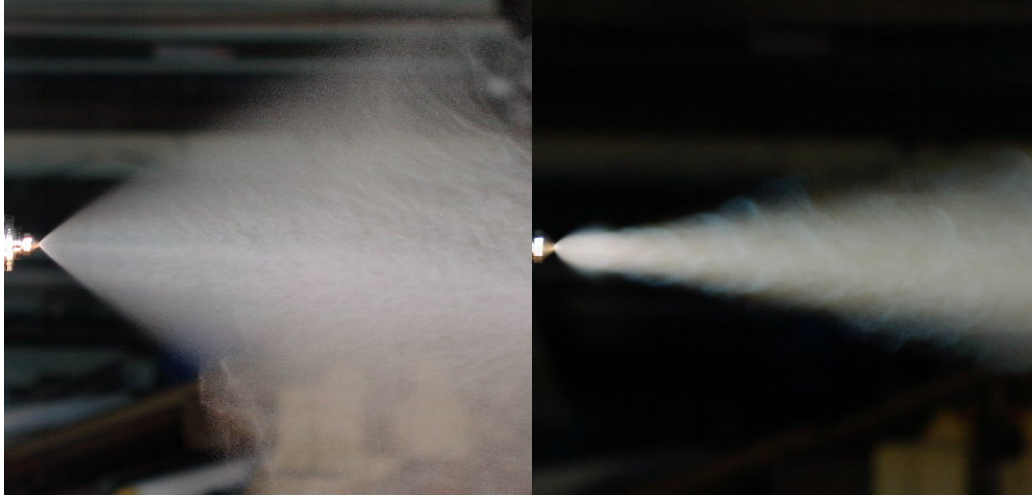
	(a)	(b)
P_{inj}/P_c	0.0045	0.0045
T_{inj}/T_{sat}	0.7860	2.0000
P_{inj}/P_{chm}	41.600	41.600

Figure 5.2 High pressure atomized water (a) and vaporized water (b).[49]

To eliminate the possibility of condensation during the fuel injection process into stagnant air, which is analogous to the water tests performed above but not to the mixing performed in this research, the fuel temperature must exceed the critical temperature. Consider the shadowgraph photos of a supercritical methane and ethylene jet at pressures and temperature above the critical points (Fig. 5.3) into a stagnant chamber filled with N_2. The mixture is 90% ethylene and 10% methane and the throat diameter is 1 mm. The photo on the left has an injection temperature slightly above the critical temperature. The

plume is not translucent, thus the vaporized mixture has condensed back to a liquid due the pressure and temperature drop during the expansion process. The shadowgraph on the right side, however, is sufficiently above the critical temperature (23%) that the vapor does not condense back into a liquid and has transparent gaseous features. A gaseous fuel jet is transparent and will only be visible with a Schlieren or shadowgraph system. The results will show that a fully gaseous jet is not required to adequately achieve flash vaporization so long as the mixing with air occurs quickly.
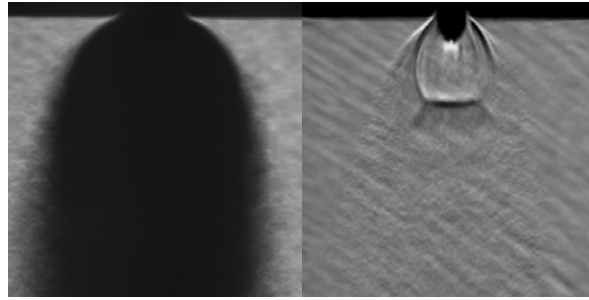
P_{inj}/P_c	1.16	1.15
T_{inj}/T_c	1.03	1.23
P_{inj}/P_{chm}	36.7	35.7

Figure 5.3 Shadowgraph images of supercritical methane/ethylene jets.[80]

During this research, fuels were injected into the air at temperatures above the auto ignition temperatures of the fuel (Table 2.3). Auto ignition was averted because the fuel temperature dropped during the injection expansion in the manifold, and the fuel quickly reached thermal equilibrium with the cooler air before the auto ignition process could occur.

Fuel Phases during Injection

To completely zero the evaporation times, fuel is injected into air at a high enough temperature that no energy from the air is required to achieve a liquid free equilibrium condition of the mixture. This specific fuel temperature is quantified later in the chapter. The fuel is pressurized above the critical pressure so that it can be heated within the furnace to temperatures above the critical temperature (Table 5.5) without entering the saturation region of the vapor dome. The phase change occurs at the fuel nozzles where pressure drops from the furnace pressure (30 bar) to the relatively low (2 bar) manifold pressure.

Table 5.5 Critical properties of relevant fuels.

Fuel	$T_{critical}$ (K / °F)	$P_{critical}$ (atm) / (psia)
Propane[81]	369.9 / 206.1	41.9 / 616.4
n-heptane[81]	540.0 / 512.3	27.0 / 397.4
av gas[16]	548.0 / 526.7	n/a
Isooctane[81]	543.9 / 519.35	25.33 / 372.31
JP-7[82]	669.9 / 746.2	20.8 / 305.76
JP-8 / Jet A[83]	683.0 / 769.7	23.3 / 342.4

The fuel nozzles are treated as adiabatic devices, and thus a constant total or stagnation enthalpy (h_{TOTAL}) injection process will be represented by the vertical line descending from one pressure line to another as shown in Fig. 5.4 at the 520 K data point. The first law of thermodynamics is applied to an adiabatic nozzle in Eqn. 5.5.

$$h_{TOTAL} = (h + ke)_{IN} = (h + ke)_{OUT}$$

(5.5)

The process of injection causes the fuel to attain a very high velocity as the fuel static enthalpy, h, is converted to kinetic energy, ke, with the ensuing temperature and

pressure drop. Since the air has a much lower velocity, the shear forces between the gases will slow the fuel and convert the kinetic energy back into static enthalpy. The resulting rise in static enthalpy for a calorically perfect gas can be related to a corresponding rise in temperature through the following equation.

$$h = C_P \cdot T \tag{5.6}$$

The constant enthalpy injection process is shown in Fig 5.4 and is representative of the water and methane/ethylene jets into stagnant air/N_2 discussed in the previous section. At some intermediate pressure dictated by the area ratio of the nozzle, the fuel will begin to mix with the air. At that location, the n-heptane vapor dome (Fig. 5.4) fails because the enthalpy of the air is not included in determining the phase or the final state properties of the components in the mixture.
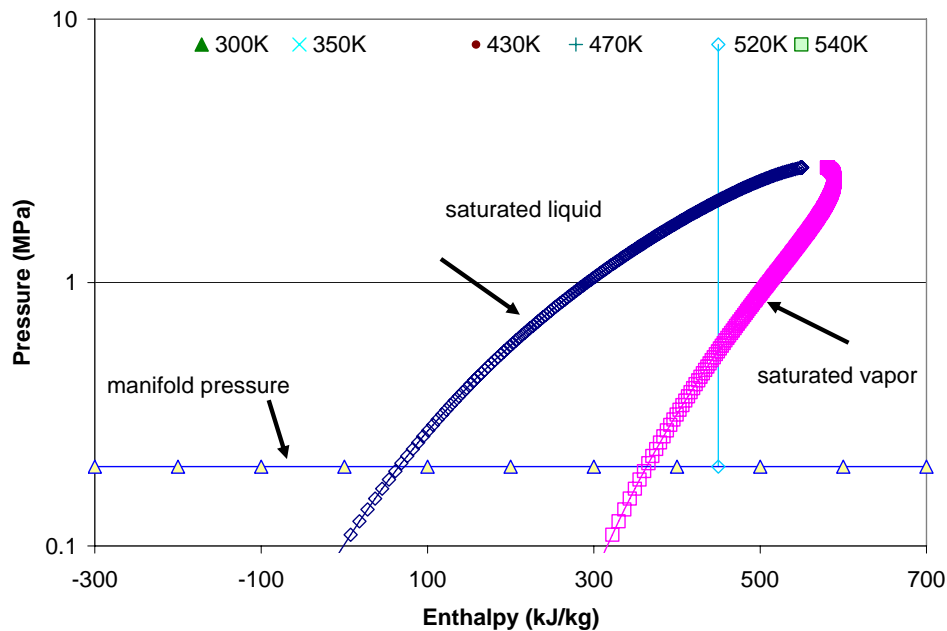
Figure 5.4 N-heptane pressure-enthalpy diagram. The vapor dome is the region between the two saturation lines. Data from Ref. 81.

The 520 K fuel temperature data point in Fig. 5.4 is shown at the nominal injection pressure of the FVS. As the fuel passes through the nozzle driven by the pressure drop across the nozzle, the fuel state properties descend through the vapor dome and finishes to the right of the saturated vapor line as a gas. Since the fuel is mixing with air, the air could be at a low enough temperature (or energy level) to cause the fuel to condense back into a liquid. The combined fuel and air conditions required to achieve a mixture capable of sustaining a gaseous fuel and air mixture are modeled to predict the performance of the FVS and is described in the next section.

Flash Vaporization Fuel and Air Mixture Model

As described in Chapter III, the fuel and air are premixed in the intake manifold prior to being valved into the PDE thrust tubes. The pressure conditions in the intake manifold are an important factor in determining the final required conditions to achieve a fully gaseous mixture prior to combustion.

The National Institutes of Standards and Technology (NIST) program SUPERTRAPP version 3.1 was used to model and predict how much liquid was in the fuel and air mixture in the manifold if left at a specified pressure and temperature until equilibrium was reached. The program uses the thermophysical properties of hydrocarbon mixtures database and computes the vapor-liquid equilibrium using the Peng-Robinson model.[85] The theory and performance of the model is discussed in more detail in Appendix C. A stoichiometric fuel and air mixture was entered into the program at a constant pressure of 2.0 bar. This pressure is slightly above the maximum pressure measured in the manifold during testing. The final mixture temperature in Fig. 5.5 and

Fig. 5.6 was varied to determine the percentage of fuel vapor present at equilibrium. The desired mixture condition was to achieve 100% fuel vapor. JP-8 was modeled using a surrogate mixture described in Appendix C. No attempt was made to model the multi-component aviation gasoline. The 100% vapor mixture temperatures in the manifold for three fuels are summarized in Table 5.6.

Table 5.6 Minimum stoichiometric fuel and air mixture temperatures required to achieve 100% vapor at equilibrium in the intake manifold at 2 bar.

Fuel	Temperature (K)
n-heptane	282
isooctane	287
JP-8	400
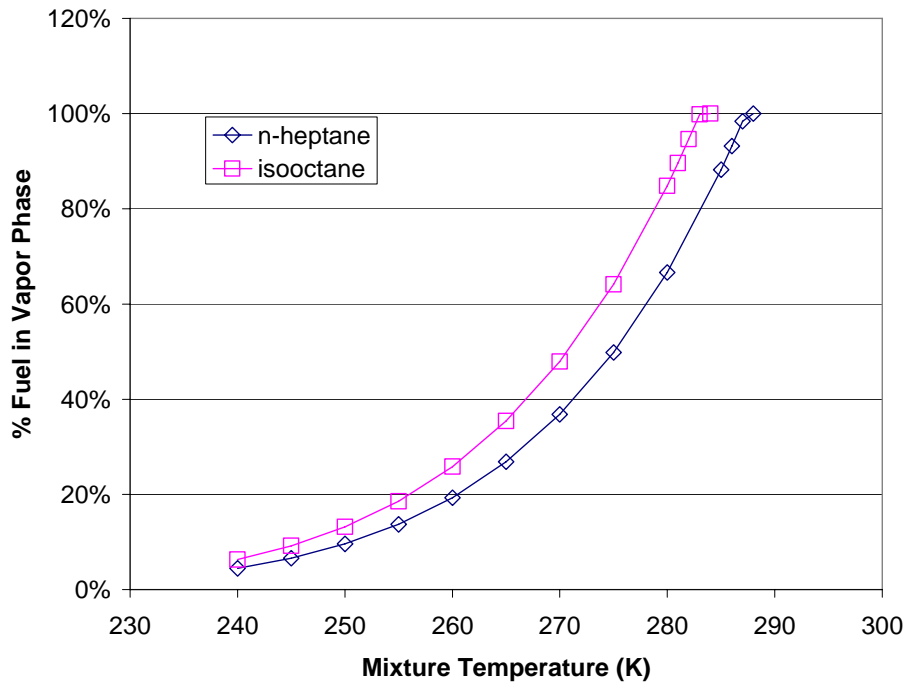
Figure 5.5 Percentage of the fuel in vapor phase for a stoichiometric mixture at 2 bar.[49]

At the mixture temperatures required to achieve 100% vapor with the heptane and isooctane, the JP-8 and air mixture is below 20% vapor. This shows the importance of the FVS to achieve a vaporized mixture of the JP-8 (Fig. 5.6).
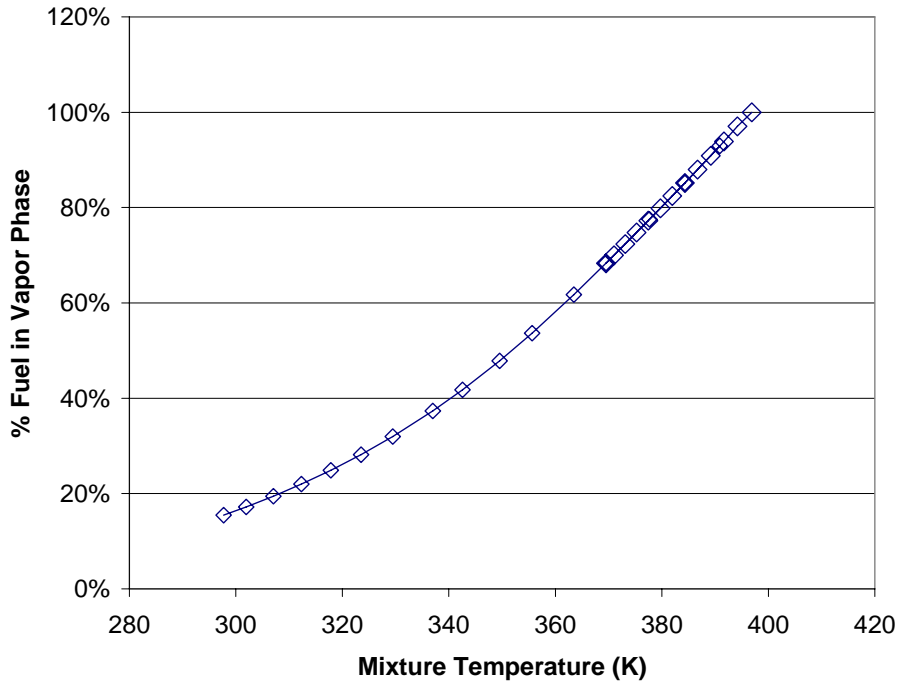
Figure 5.6 Percentage of fuel in vapor phase for a stoichiometric JP-8 surrogate and air mixture at 2 bar.

As long as the resultant mixture temperature did not drop below those shown in Table 5.6, the fuel vapor should not condense back into a liquid. If the manifold pressure was increased, such as for higher frequency operation, the minimum mixture temperature to maintain the fuel in the vapor state would also increase (Fig. 5.7). The increase in manifold pressure from 2 to 3 bar increases the minimum mixture temperature by 8 °C.
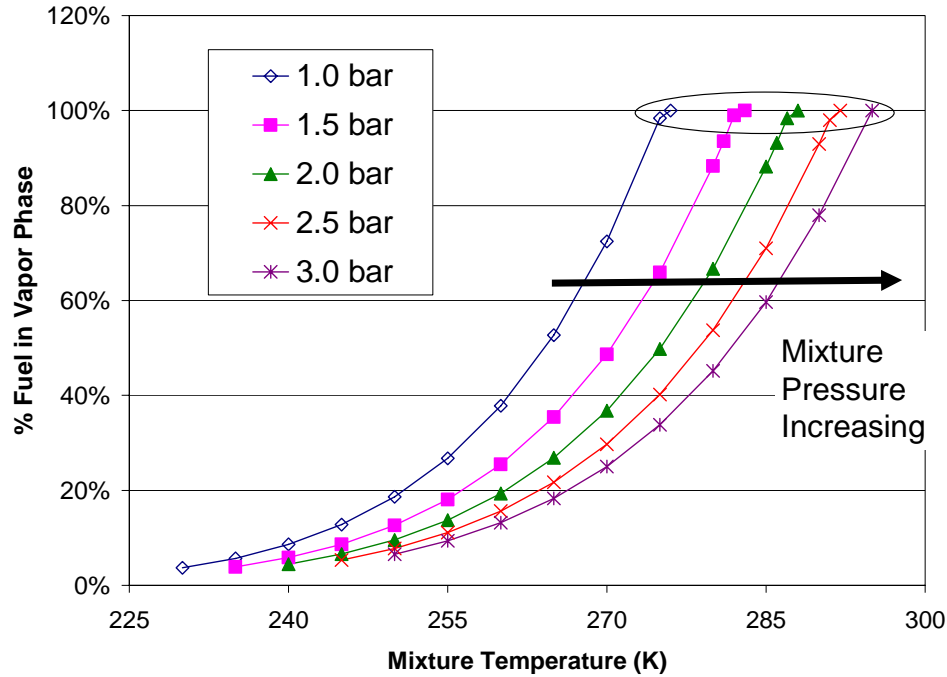
Figure 5.7 Equilibrium liquid vapor state for a stoichiometric n-heptane and air mixture at various manifold pressures.[69] The circle captures the 100% vapor state.

Figures 5.8, 5.9, and 5.10 represent the fuel injection envelopes as determined by the stoichiometric fuel and air model. The model assumes unlimited time to reach equilibrium with adiabatic (constant enthalpy) conditions. The horizontal line below the hatched box denotes liquid vapor equilibrium point of the mixture temperature. The x-axis represents the fuel injection temperature, and the data lines on each plot represent the initial air temperature prior to mixing with the fuel. The y-axis represents the final mixture temperature at equilibrium. Operation within the hatched region ensures flash vaporization and 100% fuel vapor throughout. Operation to the left of the hatch region, but above the liquid vapor equilibrium point, will eventually achieve 100% fuel vapor, but requires heat transfer from the air and droplet evaporation time to do so.
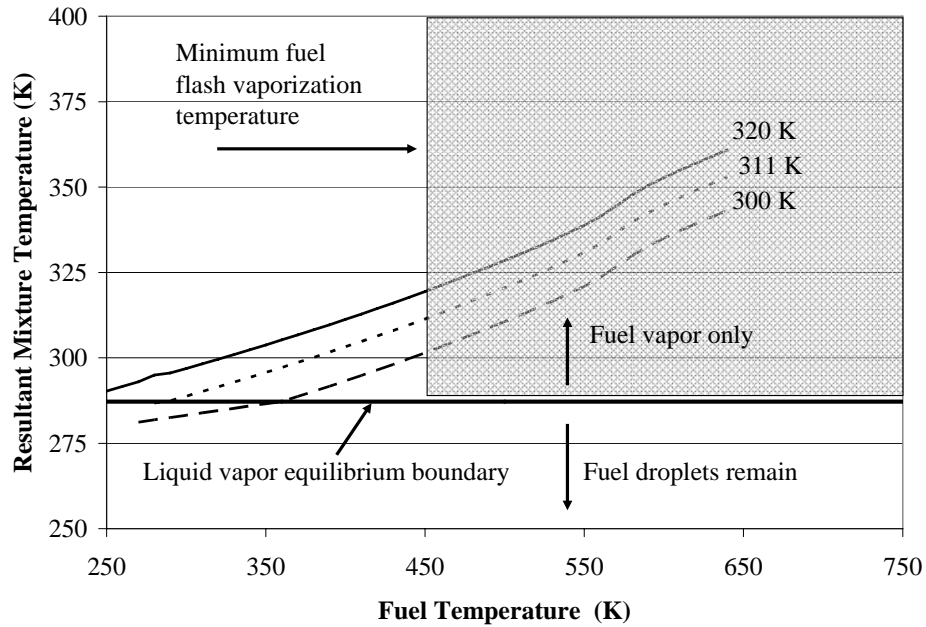
Figure 5.8 Stoichiometric n-heptane air mixture liquid vapor equilibrium in the intake manifold for 3 air temperatures at 2 bar. Flash vaporization occurs within the hatched region.
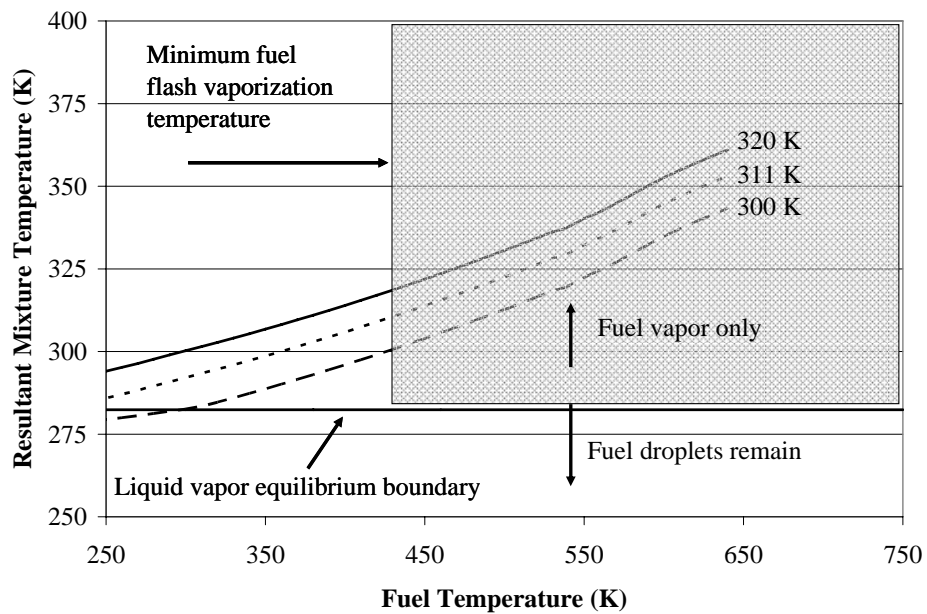
Figure 5.9 Stoichiometric isooctane air mixture liquid vapor equilibrium in the intake manifold for 3 air temperatures at 2 bar. Flash vaporization occurs within the hatched region.
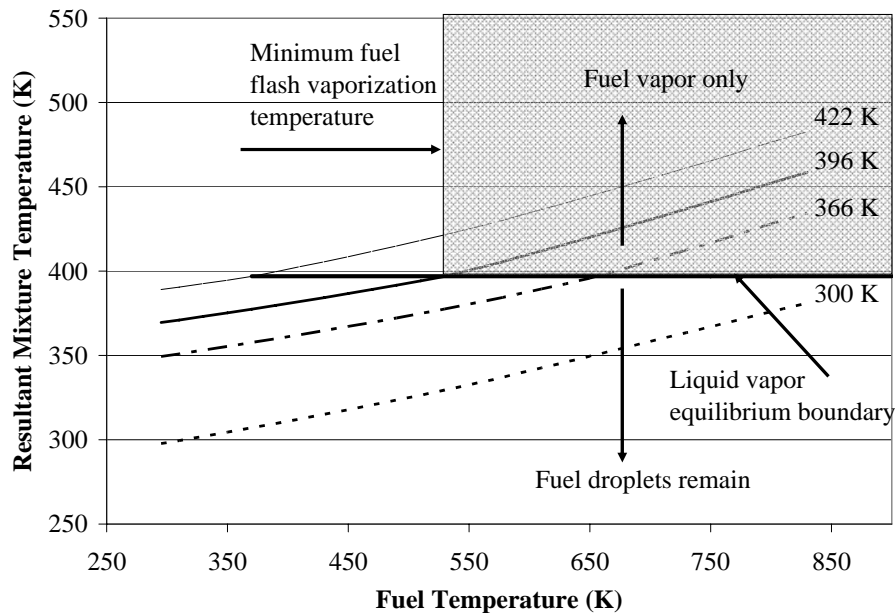
Figure 5.10 Stoichiometric JP-8 surrogate air mixture liquid vapor equilibrium in the intake manifold for 4 air temperatures at 2 bar. Flash vaporization occurs within the hatched region.

The previous three figures are important to understanding the fuel and air conditions necessary to reach a mixture composition capable of sustaining or fully evaporating all of the liquid fuel droplets. The high vapor pressure fuels (Figs. 5.8 and 5.9) show that for most fuel and air temperatures at or above ambient, the mixture could reach an equilibrium condition without any liquid present. The low vapor pressure JP-8 surrogate, however, could never reach a liquid free equilibrium at an air temperature of 300 K without going to fuel temperatures above 800 K. At temperature above 723 K, the model will fail to accurately predict the liquid vapor equilibrium condition due to the expected endothermic reactions and the new species created. The model provides crucial insight into what air temperatures are required to sustain a liquid free mixture. The model also shows the benefits of heating the fuel to higher temperatures and the increased margin over the liquid vapor equilibrium line. The minimum fuel temperature required to

93

fully vaporize is determined by the equilibrium condition where the resultant mixture temperature is the same as the incoming air temperature. This condition is defined as the fuel flash vaporization temperature and implies that no energy was extracted from the air to move the liquid fuel to a fully gaseous mixture. The minimum fuel injection temperatures to flash vaporize the fuels are listed in Table 5.7. The resulting fuel and air mixture temperature must remain above the temperatures listed in Table 5.6 or the fuel will condense and separate from the mixture.

Table 5.7 Flash vaporization fuel temperature into air at 2 bar manifold pressure.

Fuel	Fuel Temperature (K)
n-heptane	450
isooctane	430
JP-8	530

PDE Heat Generation

A goal of this research is to determine what fuel temperatures are required to flash vaporize during mixing. After the fuel temperatures are defined, the amount of energy required to raise the fuel from ambient to the FVS temperature must be available as waste heat on the PDE. This research uses an industrial furnace to raise the fuel temperature statically between tests, but for a flight worthy PDE, the energy must be available onboard. The largest waste heat source available is the exterior of the PDE thrust tubes. Experiments were performed using a water cooled thrust tube to determine the amount of heat available relative to the detonation cycle rate of the PDE thrust tube. A stoichiometric hydrogen and air detonation was used to generate the heat at different firing frequencies. The water cooled tube was a 0.91 m long pipe with a 7.62 cm exterior tube with a 5.72 cm diameter PDE thrust tube within it. The heat transfer measurements

were made by measuring the incoming and outgoing water temperatures for differing flow rates and are shown in Fig. 5.11. The results show that the power extracted from the thrust tube scales roughly linearly with detonation cycle frequency.
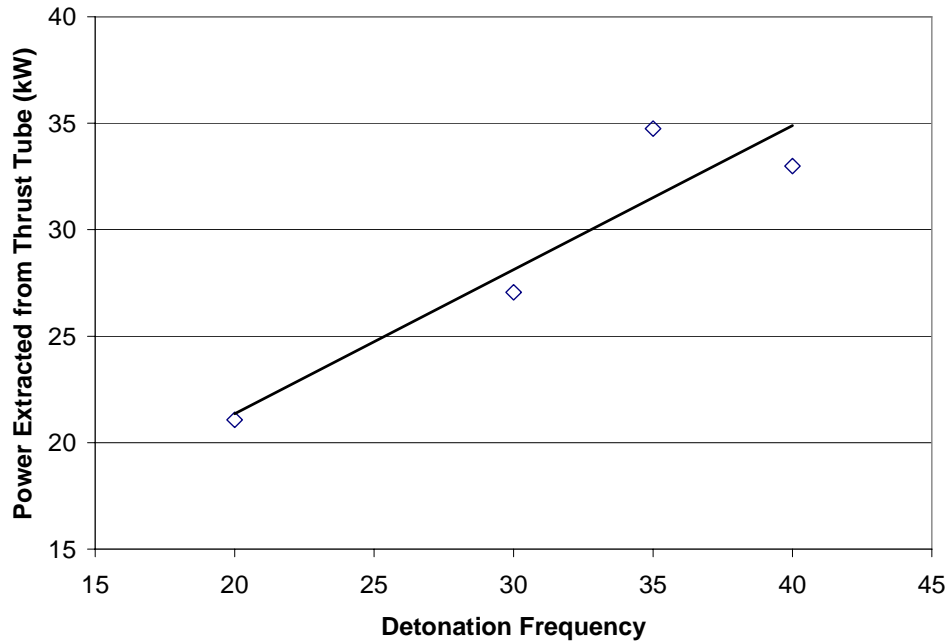
Figure 5.11 Heat transfer from a single water cooled thrust tube for a stoichiometric H_2 and air detonations at several firing frequencies.

The total energy required to raise the temperature of the fuel from ambient to its critical temperature (Table 5.5) is provided in Table 5.8. The table projects the energy requirements for the fuel mass flow rates used in this research. The amount of energy required to heat the JP-8 for two tubes at stoichiometric conditions from ambient to the fuel critical temperature (above the flash vaporization temperature) is roughly half of what is available from the entire length of a single PDE thrust tube. As the firing frequency increases, the power requirement for the fuel will go up, but if the relationship shown in Fig. 5.11 stays constant, then there would be sufficient power available to heat the fuel and thus the system should self sustain. A likely design choice would be to cool

the hottest portion of the thrust tube to extend the life of those components and minimize

the length and weight of the fuel system.

Table 5.8 Power requirements to heat fuel from $T_{ambient}$ to $T_{critical}$ for two 1.22 m long, 5.2 cm diameter circular tubes at 15 Hz.

Fuel	Molecular Weight	Stoichiometric Fuel to Air ratio	PDE Frequency	Fuel Mass Flow Rate (kg/min)	Power to Heat Fuel to $T_{critical}$
Propane	44	0.063800	15 Hz	0.434	1.912 kW
Isooctane	114	0.066067	15 Hz	0.450	5.213 kW
JP-8	160 (equiv)	0.068287	15 Hz	0.465	8.109 kW

VI. Results

The combustion results for aviation gasoline, isooctane, n-heptane, and JP-8 are presented. The results include ignition time, deflagration-to-detonation transition (DDT) time, and combustion wave speeds. Each of these combustion parameters is plotted versus equivalence ratio. The individual data points represent an average value of 8 to 12 combustion cycles per data set. Two tubes were run simultaneously, so two data points are given at each equivalence ratio.

The heated fuel system performance is also presented. Thermal oxidation was not experienced for any of the fuels, but some endothermic reactions were noted during the heating of the aviation gasoline and JP-8. Neither the thrust nor the specific impulse of the PDE was measured, and the only the presence of a detonation is considered the relevant combustion feature of this work.

Pressure and Temperature Effects on Combustion

Combustion data was taken at spark delays of 6 ms and 8 ms. The spark delay time is measured from the time the intake valves close until the spark is deposited in the combustible mixture (Fig. 6.1). At the PDE cycle frequency of 15 Hz, the firing portion of the cycle has 22.2 ms available to ignite the mixture, transition to a detonation, and exhaust the tube to atmospheric pressure. After a detonation wave has exited the tube, the pressure stored in a 1.52 m tube takes roughly 5 ms to completely exhaust to atmospheric pressure, and it is the pressure acting on the interior thrust wall (Appendix A, Fig. A.7) that is the force producing thrust during the cycle. Due to these time constraints, the ignition times are limited to a maximum of 10 ms to 12 ms. At the leaner

mixtures, ignition values were measured that exceeded the aforementioned time limits. This caused an increase in the purge manifold temperature and pressure since the pressure in the thrust tube had still not relaxed before the purge valves opened. When this occurred, the PDE became susceptible to backfire due to insufficient purge gases between the exhausting hot products and the incoming fresh reactants. To increase this window, the spark delay could be reduced, but ignition events were difficult to obtain at spark delays of less than 4 ms due to the reduced pressure and increased velocity in the head immediately after the intake valves closed. The correlation between spark delay and pressure is discussed in the next section.

PDE Cycle

Fill   Fire   Purge

Spark Delay   Ignition Time   DDT Time   time

Intake Valves Close   Spark Deposited   Ignition Occurs   Detonation Wave Exits Spiral   Detonation Wave Exits Thrust Tube
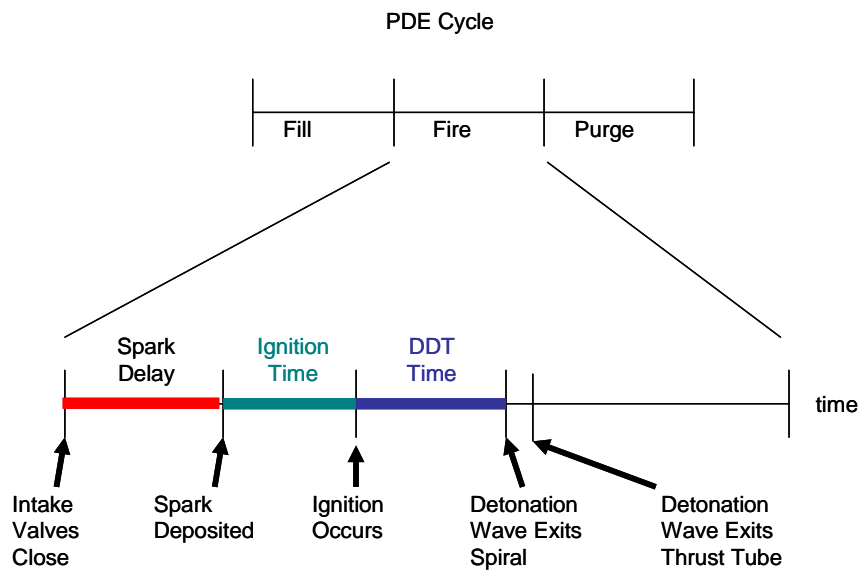
Figure 6.1 Combustion time definitions.

Spark Delay and Initial Pressure

The spark delay was varied to create a different pressure condition within the tube during combustion and thereby determine any pressure effects on the combustion performance of the fuels. As stated previously in Chapter II, the octane number is a combined temperature and pressure effect so it is necessary to vary both to better capture

98

any octane number influence. The pressure in the PDE thrust tube without combustion is shown in Fig. 6.2 where the zero time is defined as the moment the intake valves close. The vertical lines denote the two spark delays used for the combustion data and the associated initial pressure.
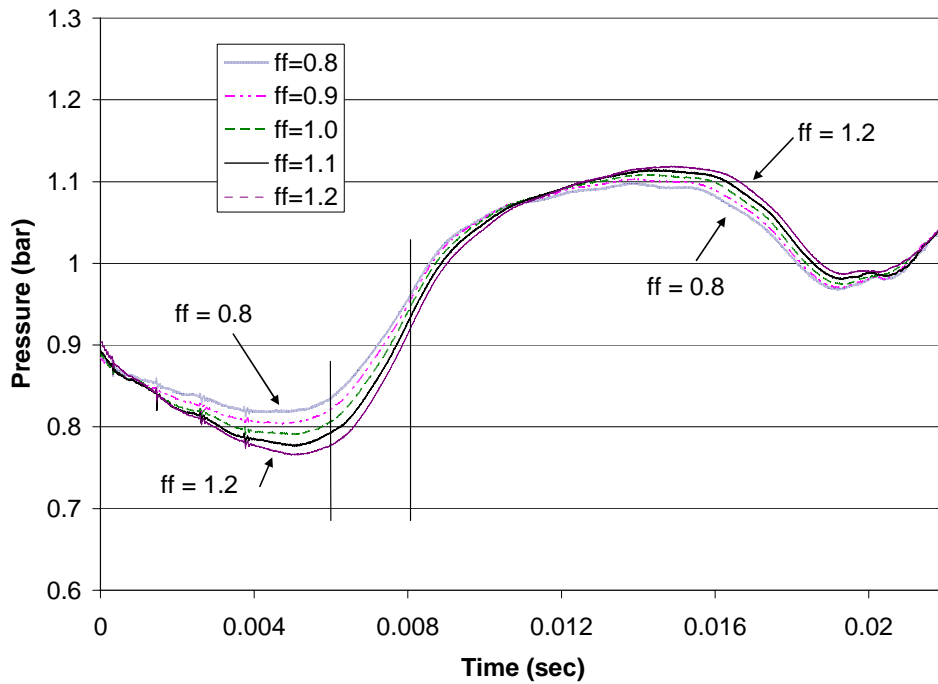
Figure 6.2 Head pressures for 310 K air at 15 Hz for fire portion of cycle without combustion for varying fill fractions. Vertical lines denote two spark delay initial pressure values.

The pressure within the tube changes with time and both spark delays allow the combustion to occur within a compression wave. With a zero spark delay, however, the combustion would occur within an expansion wave for the first 5 ms. A 4 ms spark delay was the minimum spark delay for which a successful ignition was achieved for the 15 Hz test condition. One difficulty in discerning the pressure effects is that the pressure in the head and along the length of the tube varies with time. The average pressures in the closed end of a PDE thrust tube during the 8 ms following the spark deposit (without

fuel) are shown in Table 6.1. Though the initial and final pressures differ, the average pressure difference during that time is less than 0.06 bar (5.6%) and is not considered significant.

Table 6.1 Pressures in the closed end of the PDE thrust, without combustion, during the 8 ms following the spark deposit.

spark delay	initial P (bar)	final P (bar)	average P (bar)
6 ms	0.803	1.104	1.009
8 ms	0.937	1.095	1.069

Test Time and Initial Hardware Temperature

The temperatures in the PDE rapidly change with time and can affect the combustion performance of the PDE. In Fig. 6.3, the time history of the head (closed end) and wall temperatures are shown during a 15 Hz firing frequency run. The tube wall temperature is taken at the exit of the spiral, 1.22 m from the entrance of the thrust tub with a PDE tube wall thickness of 3.9 mm. The head temperature, as compared to the thrust tube, does not get as hot due to the fact that the aluminum head is water cooled and increases from slightly below the air temperature at startup until maintained at roughly 65 °C within 20 seconds. Since ignition begins in the closed end of the tube, ignition time consistency will be shown to be sensitive to wall temperature during the first data set taken for the high vapor pressure fuels (T_{Air} = 310 K).

When the data was taken during a run is important to determine the tube wall temperature affect on the combustion. As stated previously, data was taken at both 6 ms and 8 ms spark delays during each data acquisition run, roughly 30 seconds apart. For the aviation gasoline, isooctane, and n-heptane the 6 ms case was taken first, on average

15 seconds into the run. Saving the data took roughly 30 seconds and after its completion the 8 ms data case was taken and the engine was shut down. The spark delay was then taken in the opposite order (8 ms then 6 ms) during the acquisition of the JP-8 combustion data. This was an effort to isolate whether or any combustion effects were observed between the two spark delays and if they were temperature or pressure related.
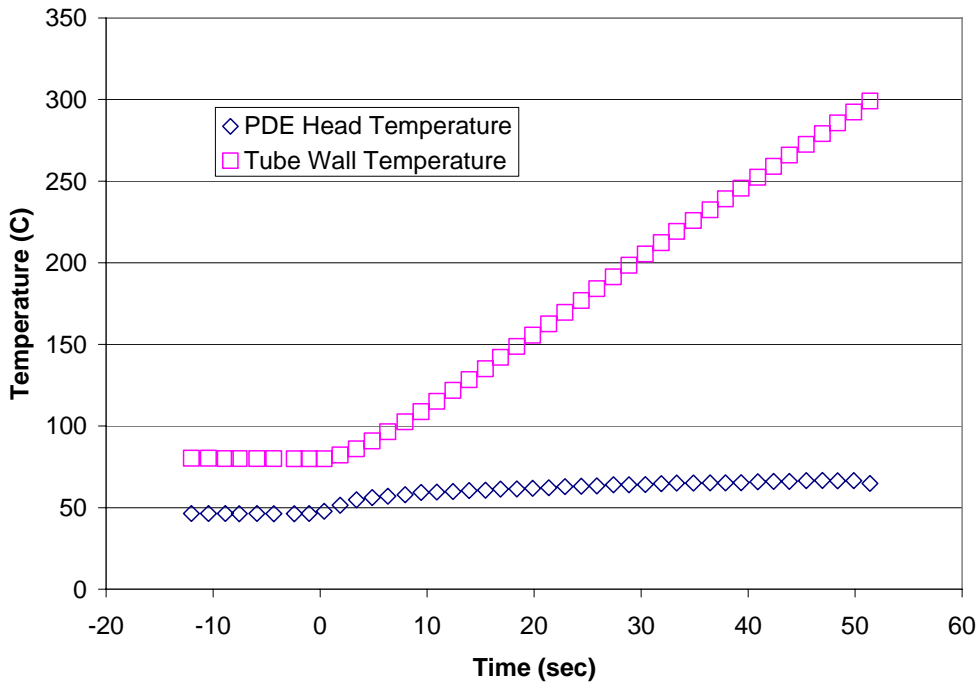
Figure 6.3 PDE thrust tube closed end head and tube wall (3.9 mm thick tube and 1.22 m from head) for a stoichiometric 555 K JP-8 and 422 K air mixture firing at 15 Hz.

The data will show that the temperature effects are a stronger influence on the combustion performance than the pressure effects due to the spark delay. The higher temperature difference between the detonation wave and the cold tube during the first data set increased the heat transfer out of the combustion wave and affected the detonable equivalence ratio range. As the temperature of the tube went up, the heat transfer out of the combusting gases went down and the detonability of the mixture increased.

Fuel Injection Temperature and Resultant Manifold Mixture Temperature

The fuel and air mixture temperature within the manifold should change based on the incoming fuel temperature as modeled in Fig. 6.4. The experimentally recorded temperatures in the manifold, down stream of the fuel injector, did not capture the expected resultant temperature change due to fuel evaporation or flash vaporization. The smaller than expected change was due to the non-adiabatic behavior of the 6.5 m long mixing length. The manifold was a significant thermal mass and provided heat transfer that sustained the mixture temperature at the previous air temperature during a 1 minute run. The premixed manifold took roughly 15 minutes to reach thermal equilibrium prior to the fuel injection and returned quickly (1 minute) the set point temperature after the fuel flow was terminated. The heat transfer from the manifold into the mixture resulted in a consistent mixture temperature for comparison between test cases and fuel flow rates.
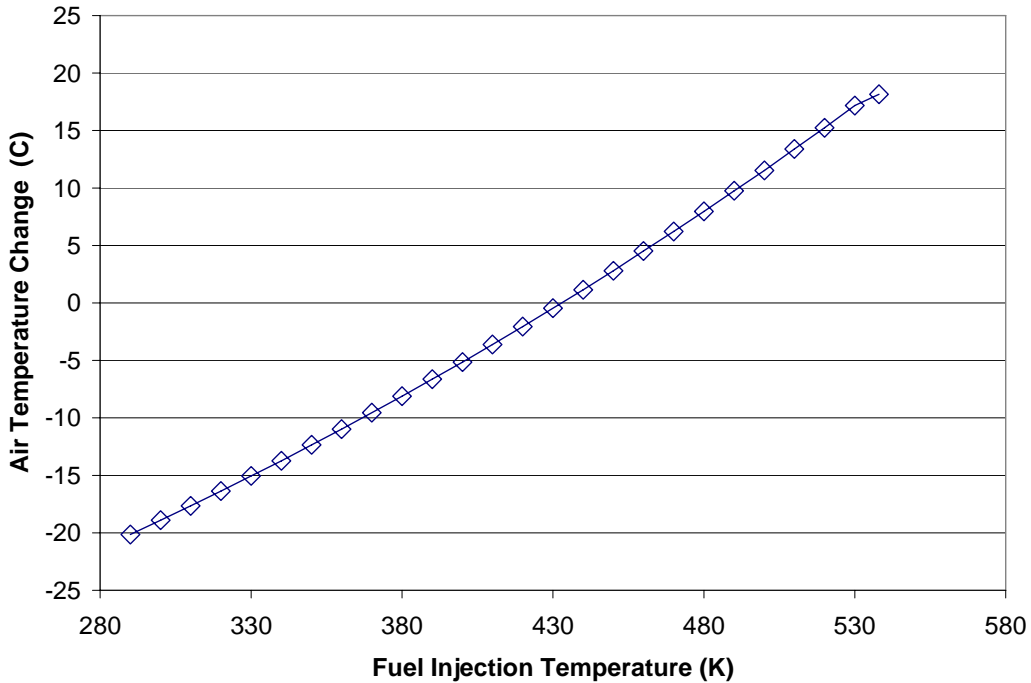
Figure 6.4 Predicted change in resultant mixture temperature due to a stoichiometric i-C_8H_{18} fuel injection and an adiabatic wall condition.

Ignition Results

       The ignition times are determined using the dynamic pressure transducer and the data reduction algorithm discussed in detail in Chapter IV. The consistency of the data points is determined by the standard deviation among the cycles that make up the average. The standard deviations (STD) are plotted with same symbols, but are presented in a smaller font and appear at the lower region of the plots. The aviation gasoline, isooctane, and n-heptane were tested with a 6.5 meter mixing length with an inline axial mixer. These three high vapor pressure fuels represent the best case because of the longer residence times (0.237 ms) available for the fuel to fully evaporate and mix with the air prior to combustion. The JP-8 fuel injection tests have a 1.3 m mixing length and are considered more challenging to mix because of the much lower vapor pressure, which discourages evaporation, and the stronger pressure and velocity fluctuations (Appendix B) which discourage the homogeneity of the resultant mixture. The shorter JP-8 setup results in a shorter residence time (0.046 ms) available to evaporate and mix prior to combustion.

Aviation Gasoline Ignition Data

       The ignition times for spark delays of 6 ms and 8 ms are shown in Fig. 6.5 and Fig. 6.6. Though the ignition times are nearly identical between the spark delays of 6 and 8 ms, the data set standard deviations between the two spark delays are not. The data set standard deviations represent the repeatability between the 8 to 10 individual ignition events used for the plotted point and include one point for each thrust tube. The standard deviation is lower (consistency is higher) for the 8 ms case because the PDE had reached a steady state thermal condition in the head.
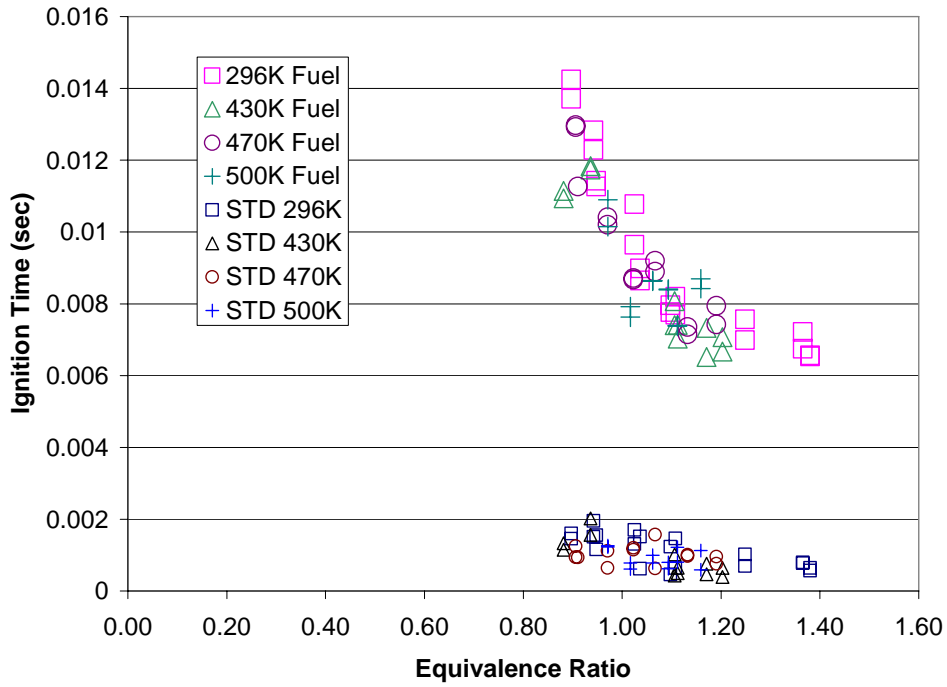
Figure 6.5 Aviation gasoline ignition times and data set standard deviations (STD) at a spark delay of 6 ms. Air temperature is 311 K.
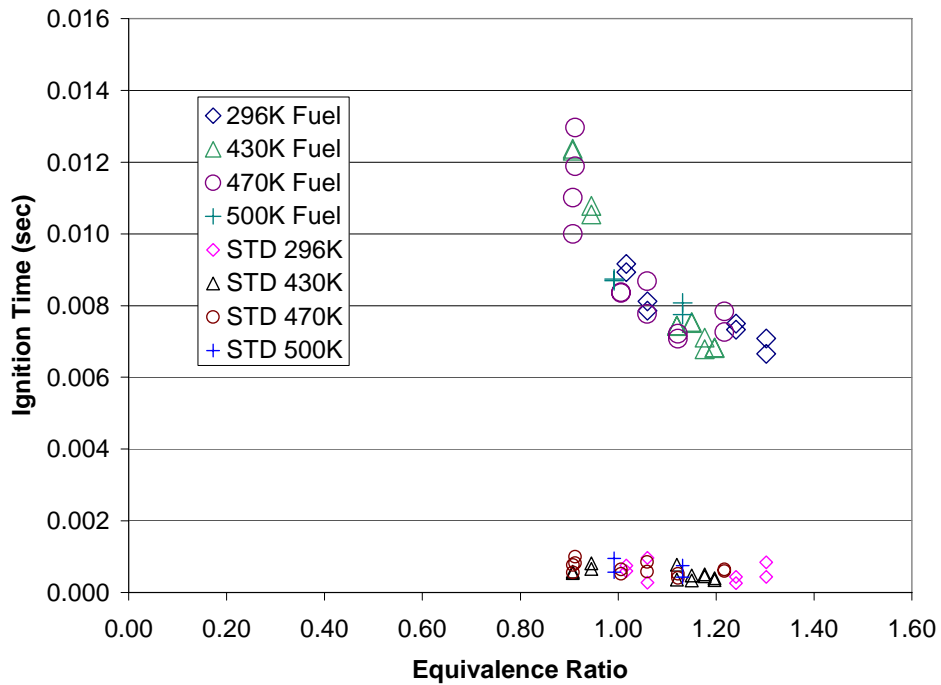
Figure 6.6 Aviation gasoline ignition times and data set standard deviations (STD) at a spark delay of 8 ms. Air temperature is 311 K.

The longer run times associated with the 8 ms spark delay reduced any cold wall effects, such as quenching, and improved the overall combustion performance. The improvement is best identified by the consistency between the data points that make up the individual data points. The ignition time standard deviations were on the order of 15% for the 6 ms spark data (taken 15 sec into the run), and at 7% for 8 ms spark data (taken 30 to 45 sec later). The ignition times, for stoichiometric aviation gas and air, were near 9 ms for both spark delays. There were no strong fuel injection temperature effects on the ignition times or on the consistency of the data sets for aviation gasoline.

Isooctane Ignition Data

Both the aviation gasoline and isooctane had an octane number of 100 and an auto ignition temperature within 17 °C of one another (Table 2.3). The isooctane exhibited an ignition time near 9 ms at an equivalence ratio of one. There was little to no change in ignition times between the 6 and 8 ms spark delays, though a slight reduction (~3%) in the standard deviations at the 8 ms spark delay was observed
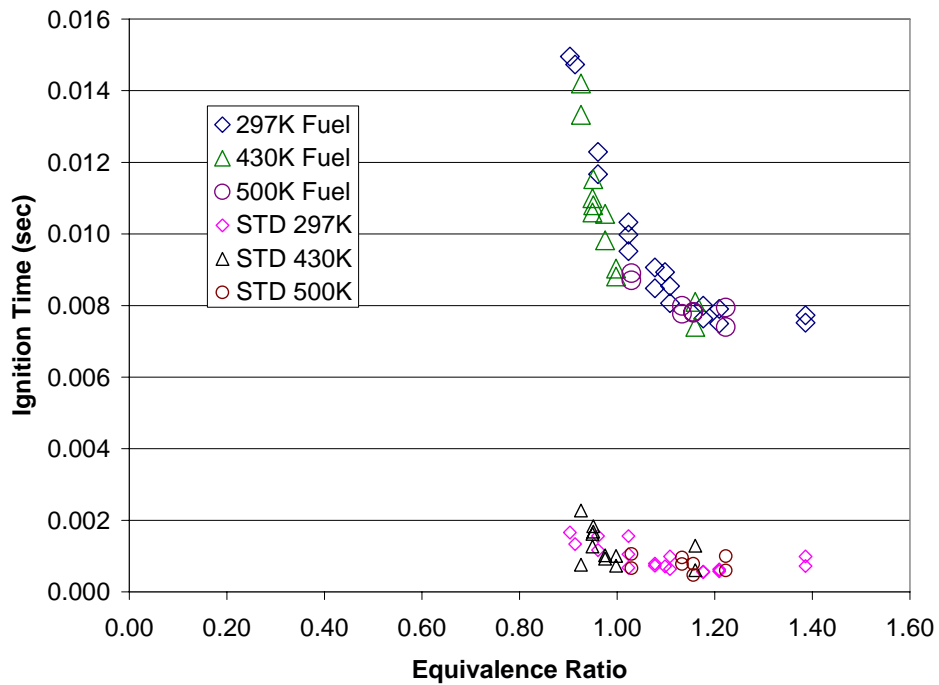
Figure 6.7 Isooctane ignition times and data set standard deviations (STD) at a spark delay of 6 ms. Air temperature is 311 K.
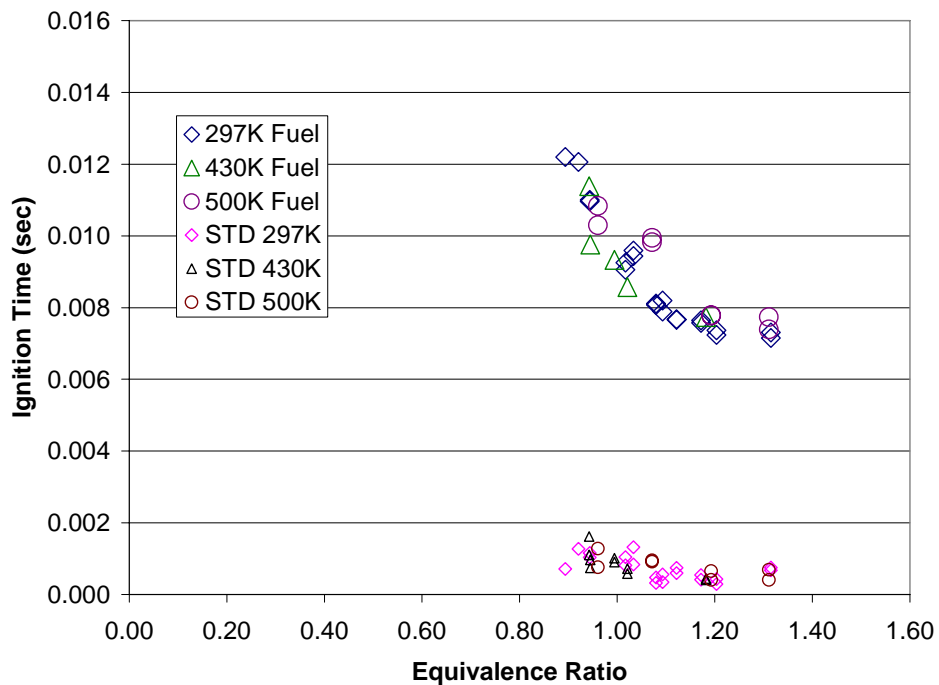
Figure 6.8 Isooctane ignition times and data set standard deviations (STD) at a spark delay of 8 ms. Air temperature is 311 K.

106

n-Heptane Ignition Times

The n-heptane ignition times for both spark delays (Fig. 6.9 and 6.10) were near 8 ms at an equivalence ratio of one, or 1 ms less than the isooctane and aviation gasoline. The faster ignition times were consistent across the range of equivalence ratios tested. The trend of ignition data with equivalence ratio takes a similar shape to the other two fuels but with less flattening of the times from an equivalence ratio of 1.2 to 1.4. The absence of the perceived minima lends support to the correlation between ignition time and the minimum ignition energy which occurs at $\varphi=1.8$ shown in Fig. 2.3. The ideal combustion regime is to operate the PDE as fuel lean as possible to conserve fuel so there was no benefit to increase the equivalence ratio past 1.4. The n-heptane standard deviations also experienced the drop shown in the previous two fuels when going from the 6 ms to 8 ms spark delay due to the benefits of thermal equilibrium in the head.
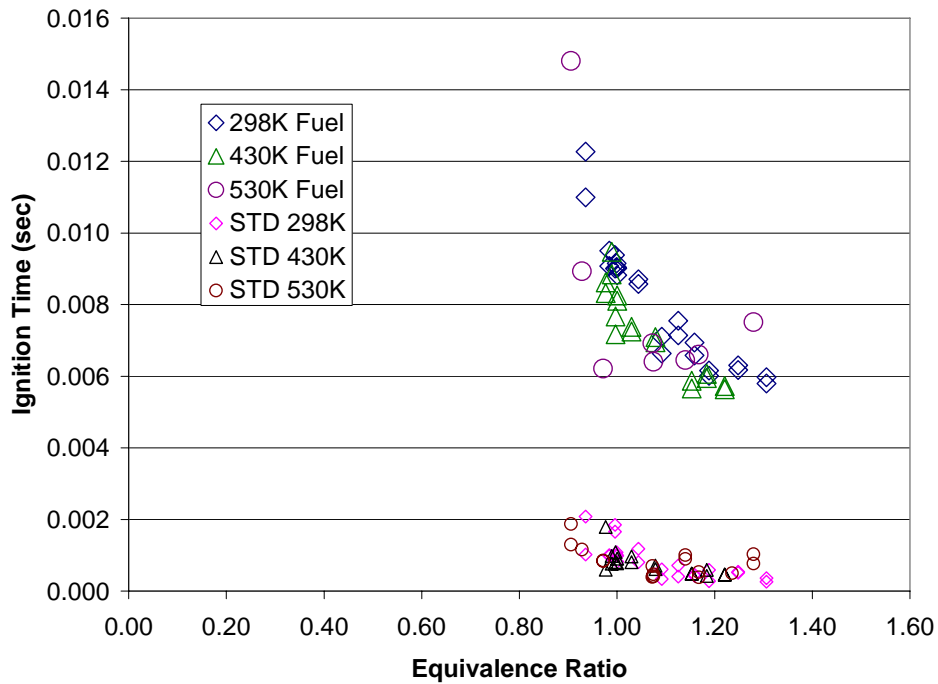
Figure 6.9 n-Heptane ignition times and data set standard deviation (STD) at a spark delay of 6 ms. Air temperature is 311 K.
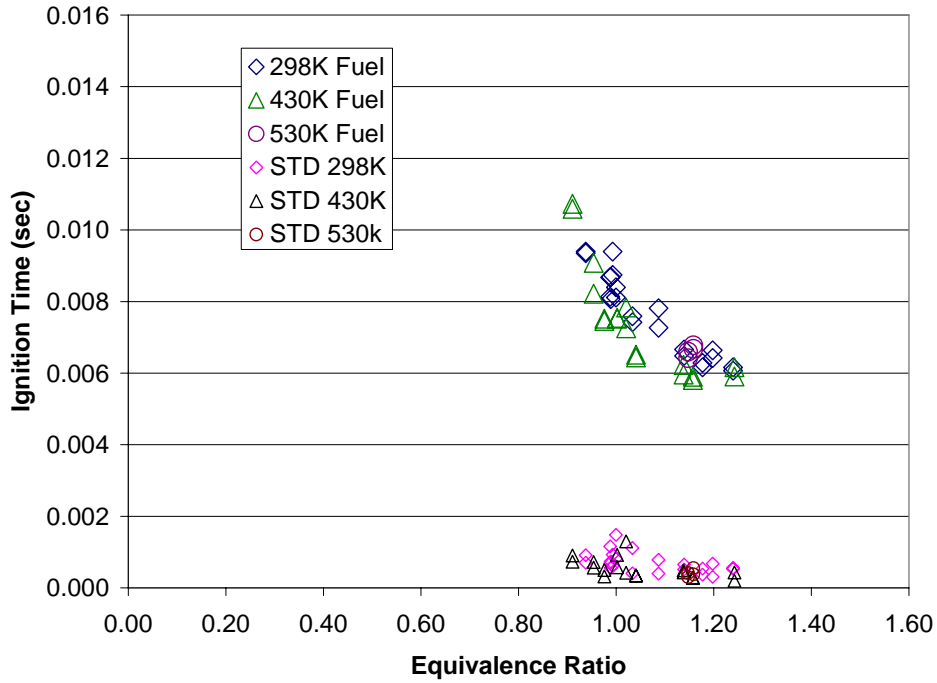
Figure 6.10 n-Heptane ignition times and data set standard deviation (STD) at a spark delay of 8 ms. Air temperature is 311 K.

High Vapor Pressure Fuels Trends

Each of the high vapor fuels showed similar ignition and equivalence ratio behavior. The range of equivalence ratios where ignition was observed (within the cycle constrained 14 ms) varied from 0.89 to 1.39. Increasing the fuel injection temperature did not have a measurable effect on ignition times for the high vapor pressure fuels, and the majority of the data fell within ±1 standard deviation of each fuel temperature tested. The absence of fuel injection temperature dependence shows that the droplets were not a factor for the ignition of the high vapor pressure fuels. The fuel injection envelope prediction (Figs. 5.8 and 5.9) and the droplet lifetime prediction (Table 5.4) supports the assumption that given adequate time (or mixing length), the droplets will approach 100% vapor. The 6.5 meter mixing length, in conjunction with the axial mixer, adequately evaporated any droplets prior to combustion, and therefore created the best case

108

performance for the fuel injection system. A difference in ignition time was observed between the 100 octane (aviation gasoline and isooctane) and 0 octane (n-heptane) number fuels. The n-heptane was consistently 1 ms faster for all equivalence ratios. The reduction in ignition time between the fuels is small (11.1%) considering the large reduction in both auto ignition temperature (200 °C) and octane number (100) (Table 2.3).

JP-8 Ignition Times

The JP-8 ignition results show a strong dependence on the fuel temperature and the air temperature due to the effect of fuel droplets. When compared to the previous high vapor pressure fuel setup, the mixing length was shortened from 6.5 m to 1.3 m, and the axial mixer was removed to prevent fuel from condensing in the mixer and creating a hazard. Reducing the manifold length also reduced the amount of structure to be heated and maintained with the air heater. The most noticeable result was the reduced operating equivalence ratio range. For the unheated JP-8 fuel injection case, regardless of the air temperature, the minimum equivalence ratio where ignition was achieved, within the 14 ms maximum ignition time, was 1.05. This value is significantly higher than the 0.89 obtained for the unheated high vapor pressure fuels. As discussed earlier, any ignition times over 12 to 14 ms could damage the PDE (backfire) and were avoided. The reason the minimum equivalence ratio was higher for the unheated JP-8 was because much of the fuel was still suspended in droplets without sufficient time and energy to adequately evaporate prior to combustion. The resulting mixture was globally fuel rich, but locally fuel lean since the droplets had not evaporated and mixed with the air. Three air

temperatures were used to determine the effect of the air temperature and the capacity of the mixture to keep the fuel vapor from condensing back into a liquid. The JP-8 data sets were taken first at an 8 ms spark delay and then the 6 ms spark delay. This spark delay order is the opposite of the high vapor pressure data, and results show that the standard deviation trends for the ignition data were again lower for the later data set (6 ms spark delay) and had more scatter for the initial set (8 ms spark delay). This trend was strongest in the unheated fuel case. Other fuel injection temperature data sets showed little to no difference in data set standard deviations from run to run. The higher inconsistencies in the data sets, denoted by the STD symbols, are more likely an effect of the short mixing length and less an effect of the thermal transients. As in the high vapor pressure data, the ignition times did not show strong pressure dependence (varied spark delay). The ignition data for Fig. 6.11 and 6.12 are presented for unheated JP-8.
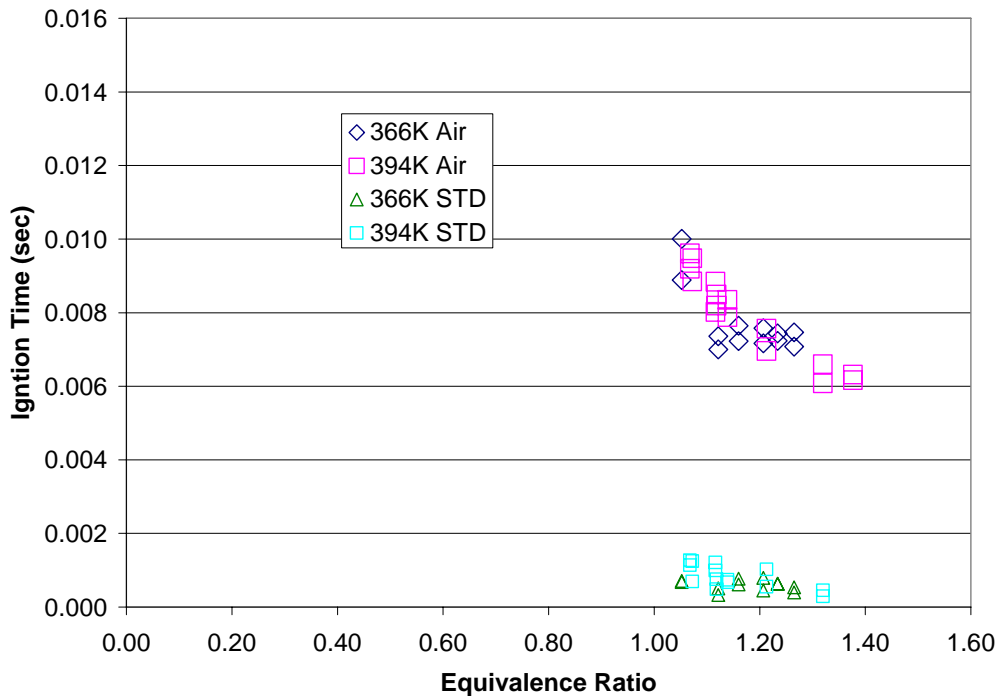
Figure 6.11 JP-8 ignition times and data set standard deviation (STD) at a spark delay of 6 ms. Fuel at 300 K.

110
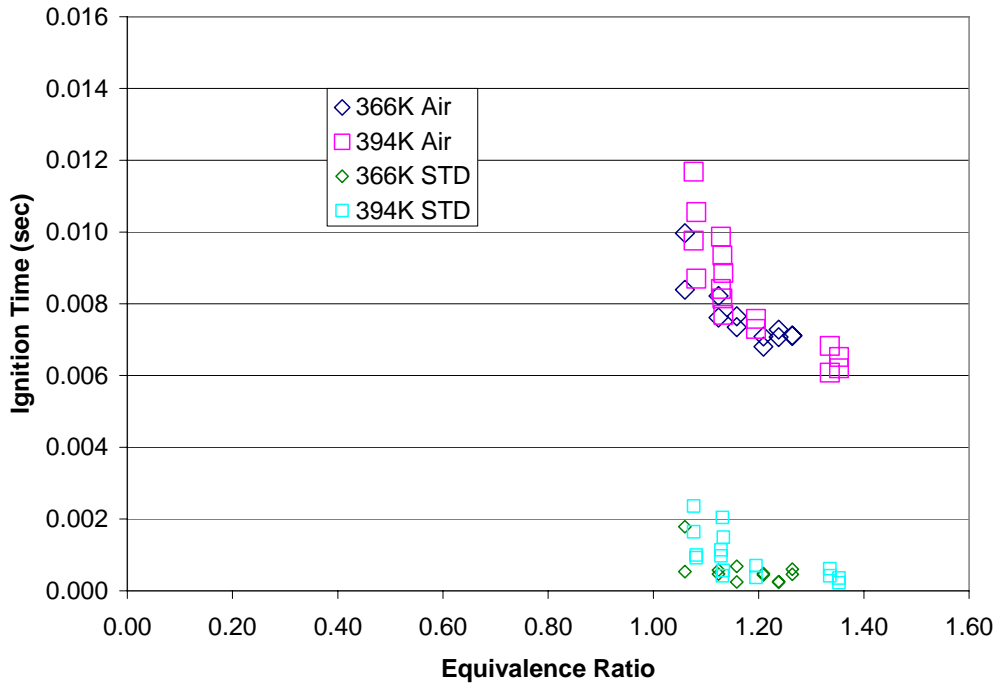
Figure 6.12 JP-8 ignition times and data set standard deviation (STD) at a spark delay of 8 ms. Fuel at 300 K.

Figures 6.13 and 6.14 are presented for a 473 K fuel temperature and show a widened operating equivalence ratio with the increased fuel temperature. The leanest ignitable equivalence ratio has now been reduced to 0.93 from 1.05 observed previously with the ambient temperature fuel. Increasing the air temperature with the 473 K fuel shifts the lean operating equivalence ratio from 0.99 at the 366 K air to 0.93 with the 422 K air. The shifts lean are a result of a higher temperature droplet with a resulting increase in vapor pressure (Table 5.2), and an increased enthalpy of the air. As predicted in Fig. 5.10, the mixture has not overcome the liquid vapor equilibrium boundary to ensure that the mixture is droplet free. The 366 K and 394 K air data points fall below the liquid vapor equilibrium line where droplets are expected, and although the 422 K data point is above the line, the fuel temperature is still below the flash vaporization temperature and the evaporation time was not sufficient to reach a droplet free mixture.

111
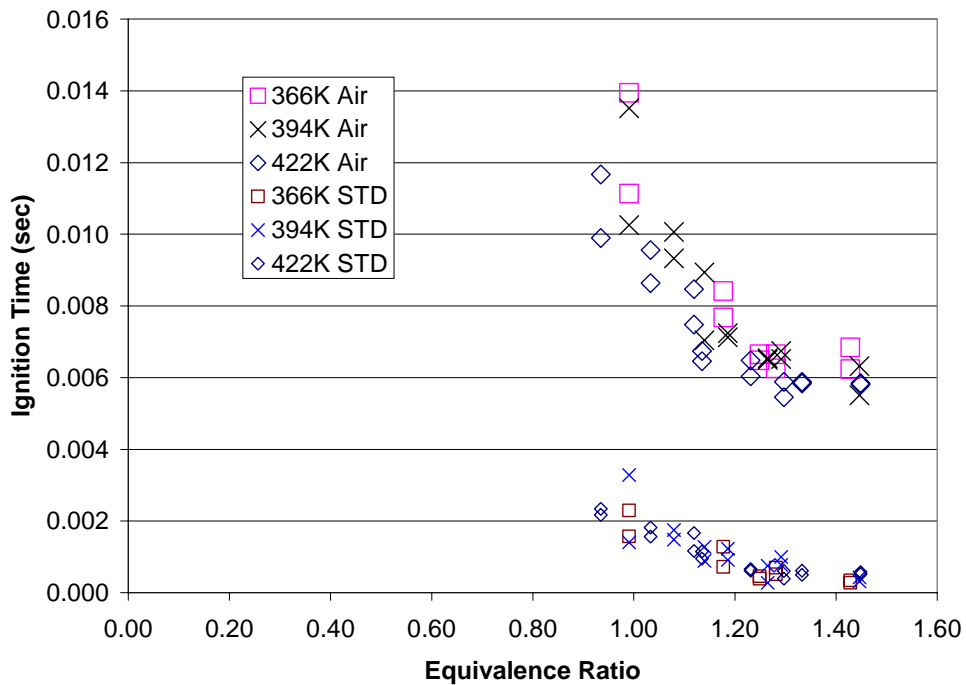
Figure 6.13 JP-8 ignition times and data set standard deviation (STD) at a spark delay of 6 ms. Fuel at 473 K.
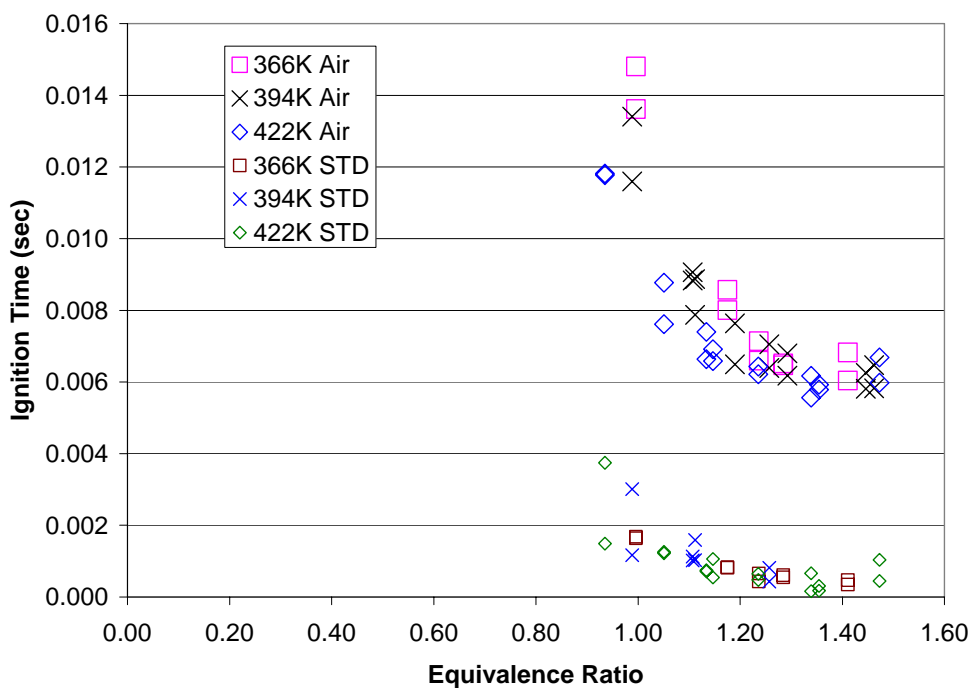
Figure 6.14 JP-8 ignition times and data set standard deviation (STD) at a spark delay of 8 ms. Fuel at 473 K.

The fuel temperature was increased further to 555 K which exceeded by 25 °C the expected flash vaporization temperature predicted for JP-8 in Fig. 5.10. Figures 6.15 and 6.16 show the ignition times collapse tightly together (within 2%) for both air temperatures. These results are similar to the high vapor pressure results where the droplet effects have been adequately eliminated, and the JP-8 minimum ignition equivalence ratio has been lowered to 0.86, bettering the 0.89 achieved previously with the n-C_7H_{16} and air mixture. The data set standard deviations no longer differ appreciably between the two data sets.
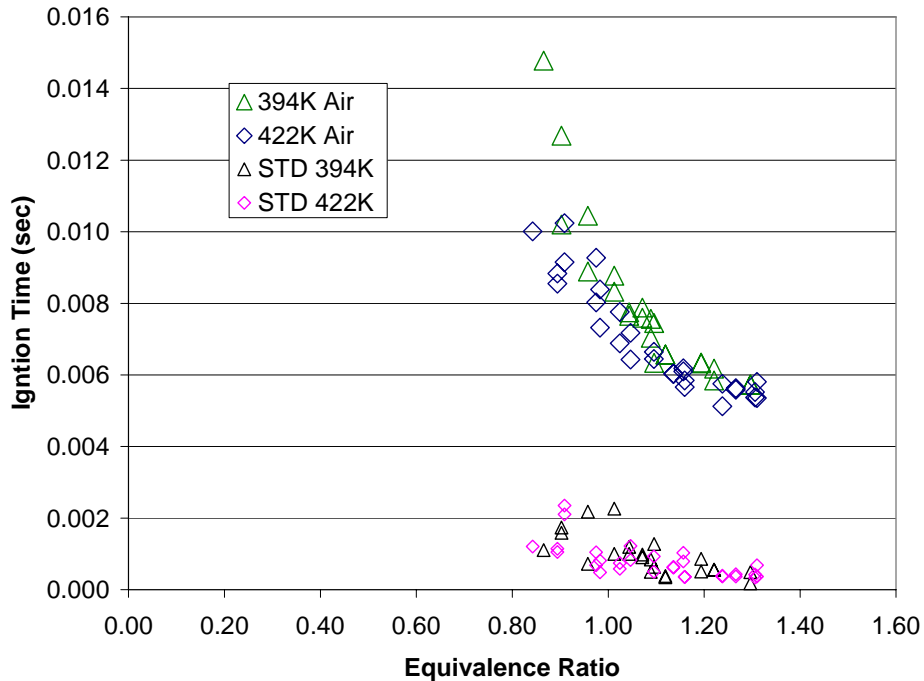
Figure 6.15 JP-8 ignition times and data set standard deviation (STD) at a spark delay of 6 ms. Fuel at 555 K.
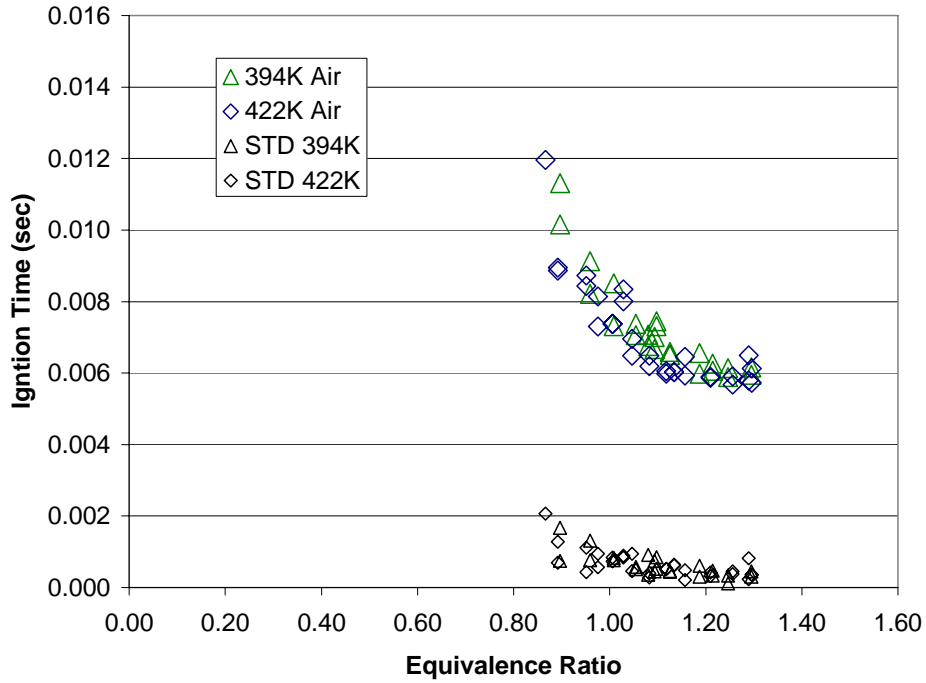
Figure 6.16 JP-8 ignition times and data set standard deviation (STD) at a spark delay of 8 ms. Fuel at 555 K.

Combined Effects with JP-8

The ignition time data in Figs. 6.12, Fig. 6.14, and Fig. 6.16 are plotted together in Fig. 6.17 to show the effect of the combined fuel and air temperatures for the 8 ms spark delay cases. The JP-8 droplet effects are clearly observed in the combustion data when compared to the high vapor pressure fuels where all droplet effects were negligible.
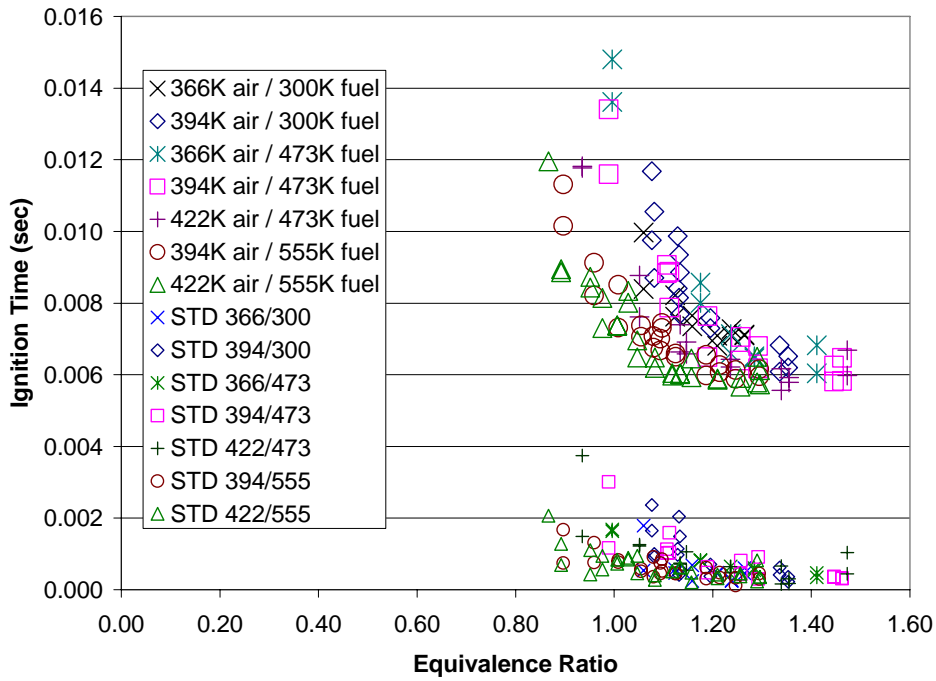
Figure 6.17 Variation of air and fuel temperature on ignition time of a JP-8 and air at 8 ms spark delay.

To better show the droplet effects, the ignition trends in Fig. 6.17 were captured using a second order polynomial curve fit and are plotted in Fig. 6.18. The shapes of the curves are similar, but the lower fuel and air temperature curves are shifted fuel rich. Referring back to the predicted droplet lifetimes from Table 5.4, the percentage of liquid fuel remaining after 70 µm droplet evaporates during a 46 ms manifold residence time is plotted in Fig. 6.19. The higher the droplet and air temperatures, the more quickly evaporation occurs and a higher percentage of fuel vapor is available for combustion. The liquid fuel remaining in the mixture is effectively unusable for combustion due to the fast combustion (6 to 15 ms) required by the PDE. This supports the trends observed in Fig. 6.18 and measured in Table 6.2. The same ignition times were observed at higher fuel equivalence ratios, supporting the hypothesis that the two-phase mixture is behaving as if only the fuel vapor is being consumed.

115
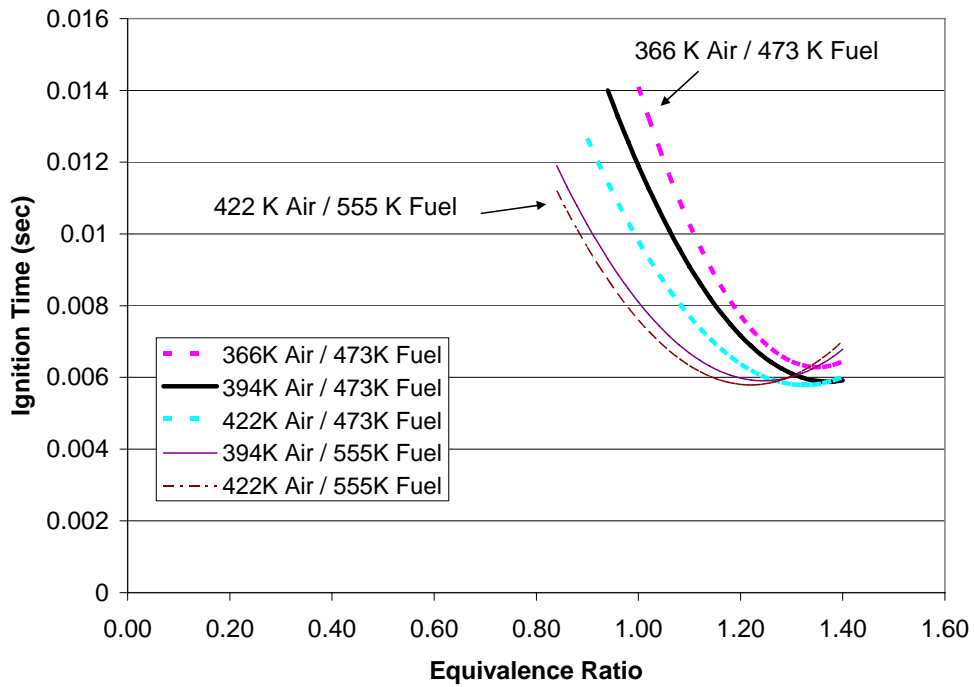
Figure 6.18 Best fit lines for 6 fuel and air temperature variations for JP-8 and air ignition. Fits are representative of data in Fig 6.17.
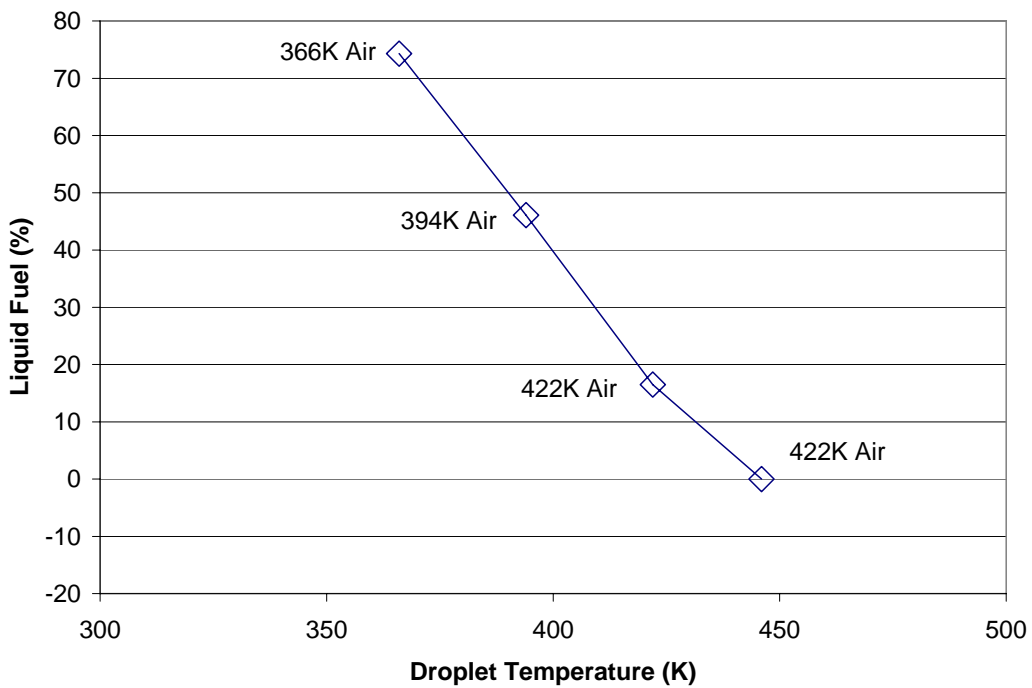
Figure 6.19 Estimated liquid JP-8 remaining after a 70 µm droplet evaporates during a 46 ms manifold residence time from Table 5.4.

The flash vaporization system reduced the required fuel flow by 20% (Table 6.2) to achieve the same 10 ms ignition time. To compare the ignition times in Fig. 6.18 at a fixed equivalence ratio of one, the 366 K air and 473 K fuel requires 16 ms, but the flash vaporized fuel requires less than 8 ms to ignite, a 50% reduction in ignition time.

Table 6.2 Measured equivalence ratio at an ignition time of 10 ms from Fig. 6.18. Estimated fuel vapor assumes a 70 µm droplet flow field with a 46 ms manifold residence time before combustion.

Air Temperature (K)	Fuel Temperature (K)	Equivalence Ratio	Average fuel and air temperature T_{avg} (K)	Estimated fuel vapor percentage at T_{avg}	Estimated fuel vapor equivalence ratio at T_{avg}
366	473	1.1	420	81.7	0.90
394	473	1.06	433	92.8	0.98
422	473	0.98	447	99.9	0.98
394	555	0.9	474	100	0.90
422	555	0.88	555	100	0.88

The amount of fuel vapor available for the 5 injection cases in Table 6.2 was estimated using an average droplet temperature. This crude estimate is for a fuel spray with 70 µm droplets and a 46 ms manifold residence time. The average temperature was chosen because droplet lifetimes and the heat transfer times were closely matched. The estimate captures the expected fuel vapor trends very well for the 366 K air and 473 K fuel case, and the next two cases over predict the amount of fuel vapor available before matching the final two flash vaporization cases. The proper fuel vapor trends are observed and the hypothesis that any remaining liquid fuel is effectively unusable due to the fast combustion times in the PDE is reinforced.

Detonability

The detonability of a fuel is defined as the range of equivalence ratios that a particular fuel and air mixture can transition a deflagration into a detonation using a fixed length obstacle such as Schelkin spiral. Two experimental methods are used to determine the detonability of the fuels. The first method is to determine the time the combustion wave arrived at the exit of the DDT spiral after ignition has been established. The shorter the time for the combustion wave to traverse the spiral, the shorter the length required to achieve a detonation. The second method is to determine whether or not the combustion wave speed was at or near the Chapman-Jouguet detonation wave speed and therefore a detonation. The wave speed results will be shown in the next section. The length of the obstacle that is required to achieve a detonation is critical to the engine designer as it sets the minimum length for the thrust tubes. While the spirals are necessary to transition to a detonation in this research, a longer than required spiral causes performance losses and the length should be minimized (Appendix A).

The two major trends observed in the DDT data are shown in Fig 6.20. The DDT times are roughly flat until the mixture becomes more difficult to detonate at the higher equivalence ratios and the times begin to increase. In Fig. 6.20(i), a shift from lean to rich equivalence ratios is highlighted with a shift from corner (a) to corner (b). The increase in the rich limit was observed when the fuel was changed from a 100 octane number (ON) fuel to the lower ON n-heptane and JP-8. A second trend shown in Fig. 6.20(ii) represents a reduction in the overall DDT time due to the changing of the fuel ON and also from the hotter PDE tubes from the data set taken later in a test sequence. The hotter

PDE thrust tubes have lower heat transfer out of the emerging detonation wave and have more energy available to transition to a detonation.
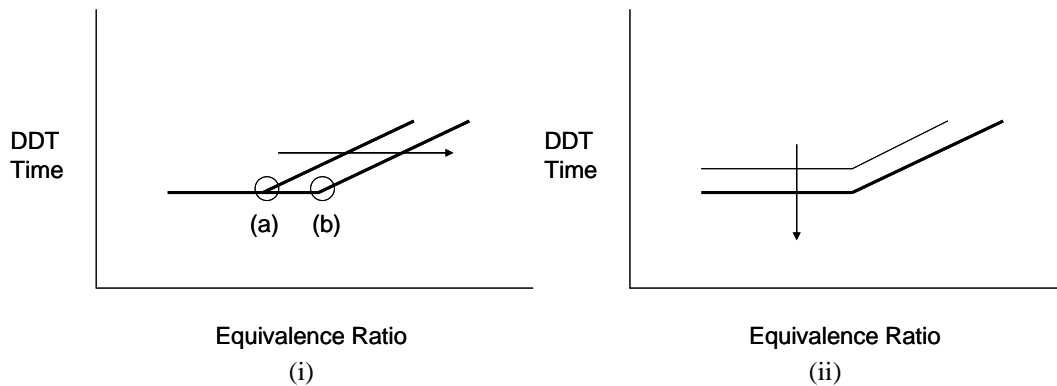
Figure 6.20 Key features of DDT time plots (i) increase in equivalence ratio where detonations are observed, or (ii) decrease in overall DDT times. Both are caused by changing fuel ON and hotter PDE tube temperatures.

Aviation Gasoline DDT Times

Figures 6.21 and 6.22 show the times the combustion waves reached the end of the DDT spiral (second ion sensor) in both tubes for different injection temperatures and equivalence ratios. The two plots agree well with stoichiometric mixture time of arrival just around 2.5 ms ($\pm$ 0.15 ms) for the 6 ms spark delay and an arrival time of 2.37 ms ($\pm$ 0.11 ms) at the 8 ms spark delay. As the spark delay is increased, the equivalence ratio corner shifts from 1.15 for the 6 ms spark delay to a value near 1.2 for the 8 ms spark delay. The improvement in time and detonability is less than 5% and within the error bars, and no improvement was observed by increasing the fuel injection temperature.
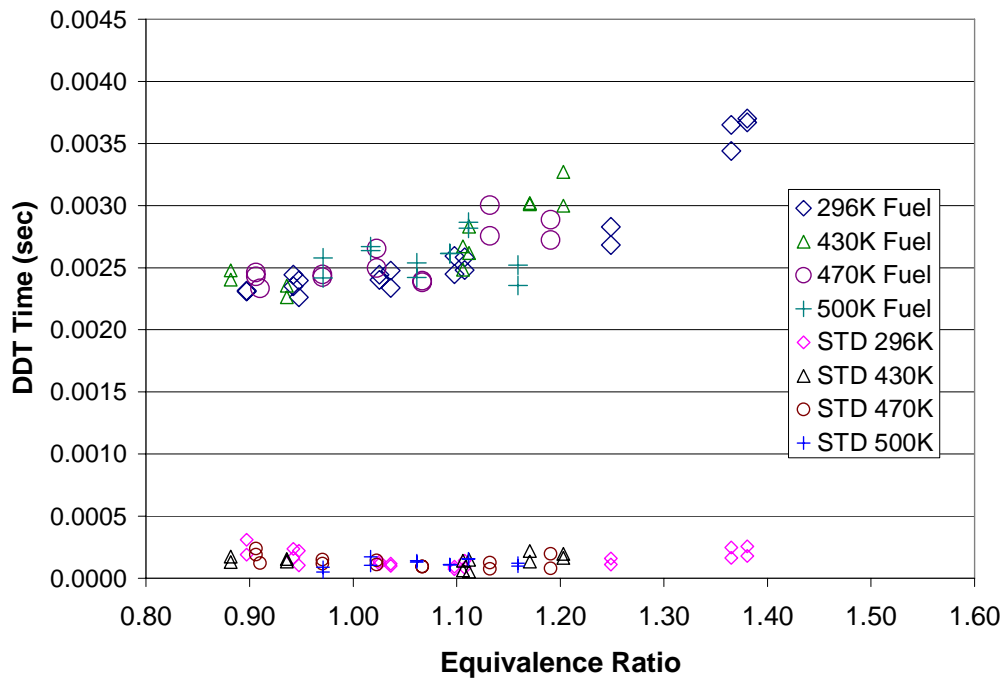
Figure 6.21 Aviation gasoline combustion wave times to second sensor at a 6 ms spark delay. Air temperature is 311 K.
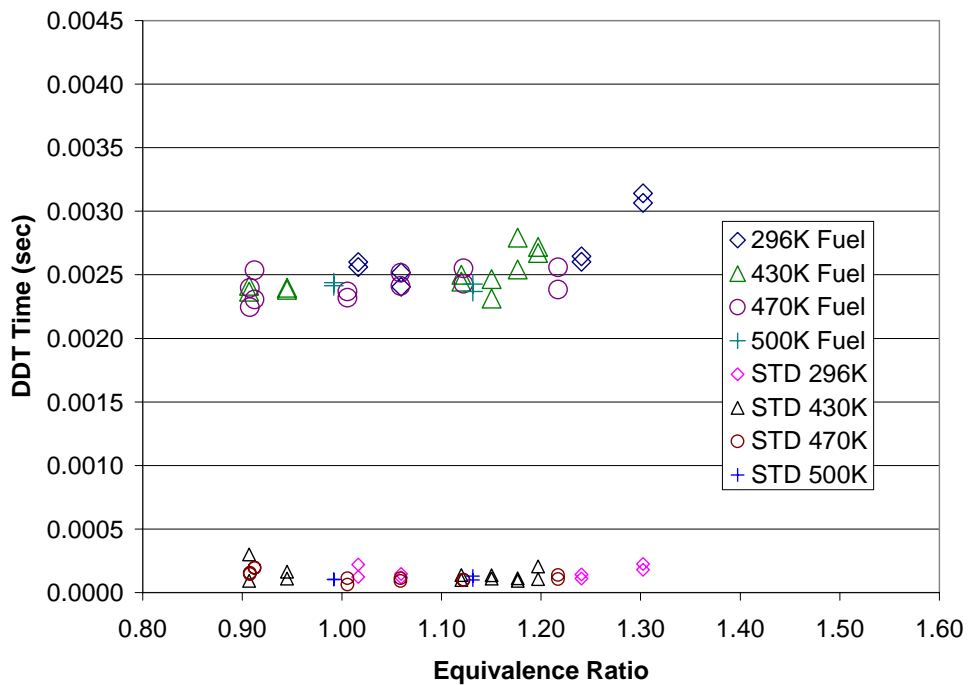
Figure 6.22 Aviation gasoline combustion wave times to second sensor at an 8 ms spark delay. Air temperature is 311 K.

Isooctane DDT Times

The isooctane DDT time data (Figs. 6.23 and 6.24) closely resembles the shape of the aviation gasoline data, but with slightly longer times. The times were near 2.57 ms (± 0.14 ms) for a stoichiometric mixture for the 6 ms spark delay, and a slightly lower time of 2.45 ms (± 0.13 ms) for the 8 ms spark delay. For the 6 ms spark delay, the DDT corner occurs at an equivalence ratio of roughly 1.10, but is extended to near 1.18 for the 8 ms spark delay case. This corresponds to a 7% increase in the detonable equivalence ratio corner and is confirmed later in the combustion wave speed data. The overall DDT time reduction was considered to be within the scatter of the data.
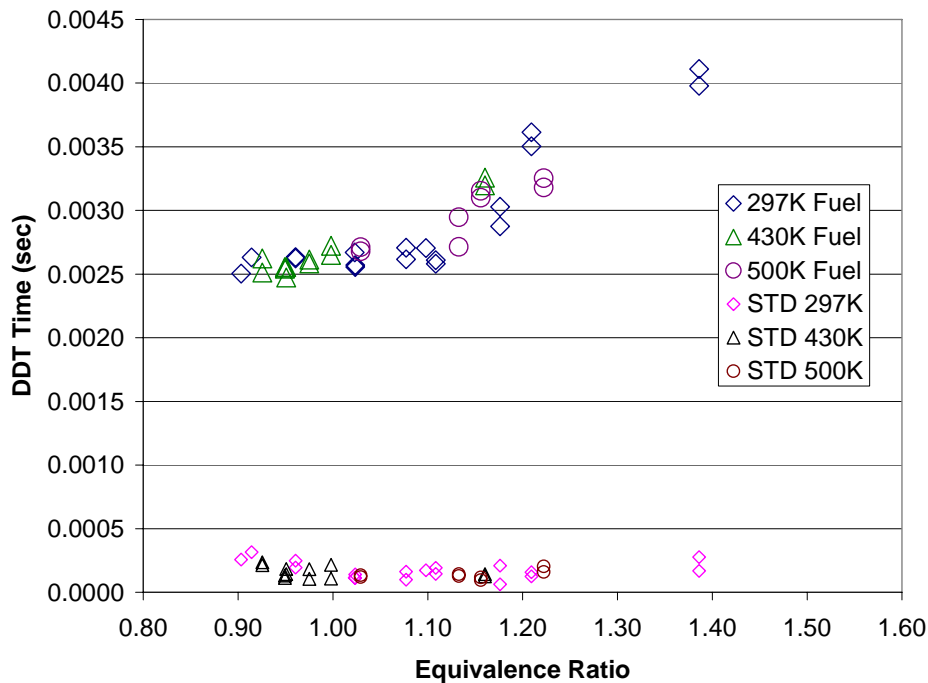
Figure 6.23 Isooctane combustion wave times to second sensor at a 6 ms spark delay. Air temperature is 311 K.
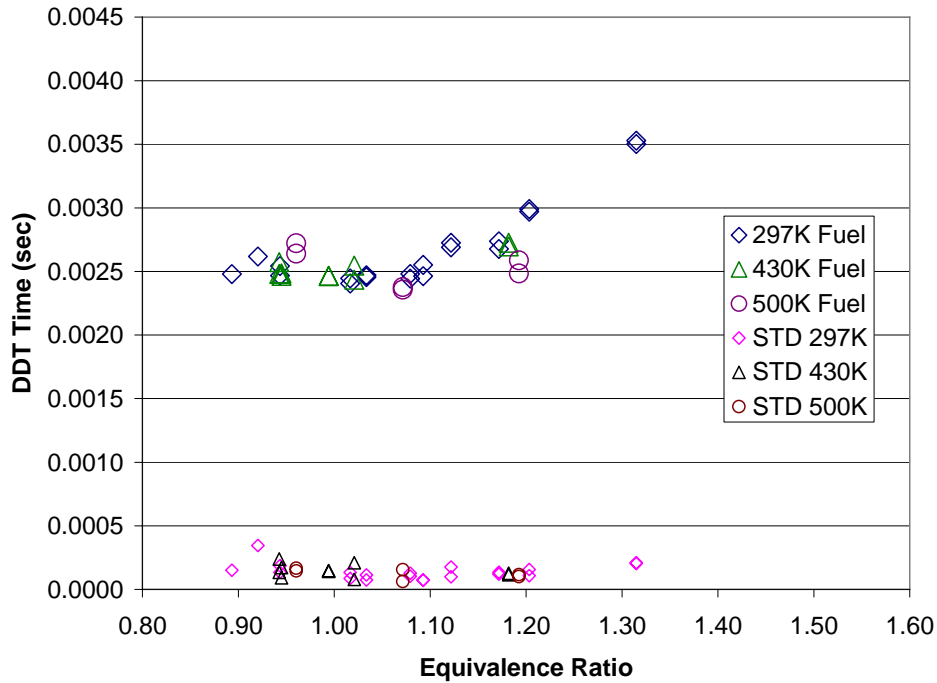
Figure 6.24 Isooctane combustion wave times to second sensor at an 8 ms spark delay. Air temperature is 311 K.

n-Heptane DDT Times

The n-heptane DDT data in Figs. 6.25 and 6.26 shows the largest change due to the increased average pressure and hotter PDE tube temperature. The 6 ms spark delay shows a combustion wave arrival time at 2.5 ms, but the combustion arrival time drops a full 0.25 ms to 2.25 ms to the second sensor for the 8 ms spark delay. The scatter of the 6 ms spark delay data falls within a 1 ms band whereas the 8 ms spark delay band is within a 0.5 ms band. Another important feature is that the DDT times are relatively flat without the sudden rise (corner) encountered in the previous two fuels. The result is that detonations occurred at nearly every equivalence ratio tested. There is a slight increase in DDT time with equivalence ratio, but the slope change is not nearly as steep as seen previously in Figs. 6.23 and 6.24 for the isooctane.
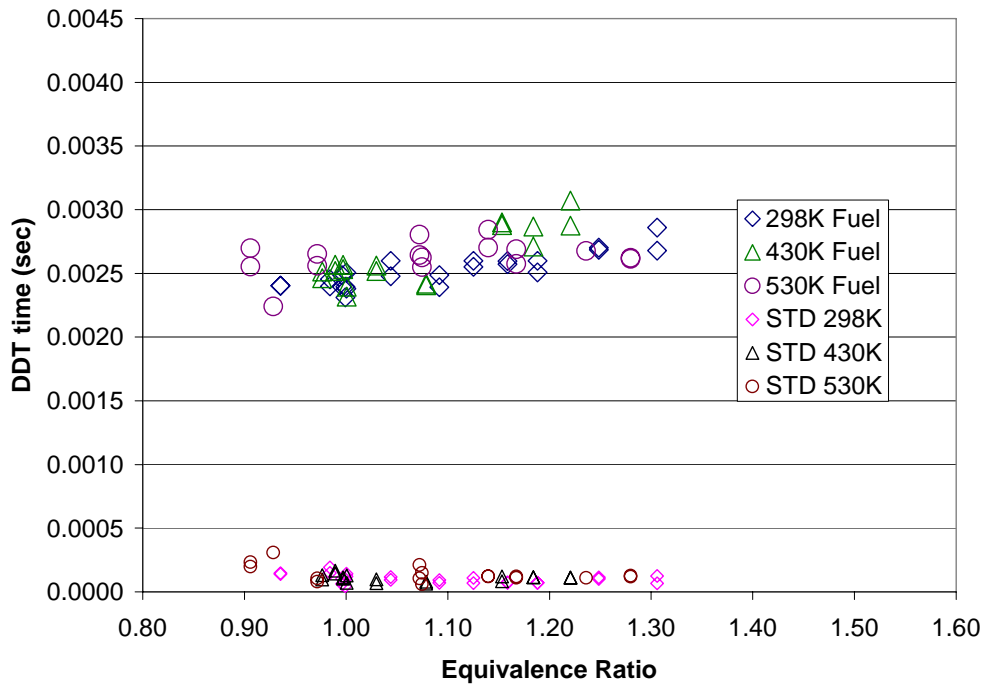
Figure 6.25 n-Heptane combustion wave times to second sensor at a 6 ms spark delay. Air temperature is 311 K.
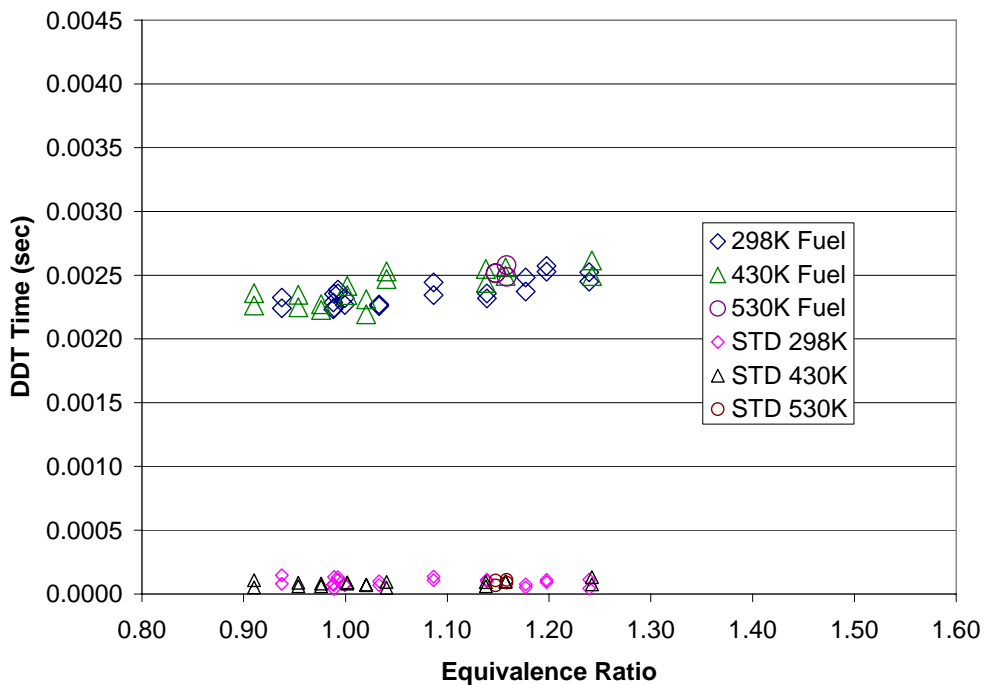
Figure 6.26 n-Heptane combustion wave times to second sensor at an 8 ms spark delay. Air temperature is 311 K.

JP-8 DDT Times

The JP-8 DDT times were the lowest of the four fuels. Figures 6.27 and 6.28 show the results for the ambient fuel injection temperature at two different air temperatures. In comparison with the high vapor pressure fuels, the unheated JP-8 has much more scatter (1 ms versus 0.25 ms) and an increased variation from tube to tube. Two data points are given at each equivalence ratio and the increased variation between them is a result of poor mixing and liquid droplets remaining due to the reduced mixing length (6.5 m to 1.3 m). As the fuel temperature increases to the flash vaporized case, the data variation between the two tubes becomes less pronounced due to better mixing. The JP-8 DDT data displays a minima occurring at a given equivalence ratio. The minimum time for the combustion wave to traverse the spiral should occur closer to an equivalence ratio of one where the fuel is most easily detonated (Fig. 2.12). The unheated fuel data had too much scatter to accurately ascertain the minima, but subsequent heated fuel plots begin to show a shift from a slightly rich limit towards an equivalence ratio of one.

The wave speed data in the next section will show that if the DDT times are at or below 2.6 ms then a detonation was usually observed. For the range of equivalence ratios tested, the JP-8 DDT data falls below the 2.6 ms limit and detonations are observed without heating the fuel; however, as discussed previously in the JP-8 ignition data, the minimum equivalence ratio was 1.05 for the unheated fuel which is 23% higher than for the flash vaporized fuel case. This shift is a result of the locally lean behavior of a fuel and air mixture with a significant amount of fuel still in an unusable liquid condition.
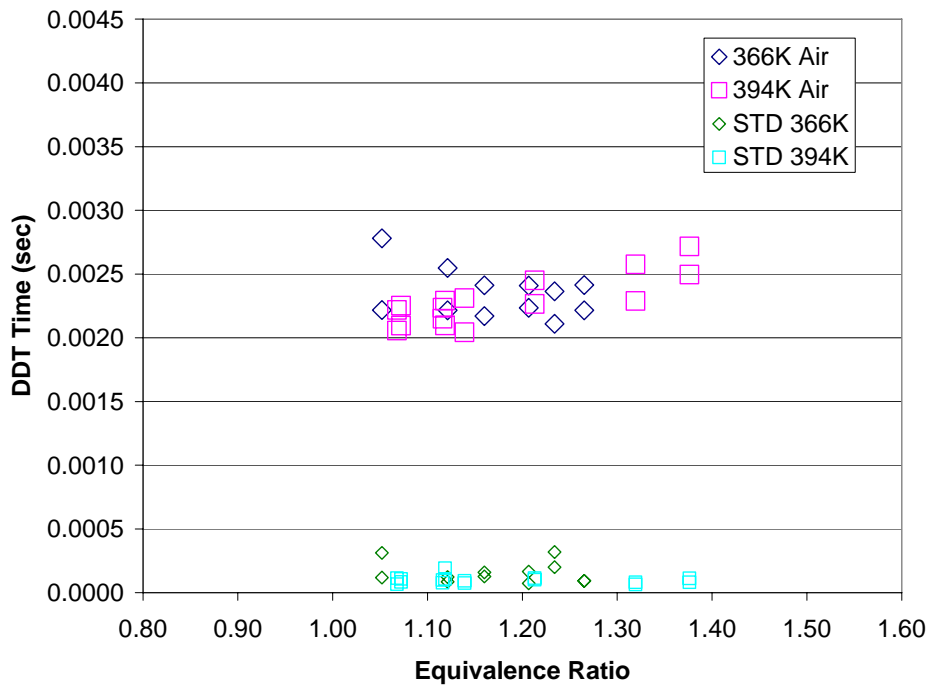
Figure 6.27 JP-8 combustion wave times to second sensor at a 6 ms spark delay, 300 K fuel.
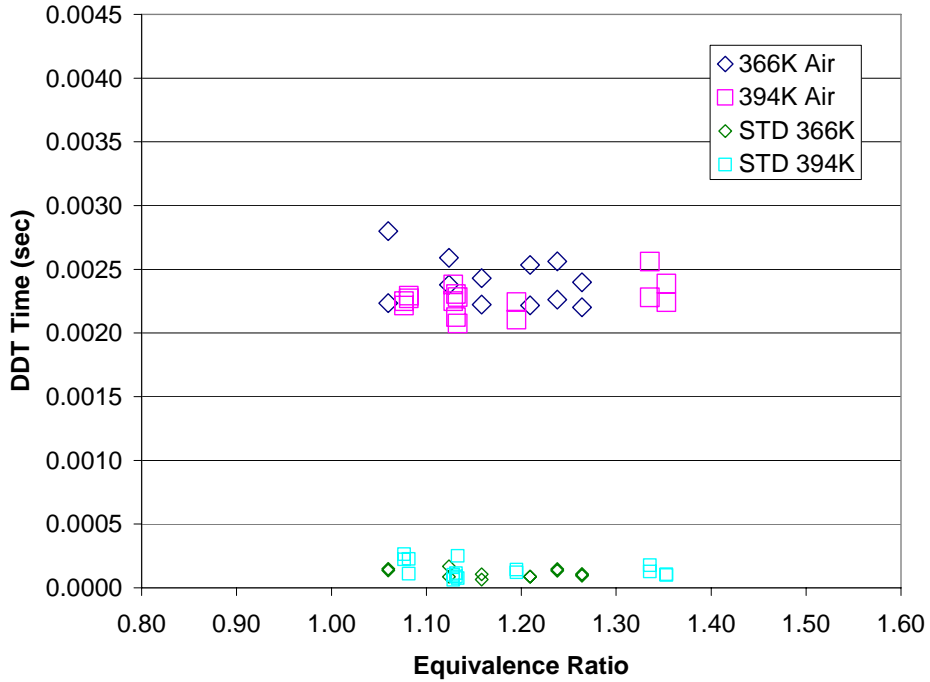
Figure 6.28 JP-8 combustion wave times to second sensor at an 8 ms spark delay, 300 K fuel.

For the 473 K temperature fuel DDT data shown in Fig. 6.29 and Fig. 6.30, the variation from tube to tube is much smaller. Also important is the improved operating stoichiometry discussed with the ignition results. The minimum DDT time occurs near an equivalence ratio of 1.1. This agrees well with the minimum cell size relationship to equivalence ratio occurring near a value of one (Fig. 2.12). The minimum cell size then correlates to detonation initiation energy (Fig. 2.10) which means the smaller the cell size the more easily the fuel can be detonated. The JP-8 DDT times are near that of n-heptane and thus require a similar distance of roughly 1 meter to achieve the DDT at an equivalence ratio of one
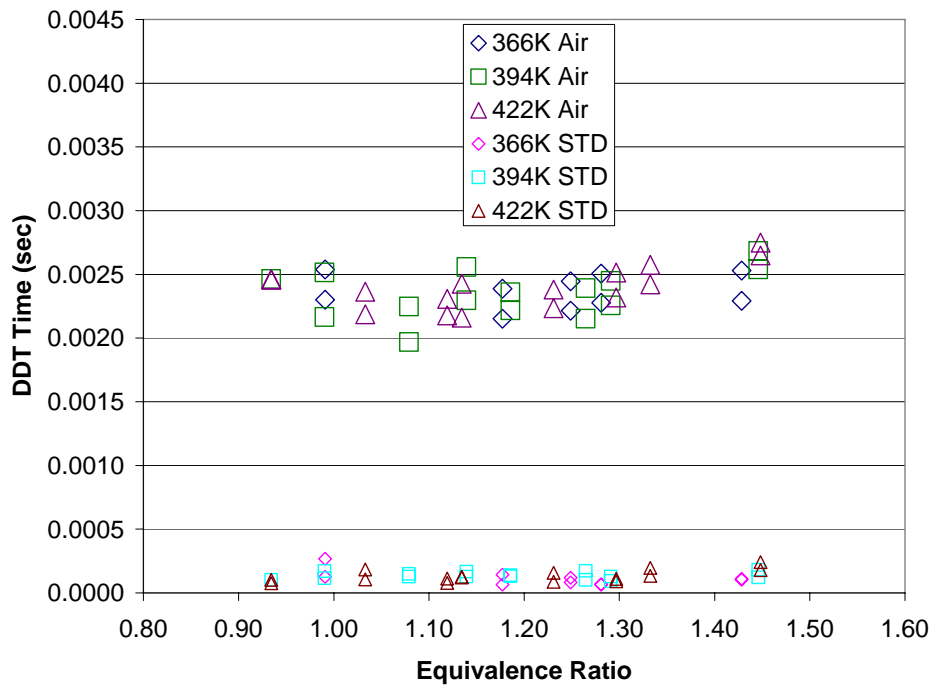
Figure 6.29 JP-8 combustion wave times to second sensor at a 6 ms spark delay, 473 K fuel.
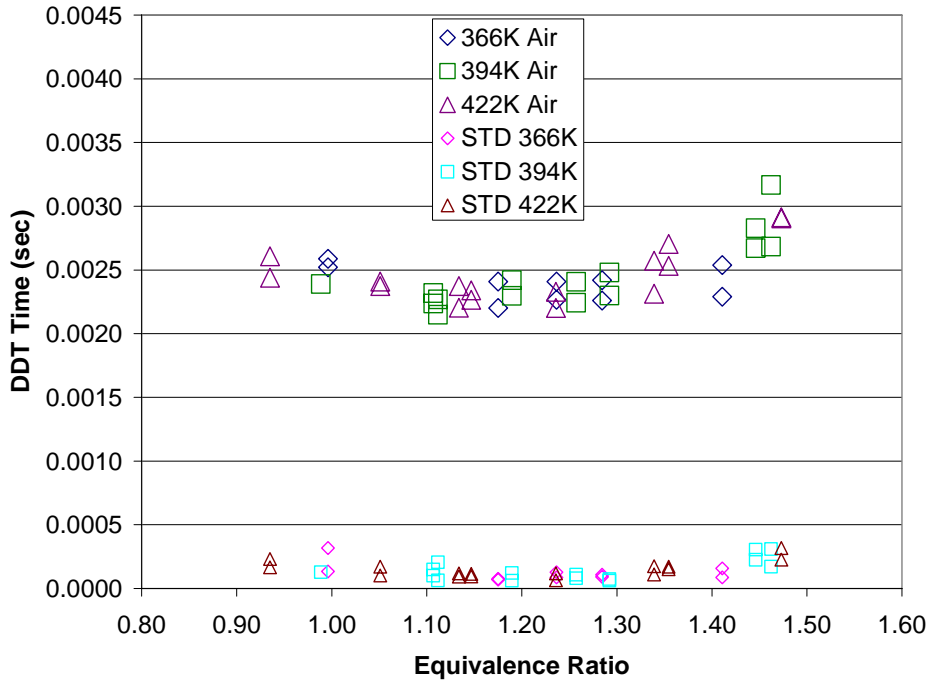
Figure 6.30 JP-8 combustion wave times to second sensor at an 8 ms spark delay, 473 K fuel.

As the fuel temperature is further increased to 555 K, the variation from tube to tube is much smaller and the minimum DDT time shifts to an equivalence ratio near 1. The minimum DDT time is 2.27 ms (± 0.15 ms) for the 6 ms spark delay (Fig. 6.31) and a value of 2.35 ms (± 0.2 ms) at the 8 ms spark delay case (Fig. 6.32).
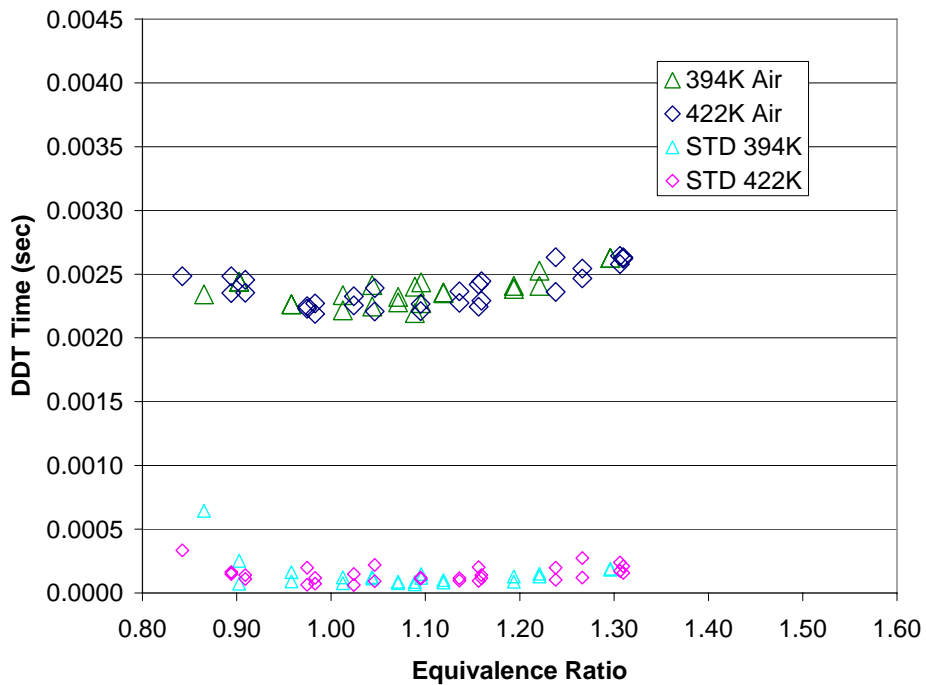
Figure 6.31 JP-8 combustion wave times to second sensor at a 6 ms spark delay, 555 K fuel.
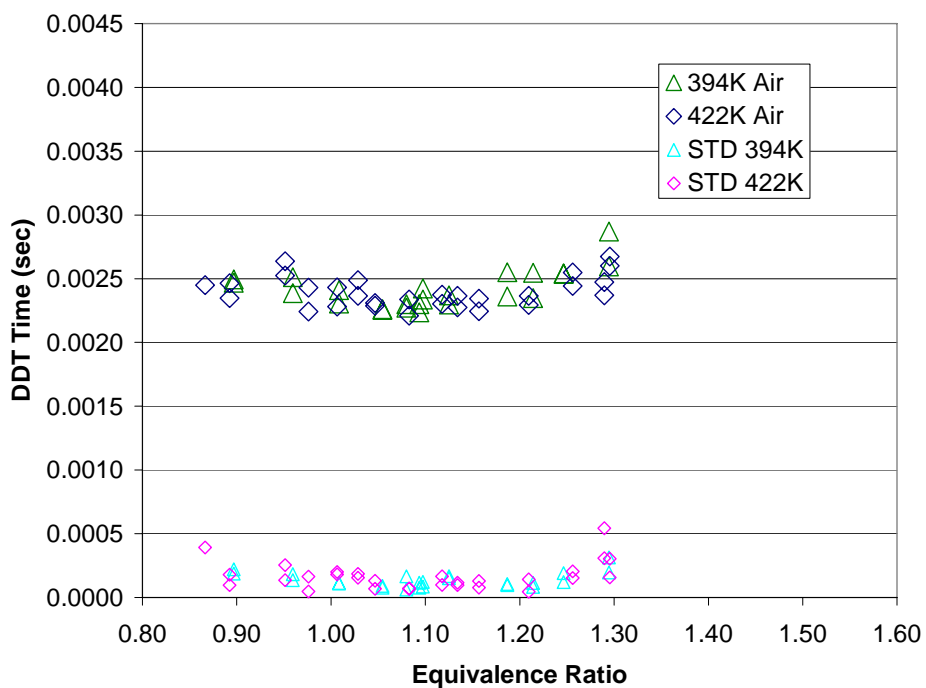
Figure 6.32 JP-8 combustion wave times to second sensor at an 8 ms spark delay, 555 K fuel.

The DDT times captured for the three fuel and three air temperatures are plotted in Fig. 6.33 for the 8 ms spark delay case. The DDT times do not significantly differ in magnitude for the given range in fuel and air temperatures. The lean limiting equivalence ratio is dependent on the fuel and air temperatures described earlier in the ignition data and are denoted by the three vertical lines. As the fuel and air temperatures increase, the lines progressively shift to the leaner equivalence ratio as more fuel transitions from liquid to vapor.
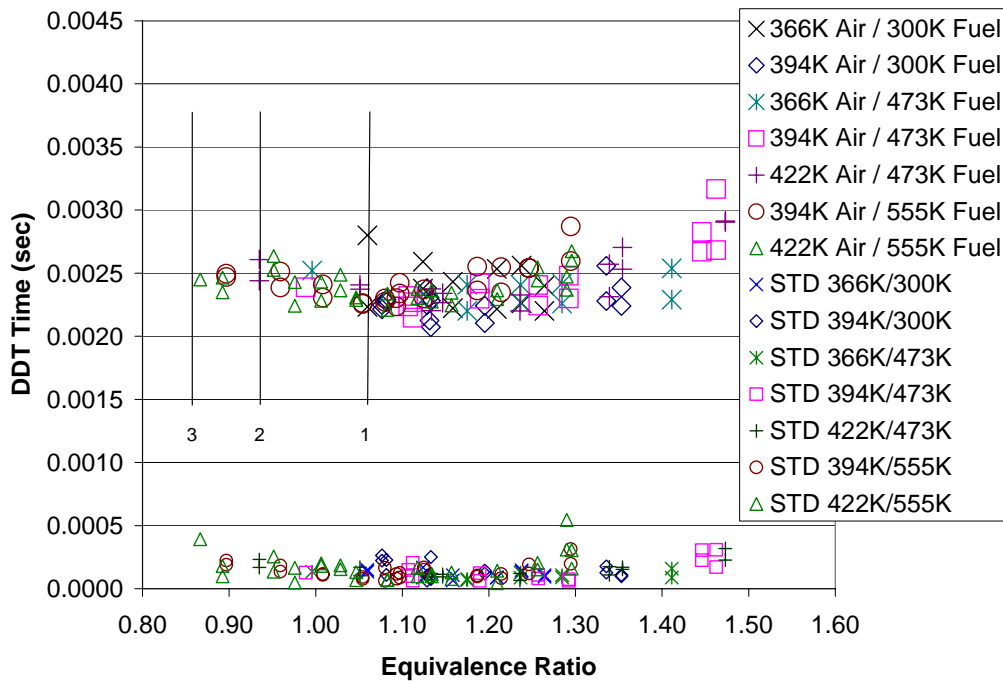
Figure 6.33 JP-8 combustion wave times to second sensor at an 8 ms spark delay, all data. Raising fuel and air temperature causes the minimum equivalence ratio to shift from line 1 (300 K fuel), line 2 (473 K fuel) to line 3 (555 K fuel).

Combustion Wave Speeds

The combustion wave speed is the primary method to determine whether or not a detonation occurred. How the wave speed changes with equivalence ratio provides insight into understanding the detonability of the different fuels using the transition

129

methods described in Chapter II. The theoretical Chapman-Jouguet (CJ) wave speed varies with equivalence ratio as shown in Fig. 6.34, and shows that most hydrocarbon fuels with air as the oxidizer reach a maximum steady state wave speed near an equivalence ratio of 1.3. Since the minimum energy required to generate a detonation goes up with mixtures off stoichiometric, detonations may not be achievable for all the equivalence ratios plotted. Combustion waves are usually considered detonations if the velocity was within ± 10% of the predicted CJ velocity. [86] During this research, the average wave speeds were taken at locations before and after the spiral at locations given in Table 6.3. The WS1 location is the average distance between sensors one and two near the exit of the spiral. The WS2 location is the average distance between sensors two and three after the exit of the spiral. See Fig. 3.15 for the tube setup schematic.
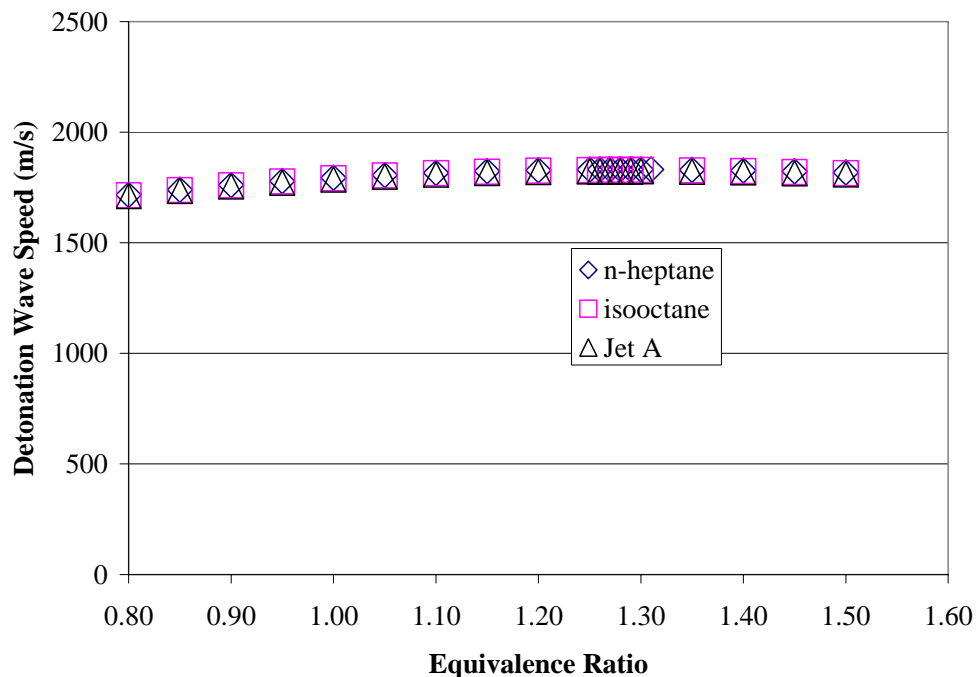
Figure 6.34 Theoretical Chapman-Jouguet detonation wave speeds for gaseous fuels with air at 298 K and 1 atm. Data from Ref. 34.

130

Table 6.3 Average wave speed and spiral locations in the thrust tube dimensions.

Tube	WS1 (m)	Spiral exit (m)	WS2 (m)
One	1.197	1.271	1.356
Four	1.202	1.277	1.353

The combustion wave speed plots used make a characteristic horseshoe shape (∩) representative of the inability to achieve detonations (i.e. lower wave speed) at the limiting equivalence ratios both lean and rich of stoichiometric. When detonations are not achieved, the values of the combustion waves often drop below 1000 m/s. The detonation cell size increases at a much greater rate as the mixture becomes leaner (Fig. 2.11); therefore, the energy required to generate a detonation at leaner mixtures is greater than for a similarly rich mixture. At the equivalence ratios where detonation wave speeds are at the rich and lean limits, the wave speed standard deviations are much higher. The increase in the standard deviation is due the combustion waves within the data set either not achieving a detonation or capturing an overdriven transitioning detonation wave. The theoretical CJ speed was not calculated for the aviation gasoline but was expected to agree well the other hydrocarbon fuels plotted previously in Fig. 6.34 because the heat release for most hydrocarbon fuels is similar.

Many of the combustion waves exiting the spiral (WS1) are at overdriven conditions. That is, the wave speeds exceed the Chapman-Jouguet wave speed as a result of the transition process, and the wave has not yet settled to the steady state value. The wave speeds at the second set of sensors (WS2) have relaxed to the steady state Chapman-Jouguet wave speeds. The two tubes, however, often do not measure the same wave speed despite the near identical geometries. The variation between the two tubes is

possibly due to either broken portions of the DDT spiral or mixing variations between the two tubes. The fuel and air mixture nearest the open end of the PDE thrust tubes moves in and out of the tube during the filling process as a result of expansion and compression waves traveling in the tube. This process could lean out the mixture at the open end of the tube and may cause the steady state wave speed to decrease (Fig. 6.34). This reduction in wave speed was not totally understood.

Aviation Gasoline Wave Speed Data

The aviation gasoline data in Figs. 6.35 to 6.38 match well with the CJ theoretical velocity trend denoted by the solid line and shown previously in Fig. 6.34. The range of detonable equivalence ratios widened when the fuel was heated as summarized in Table 6.4. Several of the limits were not captured and marked with the greater than and less than symbols. Aviation gasoline, like JP-8, is a multi-component fuel made up with various hydrocarbons to obtain combustion performance that falls within a prescribed specification. The specific components in the fuel differ between manufacturers, though most all aviation gasolines contain a lead additive to increase ON. The heating process used in the FVS widens the detonable range of aviation gasoline equivalence ratio because the tetraethyl lead reacted with the ethylene dibromide within the fuel. The newly formed lead sludge came out of solution and remained in the furnace during operations. Since the lead remained in the furnace, the fuel ON is effectively lowered by some unknown amount.

132

Table 6.4 Detonation equivalence ratio limits for unheated and heated aviation gasoline.

	6 ms case		8 ms case	
	lean	rich	lean	rich
unheated	0.95	1.25 - 1.3	< 1.01	1.25 - 1.3
heated	0.88	1.19 <	< 0.91	1.22 <

The standard deviations of the aviation gasoline wave speeds are higher as a result of the detonations transitioning later in the spiral and measured prior to the wave settling to the steady state (CJ) value. For the four aviation gasoline wave speed figures, the lowest standard deviations occur near an equivalence ratio of one, nearest the condition where the detonation requires the least amount of energy to be directly initiated. At this mixture condition, a steady state detonation wave speed has been measured and corresponds to an earlier detonation transition in the spiral. The standard deviations in Fig. 6.38 are the lowest for the four figures and are a result of the higher thermal equilibrium of the 8 ms case being taken later during a data acquisition run. As a side note, the two points (x) circled in Fig. 6.35 were unique in that the detonation did not transition until after the spiral noted by the upper circle (o) at an overdriven wave speed.
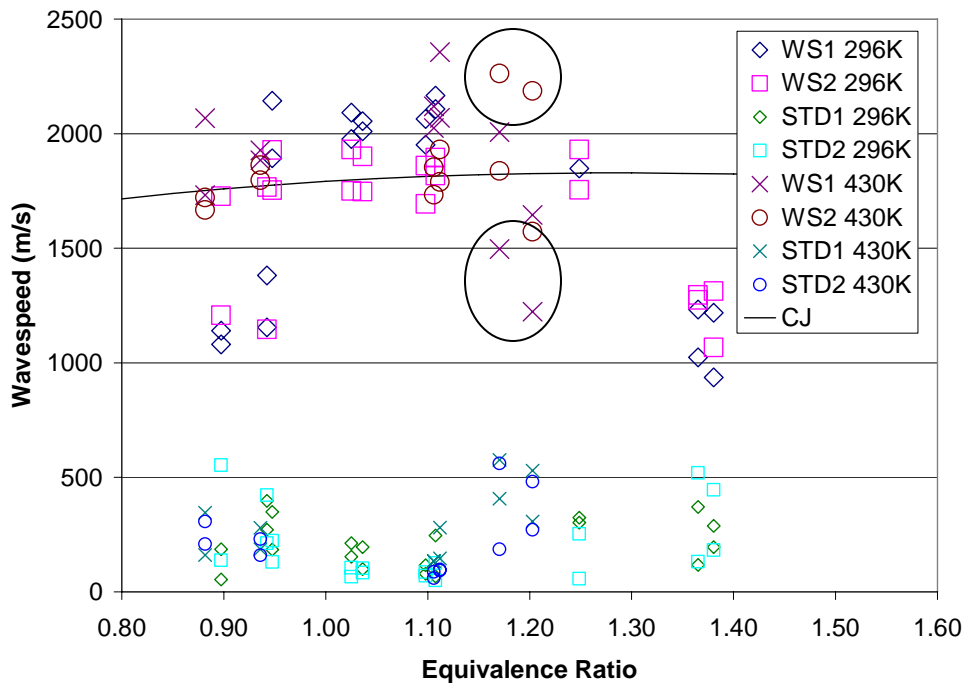
Figure 6.35 Aviation gasoline wave speeds at both WS1 and WS2 at a 6 ms spark delay and 296 K and 430 K fuel. Circles denote late transitioning detonation.
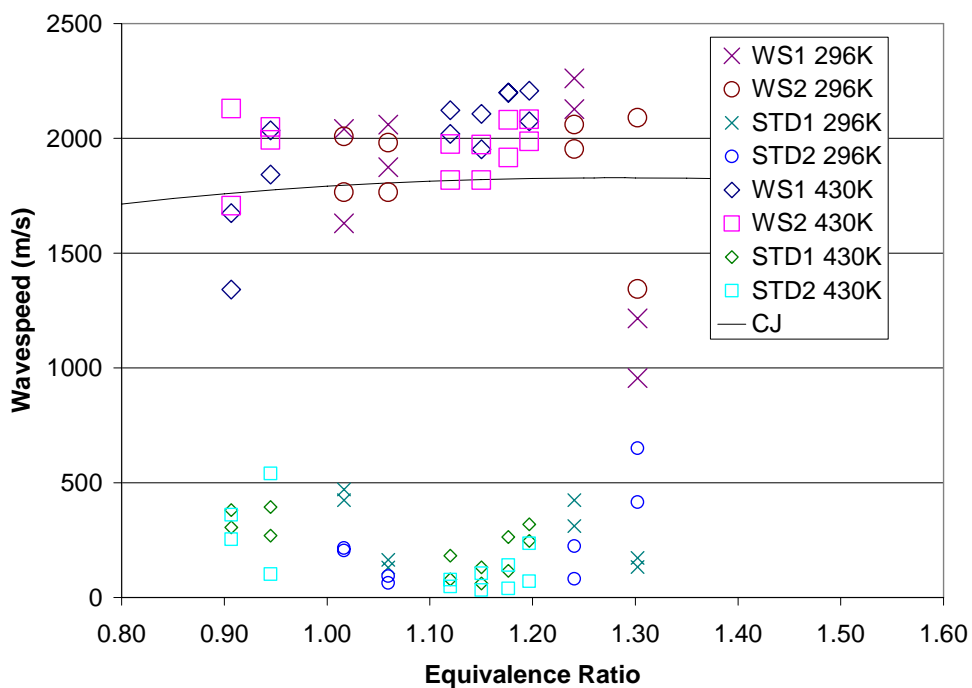
Figure 6.36 Aviation gasoline wave speeds at both WS1 and WS2 at an 8 ms spark delay and 296 K and 430 K fuel.
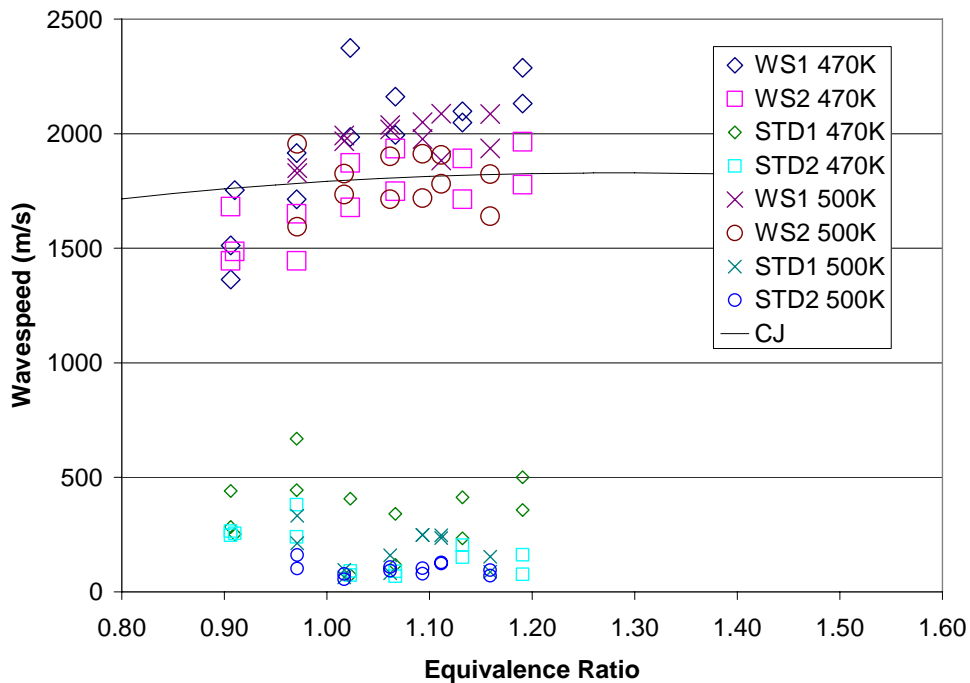
Figure 6.37 Aviation gasoline wave speeds at both WS1 and WS2 at a 6 ms spark delay an 470 K and 500 K fuel.
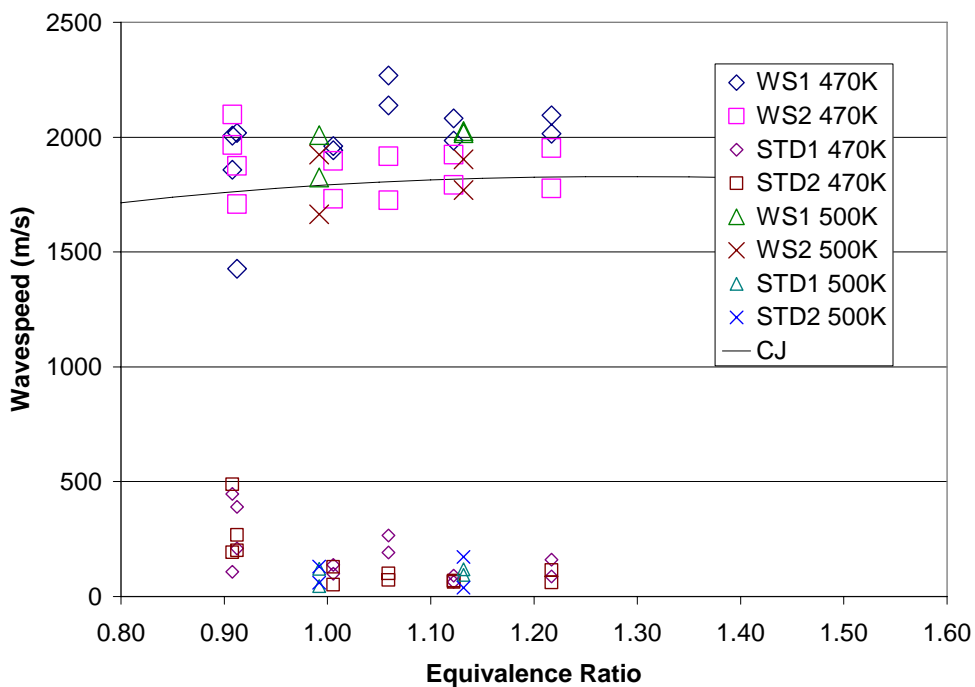
Figure 6.38 Aviation gasoline wave speeds at both WS1 and WS2 at an 8 ms spark delay and 470 K and 500 K fuel.

Isooctane Wave Speed Data

The isooctane fuel was the most difficult to detonate and had the smallest range of detonable equivalence ratio operation from 0.95 to 1.18 (Fig. 6.39 to Fig. 6.42). A longer DDT spiral may have widened the detonable equivalence ratio for this fuel and air mixture. The spiral length, however, was kept constant (1.22 m) for all fuels tested in this work. Earlier tests showed that detonations could not be achieved for any equivalence ratio for the isooctane and air mixture with a 0.914 m spiral.
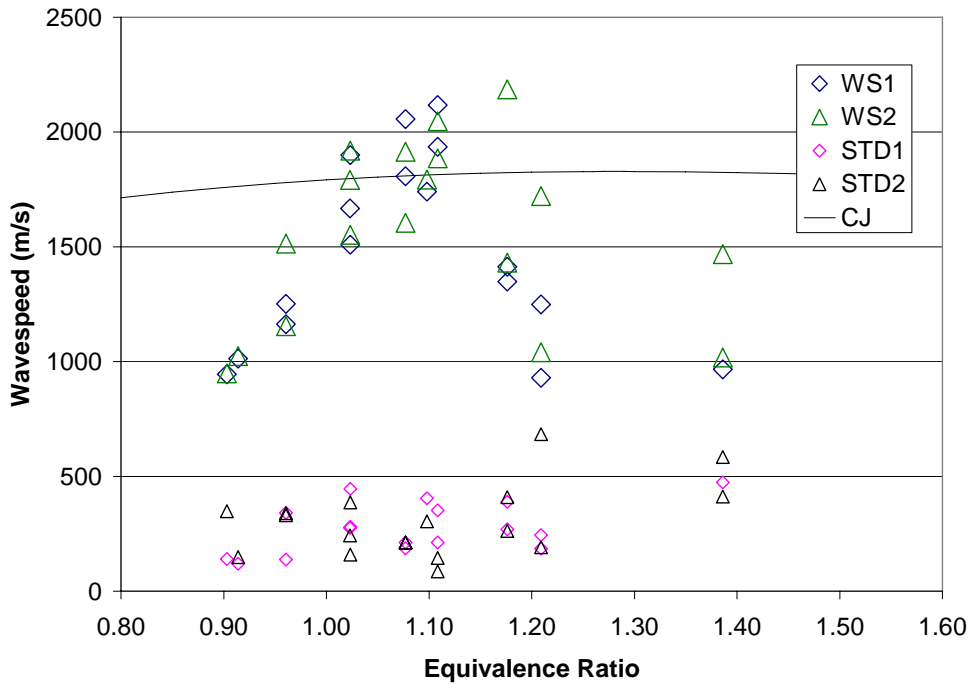
Figure 6.39 Isooctane wave speeds at both WS1 and WS2 for a 6 ms spark delay and 297 K fuel.
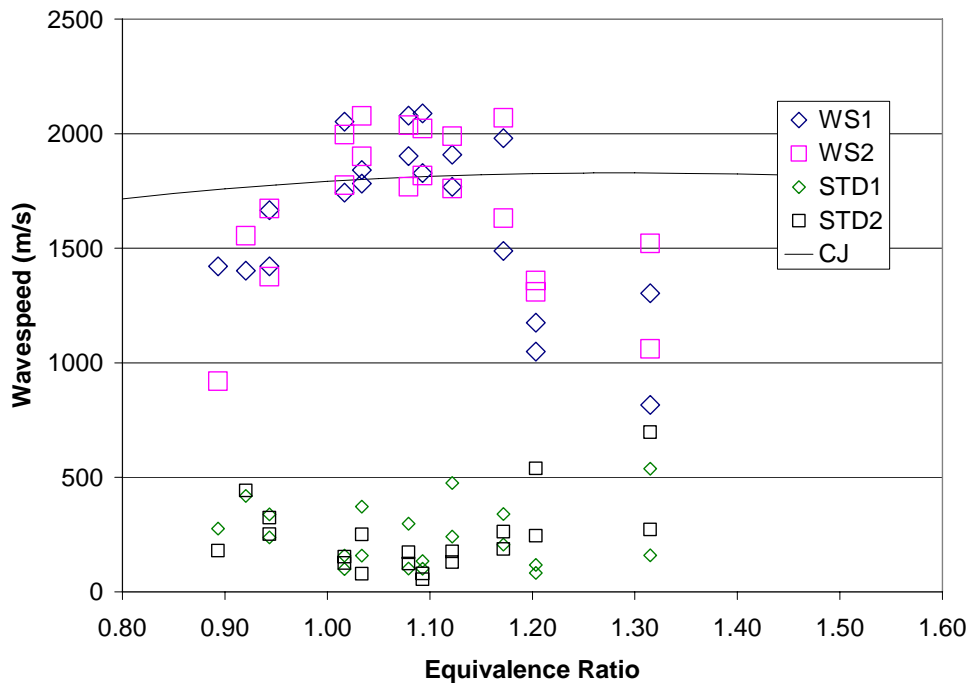
Figure 6.40 Isooctane wave speeds at both WS1 and WS2 for an 8 ms spark delay and 297 K fuel.
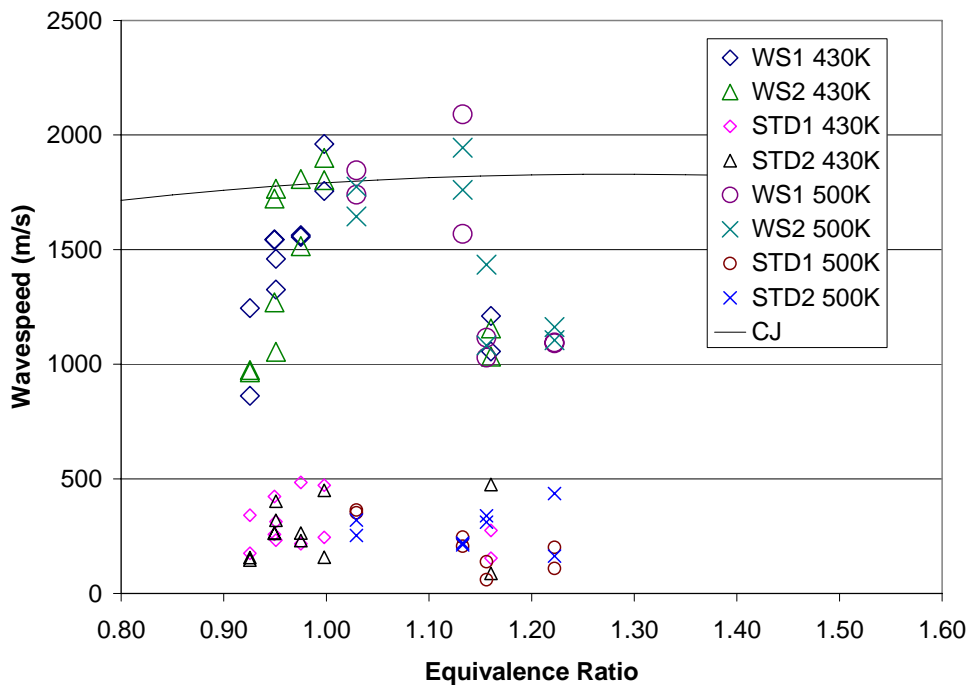
Figure 6.41 Isooctane wave speeds at both WS1 and WS2 for a 6 ms spark delay and 430 K and 500 K fuel.
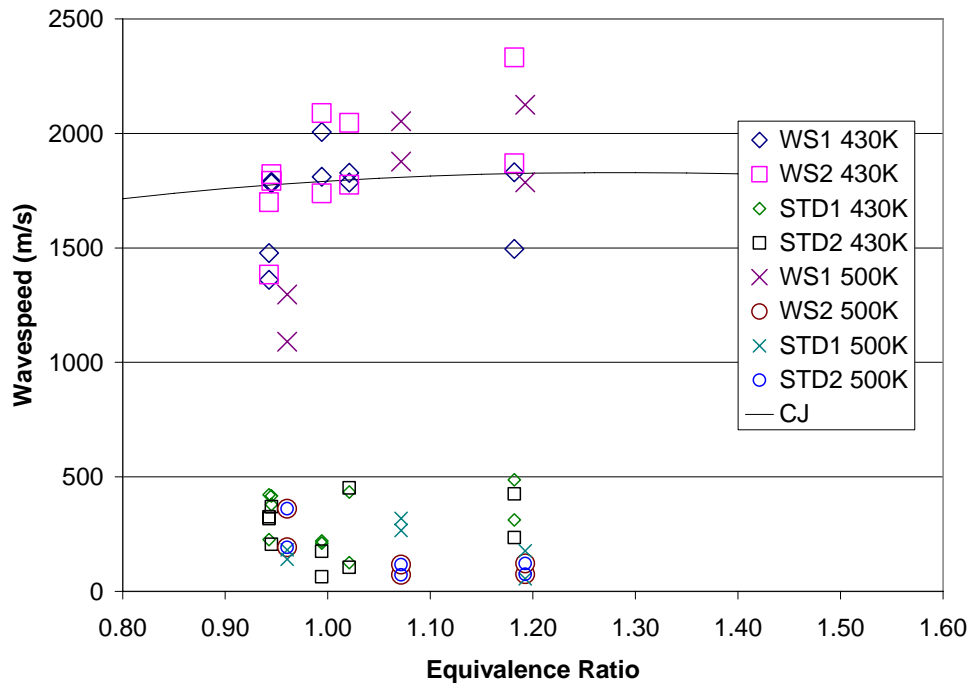
Figure 6.42 Isooctane wave speeds at both WS1 and WS2 for an 8 ms spark delay and 430 K and 500 K fuel.

For both the aviation gasoline and isooctane data (Figs. 6.35 to 6.42), the standard deviations of the wave speeds were between 100 m/s and 500 m/s and much larger than the standard deviations of the n-heptane and JP-8 (Figs. 6.43 to 6.58). The higher standard deviations are expected due to the late detonation transition observed with the higher ON aviation gasoline and isooctane. The standard deviations would be smaller if a longer tube and spiral were used to transition to the detonation. These two modifications would allow the detonation to settle to the steady CJ speed, and sensors placed further down the tube would measure fewer overdriven transitioning detonation waves and instead encounter more steady state values.

n-Heptane Wave Speed Data

On a similar experimental setup, n-heptane has been shown to transition to a detonation at around 1 meter[32] and is roughly 12 cm before the first wave speed sensor used in this experimental setup. The n-heptane (Figs. 6.43 to 6.46) wave speeds are at or near the Chapman-Jouguet wave speed. The absence of overdriven wave speeds is a result of the detonations occurring earlier in the PDE thrust tube and reaching the steady state values prior to the first set of ion sensors. In fact, the wave speed data at WS1 is within $\pm 5\%$ of the CJ wave speed. The wave speeds at the second set of sensors, however, have dropped to a value roughly 10% below the CJ point at stoichiometric.

Most of the standard deviation values for the n-heptane (Figs. 6.43 to 6.46) are in the range of 10% or lower. The rich detonation limits were not reached and only one lean limit (Fig. 6.45) was measured at 0.93. The lower equivalence ratio limit for the 8 ms spark delay and heated fuel (Fig. 6.46) had not been reached by an equivalence ratio of 0.91. Again, the steady state thermal conditions in the tube were more influential than the fuel injection temperature for the high vapor pressure fuels.
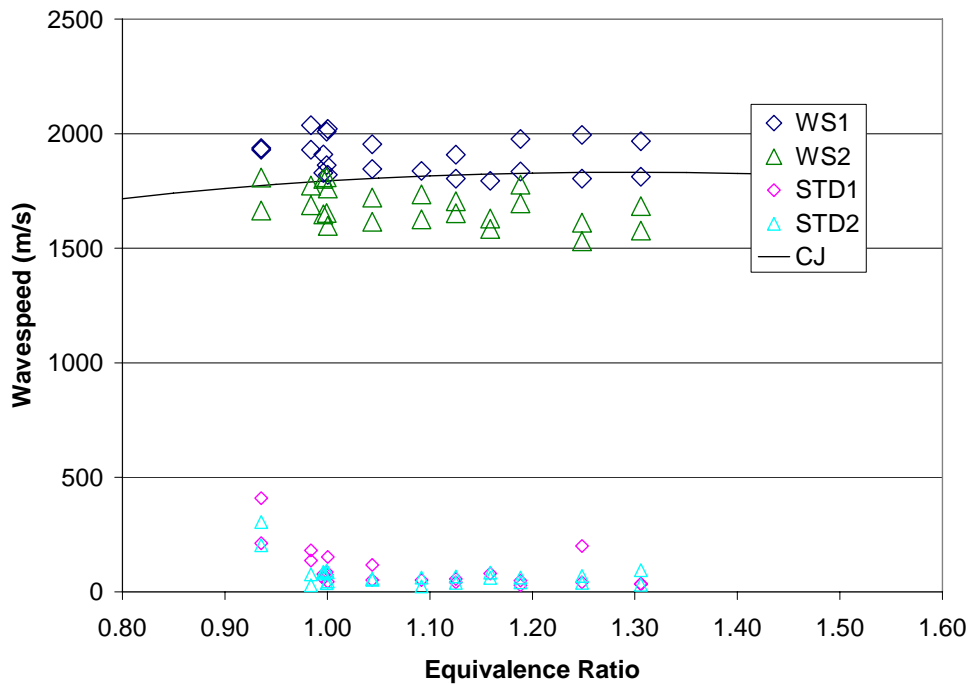
Figure 6.43 n-Heptane wave speeds at both WS1 and WS2 for a 6 ms spark delay and 298 K fuel.
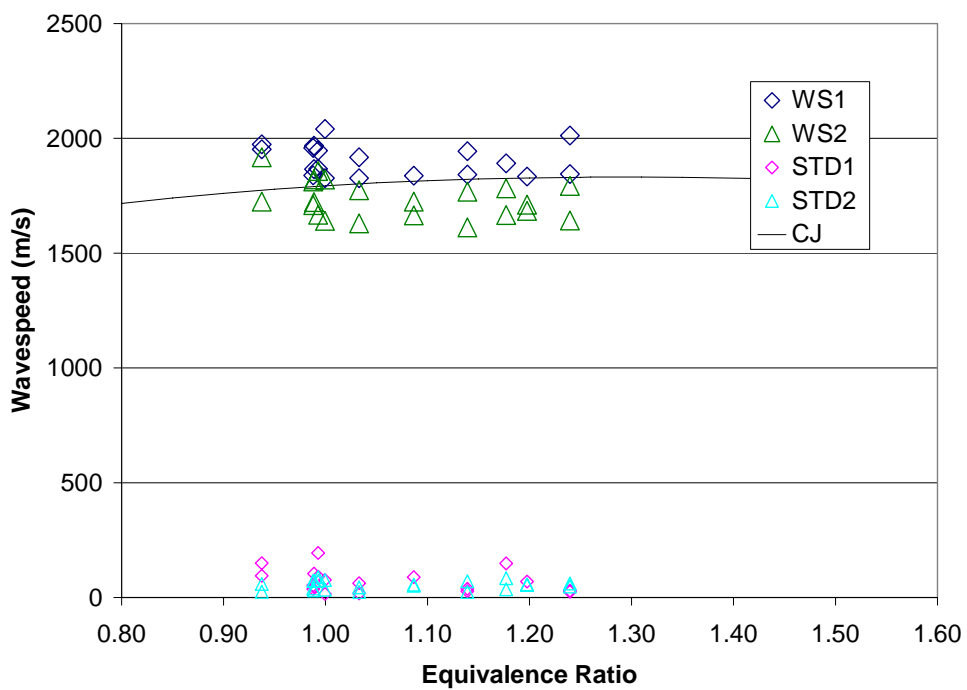
Figure 6.44 n-Heptane wave speed for an 8 ms spark delay and 298 K fuel.
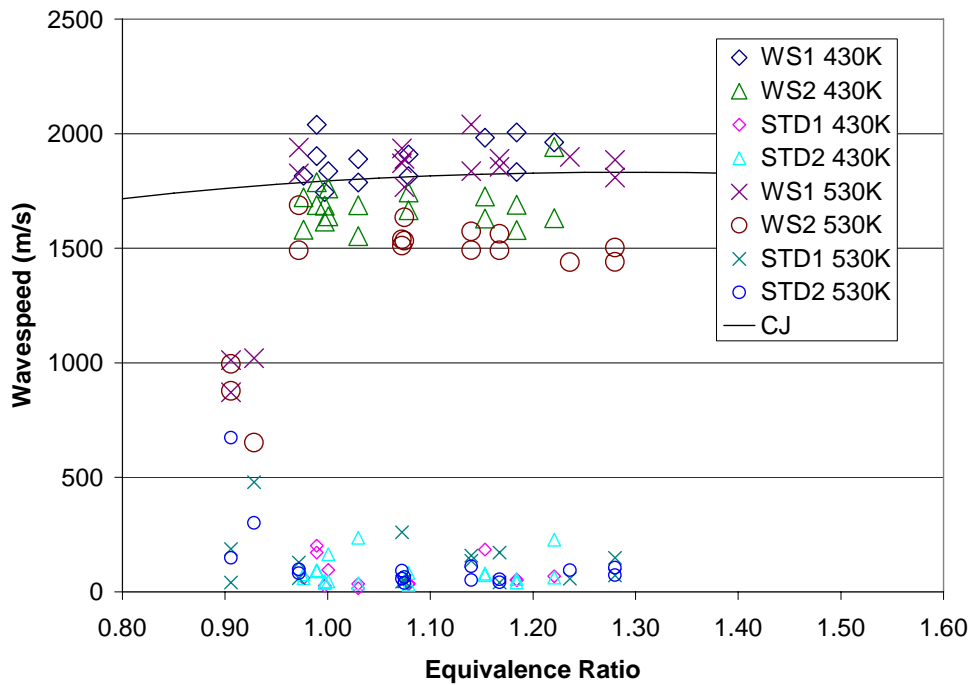
Figure 6.45 n-Heptane wave speed for a 6 ms spark delay and 430 K and 530 K fuel.
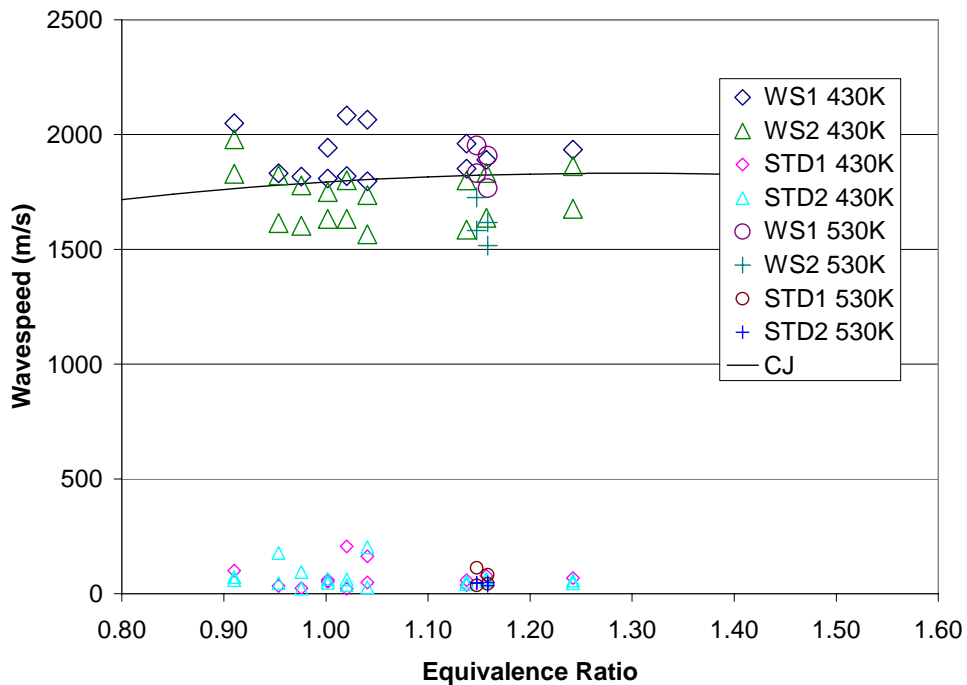
Figure 6.46 n-Heptane wave speed for an 8 ms spark delay and 430 K and 530 K fuel.

JP-8 Wave Speed Data

As stated previously, the JP-8 wave speed data was taken with the spark delays reversed, that is the 8 ms spark delay was taken first and the 6 ms spark delay second. Reversing the spark delay order was an effort to determine if the slight pressure change or the increase in thermal equilibrium was the stronger influence. The later data set (6 ms) had lower wave speed standard deviations and a slightly lower pressure. Since a higher pressure should make an easier transition to a detonation (Fig. 2.13), the steady state detonation waves observed at the 6 ms spark delay were due to a higher thermal equilibrium within the thrust tube.

The unheated (300 K) JP-8 and air mixture did not ignite (within the required timeframe) at equivalence ratios of less than 1.05. Once ignition was achieved, however, the fuel was readily detonated. The earlier data sets (8 ms) shown in Fig. 6.50 and Fig. 6.51 had consistently larger wave speed standard deviations and a narrower range of detonability on the lean side of 1.12 (Fig. 6.50) compared to the 1.05 (Fig. 6.48) for the 6 ms spark delay case. Regardless of spark delay, the wave speeds again slow down from WS1 (Fig. 6.47 and Fig. 6.49) within the spiral to the steady state values at WS2 (Fig. 6.48 and 6.50).
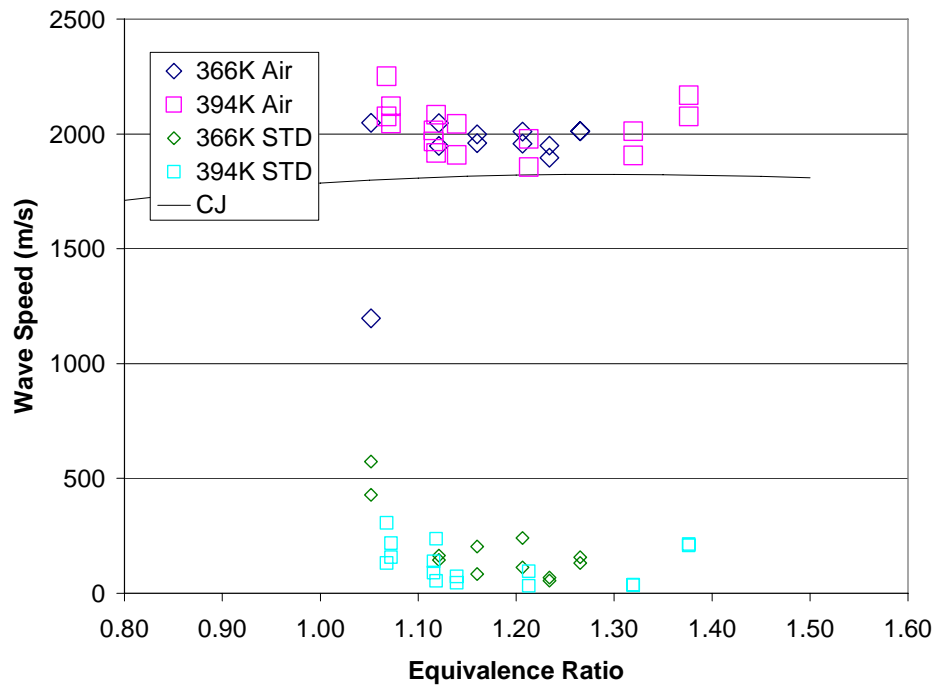
Figure 6.47 JP-8 at 300 K with a 6 ms spark delay at the WS1 location.
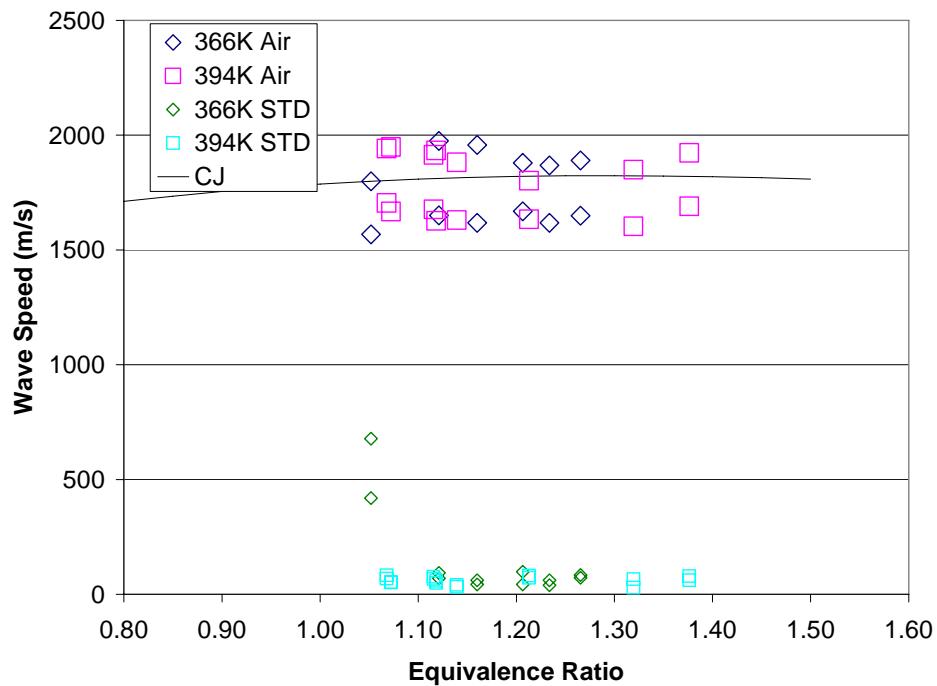
Figure 6.48 JP-8 at 300 K with a 6 ms spark delay at the WS2 location.

143
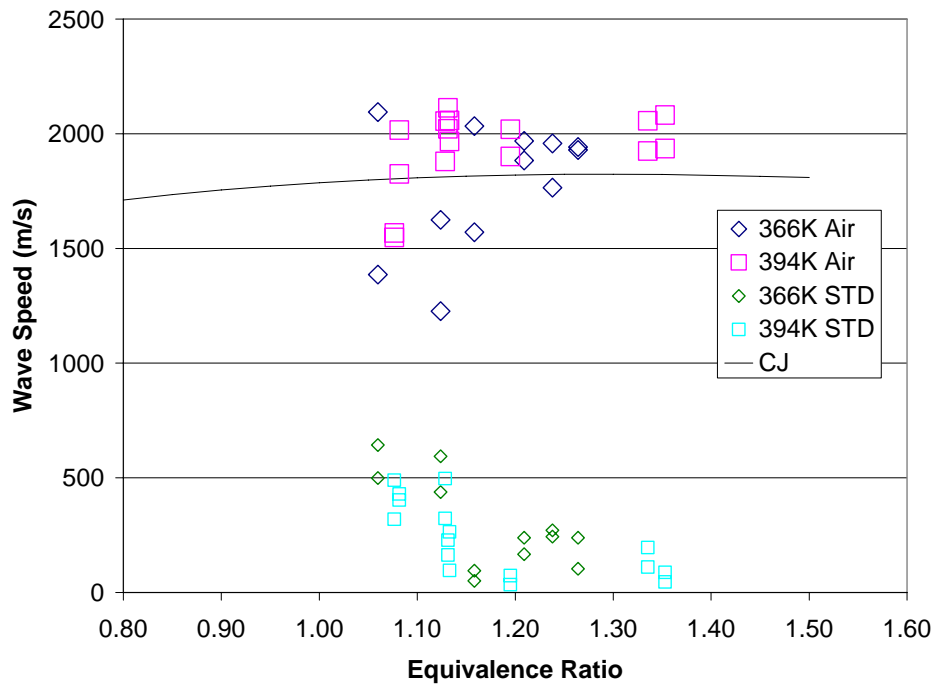
Figure 6.49 JP-8 at 300 K with an 8 ms spark delay at the WS1 location.
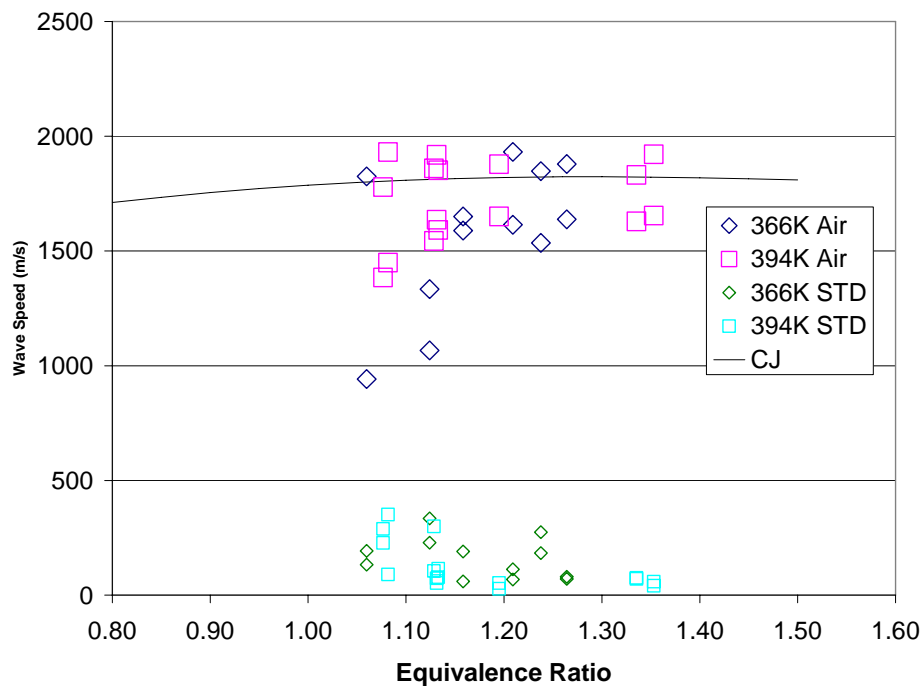
Figure 6.50 JP-8 at 300 K with an 8 ms spark delay at the WS2 location.

The fuel was heated to 473 K (Figs. 6.51 to 6.54) and is still below the predicted liquid vapor equilibrium line (Fig. 5.10). As in the unheated case, the standard deviations are much lower for the 6 ms spark delay wave speeds and reflect the improved performance at this hotter tube condition. The wave speed standard deviations reach a minimum at an equivalence ratio between 1.2 and 1.3. The minimum occurs at an equivalence ratio where the detonation is easiest to achieve (or transition) and represents where the mixture effectively behaves at stoichiometric. As will be shown later with the 555 K data, the minima will shift lean to a value near an equivalence ratio of 1.05 when all of the droplets are eliminated and the mixture exists above the predicted liquid vapor equilibrium line.

The lean equivalence ratio detonability limit has shifted lower due to the ignition being achieved at a leaner equivalence ratio and a higher percentage of fuel vapor. The rich detonability limit is first observed when the mixture approaches an equivalence ratio of 1.47 (Fig. 6.53 and 6.54).
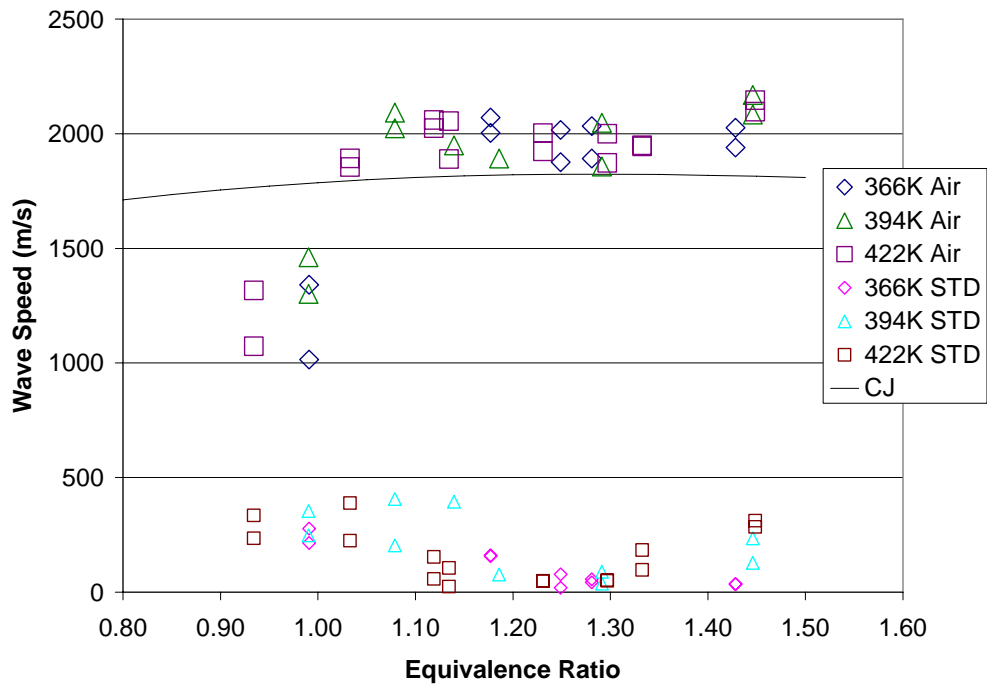
Figure 6.51 JP-8 at 473 K with a 6 ms spark delay at the WS1 location.
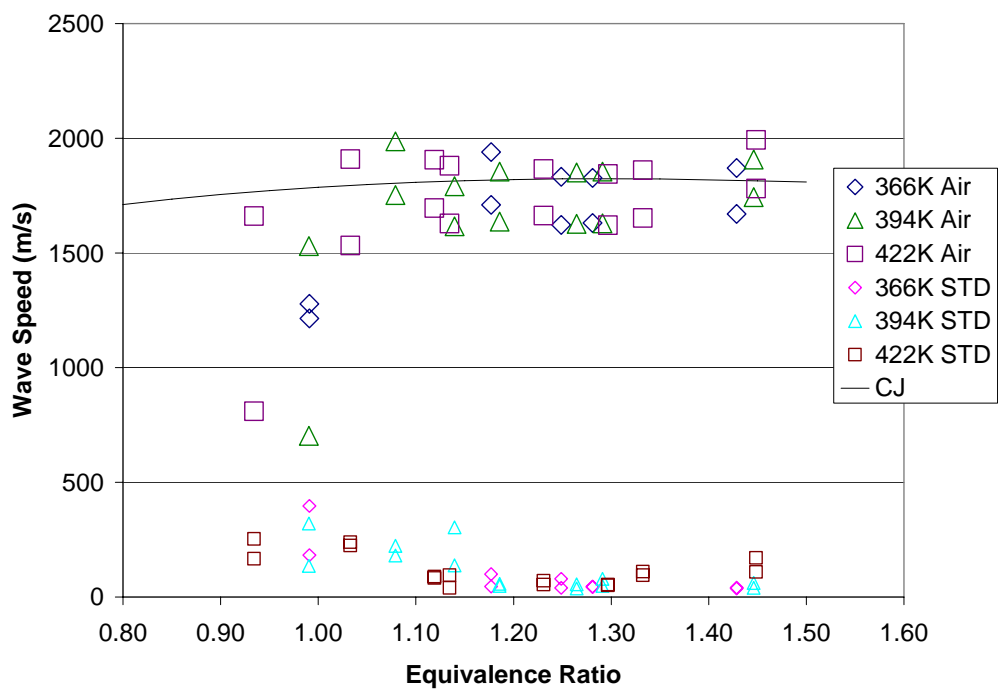
Figure 6.52 JP-8 at 473 K with a 6 ms spark delay at the WS2 location.

146
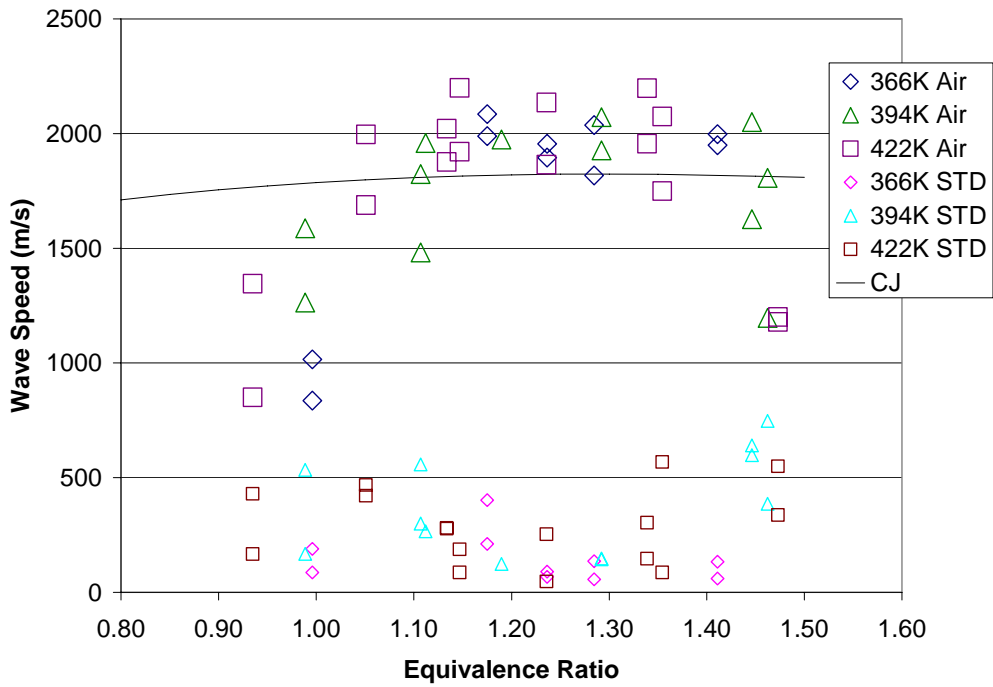
Figure 6.53 JP-8 at 473 K with an 8 ms spark delay at the WS1 location.
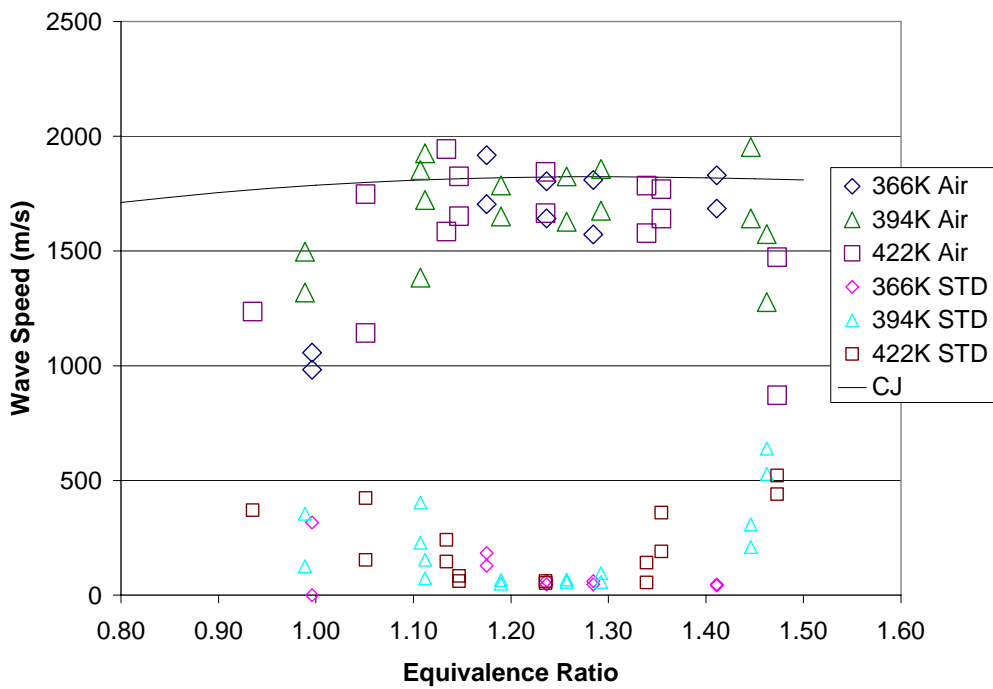
Figure 6.54 JP-8 at 473 K with an 8 ms spark delay at the WS2 location.

The fuel temperature is increased above the flash vaporization temperature to 555 K, and two primary effects are observed in Figs. 6.55 to Fig. 6.58. The biggest improvement is the reduced overall standard deviations for a wider range of equivalence ratios for both spark delays when compared to the same ranges of the lower fuel injection temperatures. With a 6 ms spark delay, the wave speed standard deviations are large from equivalence ratios from 0.84 to 1.0, denoting the increased difficulty achieving consistent detonations at those conditions. From 1.0 to 1.3, however, the standard deviations are less than 100 m/s or 6.5% of the measured values. At the 8 ms spark delay, taken earlier during the run, the range of equivalence ratios where small standard deviations were observed decreased from 0.25 (Fig. 6.55) to 0.15 (Fig. 6.57). The ability of the fuels to detonate at off stoichiometric conditions improves with longer run times and increased tube temperature at the later data set (6 ms) spark delay.
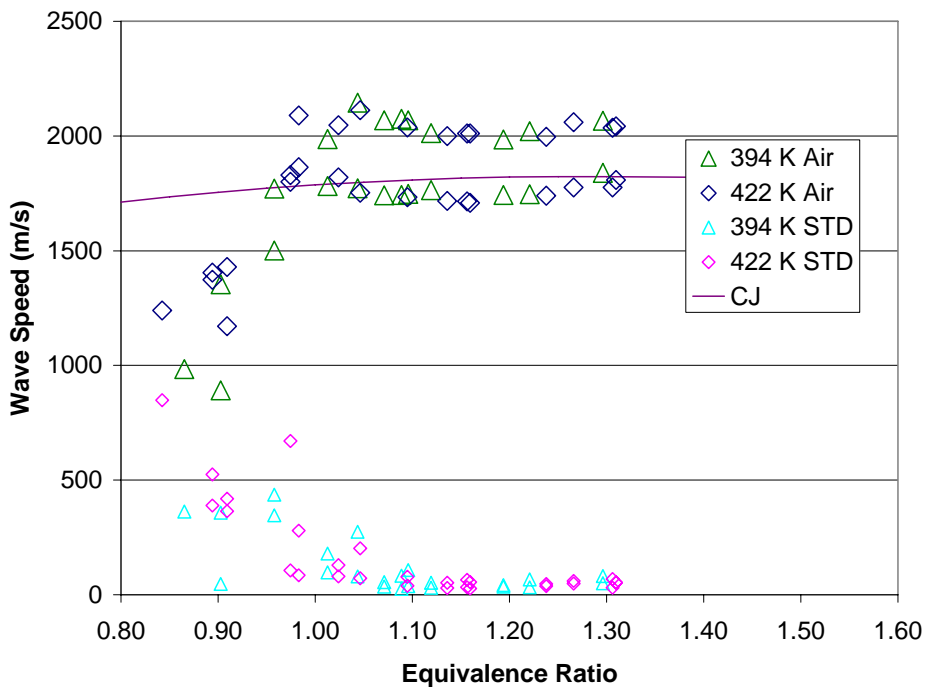
Figure 6.55 JP-8 at 555 K with a 6 ms spark delay at the WS1 location.
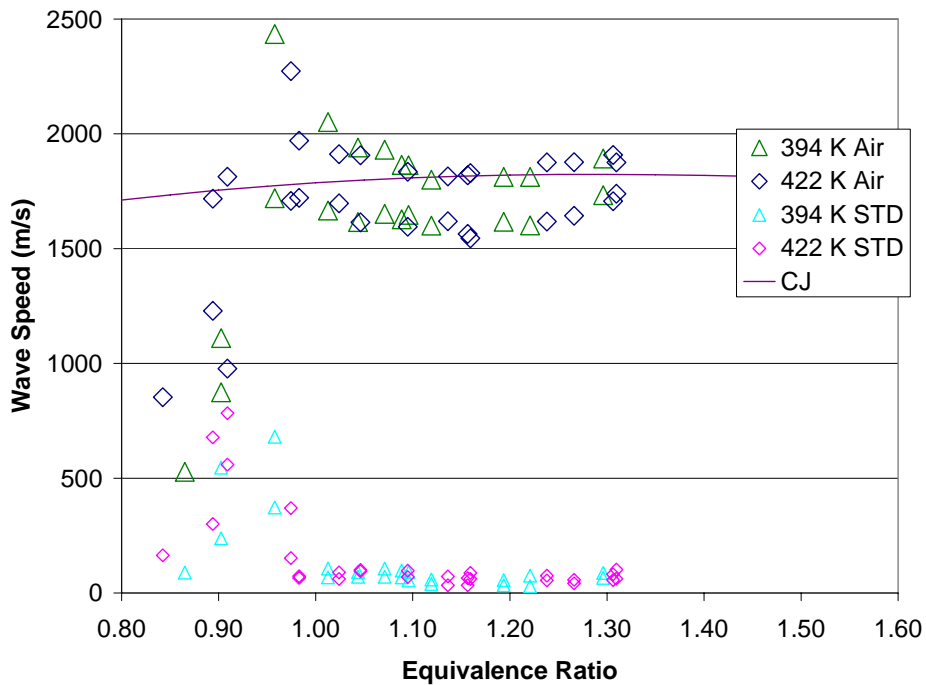
Figure 6.56 JP-8 at 555 K with a 6 ms spark delay at the WS2 location.
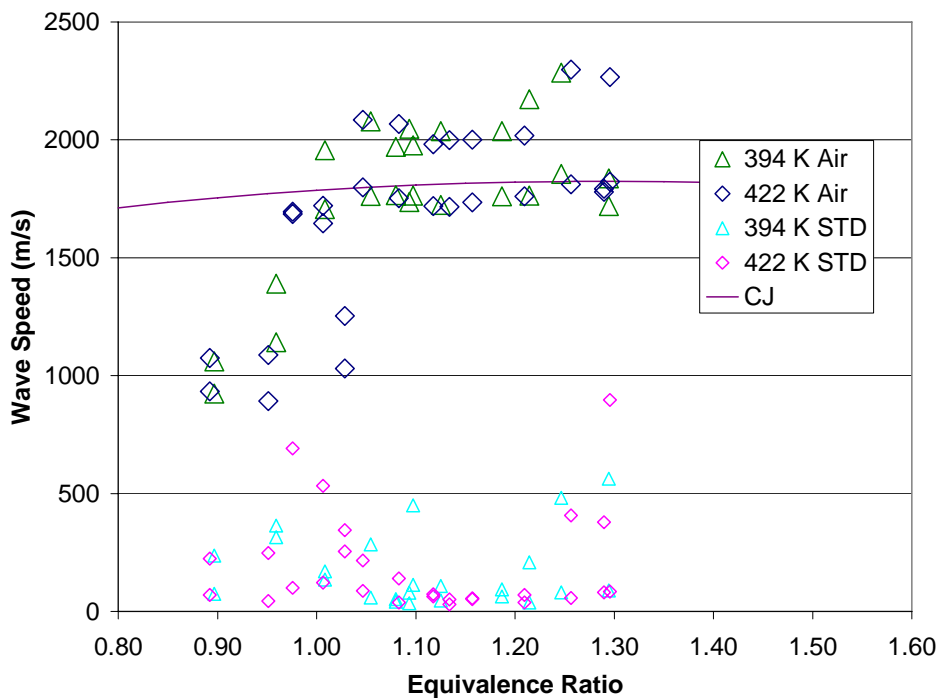
Figure 6.57 JP-8 at 555 K with an 8 ms spark delay at the WS1 location.
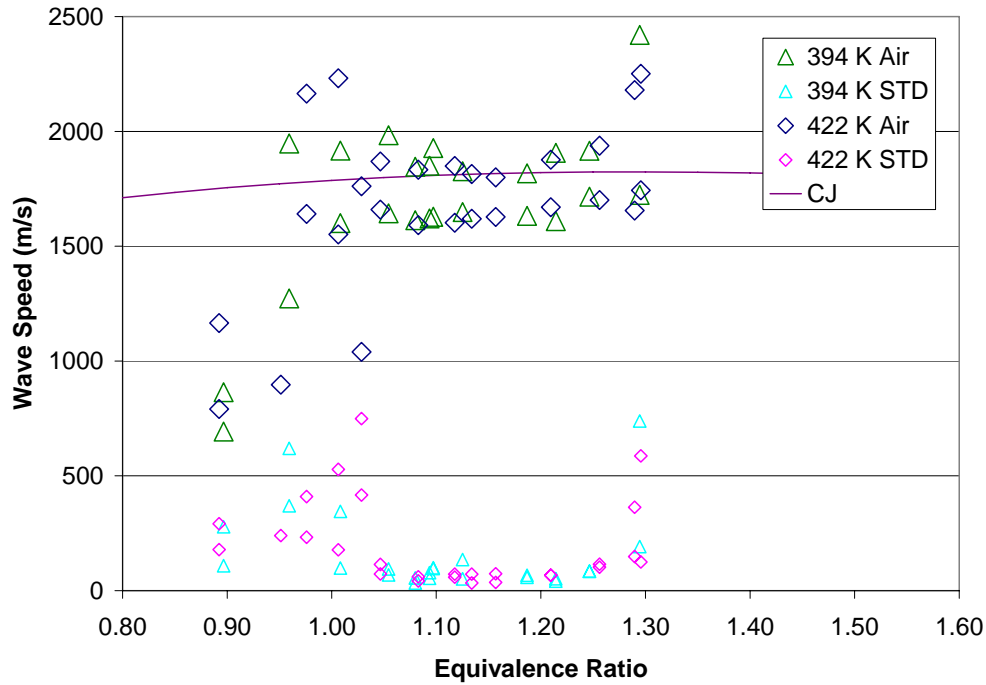
Figure 6.58 JP-8 at 555 K with an 8 ms spark delay at the WS2 location.

Discussion

Combustion Performance

The high vapor fuel tests using n-heptane, isooctane, and aviation gasoline provide the best case (droplet free) combustion performance results. The results are deemed best case, first, because of a very long mixing length (6.5 m) used in conjunction with an axial mixer, and second, due to the high vapor pressure (Table 5.2) the fuels are readily evaporated even without the benefits of the FVS. Figure 6.51 shows the best-fit ignition time curves for all four fuels, at an 8 ms spark delay. The flash vaporized JP-8 data, with 555 K fuel and 422 K air, agrees well with the ignition performance of the high vapor pressure fuels and specifically the low octane n-heptane. This important result shows that when the low vapor pressure JP-8 is flash vaporized ($T_{fuel} > 530$ K), even with

150

a much shorter mixing length (1.3 m), the ignition results match closely to the best case

high vapor pressure fuels.
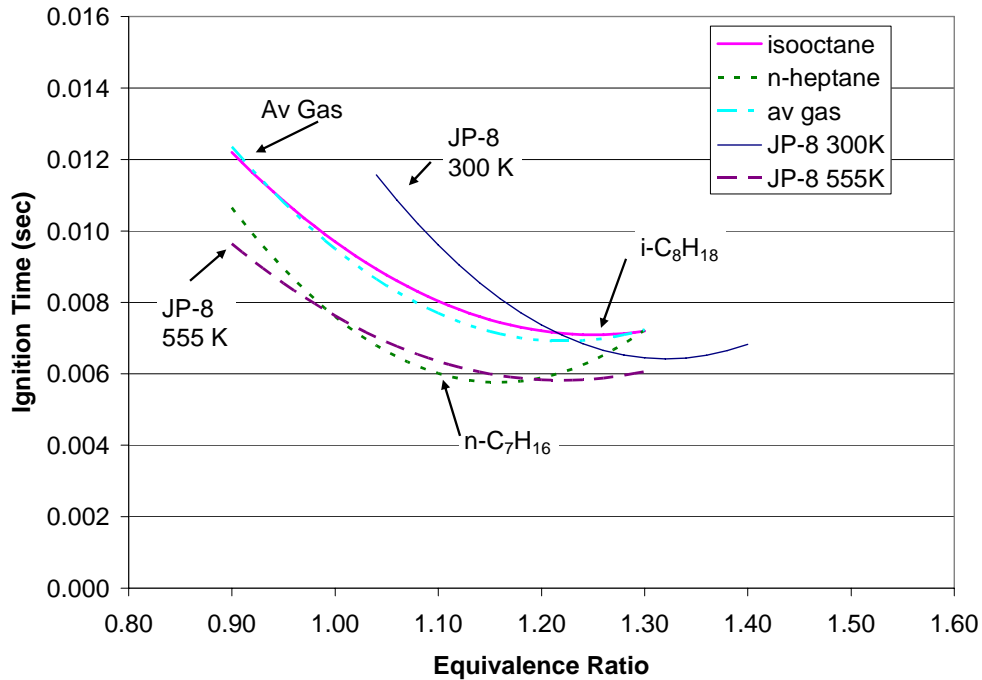
Figure 6.59 Ignition time comparisons for all 4 fuels with an 8 ms spark delay.

Mixture Homogeneity

The absence of liquid droplet effects on the combustion performance of the PDE

implies that the flash vaporization system provides a suitable fuel vapor into the flowing

air. These results are in excellent agreement with the SUPERTRAPP model prediction of

where droplet effects are expected and thus what temperatures should be used to operate

above the liquid vapor equilibrium limit. In particular, the high vapor pressure fuel results

showed little combustion improvements with increasing fuel temperature. In the modeled

results for n-heptane (Fig. 5.8) and isooctane (Fig. 5.9), all the test conditions were well

above the liquid vapor equilibrium limit even if below the fuel flash vaporization

temperature. The combustion results agree and show no fuel injection temperature or

droplet effects. Compared to the JP-8 and air model in Fig. 5.10, however, the results showed that operating in the region below the liquid vapor equilibrium line would still have liquid droplet effects. The droplet effects are seen in Fig. 6.17, when the PDE is operated in the region with sustained droplets. The droplet effects were still observed at test conditions above the modeled liquid vapor equilibrium limit (473 K fuel and 422 K air). Since the fuel was not yet flash vaporized, the remaining droplets still required time to allow the heat and mass transfer to evaporate and mix with the air prior to combustion (Table 5.4). Increasing the fuel and air temperature continued to increase the droplet evaporation and mixing rate and resulted in reduced ignition times at a given equivalence ratio. The droplet effects were negligible only after the fuel injection temperature exceeded the flash vaporization temperature. The FVS reduced the lean operating ignition limit from an equivalence ratio of 1.05 with ambient temperature fuel to a value of 0.84 with the 555 K fuel. In agreement with previous researchers,[11] the larger percentage of the fuel that is in the vapor state, the better the overall performance of the PDE.

The detonability limits of the FVS created mixtures fall within the equivalence ratio bounds reported in the literature for gaseous normal alkane fuels with a 1 MJ high explosive (HE) initiator (Table 6.5). The range of equivalence ratios that can sustain a detonation is narrow, and although the detonation transitioning method differs, these results fall near the 1 MJ direct initiation energy values. Early in this research, the detonation transition was attempted with a 0.914 m spiral. The stoichiometric n-heptane and air mixture was successfully transitioned to a detonation, but the stoichiometric isooctane and air mixture did not. The spiral was lengthened to 1.22 m and the isooctane and air mixtures were successfully transitioned to detonations. This experience has shown

152

that a longer spiral could transition detonations past the limiting equivalence ratios measured and published in Table 6.6, but would not likely exceed the limiting equivalence ratios found in maximum limits in Table 6.5. While increasing the length of the spiral may widen the detonation equivalence ratios limits, it also has ramifications that include increased weight, PDE thrust tube length, and pressure losses.

Table 6.5 Detonation limits for gaseous alkane hydrocarbon fuels in air at 293 K and 1 atm with a 1 MJ initiation energy and the max available energy. Data estimated from Ref. 9.

Fuel	Formula	1 MJ Lean Limit φ_L	1MJ Rich Limit φ_R	Max Lean Limit φ_L	Max Rich Limit φ_R
ethane	C_2H_6	0.81	1.65	0.69	2.0
propane	C_3H_8	0.93	1.45	0.70	1.9
n-butane	$n\text{-}C_4H_{10}$	0.88	1.50	0.70	2.03

Table 6.6 Detonation limits for flash vaporized hydrocarbon fuels in air at 1 atm with 1.22 m Schelkin like spiral.

Fuel	Formula	Mixture Temperature (K)	Lean Limit φ_L	Rich Limit φ_R	Figure
av gas (ambient)	n/a	311	0.95	< 1.30	6.35/6.36
av gas** (≥430 K)	n/a	311	0.91	1.22 <	6.35-6.38
isooctane	$i\text{-}C_8H_{18}$	311	0.94	1.18	6.40
n-heptane	$n\text{-}C_7H_{16}$	311	< 0.92	1.30 <	6.43/6.46
JP-8	$C_{11.9}H_{21.6}$	422	0.90	1.30 <	6.56

** The thermally decomposed aviation gasoline has a lower undetermined octane number.

Heated Fuel System Performance

The fuel preparation sparging system provided a fully deoxygenated fuel that allowed operation at temperatures well above the auto ignition temperature of the fuels

and no fuel coking was observed. The ability to heat the fuels without reduction in fuel system performance is the cornerstone to making this a viable system for future efforts. The heated aviation gasoline was unique in that reactions were observed while in the furnace. The reactions were not due to dissolved oxygen, but instead occurred between tetraethyl lead and ethylene dibromide, which are common additives in aviation gasoline. The result was a gray sludge that was suspended within the heated aviation gasoline. The sludge was analyzed and the results showed the tetraethyl lead and lead bromide peaks in the chromatogram.[87] There was no measurable system degradation from the sludge and the fuel nozzles were not obstructed because the sludge remained in the furnace. Overall, the aviation gasoline performed adequately without heating, and the long-term effects of the heated fuel reactions on the fuel system are not known.

The JP-8 was heated to the highest temperatures (725 K) of the four fuels tested. Due to the static heating method used in this work, the time the fuel spent at the higher temperatures needed to be minimized to prevent the endothermic reactions which would clog the fuel lines. Three vials of JP-8 under various thermal stresses are shown in Fig. 6.60. The left most vial (Fig. 6.60a) contains clear unheated JP-8. The fuel collected in the rightmost vial in Fig. 6.60(c), caused the fuel line to be obstructed with solid carbon deposits and prevented any fuel from passing. The 7.5 cm long blocked passage was removed and cleaned. Since the condition of the remaining passages could not be easily determined, the fuel pressure vessel was emptied of fuel and the metal structure was heated to 800 °C while air flowed through the lines to burn out any remaining carbon. Subsequent fuel heating tests did not exceed 330 °C and no further endothermic reactions or related damage was observed. The fuel in 6.60 (b) was slightly darkened due

to heating for four hours at 330 ℃. The fuel did not lose the translucent characteristics nor did the heating produce measurable insoluble carbon.
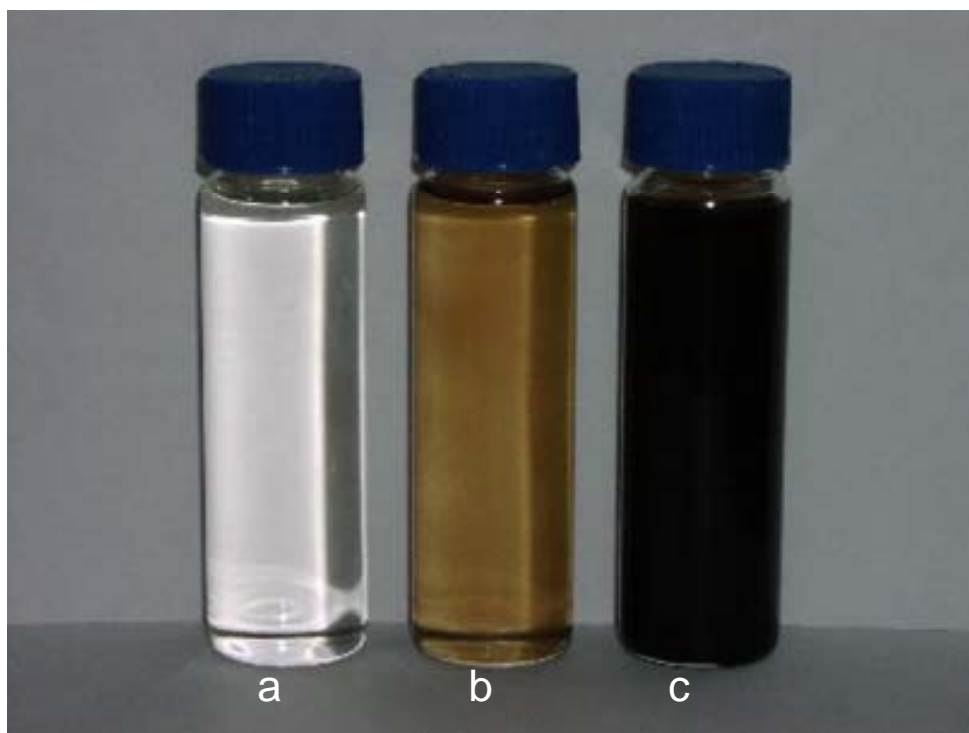
Figure 6.60 (a) Unheated JP-8, (b) statically heated JP-8 at 330 ℃ for four hours (c) statically heated JP-8 at 450 ℃ for two hours.

Octane Number Impact

The high ON fuels produced ignition times of 9 ms at an equivalence ratio of one, or 1 ms longer than the lower ON n-heptane and JP-8 at the same equivalence ratios (Fig. 6.59). The ignition times showed no dependence on the increased spark delay and the associated average pressure rise. The higher ON fuels have a correspondingly high auto ignition temperature shown previously in Table 2.3. The DDT times were reduced slightly by 0.1 ms to 0.2 ms with a decrease in ON and an increase in thermal equilibrium.

The range of equivalence ratios for which the fuels would detonate, as determined by the detonation wave speed, was a more quantifiable measure. In Table 6.6, the range of equivalence ratios narrowed as the ON was increased. The ambient temperature aviation gasoline compares well to the isooctane for the both the lean and both upper limits. The lower ON n-heptane and JP-8 both had broader ranges with the lean detonability limit at roughly 0.9 and the upper equivalence ratio limit was not yet reached at 1.3. The increase in operability is further supported when the standard deviations of the wave speeds are included for the range detonable mixtures.

VII. Conclusions and Recommendations

Flash vaporized JP-8 can be successfully mixed with air and detonated without a pre-detonator or oxygen enrichment. Aviation gasoline, isooctane (i-C_8H_{18}), n-heptane (n-C_7H_{16}), and JP-8 have been successfully heated to temperatures above the individual auto ignition temperature of the fuels without coking or reduction in fuel system performance. Deoxygenating the fuel prior to heating does successfully eliminate the thermal oxidation reactions. The unsteady inlet air flow inherent in a PDE is integrated with a steady flow fuel system with little observed penalty in fuel stoichiometry variation. The combustion results show the fuel injection temperature has little to no effect on the ignition and detonation limits for the three high vapor pressure fuels for the range of fuel and air temperatures tested. The low vapor pressure JP-8, however, does exhibit a strong dependence on the fuel injection temperature. The combustion results show that by flash vaporizing JP-8 prior to mixing with air that a 20% reduction in fuel flow can be achieved when compared with unheated fuel as well as widening the detonable equivalence ratio limits.

Impact of Research

This research is the first reported successful effort to flash vaporize and detonate a wide variety of liquid hydrocarbon fuels with air, in particular the low vapor pressure JP-8, in a working pulse detonation engine. The detonations were achieved with an operating equivalence ratio from 0.9 to over 1.3. The fuel injection temperature had no measurable influence on the combustion for the aviation gasoline, i-C_8H_{18}, and n-C_7H_{16} due to both the high vapor pressure of the fuels as well as the long mixing length. The

157

low vapor pressure JP-8 droplets effected the ignition of the fuel and was primarily characterized by a shift to a higher (fuel rich) equivalence ratio. When the JP-8 fuel temperature reached values that insured flash vaporization (> 530 K), the combustion data shifted to near that of the performance of the high vapor pressure n-heptane (Fig. 6.59).

Flash Vaporization System

The FVS injected gaseous JP-8 and eliminated all of the perceived droplet effects. The JP-8 combustion results were similar to or better than the results of three high vapor pressure fuels. The FVS and the associated fuel injection scheme gave comparable ignition and detonation results with JP-8 even with a much shorter mixing length. The FVS also validated the ability to safely heat fuel to temperatures over 330 °C without thermal oxidative reactions and without endothermic reactions damaging the fuel system.

The conditions required to successfully flash vaporize and achieve a mixture without droplets has been successfully modeled. The JP-8 and air modeling showed that for 300 K fuel and 422 K air at a manifold pressure of 2 bar, the enthalpy available in the fuel and air was insufficient to completely evaporate the fuel. Likewise, for ambient air, no fuel temperature (short of endothermic temperatures) could sufficiently ensure a fully gaseous mixture after equilibrium. The fuel temperatures used during this research were both above and below the predicted flash vaporization region. The combustion results validated the temperature and pressure envelope to provide a droplet free mixture. The results also validated the JP-8 surrogate co-developed with Dr. Scott Stouffer, described in Appendix C.

Octane Number

The isooctane and n-heptane are the basis for the automotive derived octane number (ON). The combustion results, as distinguished by ON, were considered as a fuel detonability parameter. The aviation gasoline and isooctane both had an ON equal to 100, and the n-heptane (0) and JP-8 (~25) were rated with lower ONs. The two 100 ON fuels had a 9 ms ignition time and the two lower ON fuels had an 8 ms or an 11% lower ignition time. Likewise, the higher the ON, the longer the DDT times and the narrower the equivalence ratio range where detonations were observed (Table 6.6). The DDT times were not as strong an indicator of the detonability as hoped, though a reduction in 100 µsec equates to roughly a 0.1 m reduction in DDT spiral length. An increase in the ON of a fuel does not predict a significant rise in the time to ignite and detonate a fuel and air mixture. The increase does however, denote an increase in the required length to transition to a detonation, as well as narrow the range of equivalence ratios that the detonation can transition for a fixed length DDT obstacle such as a Schelkin spiral.

Unexpected was the increased range of equivalence ratios for the flash vaporized 100 ON aviation gasoline. When the fuel was heated, the ON was lowered as a result of the chemical reactions between the tetraethyl lead and ethylene dibromide. These reactions caused the ON of the heated aviation gasoline to be lower (by an undetermined amount) than the unheated fuel. A remaining step to properly correlate ON and detonability would be to significantly increase or decrease the initial pressure for these fuels and determine the associated combustion performance impact.

Ignition Times and Equivalence Ratio

The ignition times for the three high vapor pressure fuels were not sensitive to the fuel injection temperature. Any perceived benefit was within the error bars. For the low vapor pressure JP-8, however, the reduction in ignition time was significant due to the improved mixture qualities and the increased range of ignition equivalence ratios attainable. These benefits were shown previously in Figs. 6.17 and 6.18 and represent an improvement from 16 ms to less than 8 ms to operate at an equivalence ratio of one. Since ignition occurs in the vapor phase and the ignition time scales are smaller than the evaporation time scales, any remaining fuel trapped in the droplets is essentially unusable during the spark ignition process. In Fig. 7.1, the unheated fuel ignition time curve has a similar shape as the flash vaporized line, but behaves as if roughly 20% of the total fuel is still trapped in the droplets as unusable liquid causing the overall equivalence ratio to be higher than the fully vaporized mixture. As the fuel and air temperatures increase, the droplet lifetimes decrease and percentage of fuel vapor increases to match the flash vaporized case (Fig. 6.19). No combustion improvement was observed by increasing the fuel and air temperatures past the flash vaporization temperature, and the FVS sufficiently achieved the goal of eliminating the droplet effects.
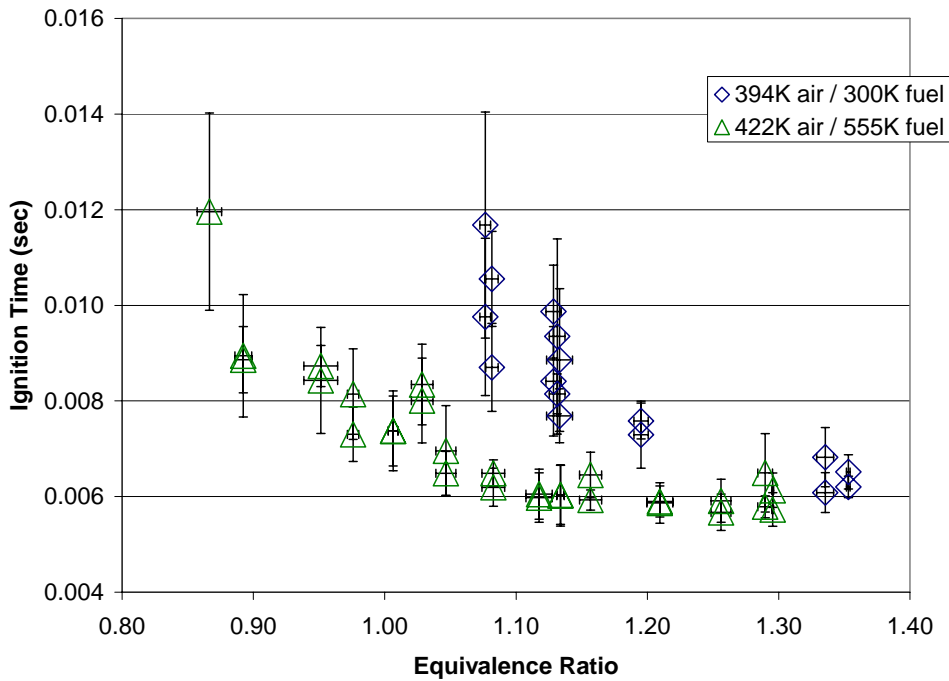
Figure 7.1 JP-8 and air ignition time with unheated (300 K) and flash vaporized (555 K) fuel. Error bars are ± 1 standard deviation.

In Figs. 7.2 to 7.5, the total time from spark deposit until the combustion wave exited the Schelkin spiral is plotted for the four fuels used in this research at the later spark delay data set. The ignition times dominated the overall time required to achieve a detonation and were on the order of 3 to 4 times larger than the DDT times for each of the fuels tested. At an equivalence ratio of one, where the transition to detonation is least difficult, the reduction in ignition time (~1 ms) was an order of magnitude larger than the reduction in DDT time (~0.1 ms). To improve the overall combustion performance for PDEs, both the ignition and DDT times must be reduced by an order of magnitude to achieve the repetition rate required to reach the goal of high frequency operation.
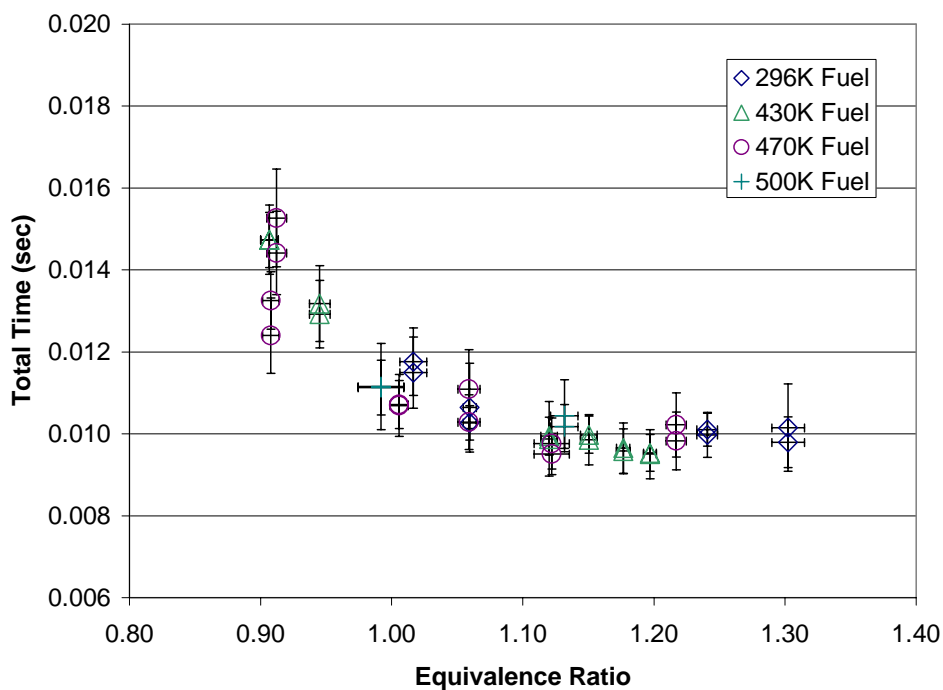
Figure 7.2 Aviation gasoline and air combined ignition and DDT times with 8 ms spark delay. Error bars are ± 1 standard deviation. Air is at 311 K.
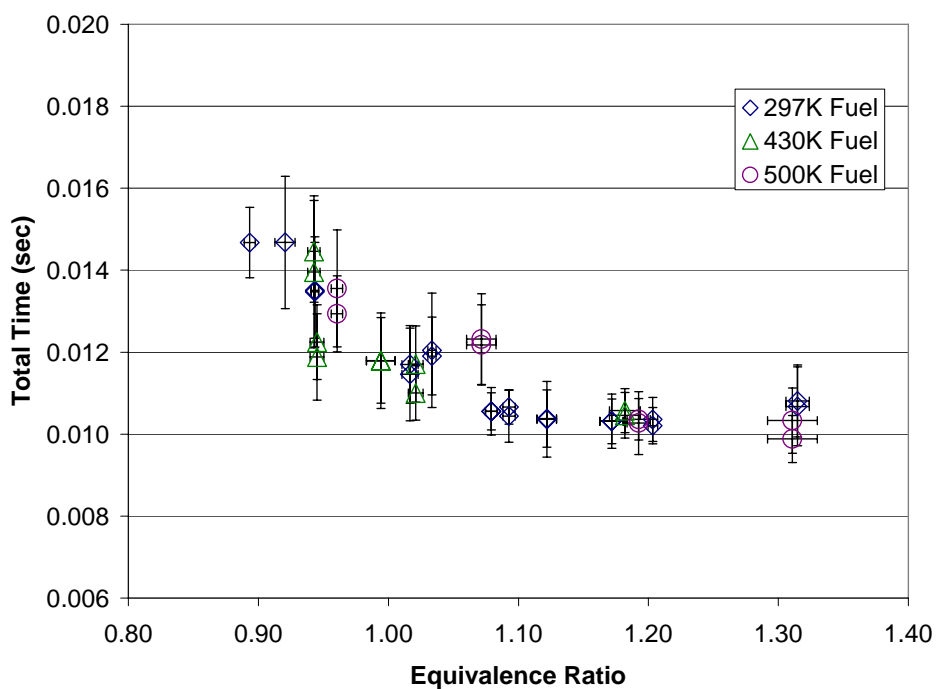
Figure 7.3 Isooctane and air combined ignition and DDT times with an 8 ms spark delay. Error bars are ± 1 standard deviation. Air is at 311 K.
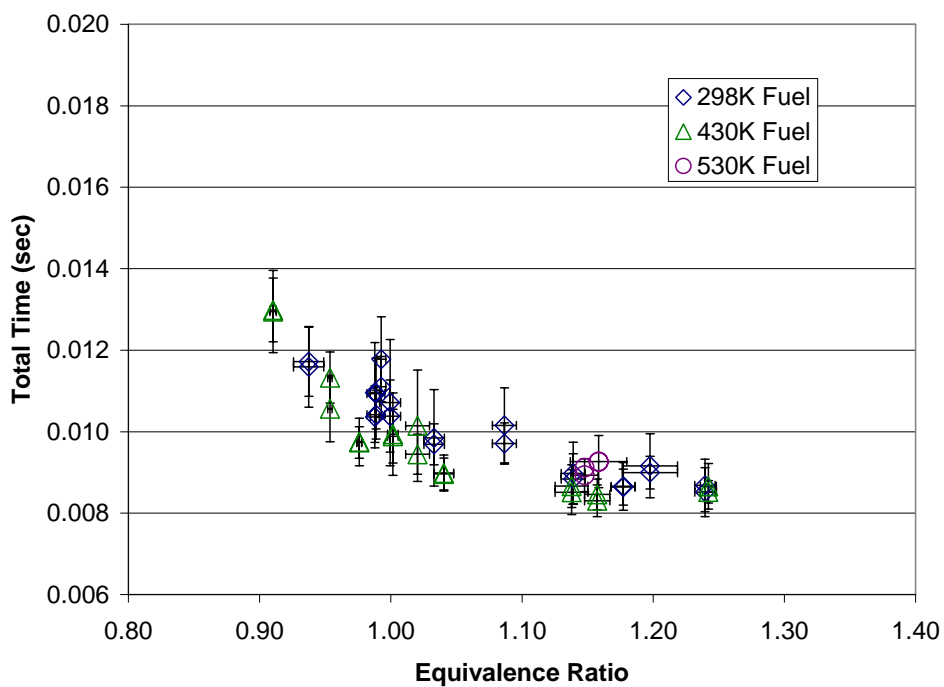
Figure 7.4 n-Heptane and air combined ignition and DDT times with an 8 ms spark delay. Error bars are ± 1 standard deviation. Air is at 311 K.
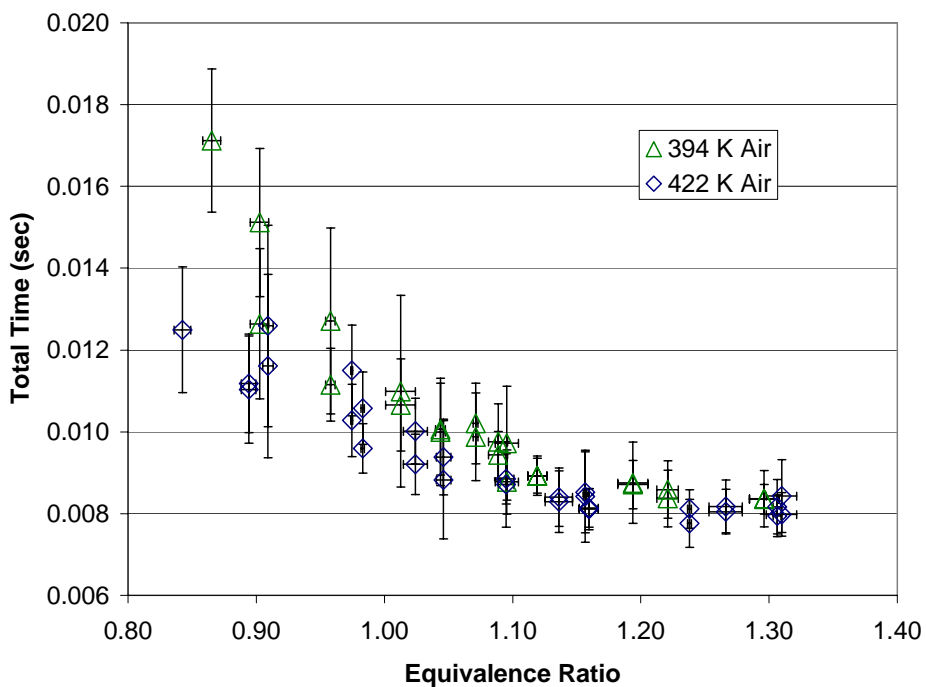
Figure 7.5 JP-8 at 555 K and air combined ignition and DDT times with a 6 ms spark delay. Error bars are ± 1 standard deviation.

Future Work

High temperature fuel systems have been studied since the 1930s, but the implementation of a working system in a PDE with JP-8 will impact not only the PDE community but the scramjet community as well. Flash vaporization is one method that is under consideration to rapidly mix liquid fuels and air in a scramjet.

PDE Applications

A key step to implementing a flash vaporization system in flight worthy PDEs will be the integration of a fuel system than can extract heat from thrust tubes to sufficiently raise the fuel temperature. Understanding the challenges of starting with unheated fuel and the development of a lightweight and robust system into the working PDE will be crucial steps. Assessing any combustion performance penalties due to heat transfer out of the thrust tubes will also have to be addressed.

This FVS successfully eliminated the droplet evaporation time on the ignition process and reduced the ignition times for low vapor pressure fuels when compared to an unheated fuel system. The next step should be to reduce the time required to begin the chemical reactions to ignite and detonate the fuel. One perceived method to achieve this is by operating at or above the endothermic fuel region. The high temperature structures on high supersonic and hypersonic air frames must be actively cooled to operate, and the fuel could be used as a heat sink to cool the structures. If the fuel temperature was sufficiently raised, then endothermic reactions would ensue and break down the fuel into smaller hydrocarbons and gaseous fuels. The desirable traits of the endothermic reaction products are high heating values, rapid burning rates, and short ignition times which will

164

decrease the time for combustion important to both the PDE and scramjet research community. Fuel additives, fuel line coatings and catalysts are being studied to control the products formed by endothermic reactions that may be more reactive or produce less insoluble carbon products.[41, 81]

Another PDE application of the FVS would be to directly inject the fuel into the thrust tubes without first premixing with air. The elimination of the premixed fuel system would reduce the length and weight of the vehicle and inlet. With the premixed fuel and air system used in this research, the mixture fills the tube from the closed end and requires a large mixture velocity to fill the tube at any reasonable frequency. Reducing this velocity and effectively raising the static pressure would improve the combustion performance of the PDE.

Large reductions in ignition and DDT times are projected by using a branched detonation system described earlier in Chapter II. A system of interconnecting tubes to branch detonations continuously (Fig. 7.6) would greatly increase the maximum operating frequency of a liquid fueled PDE and could exceed the combustion performance of a gaseous hydrogen and air mixture.[32] An even larger performance gain could occur if the detonation was branched from one tube to another without the detonation failing and transitioning back into a deflagration when arriving at the receiving tube. Successful transition from tube to tube would eliminate the ignition and DDT times as well as eliminate the need for a DDT spiral in the receiving tubes. The elimination of the spiral would increase thrust by eliminating the high drag in the tube as well as reduce the weight and length of the tubes, and reduce the maintenance of the PDE.
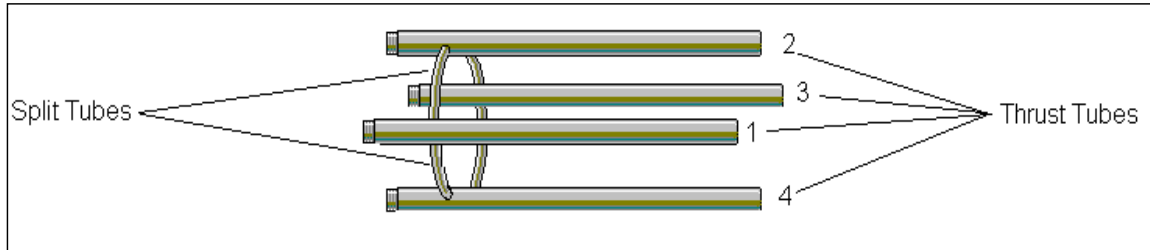
Figure 7.6 Potential detonation branching setup for a multi-tube PDE. Used with permission Ref. 29.

Scramjet Applications

The common need of a FVS for both a PDE and a scramjet application was discussed briefly in Chapter I. Scramjets, however, rely on deflagrations to release the energy in the fuel air mixture quickly. A detonation releases the chemical energy stored in the fuel tens of thousands times faster than a deflagration and would result in a much shorter combustion length. To employ the detonation wave in a steady flow scramjet, a detonation wave could be generated at the inlet within the incoming air at the steady state Chapman-Jouguet wave speed. The engine now becomes an oblique detonation wave engine.[5] Several technical difficulties must be overcome to implement this concept. First is how to generate a detonation while traveling at hypersonic speeds, and second, since the detonation wave travels at a specific speed, how to control the wave at off design flight conditions. Third would be the development of a cooling scheme to prevent the detonation wave from damaging the inlet. Fourth and finally, how to inject and mix the fuel upstream of the inlet fast enough to support the detonation wave.

166

Appendix A. The Pulse Detonation Engine

A Generic PDE Cycle

The PDE uses the detonation process to compress and heat a mass of fuel and air to produce thrust. Two intake valves per thrust tube fill the tubes with a fuel and air mixture, and two exhaust valves fill the tube with cool purge air. The cycle is fixed by the mechanical operation of the cams that open and close the valves for all four tubes. A different cam can be used to change the percentage of time spent on each portion of the cycle. The current cycle (Fig. A.1b) has three parts with equal time (120 degrees) spent to (1) fill the tube with a fuel air mixture, (2) close the valves and ignite, DDT, and exhaust the products, and (3) purge the remaining products from the tube with air to cool the tube and create a buffer before the fresh reactants are introduced into the tube.

(a)   (b)
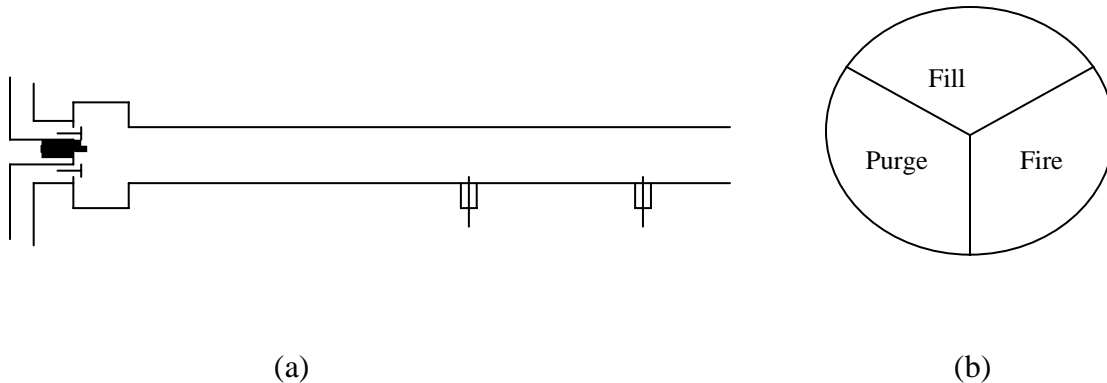
Figure A.1 PDE Tube with Valves (a) and 120 degrees per segment of the cycle (b).

The fill portion of the cycle begins when a rotating cam lobe depresses a lifter, compressing the valve spring, and opens the intake valves as shown in Fig. A.2. Premixed fuel and air rush into the closed end of the tube and begin to expand toward the

open end. The upstream manifold pressure is set to fill a specific volume of the tube. An important factor is the area of the valve. The Quad 4 head was chosen because of the increased area afforded by two intake valves and two exhaust valves. The air flow through the intake valves is nominally mid to high subsonic except when higher flow rates are required to fill larger tubes or fill the tubes at higher frequencies and can cause the air flow through the valves to choke (M_{valve}=1). An increase in valve area would reduce the manifold pressure requirements and slow the velocity of the mixture filling the pipe. The reduced velocity in the pipe would also provide a higher static pressure within the mixture.
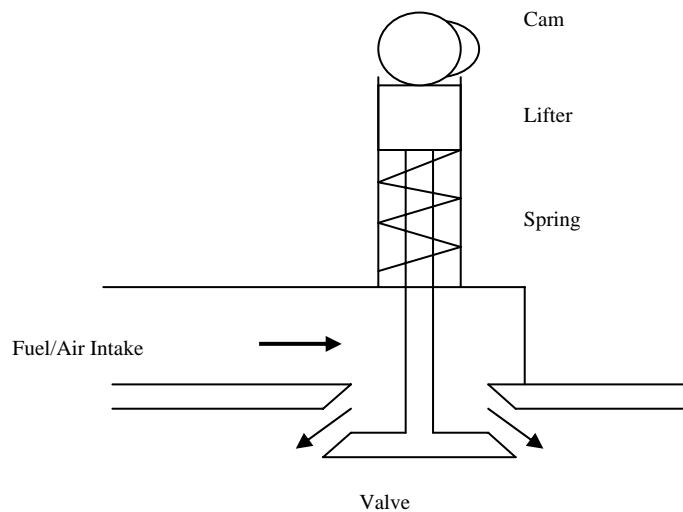
Figure A.2 Cam Driven Intake Valve Operation. The PDE thrust tube receives the mixture below the valve.

Once the tube is filled the cam closes the intake valves and the firing portion of the cycle begins. Ignition initiation can be delayed and is defined as the time between the moment the valve closes and the instant the voltage arrives at the spark plug. The spark delay is a variable and studies have shown increased thrust when the ignition coincides with the returning compression wave.[1] When the valves close, the mass of fuel and air

leaving the tube pulls a vacuum (experiences an expansion wave) because of the momentum of the flow in the closed portion of the tube. After the tube over expands, a compression wave returns the sub atmospheric fuel and air mixture in the tube to above atmospheric pressure (Fig. A.3). If the ignition is delayed until the corresponding returning compression wave, then an increase in thrust is measured due to the increased head pressure from the detonation. The penalty for waiting for the returning compression wave is the time that no thrust is being produced. The ideal circumstances are for the mixture to be ignited and detonated at the earliest opportunity to achieve the fastest cycle rate.
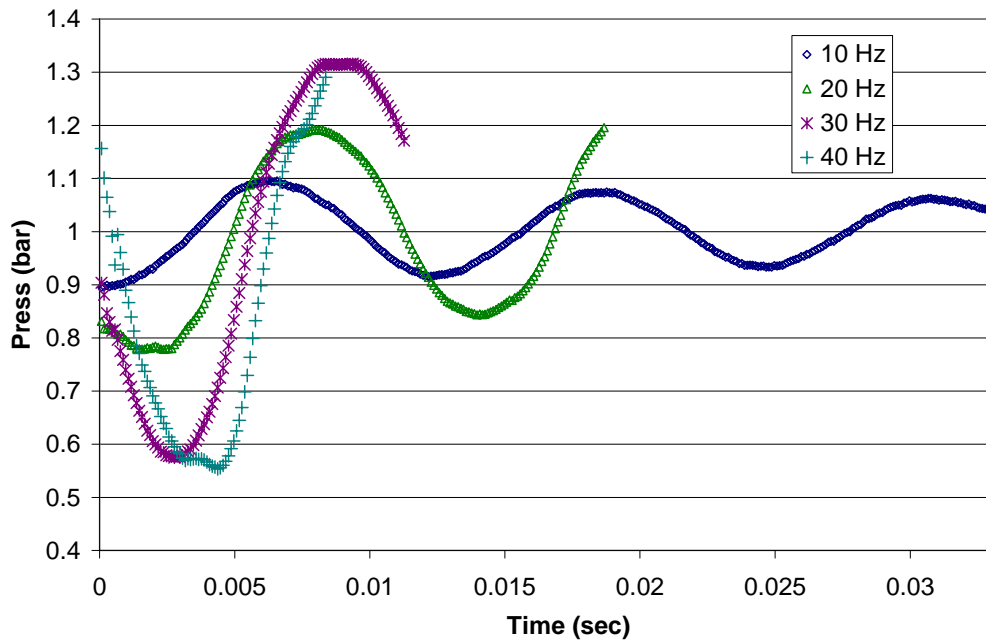
Figure A.3 Absolute pressures in head after valves close in 0.91 m tube.

The mixture ignition time is dependent on the initial pressure (Fig. A.4). The ignition times increase as the initial pressure decreases. Ignition of gaseous hydrogen air combustion is controlled by the chemical reaction time. Lefebvre[12] states for this

combustion that the minimum ignition energy is proportional to P^{-2}. This implies a reduction in ignition time with an increase in pressure for constant ignition energy.
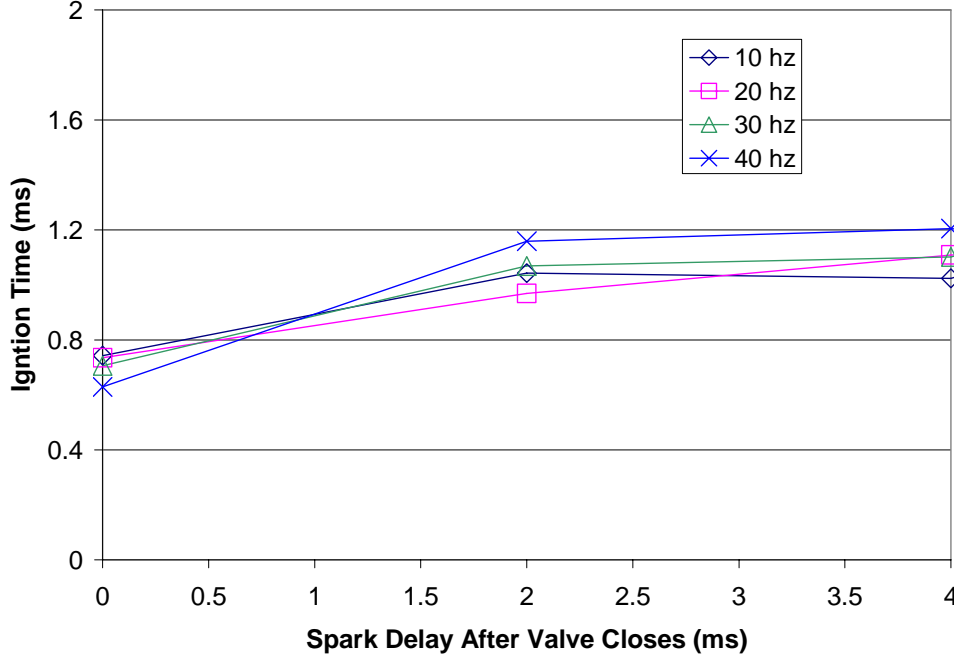
Figure A.4 H_2 and air ignition times with spark delay for different firing frequencies for a 0.91 m long, 5.2 cm diameter thrust tube.[31]

PDE Thrust Performance

A control volume analysis is applied to the PDE tube during the firing portion of the cycle. The uninstalled thrust is given by Eqn. A.1.

$$F = \dot{m}V_{exit} + \left(P_{exit} - P_{atm}\right)A_{exit} \qquad \text{(A.1)}$$

where F is thrust, V is velocity of the exit gases, P is pressure, $\dot{m}$ is the mass flow, and A is the exit area.

To increase the thrust of the PDE,

1. Fill the tube with more mass to increase the mass flow for each cycle. There is no benefit to overfilling the tube.

2. The exit velocity and pressure are fixed by the chemistry of the particular fuel chosen, but increasing the initial pressure raises the final pressure after the detonation.

3. Increase the tube diameter, which increases the exit area. However, the larger the tube diameter, the more difficult to initiate a detonation.[88]

4. Increase the frequency of the cycle. The more thrust pulses during a given amount of time, the higher the average thrust (Fig. A.5).
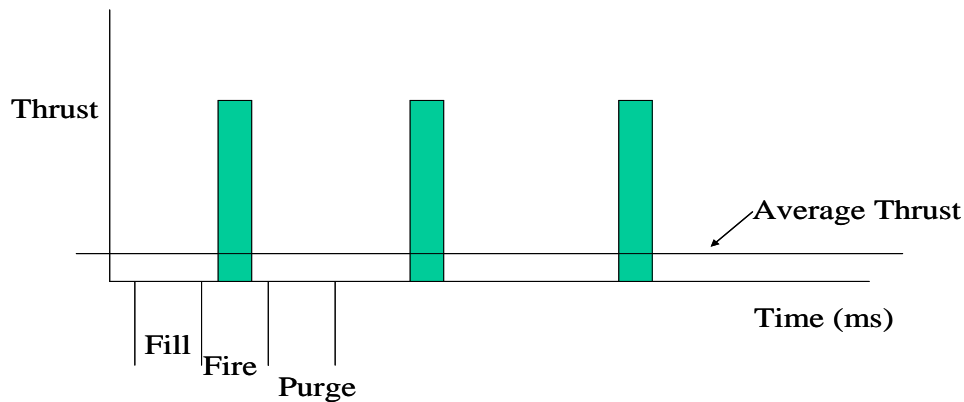
Figure A.5 Average thrust for one tube.

A second method to estimate the thrust is derived from the head pressure acting on the thrust wall inside the thrust tube. This is a reasonable approximation if you neglect any performance losses between the fluid exiting the tube and the walls or other friction causing devices such as a spiral. The head pressure in Fig. A.6 has been measured for an entire cycle. The force exerted on the interior walls can be determined by integrating the pressure multiplied by the head area, and give an equivalent thrust over the full cycle (fill, fire, and purge).
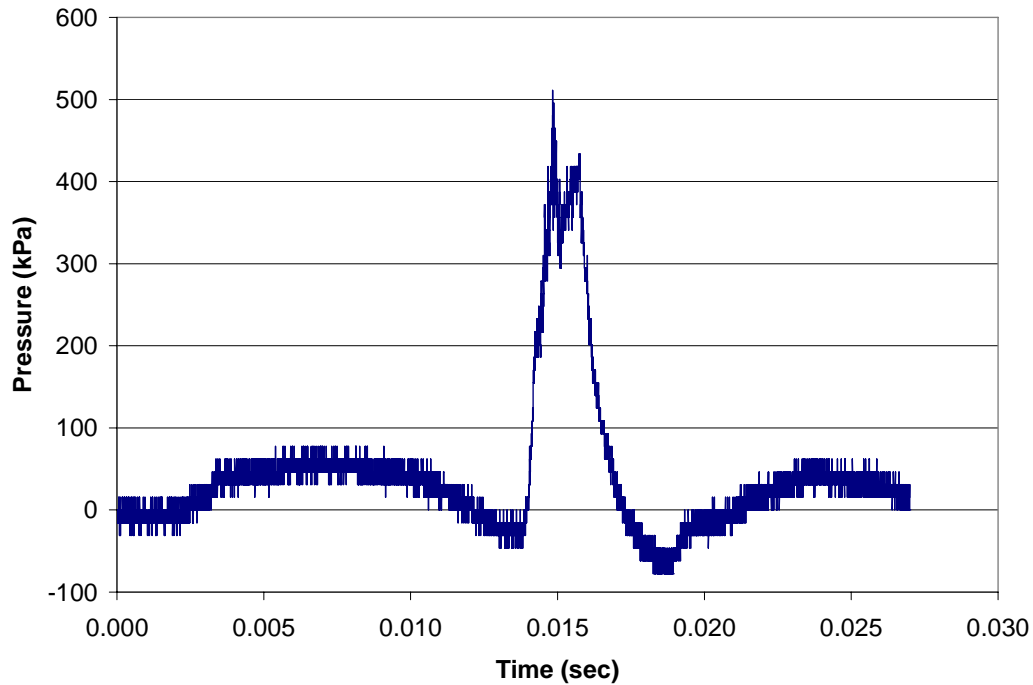
Figure A.6 Gauge head pressure for an entire cycle (30 Hz). Note the regions of sub-atmospheric pressure due to expansion waves during dynamic filling and exhaust.

If the cycles were shorter then the average pressure in the head would be higher and would equate to more thrust (Fig. A.5). Since the high temperature exhaust gas velocities are difficult to measure, the thrust can be approximated with the head pressure trace. The velocity of the gases could be approximated, but neglecting the boundary layer effects and the drag of the complex geometry within the tube will introduce signficant errors. The drag coefficent is sufficiently addressed elsewhere.[89] The sketch in Fig. A.7 is one such method to determine the thrust through the head pressure.
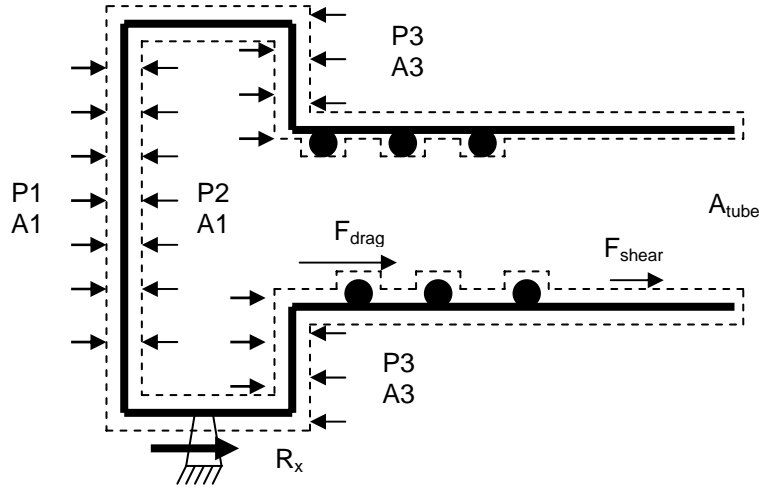
Figure A.7 Forces acting on PDE thrust tube on a test stand.

$$\sum F_x = Rx - (P1 - P2)A1 + (P2 - P3)A3 + F_{drag} + F_{shear} \qquad (A.2)$$

$$P1 = P3 \qquad (A.3)$$

$$A_{tube} = A_1 - A_3 \qquad (A.4)$$

$$R_X = P2A_{tube} - F_{drag} - F_{shear} \qquad (A.5)$$

$$F_{shear} = \int \tau dS \qquad (A.6)$$

$$F_{drag} = C_D \frac{1}{2} \rho V^2 DL \qquad (A.7)$$

where τ = shear stress

A = area

C_D = drag coefficient for a cylinder

D = diameter of spring like obstacle (m)

L = total length of obstacle (m)

The thrust equation with measured head pressure can now be presented with

$$Thrust = P_{head} A_{tube} - F_{drag} - F_{shear} \qquad (A.8)$$

Using the head pressure to approximate thrust can a useful tool; however, neglecting the obstacle drag can cause significant errors.[90] A long spiral such as used in this research to DDT is one such obstacle. It is important to keep the length of the obstacle to the minimum required to obtain a detonation to obtain the maximum thrust from each pulse.

Performance Limitations

One of the performance limitations required to make a PDE a feasible propulsion system is the inability to detonate practical and readily available fuels such as aviation gasoline and JP-8 and do so in a short enough time to allow high frequency (high thrust) operation. A second constraint is the requirement to fill multiple tubes quickly in such a way that velocities in the thrust tubes are low and static pressures high to enhance ignition and DDT. The third hurtle is to integrate the PDE into a self aspirated configuration where energy generated by the PDE can sustain the airflow and power requirements for operation.

Time Constraints

With a hydrogen and air mixture, ignition and DDT occurs within 2 ms.[31] However, with longer chain hydrocarbons such as multi-component aviation gasoline and JP-8, ignition and DDT with air can take up to 15 ms (Fig. 7.5). With the longer time requirement for hydrocarbon fuels, the firing portion is the longest in the cycle. For hydrogen and air, the fill process becomes the limiting factor. The DDT time is defined from the point ignition is first recognized until the detonation wave exits the DDT spiral.

The shorter the times to pass through the spiral the sooner the detonation wave was formed and reached the maximum wave speed. The longer the DDT time, the longer the distance required to transition the detonation and thus, the more difficult the fuel is to detonate.

Appendix B. Experimental and Computational Unsteady Air Flow Analysis

The unsteady fuel and air manifold flow conditions of a pulse detonation engine are caused by the starting and stopping of the fill process required when firing several tubes during a single cycle. This chapter summarizes the experimental and numerical results used to evaluate the unsteady pressure waves in the air and fuel manifold. The computational results give more qualitative insight into the mass flow and velocity fluctuations inherent in the system. The unsteady nature of the PDE inlet, particularly the effect of mixing steady fuel flow into an unsteady air stream, is of considerable interest to the PDE research community.

Unsteady Pressure Conditions

The PDE thrust tubes were completely filled with the fuel and air mixture regardless of air or fuel temperature. The amount of mass flow required to fill the tube did change with atmospheric pressure and mixture temperature. The equations governing the fill fraction as well as discussion of the control parameters were discussed previously in Chapter III. The filling of the tubes is not a steady process. To minimize the magnitude of the pressure and velocity fluctuations in the manifold upstream of the tubes, two tubes were filled and fired during the tests. The tubes were 180 degrees out of phase and had blocks of 120 degrees open and 60 degrees closed for each tube cycle as shown in Fig. B.1. The intake valve area varied during the cycle as shown in Figure B.2.
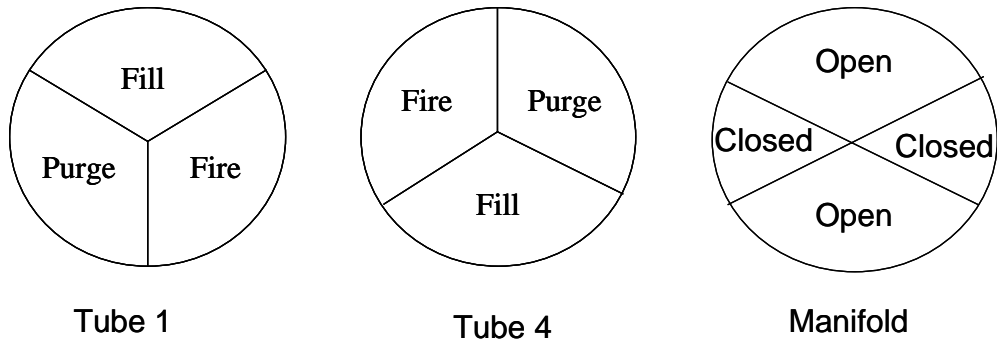
Figure B.1 Three segment cycle for each tube and the combined effect on the intake manifold. The intake manifold supplies the fuel and air mixture during the fill cycle only. The purge manifold supplies only air and experiences similar pressure fluctuations.
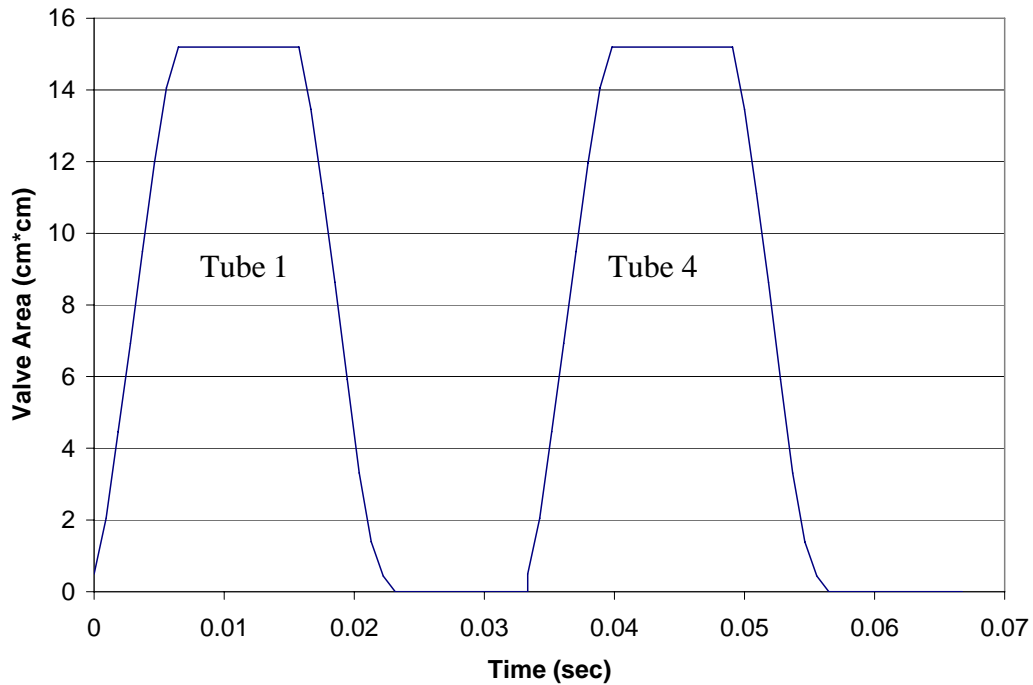
Figure B.2 Total intake valve area with time during the filling of two tubes at 15 Hz.

The opening and closing of the intake valves produce unsteady velocity fluctuations which were strongest nearest the valves in the intake manifold due to the starting and stopping of the airflow. The intake manifold pressure for five different fill fractions (mass flow rates) is shown in Fig. B.3 at a location 0.3 m upstream of the valves. For the 100% fill (fill fraction equal to one) used during the testing, the peak

177

pressure oscillates from 1.757 bar to 1.394 bar in the manifold. The velocities are predicted and shown in the CFD work in the next section.
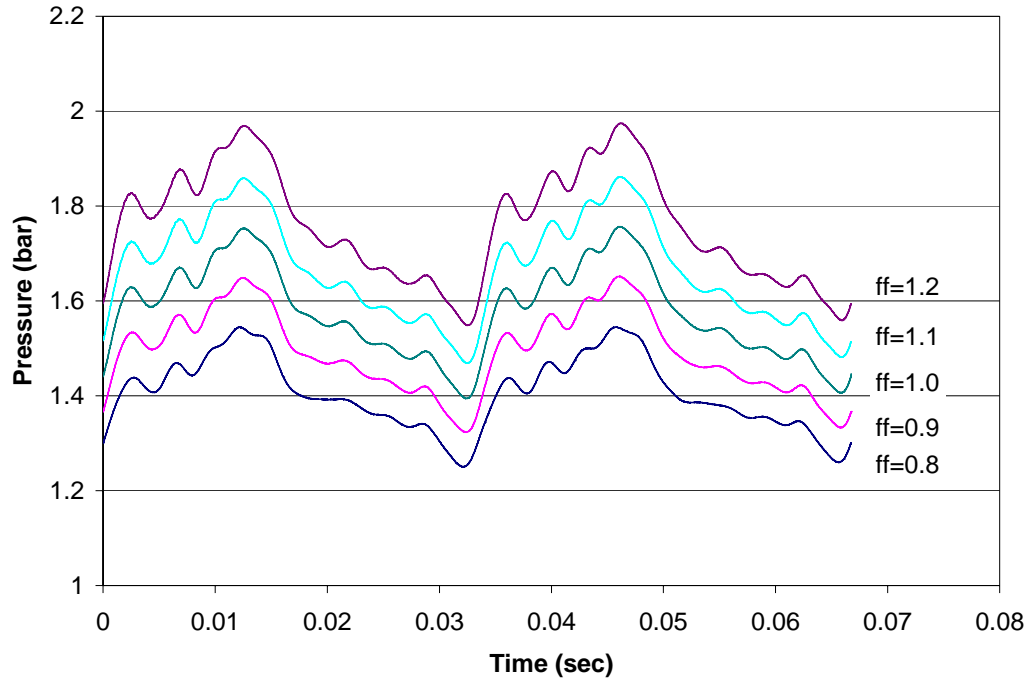
Figure B.3 Manifold pressures at 0.3 m upstream of intake valves for 310 K air at 15 Hz for two tubes with volume fills of ± 20%.

High Vapor Pressure Fuel Manifold Pressure Data

The high vapor pressure fuels (n-heptane, isooctane and aviation gasoline) were injected into the air manifold 6.5 meters upstream from the intake valves (Fig. 3.2). The increased mixing length in conjunction with the axial mixer provided lower pressure fluctuations than choosing a fuel injection location near the intake valves. The peak to peak pressure at the high vapor pressure fuel injector was 1.727 bar to 1.627 bar at a fill fraction of one shown in Fig. B.4. This 0.100 bar maximum fluctuation compares favorably with the maximum 0.363 bar fluctuation measure nearest the intake valves.
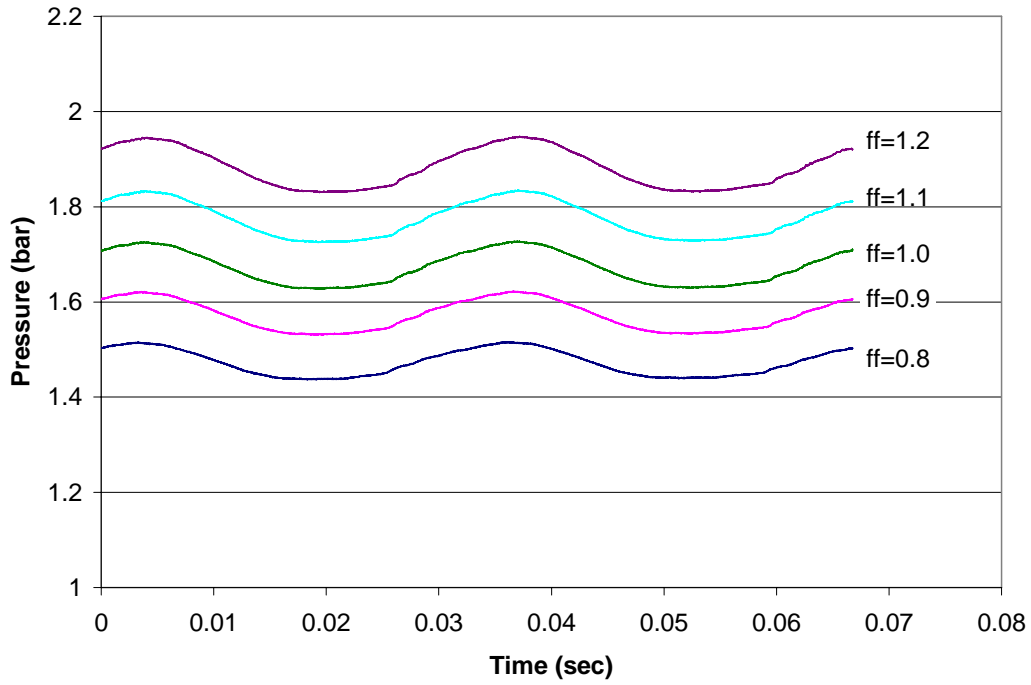
Figure B.4 Air pressure at fuel injector location 6.5 m upstream of intake values for 310 K air at 15 Hz for two tubes with volume fills of ± 20%.

The pressures in the closed end of the PDE thrust tube were important due to the pressure effect on the combustion and detonability of the different fuels. Figure B.5 shows the pressure trace on the thrust wall at the head of a single PDE thrust tube at the location of the spark plug for one cycle.
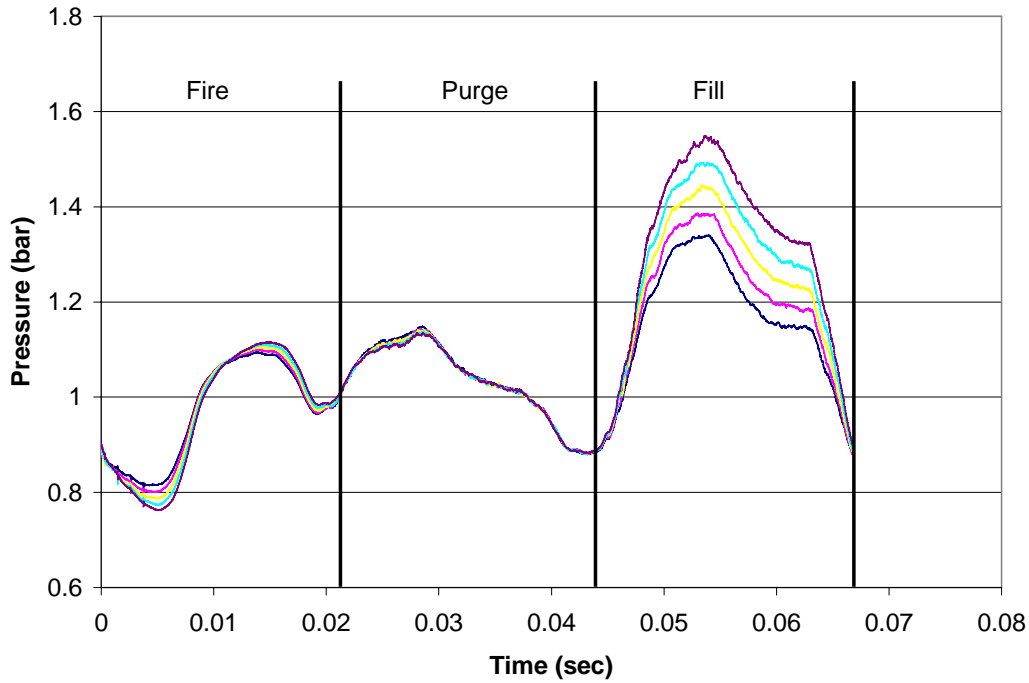
Figure B.5 Head pressures for 310 K air at 15 Hz for two tubes with volume fills of ± 20%.

As the fill fraction goes up, more mass is being fed through the intake valves. Since the maximum intake area is fixed, the air flow travels at a higher velocity. Since the tube is filled from the closed end, at the instant the intake valves close, the high momentum of the air causes a drop in static pressure in the head due to an expansion wave. The gases in the tube continue to drop below atmospheric pressure until the expansion wave exits the open end of the tube, then a compression wave returns from the open end of the tube to match pressure at the closed end of the tube. The number of expansion and compression waves that occur depend on the local speed of sound, the length of the tube, and the firing frequency. The expansion and compression waves are strongest with an over fill (ff>1) and weakest with an under fill (ff<1). To better show the expansion wave experienced after the intake valves close, the fire portion of the cycle shown previously in Fig. B.5 is enlarged in Fig. B.6 a. Of interest is the ringing of the

180

pressure sensor after the intake valves slammed closed (t=0) and have bounced four times at 1 ms intervals. The pressure sensor was located between the intake valves where the spark plug is normally found.
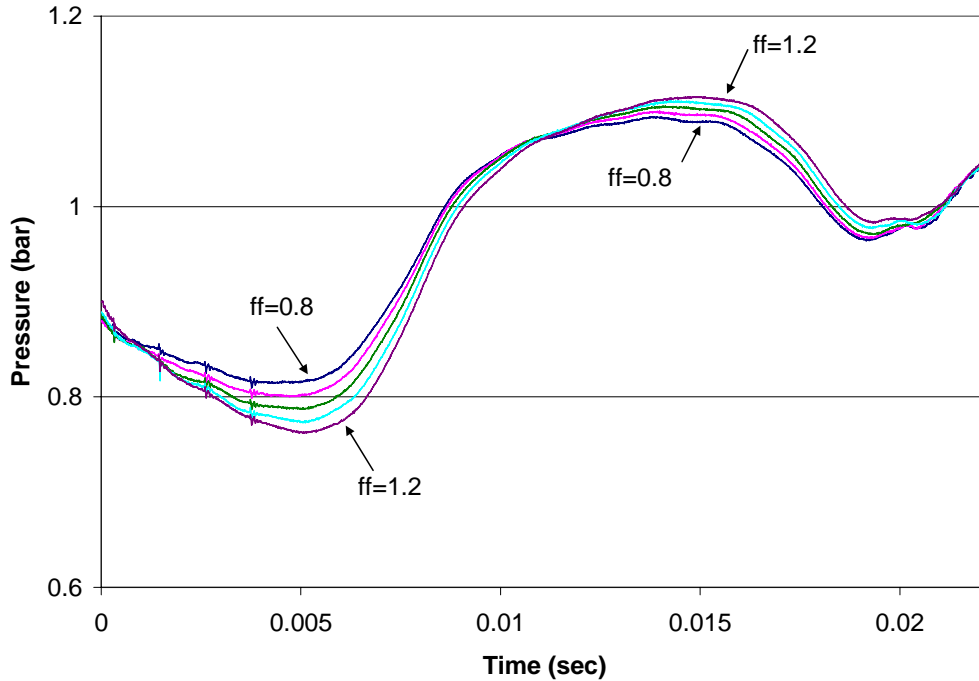
Figure B.6a Head pressures for 310 K air at 15 Hz for the fire portion of cycle for two tubes with volume fills of ± 20%.

During the testing of the four fuels, combustion data was taken at two spark delays: 6 ms and 8 ms. The measured ignition times ranged from 6 ms to 16 ms. As described in Chapter II, the pressure affects both ignition and DDT time. Knowledge of the effect of the average pressure during the ignition and subsequent deflagration-to-detonation transition time is therefore important. The average pressures are presented in Table B.1 and are varied for different spark delays and fill fractions for both an ignition event that took 6 ms and an ignition event that took 16 ms. A separate column displays the difference in average pressure between the two spark delays. For all spark delays and ignition times, the 8 ms spark delay had a higher average pressure during the length of

the ignition event. For a tube fill fraction of one, used during all the tests, the 8 ms spark delay for a measured 6 ms ignition event experienced a 0.085 bar (1.25 psig or 7.9%) higher pressure. The effect of the unsteady pressure during the ignition and DDT of the fuel and air mixture may be larger than simply the average pressure.

Table B.1 Average pressures in head for min and max ignition times at two spark delays.

Fill Fraction for air at 310 K	Spark Delay	6ms Ignition Time Average Pressure (bar)	Pressure Change (bar) Due to spark delay	16ms Ignition Time Average Pressure (bar)	Pressure Change (bar) Due to spark delay
0.8	6	0.982		1.020	
0.8	8	1.054	+0.072	1.046	+0.025
0.9	6	0.976		1.022	
0.9	8	1.054	+0.078	1.049	+0.026
1.0	6	0.970		1.023	
1.0	8	1.054	+0.084	1.051	+0.028
1.1	6	0.961		1.022	
1.1	8	1.050	+0.089	1.052	+0.030
1.2	6	0.951		1.022	
1.2	8	1.046	+0.095	1.054	+0.032

The most important aspect of the data presented in Table B.1 is the fact that even relatively large changes ($\pm 20\%$) in the fill fraction do not cause significant changes in the average pressure experienced by the reactant prior to combustion. This gives a high degree of confidence that the pressure was justifiably constant during all of the testing.

The purge portion of the cycle provides air to buffer the high temperature products remaining in the tube after the fire cycle and the incoming reactants for the fill cycle. The purge fill fraction was held constant at 0.5 and as seen in Fig. B.6b, the values

do not change appreciably due to the ± 20% change in main air fill fraction. Figure B.6b is the second portion of the cycle shown previously in Fig. B.5.
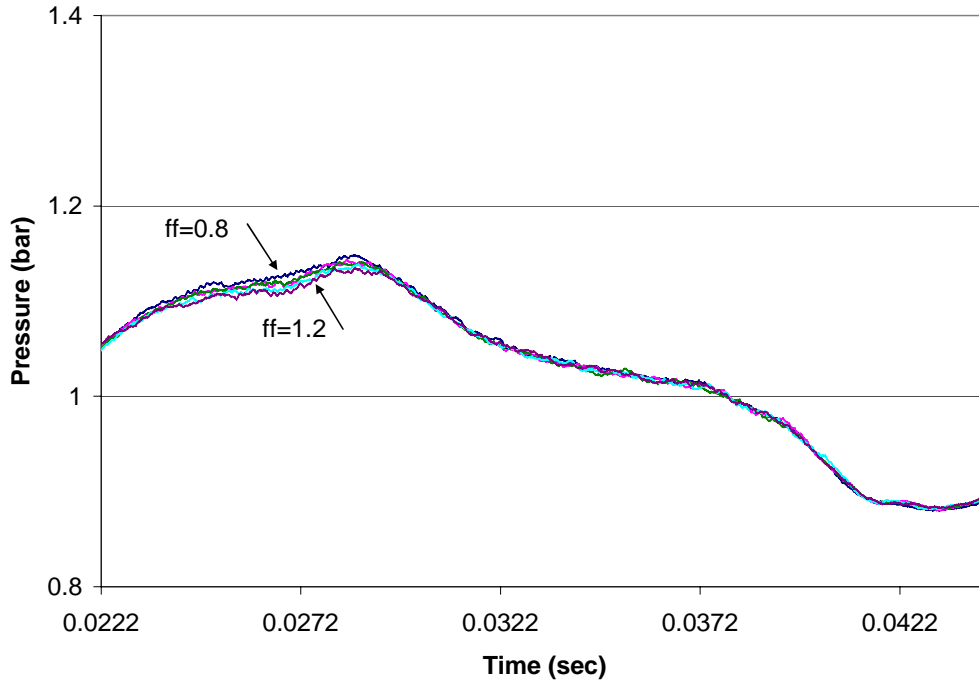
Figure B.6b Head pressures for 310 K air at 15 Hz for the purge portion of cycle. Purge fraction was held constant at 0.5.

The fill fraction effect on head pressure was largest during the fill portion (Fig. B.6c) of the cycle. The increase in pressure in the head was due to the increase in mass flow from the increasing fill fraction. For these tests, the size of the tubes and the relatively low firing frequency (15 Hz) set the tube mass flow requirements below the sonic point (Mach=1) at the intake valves. If the air flow requirements were suitably high, the flow through the intake valves would become sonic and cause a larger pressure and temperature drop across the valves. These effects would be more likely to skew the combustion data from case to case.
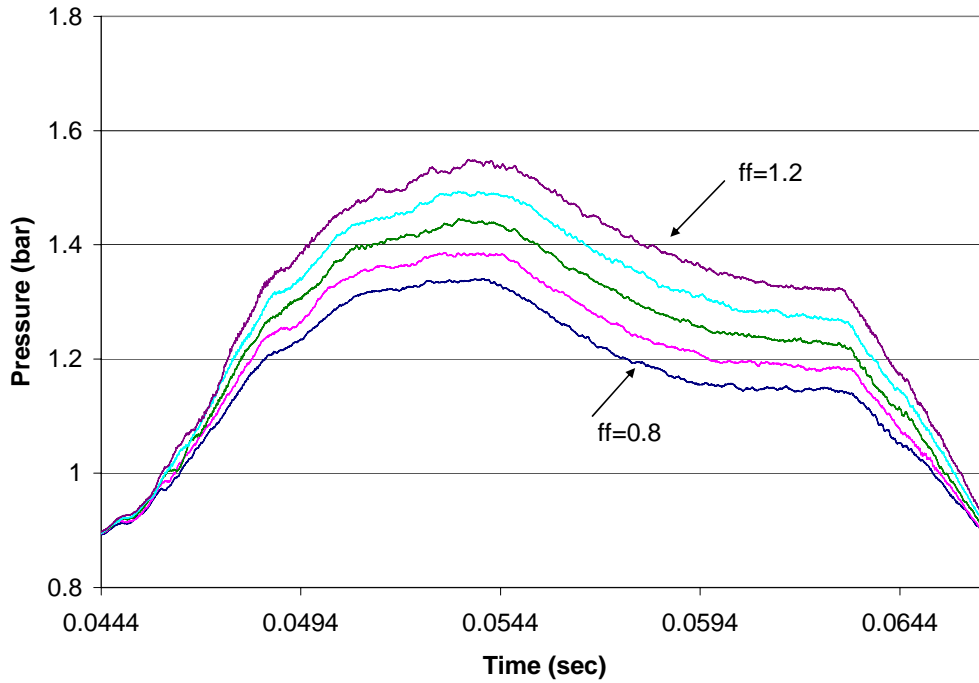
Figure B.6c Head pressures for 310 K air at 15 Hz for fill portion of cycle.

JP-8 Manifold Air Data

The air temperature was varied from 366 K to 422 K when the low vapor pressure JP-8 was tested. Figure B.7 shows the static pressure variation in the manifold at the fuel injector location 1.3 m from the intake valves for four air temperatures. It is important to note that during the tests, regardless of the fuel injector location, the manifold pressure never exceeded the upper limit of 2 bar. The upper bound of 2 bar was used in the modeling of the liquid vapor equilibrium discussed previously in Chapter V. The 422 K temperature air mass flow rate is the lowest for all the air temperatures and has the lowest fill pressure to meet the required volume.
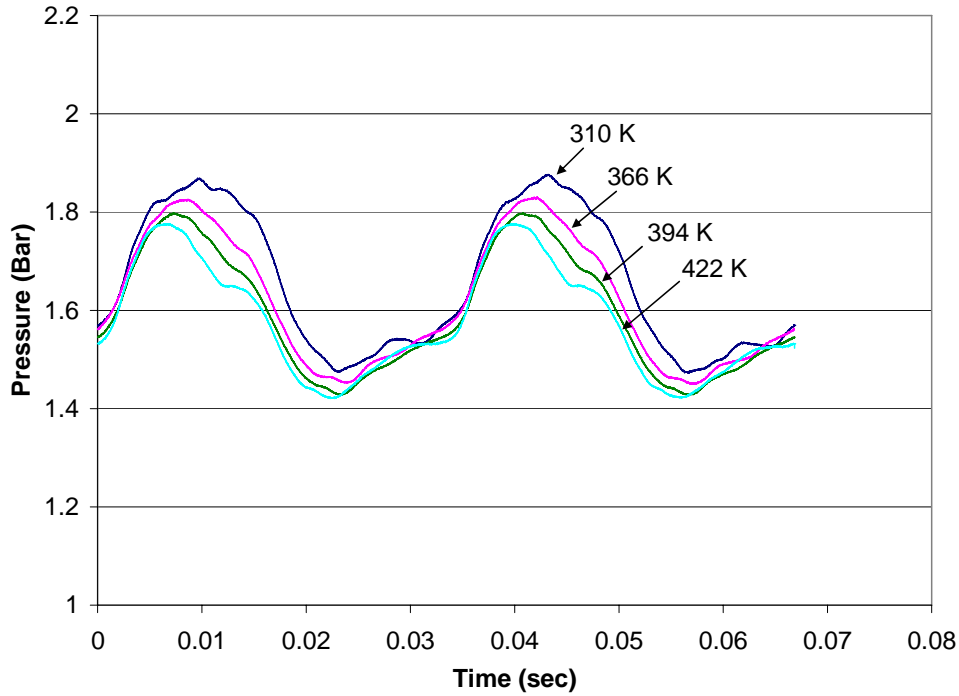
Figure B.7 Manifold air static pressures near the JP-8 fuel injector, 1.3 m upstream from the intake valves for 4 air temperatures air at 15 Hz for two tubes. Fill fraction is held constant at 1.0.

The combined fire, purge, and fill cycles are shown in Fig. B.8. When the mixture temperature varies but the fill fraction stays constant, the pressure magnitude of the expansion and compression waves does not vary as much as when the fill fraction increases as shown in Fig. B.6a. The firing portion of the cycle is shown in detail in Fig. B.9. The compression waves arrive fastest for the 422 K air temperature case and slowest for the 310 K air temperature case. This is due to the increase in the speed of sound (Equation 2.6) by 58.8 m/s and the resulting increase in the velocity of the sonic expansion and compression waves.
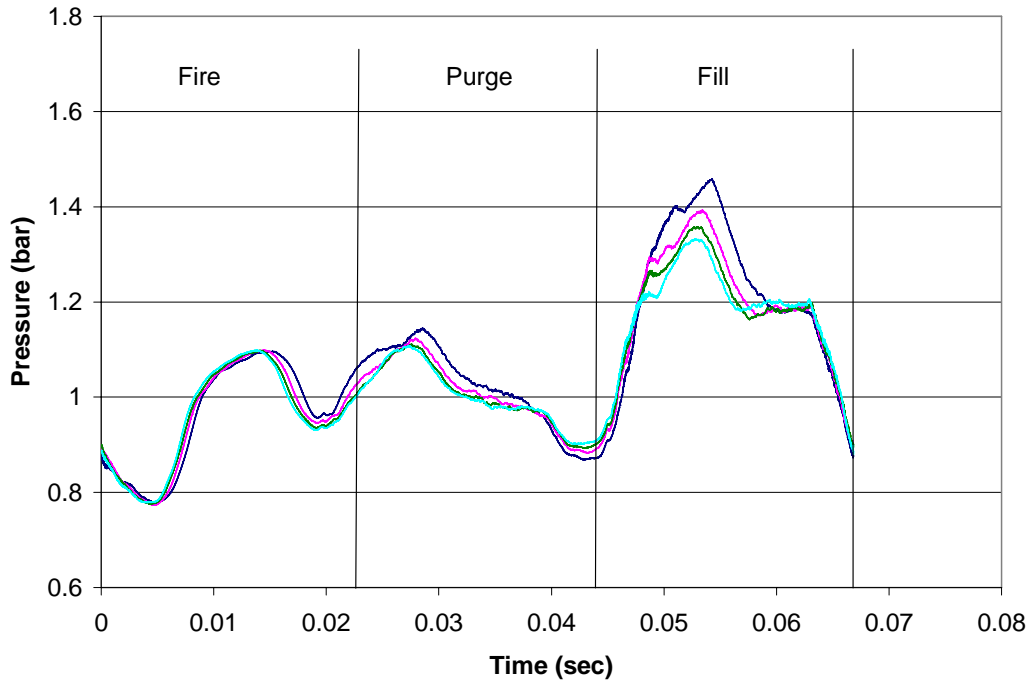
Figure B.8 Head pressure variations for 4 air temperatures with a fill fraction of one.
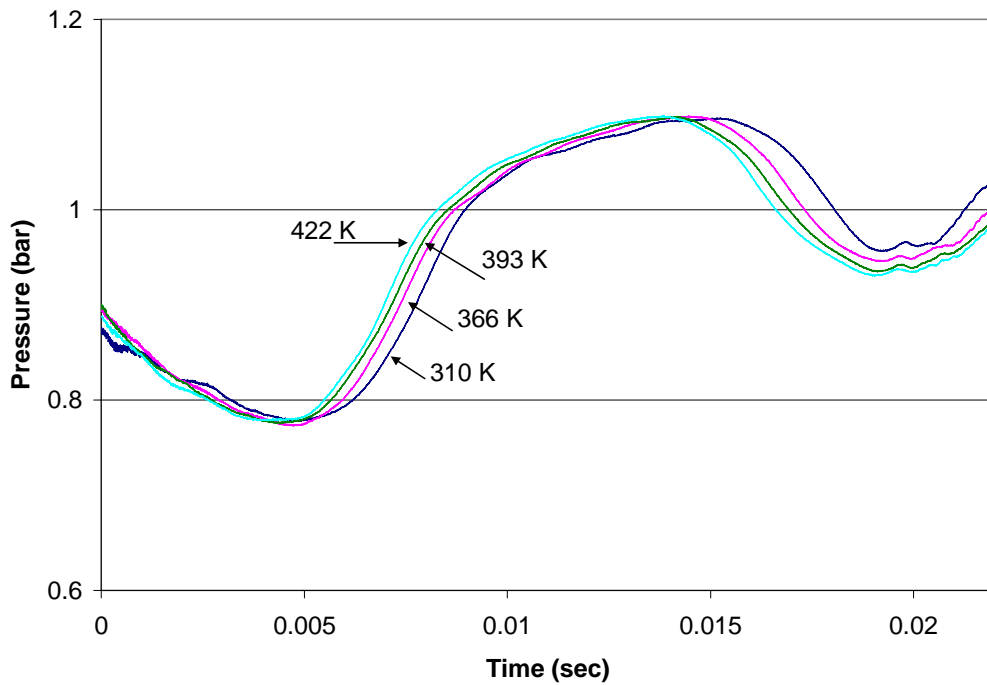
Figure B.9 Firing cycle head pressure for 4 air temperatures with a fill fraction of one.

During the JP-8 tests, combustion data was also taken at two spark delays, 6 ms

and 8 ms, but at three air temperatures, 366 K, 394 K, and 422 K that were much higher

186

than the 311 K used with the three high vapor pressure fuels. The measured ignition times

ranged from 6 ms to 16 ms as for the high vapor pressure fuels. The average pressures are

given in Table B.2 and are varied for different spark delays and air temperatures, but with

the fill fraction fixed at one. The average pressure in the head of the PDE thrust tube for

both an ignition event that took 6 ms and an ignition event that took 16 ms. A separate

column displays the difference in average pressure between the two spark delays. For all

spark delays and ignition times, the 8 ms spark delay had a higher average pressure. The

maximum pressure difference between the two spark delays, for a fixed fill fraction of

one, went down as the mixture temperature when up. The maximum average pressure in

the thrust tube differed between the four temperatures by 0.034 bar (6 ms spark delay)

and 0.019 (8 ms spark delay) and is considered negligibly small. The increase of 112 °C

in the air and thus the mixture temperature was more influential than the slight (2 to 3%)

pressure variation.

Table B.2 Average pressures in head for four different air temperatures.

Air Temperature (K)	Spark Delay	6ms Ignition Time Average Pressure (bar)	Change (bar)	16ms Ignition Time Average Pressure (bar)	Change (bar)
310	6	0.966		1.011	
310	8	1.044	+0.078	1.038	+0.027
366	6	0.980		1.007	
366	8	1.051	+0.071	1.027	+0.020
394	6	0.990		1.005	
394	8	1.057	+0.067	1.021	+0.016
422	6	1.000		1.006	
422	8	1.063	+0.063	1.019	+0.013

The changing air temperature affected the average pressure by less than 2% between the limiting cases. This provides an important insight that comparing data from the high vapor pressure fuel air temperature of 310 K to the low vapor pressure fuel air temperature up to 422 K given the same fill fraction does not significantly raise or lower the average pressure the reactants experience during the ignition and DDT events.

Computational Flow Solver

As stated earlier, the unsteady nature of the PDE intake air flow was a concern. To determine the extent of the air mass flow variation due to the intake valves opening and closing (Fig. B.1 and B.2), a CFD analysis was performed on the air feed system. The Air Force Institute of Technology Extendable Research Code (AFITERC) is a two-dimensional, structured, cell-centered, finite volume, Euler/Navier-Stokes code. Flux evaluations are accomplished using first or second order Roe averaging.[90] The code was co-developed by the author with Daniel Millman and David Lucia. The code has both time accurate and steady state options, and time integration is accomplished via either first, second, or fourth order Runge-Kutta (R-K)[91] method. The code was validated using a combination of theory and experimental data. Subsonic performance was validated using wind-tunnel data.[92]

The unsteady nature and variable pressure downstream of the intake valves in the PDE head was captured with a variable area outflow condition with a specified exit pressure depending on the specific time of the cycle. Experimental pressure data (Fig. B.6c) was input on the exit boundary condition to properly mimic the pressures

downstream of the intake valve during the fill cycle. The first order Roe scheme, with a first order R-K time accurate solver was used.

Grid Dimensions

The grid dimensions were 177 x 65 cells (Fig. B.10) and represented 8.5 meters of the air intake system. The air mass flow through the grid was fixed by a choked orifice. The choked orifice was critical to capturing the flow physics due to the large pressure oscillations that guaranteed reverse flow at a subsonic inflow boundary condition. The choked orifice is also representative of a supersonic inlet feeding a PDE. The left most circle in Fig. B.10 represents the choked orifice grid section and is enlarged in Fig. B.11.
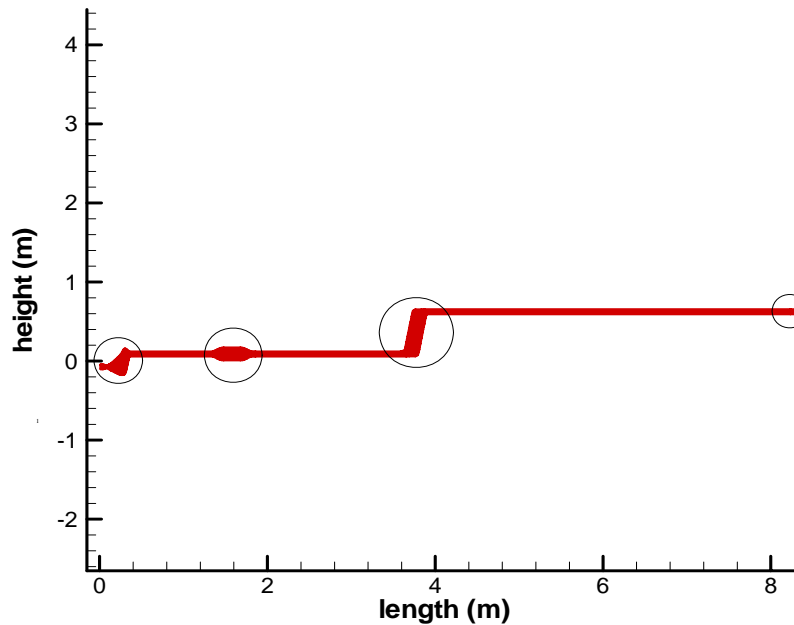
Figure B.10 Full grid of intake system. Circles denote (left to right) the choked orifice, injector, mixer, and intake valves.
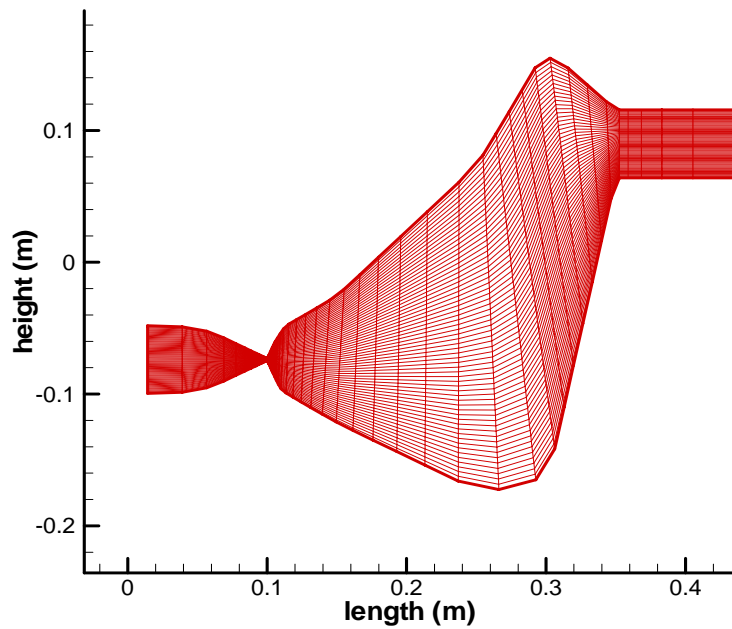
Figure B.11 Grid of choked orifice flow device for flow.

The orifice is gradually convergent with a large divergent section to model the choked plate geometry described in Chapter III. The result is the jet shown below in Figs. B.12a and b. The supersonic jet flows into a void and allows the flow to settle out before being fed into the injector flow path. The orifice does choke (Mach=1) and then accelerates supersonically until settling to a lower subsonic flow with the large area settling chamber.
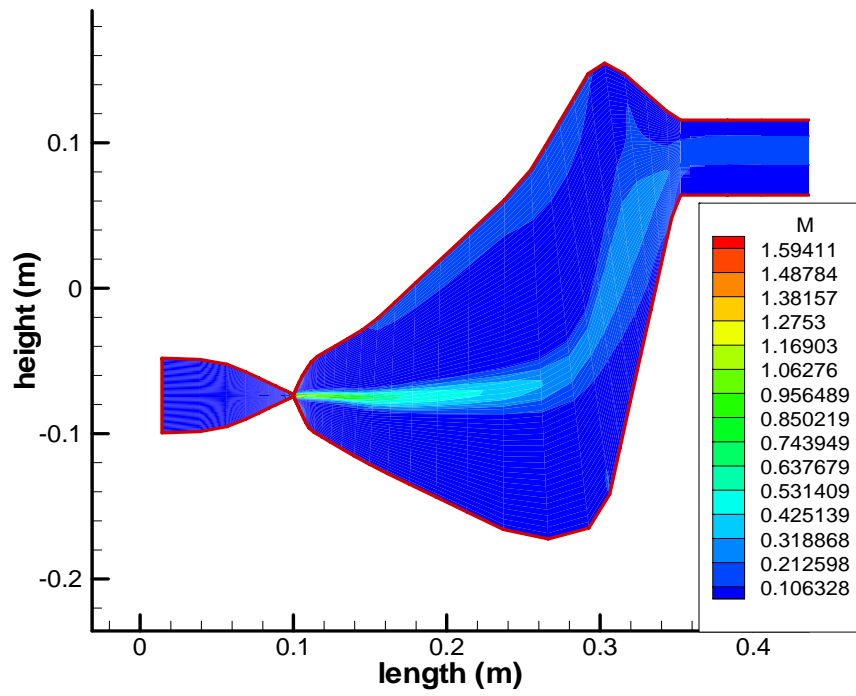
Figure B.12a Mach profiles of choked orifice flow metering device.
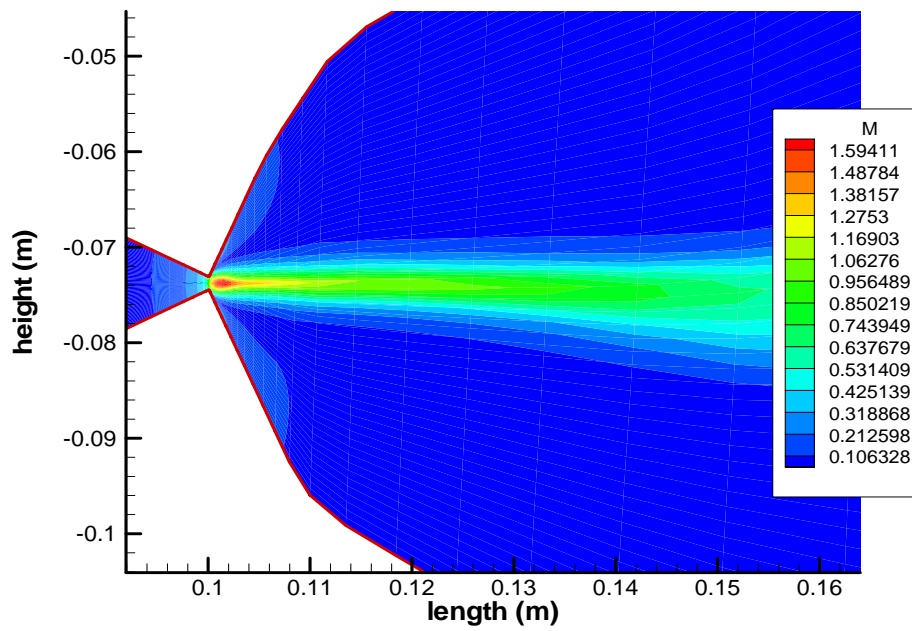
Figure B.12b Mach profiles of choked orifice flow metering device.

The portion of the air manifold where the fuel was injected and mixed (Fig. B.13) was modeled only as a void without any nozzle spray bars or other structures. The static pressure on the wall was recorded at the same location (6.5 m upstream) that the experimental data was recorded. The results are shown later in this chapter.
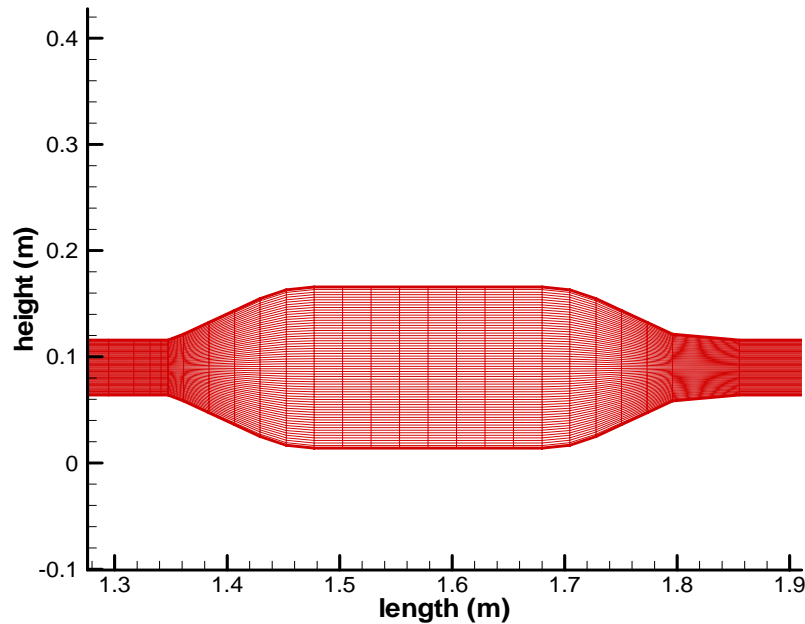
Figure B.13 Fuel injector body in air system grid.

The internal geometries of the mixer were too complex and three dimensional to adequately capture in a two dimension grid. The axial mixer (Fig. B.14) was modeled as a void but with two 90 degree bends that would force the axial flow to turn twice through the device. No attempt was made to experimentally or numerically evaluate the axial mixer as a flow improvement device. The volume of the mixer did act as a capacitor, however, and absorbed and reduced the magnitude of the air flow fluctuations
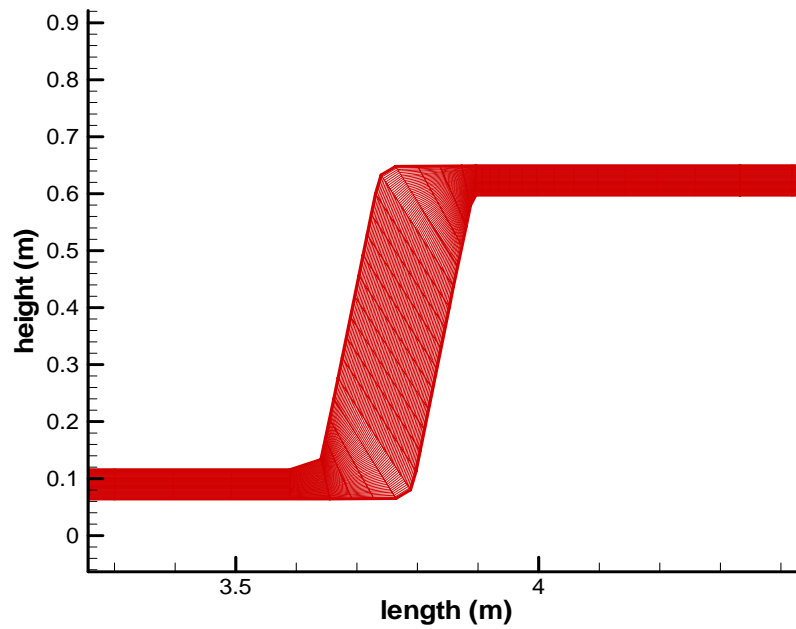
Figure B.14 Grid of mixer body and void.

The intake valve was modeled by changing the number of cells opened at the right boundary condition. The effective valve area was determined by dividing minimum valve area by total tube area and using the area ratio to convert from three dimensional pipes to two dimensional slots.
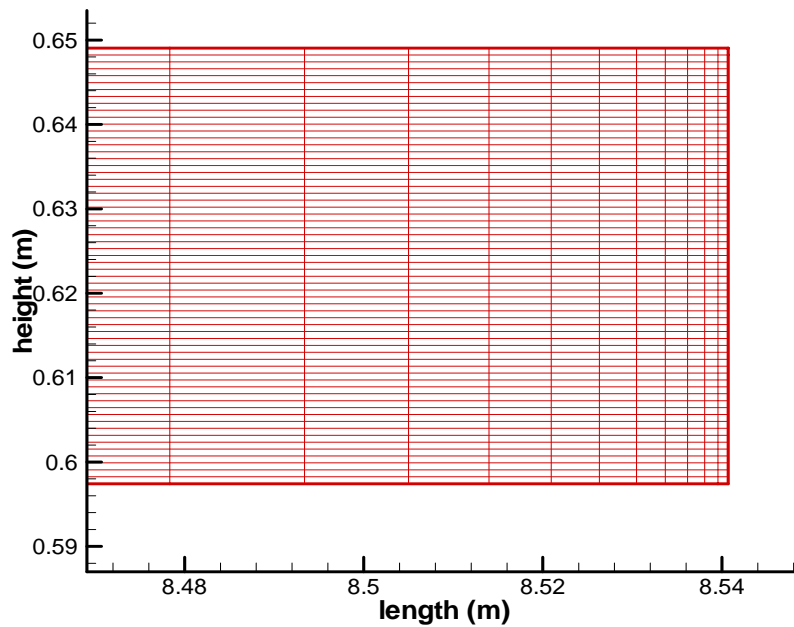
Figure B.15 Grid at valve. Right wall cells open and close to mimic the opening and closing of the intake valves.

Run Time

The program took 38 hours to run one complete cycle (valves open and close twice). The computer used was a Compaq desktop with an AMD Athlon™ XP 2600+ running at 2.13 GHz with 1.0 Gig RAM on a Windows XP Professional operating system. It took five to 10 cycles to completely settle out the pressure and velocity changes to less than 1% between cycles. Time steps were 2.28×10^{-8} seconds.

Comparison of Experimental and Computational Results

The experimental and computational data are plotted together for the injector and manifold captured static pressure traces in Figs. B.16 and B.17. The experimental pressure traces in both figures were shifted upward by 3450 Pa (2%) to match the pressures from the computational flow. This is both reasonable and expected due to the

inviscid code not capturing the inherent pressure drop due to the viscous boundary layer, the pipe flow bends and turns, and in particular the head losses at the choked orifice due to the turbulent separation not properly captured at the jet. The shapes and magnitudes of the experimental results are reasonably captured with the CFD simulations of the flow field. Most important is the capturing of the pressure wave time scales.
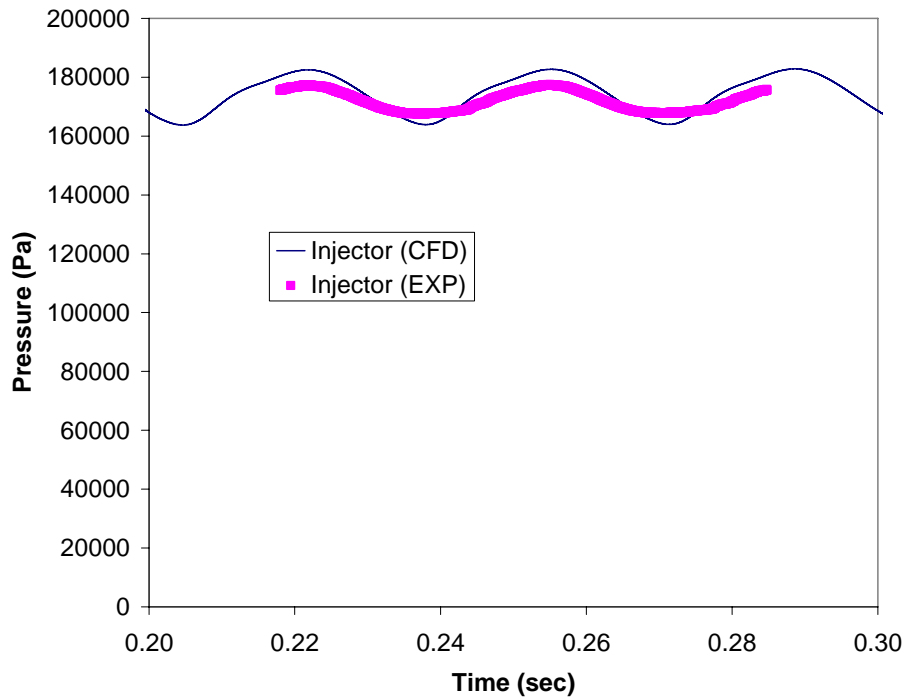
Figure B.16 Static pressure comparisons at the wall inside the fuel injector body 6.5 m from the intake valves. Experimental data is shifted upward by 3450 Pa.

The overall shape of the pressure wave at the intake manifold location, 88 cm from the intake valves, is mostly captured in Fig. B.17. Some irregular flow dynamics of the actual intake geometry manifold were not resolved with the simplified grid.
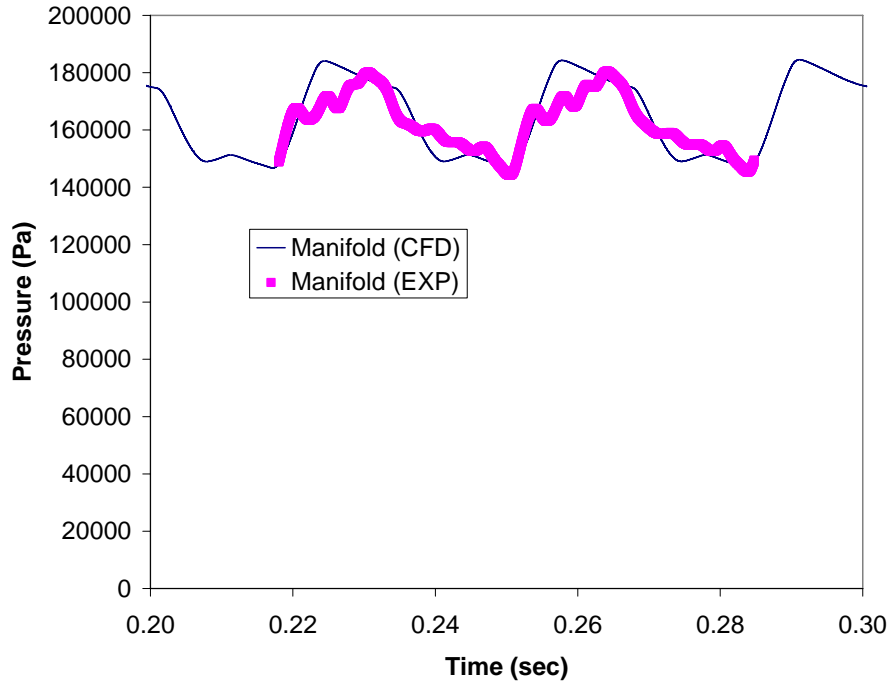
Figure B.17 Static pressure comparison at the wall 88 cm upstream from the intake valves. Experimental data is shifted upward by 3450 Pa.

The velocity profiles were difficult to measure with traditional pitot-static probes. The 46 cm length between the pitot probe tip and the transducer location in conjunction with high speed pressure fluctuations provided data that was unusable. Hotwire anemometry would have been successful but was not readily available. The CFD was used to quantify the velocity fluctuation in the flow field. Figure B.18 gives the computationally determined velocity profiles at the centerline of the main manifold at locations both 88 cm upstream of the intake valves as well as 6.5 m upstream where the fuel is injected into the air. The velocity fluctuation nearest the intake valves range from 1 m/s to 65 m/s. These large air velocity swings make this location a poor choice for steadily injected fuel. Farther upstream is a better injection location since the velocity only fluctuates from 20 to 35 m/s. The average velocity is lower because of the mass of compressible air stored in the 6.5 m length between the valves and the fuel injector body

196

(Fig. B.13). The mass of air acts as a capacitor and can absorb and dampen the oscillations.
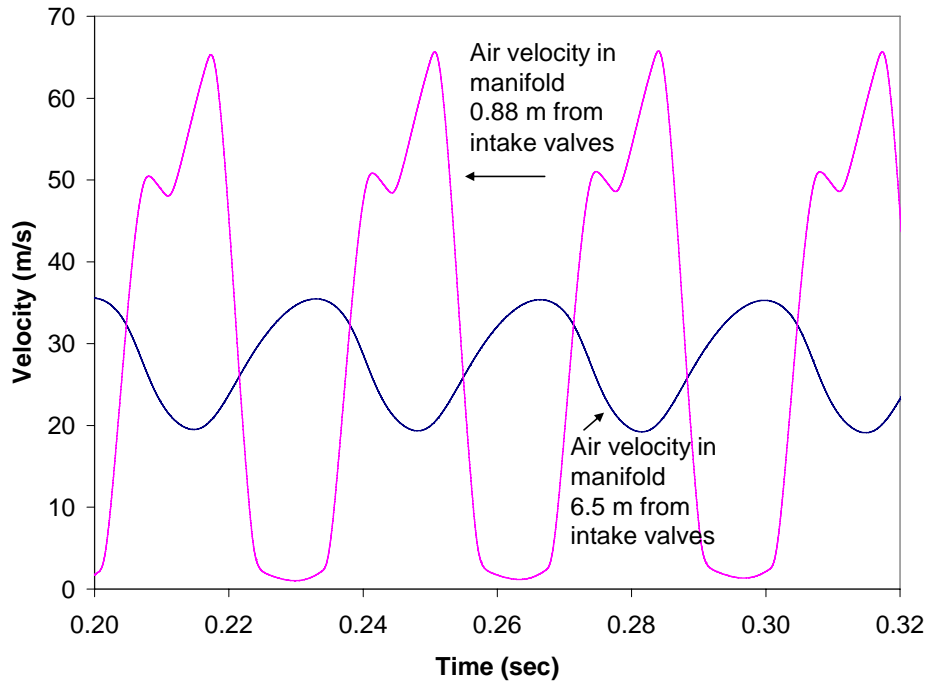
Figure B.18 CFD derived centerline velocity profiles at the fuel injection location and near the intake valves.

The air velocity fluctuations are not balanced with the steady fuel flow that comes in at a high pressure and velocity. The relatively low pressure air oscillations do not effect the supersonic fuel injection. The variation in air velocity when combined with a steady flow fuel injection should exhibit a variation in equivalence ratio of $\pm 23\%$. This variation was not observed in the combustion data, nor does it take into account any of the turbulence enhanced axial mixing due to vortices separating off the blunt fuel injector bodies (Fig. B.19). The fuel and air system should be designed to have steady air flow and low velocity fluctuations at the fuel injector to minimize mixing and stoichiometry issues. No attempt was made to further improve the stoichiometry of the injection process. The combustion results show excellent repeatable performance and much

smaller variations in phi. It is the author's opinion that these fluctuations are averaged out by the three dimensionality of the flow, as well as the mixing caused by the starting and stopping of the mixture near the intake manifold, shaking the mixture and causing the rich and lean regions of flow to collide.
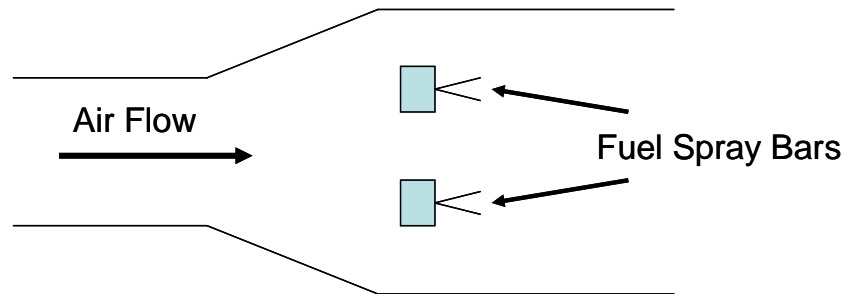
Figure B.19 Flow at the injectors (left to right).

Appendix C. Supercritical Fluids Analysis

Multiphase Fluids

The phase in which a pure substance exists depends only on two state variables such as temperature and pressure. Sub-cooled liquids exist at temperatures below the saturation temperature at a given pressure. The sub-cooled region is to the left of the saturated liquid line until the critical pressure is attained (Fig. C.1). At a given pressure there is a defined saturation temperature at which the substance begins to boil and change phase from a liquid to a gas and is known as the saturation region. This region is called the vapor dome, and is the area between the saturated liquid and vapor lines below the critical pressure. For a fixed pressure, the temperature will remain constant through the saturation region, and the energy state determines at what quality the substance exists. The quality defines the mass fraction of the substance that exists in the vapor phase. After the liquid fully changes phase to a vapor through some energy exchange, the vapor is called a superheated vapor and is shown as the region to the right of the saturated vapor line up to the critical point.

The fluid is treated as supercritical if it exists in the region above the critical pressure and temperature. In the supercritical region, the fluid behaves as a liquid and a gas and has zero surface tension between phases. Similar to a gas, the supercritical properties are defined by two state variables, but the fluid does not yet behave as an ideal gas and a compressibility factor or similar method must be employed to correct for the behavior. The fluid does not behave as a perfect gas until the temperature is much greater than the critical temperature ($T \gg T_c$). The supercritical properties of density and

viscosity are much lower than that normally associated with liquids but still higher than that of the vapor phase. Supercritical fluids also exhibit gas-like qualities of compressibility, homogeneity and gradually change from liquid to gas-like properties as the temperature increases.[93]
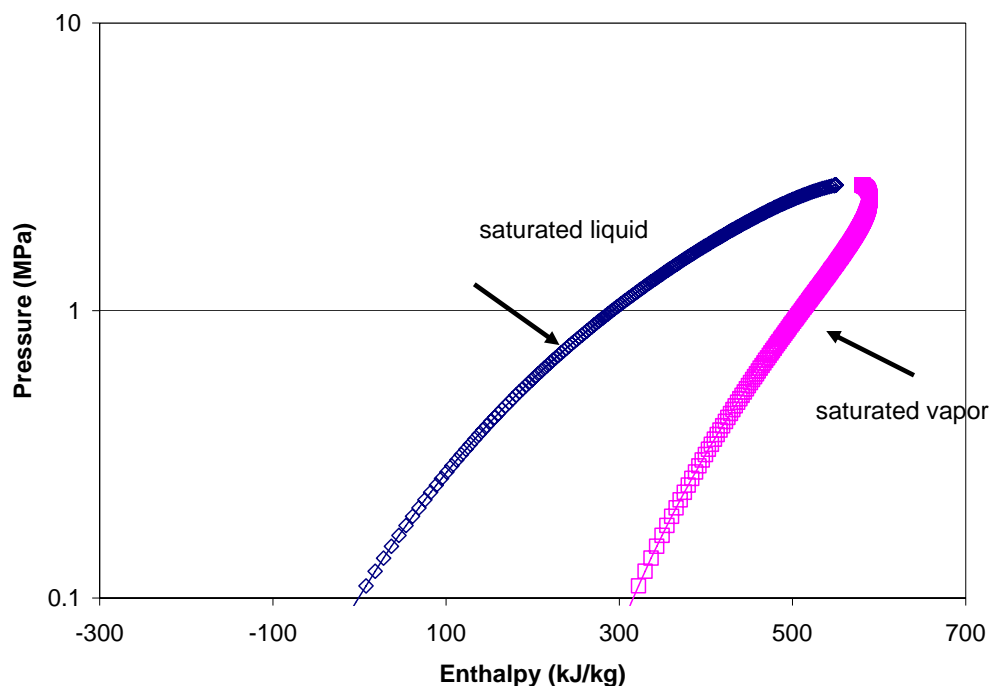
Figure C.1 n-Heptane P-h diagram. Data from Ref. 80.

Peng-Robinson Model

The program SUPERTRAPP uses the Peng-Robinson equation of state[85] (PR-EOS) to determine the vapor liquid equilibrium phase compositions of the hydrocarbon and air mixtures being studied in this work. The thermodynamic properties of the different phases are calculated using the National Institute of Standards and Technology (NIST) extended corresponding states model (EXCST). n-Heptane, isooctane, and a JP-8 surrogate are input into the program to determine the density, viscosity, and other properties of interest at the temperatures and pressures upstream of

the fuel injectors prior to mixing with air. A brief discussion of the two models is show below.

SUPERTRAPP can calculate the liquid vapor equilibrium (flash) given two state variables at the end of some mixing process and allows multiple components to be present in the mixture. The FLTP command performs the flash (FL) calculation at constant temperature (T) and pressure (P), and the FLPH command performs the flash calculation at constant pressure (P) and enthalpy (H). In addition to all the other state variables, the program calculates the final molar qualities of each component in the mixture assuming the mixture has had infinite time to reach an equilibrium condition. An example of the input is shown in Table C.1. Three components (COMP) make up the stoichiometric n-heptane (C7) and air (N_2 and O_2) mixture. The feed for each component is input in molar fractions with the requirement that the three fractions sum to one. The isothermal and isobaric flash calculation (FLTP) is invoked with the temperature in Kelvin and the pressure in bar.[94]

Table C.1 Input script for SUPERTRAPP isothermal flash calculation.

COMP	1	N2
COMP	2	O2
COMP	3	C7
FEED	1	0.77511
FEED	2	0.20615
FEED	3	0.01874
FLTP	298.15	1
FLTP	298.15	2
FLTP	298.15	3

Both the PR-EOS and EXCST models are based on an extension of van der Waals equation that applies a dimensional analysis technique to sets of known data to determine

the properties of an unknown component that may have a similar molecular behavior. Semi empirical equations of state such as van der Waals represent pressure as the sum of the repulsive and attractive pressure terms (C-1).

$$P = P_A + P_R \tag{C-1}$$

The attractive pressure can be expressed by Equation C-2 below where a is a measure of the intermolecular attraction force and $g(v)$ is a function of the molar volume v.

$$P_A = -\frac{a}{g(v)} \tag{C-2}$$

$$P_R = \frac{RT}{v - b} \tag{C-3}$$

The repulsive pressure term comes from van der Waals' hard sphere equation (C-3) where R is the universal gas constant and T is temperature. The a and b parameters account for the intermolecular attractive forces and finite molecular volumes that are present in real fluids. The van der Waals forces must be considered when the density is high enough that the molecular spacing is comparable to the range of the intermolecular forces.[95] When the density is not as high, then the model reverts to the idea gas law.

The attractive pressure term was modified to significantly improve the prediction of vapor pressures for pure substances and equilibrium ratios for mixtures (C-4).

$$P = \frac{RT}{v - b} - \frac{a(T)}{v(v + b) + b(v - b)} \tag{C-4}$$

The results[85] from this model show a prediction of n-heptane vapor pressures with a 0.79% relative error with a bias of 0.63%. Excellent agreement for many other paraffin hydrocarbons was also provided in the paper.

Extended Corresponding States Model

A two parameter corresponding states model uses a partition function to represent the thermodynamic properties of different substances as universal functions of dimensionless groups. The model is based on statistical thermodynamics and is reduced to Eqn. C-8 below.[95]

$$P_{reduced} = \frac{P_{actual}}{P_{critical}} \tag{C-5}$$

$$T_{reduced} = \frac{T_{actual}}{T_{critical}} \tag{C-6}$$

$$Z = \frac{Pv}{RT} \tag{C-7}$$

The experimentally determined compressibility Z is valued at one for ideal gases.

$$Z = f(\frac{\varepsilon}{kT}, \frac{V}{N\sigma^3}) = f(T_{reduced}, P_{reduced}) \tag{C-8}$$

where ε is the potential energy minimum in intermolecular potential, σ is the separation distance between molecules at zero potential energy, k is the Boltzmann's constant, N is Avogadro's number, V is the volume for the component being studied.

If individual substances and the reference substance fall into certain chemical and molecular categories (or conform to the same intermolecular potential function), the values will collapse quite well for reduced temperatures and pressures (Eqns. C-5 and C-6). If a substance deviates slightly from the simple (two equation) model, the model can be extended with a correction for non-symmetrical potentials of the molecules with a third parameter called Pitzer's acentric factor. Further improvement, with empirically derived shape factors,[96] correct the substance to better match the two parameter corresponding states model.

Both iso and normal alkanes (C_nH_{2n+2}) fall into the category with weak polarity and/or with a small deviation from a symmetric force field. These fuels are adequately captured with an extended corresponding states model and the inclusion of shape factors. The models thermodynamic properties such as enthalpy, entropy, and compressibility are accurate to 4.4%.[96] The accuracy of the models transport properties such as the viscosity of n-heptane is an average absolute percent deviation of 6.31 with a bias of 3.45.[97]

Leland and Chapelear state the Corresponding States Principal model requirements:[95]

1) The translational energy states of the molecules must be entirely independent of the rotational states, and the molecules translational and rotational energies are small relative to kT.

2. The internal energy states for an individual molecule are independent of density.

3. The translational and configurational portions of the partition function are assumed to be independent of quantum effects, and the Maxwell-Boltzmann statistics are considered applicable. Light molecules such as Ne, D_2 and H_2 are excluded from the simple corresponding states model.

4. The total potential energy for the system can be expressed as the product of an energy parameter and a function of dimensionless separation distances between molecular centers.

JP-8 Thermodynamic Properties Surrogate

The components combined in Table C.2 represent a proposed physical surrogate that mimics the approximate volatility and phase change behavior of JP-8 / Jet A.

Surrogates are used to capture the thermodynamic characteristics of multi-component fuels, such as JP-8 or aviation gasoline, that are too complex to represent explicitly.[98] The combination of these compounds is used in SUPERTRAPP to capture the air and fuel temperature at the highest expected manifold pressure to achieve a fully flash vaporized mixture. The surrogate is a modified version of Shultz's[99] surrogate with two compounds removed and the composition tweaked to match the approximate carbon and hydrogen numbers. As shown in Figs C.2 and C.3, the modeled values agree well with published dew and bubble point properties as well as density. The JP-8 surrogate model misses the bubble point line by 12.5 °C (1.84% of Tc) and dew point line by 22 °C (3.24% of Tc).

Table C.2 JP-8 Surrogate for modeling vaporized mixture.[100]

Name	SUPERTRAPP Symbol	Formula	MW	Mass of fuel	Moles
isooctane	224TMP	C_8H_{18}	114.229	5.0%	0.06830
methyl cyclohexane	MCC6	C_7H_{14}	98.186	5.0%	0.07945
meta-xylene	MXYL	C_8H_{10}	106.165	5.0%	0.07348
n-decane	C10	$C_{10}H_{22}$	142.282	15.0%	0.16449
butyl benzene	C4BNZ	$C_{10}H_{14}$	134.218	5.0%	0.05812
n-dodecane	C12	$C_{12}H_{26}$	170.335	22.0%	0.20152
1-methylnaphthalene	1MNAPH	$C_{11}H_{10}$	142.197	10.0%	0.10972
n-tetradecane	C14	$C_{14}H_{30}$	198.388	18.0%	0.14156
n-hexadecane	C16	$C_{16}H_{34}$	226.441	15.0%	0.10335
surrogate		$C_{11.9}H_{21.6}$	156.024	100.0%	1.00000
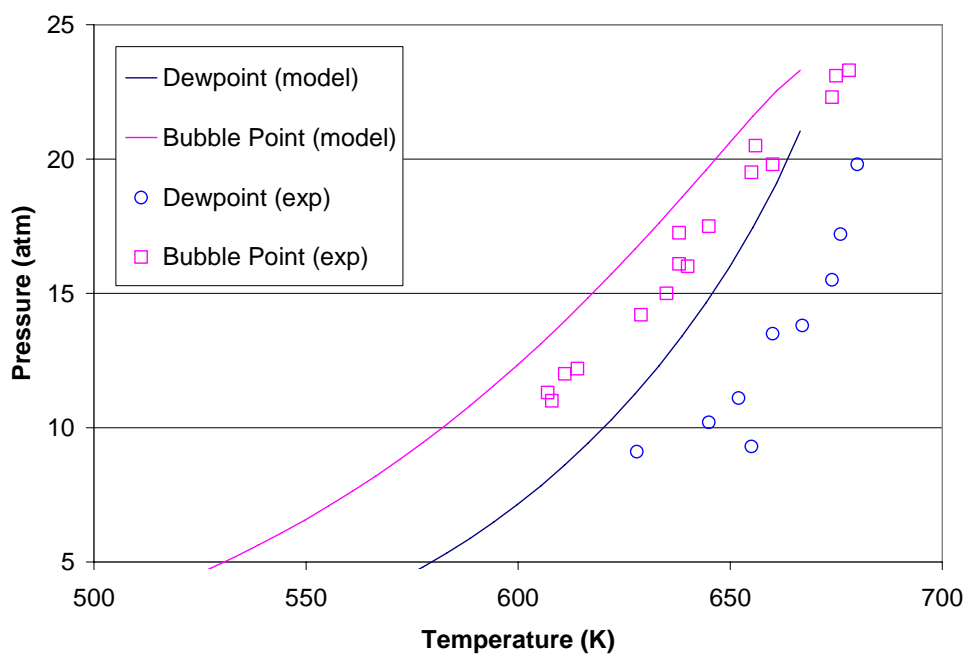
Figure C.2 Comparison of computed JP-8 vapor dome with experimental data. Data from Ref. 81.
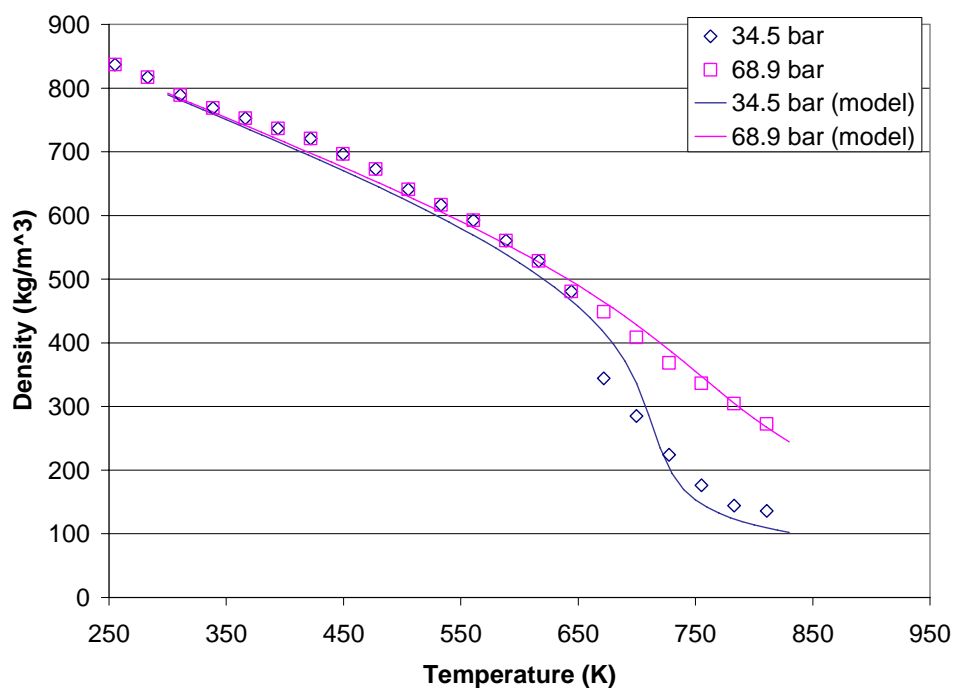
Figure C.3 Comparison of computed JP-8 surrogate with density at two pressures. Data from Ref. 101.

In Fig. C.4, each of the components that make up the JP-8 surrogates described in Table C.2 is shown as the percentage of each individual component as a gaseous vapor after injection into air relative to the final mixture temperature. The specific component percentages of the overall fuel mixture are listed on the rightmost column in Table C.2. The components that are the hardest to get to vapor are heaviest per the molecular weight of the species. The individual species in Fig. C.4 are multiplied by the species mole fraction and summed to make Fig. 5.7.
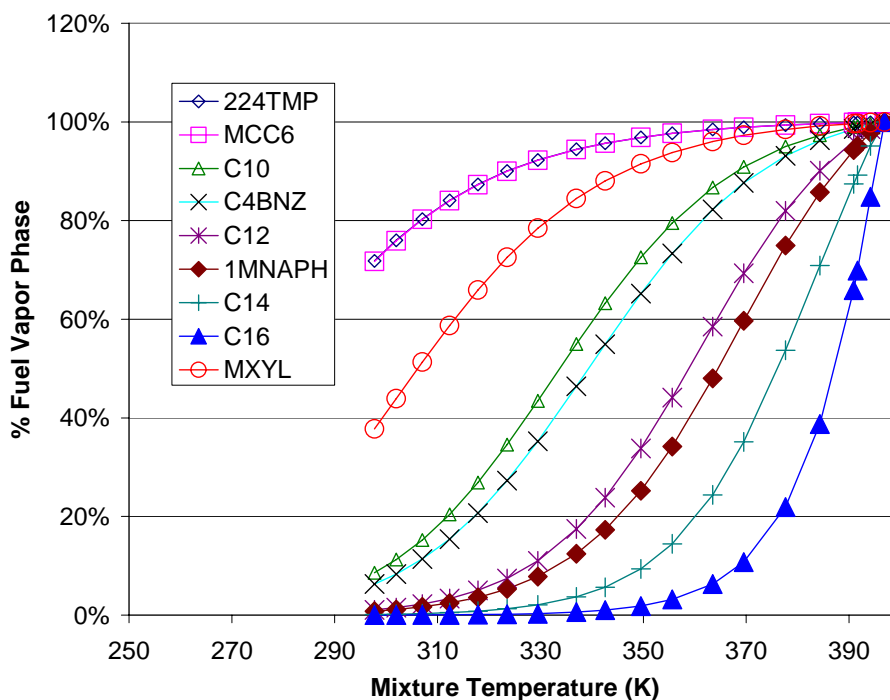
Figure C.4 Surrogate component vapor fraction for a stoichiometric fuel and air mixture at 2 bar.

The fuel density at a given temperature and pressure was important in determining how much fuel mass could be stored within the furnace during the flash vaporization system (FVS) runs. At the higher fuel temperatures, the low density limited the mass storage and thus the maximum run time. After the fuel temperature exceeded the critical

point, the density became pressure dependent (Fig. C.5), and the mass storage dropped

further to a point where runs were not feasible.
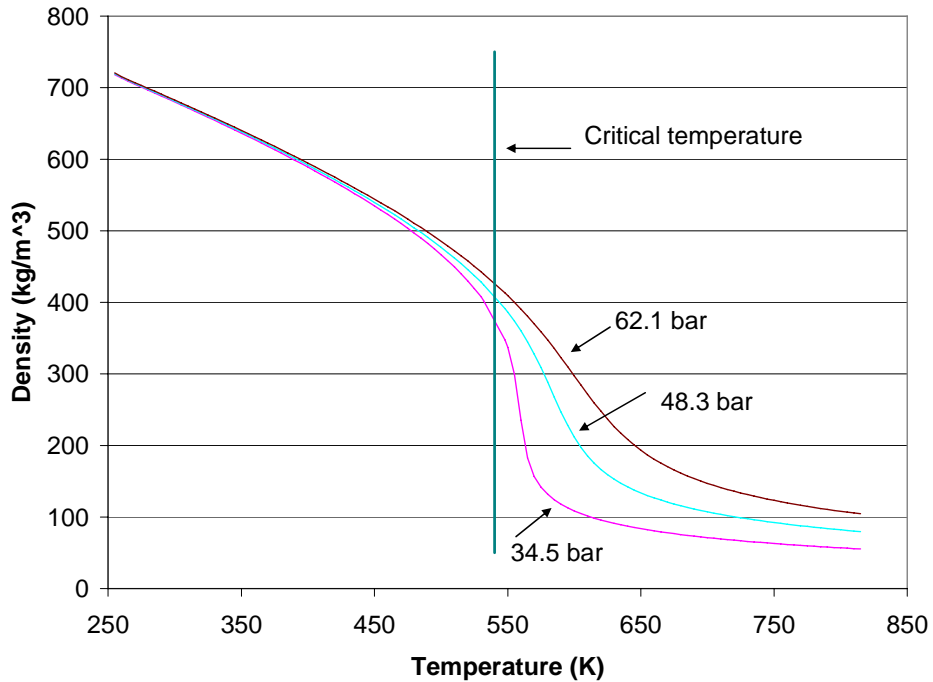
Figure C.5 Isooctane density for three pressures. Data from SUPERTRAPP.

The viscosity of the fuels was also pressure and temperature dependent at

temperatures exceeding the critical value. As seen in Fig. C.6, the viscosity of n-heptane

drops over 2 orders of magnitude during the heating, at values above the critical

temperature.
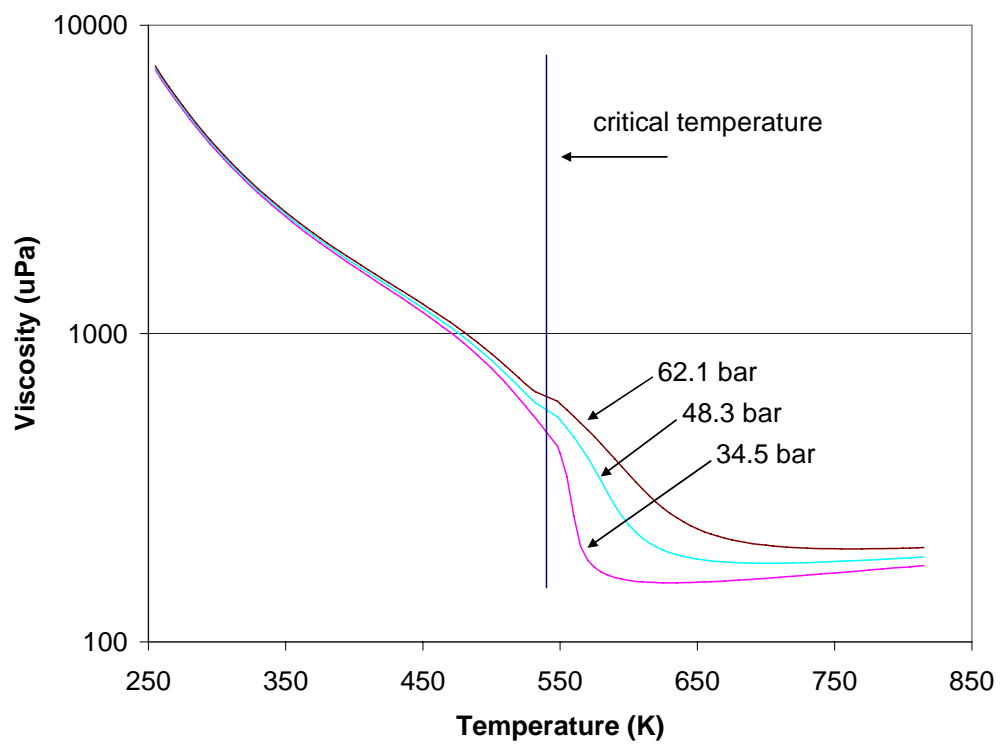
Figure C.6 n-Heptane viscosity for three pressures. Data from SUPERTRAPP.

Appendix D. Test Conditions

This appendix contains the test conditions recorded during the data collection for the results presented in Chapter VI. The air and fuel flow data are the averages over a five second window during the high speed data acquisition.

Table D.1 Barometric pressure during test days.

Fuel	Test Day Pressure (bar)	Delta (bar)	Standard Deviation
Av Gas	0.9942		0.0004
isooctane	0.9887	-0.0055	0.0007
n-heptane	0.9893	-0.0049	0.0010
JP-8	0.9869	-0.0073	0.0004

Fuel and Air Test Conditions
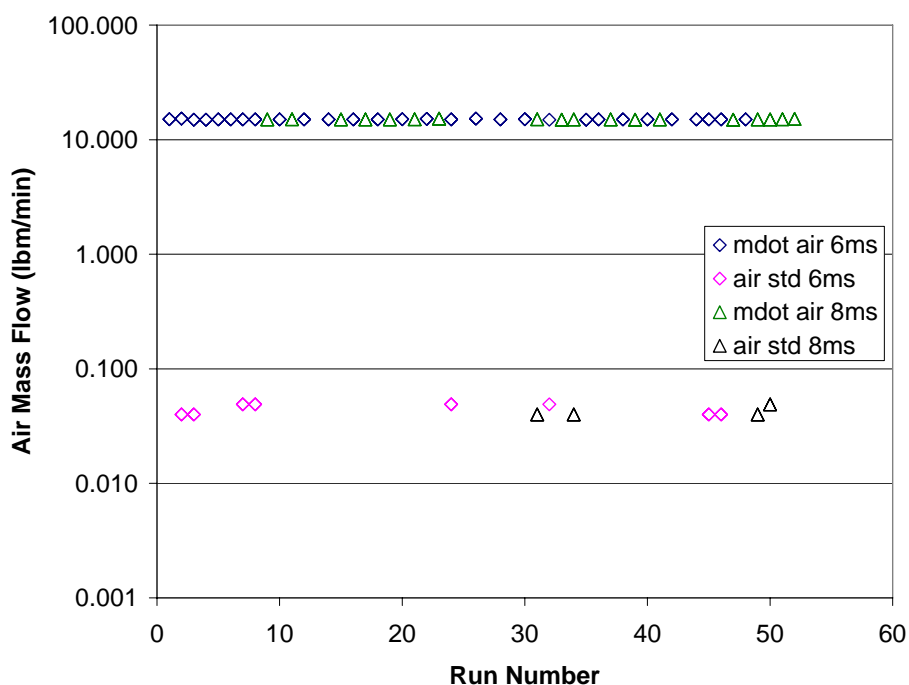
Figure D.1 Aviation gasoline tests air flow performance, missing test point standard deviations are below the threshold of 0.001 lbm/min.
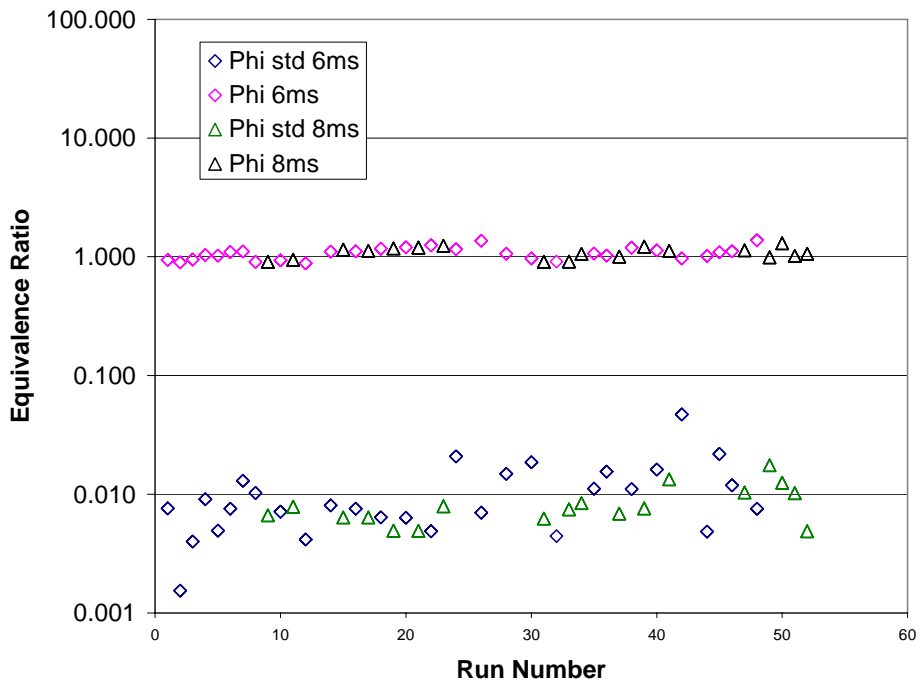
Figure D.2 Aviation gasoline fuel flow performance.
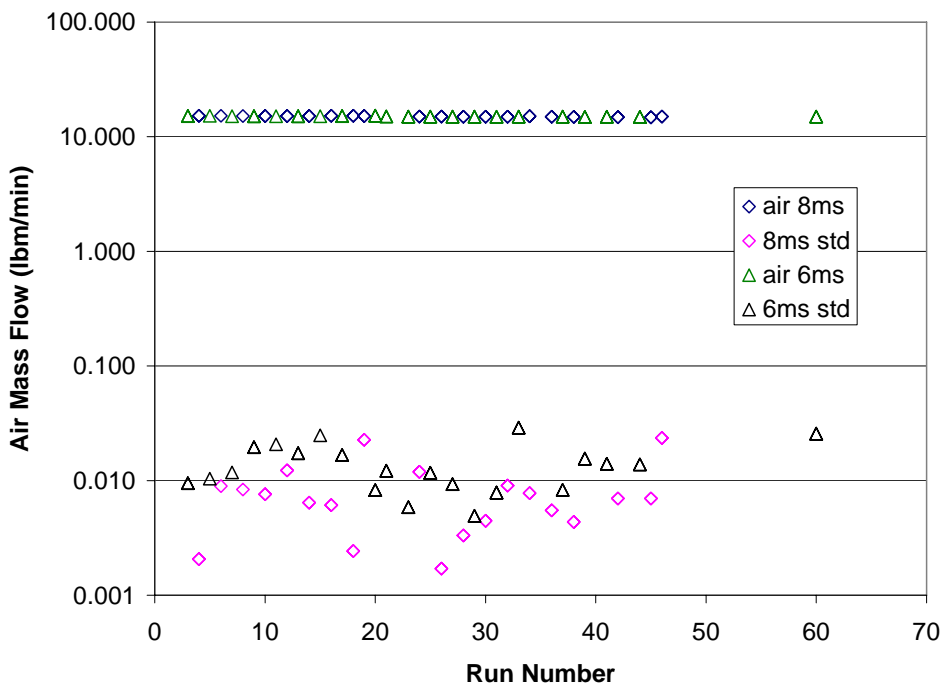
Figure D.3 Isooctane air flow performance.
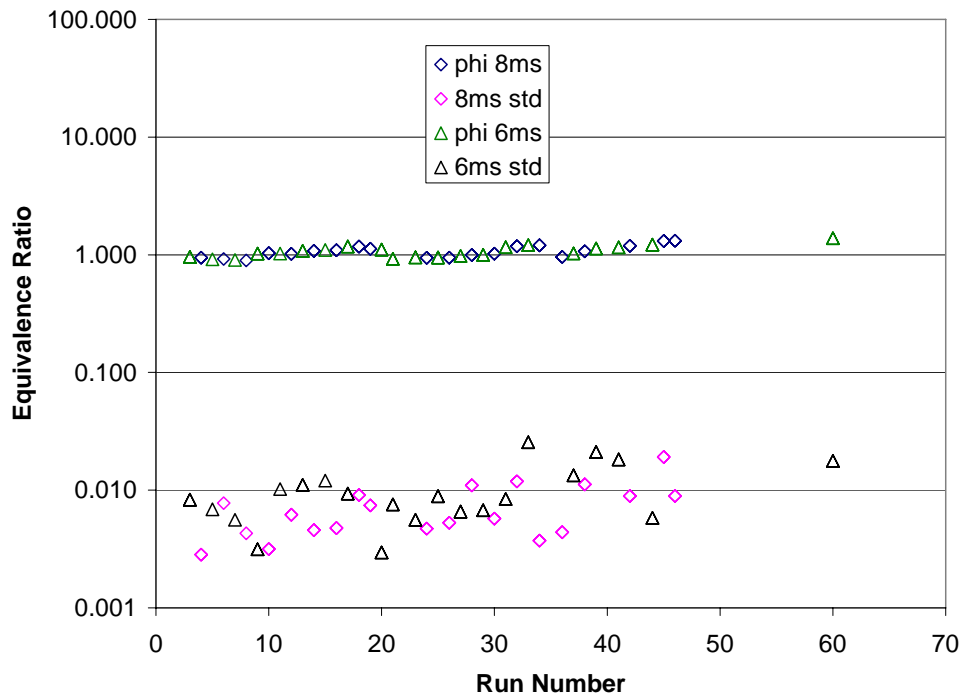
Figure D.4 Isooctane fuel flow performance.
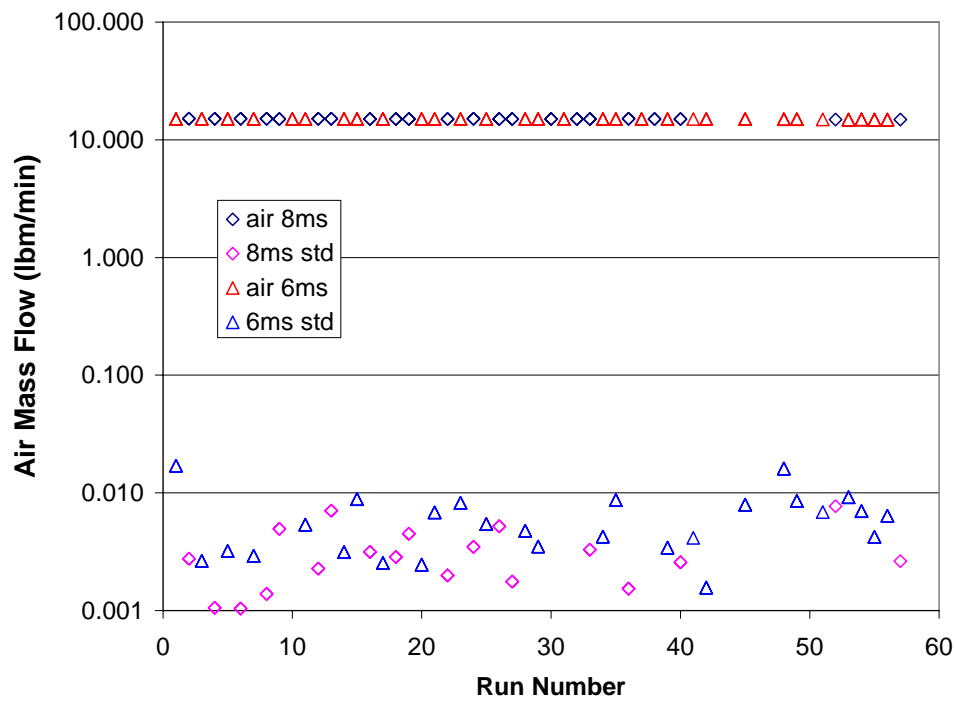
Figure D.5 n-Heptane air flow performance.
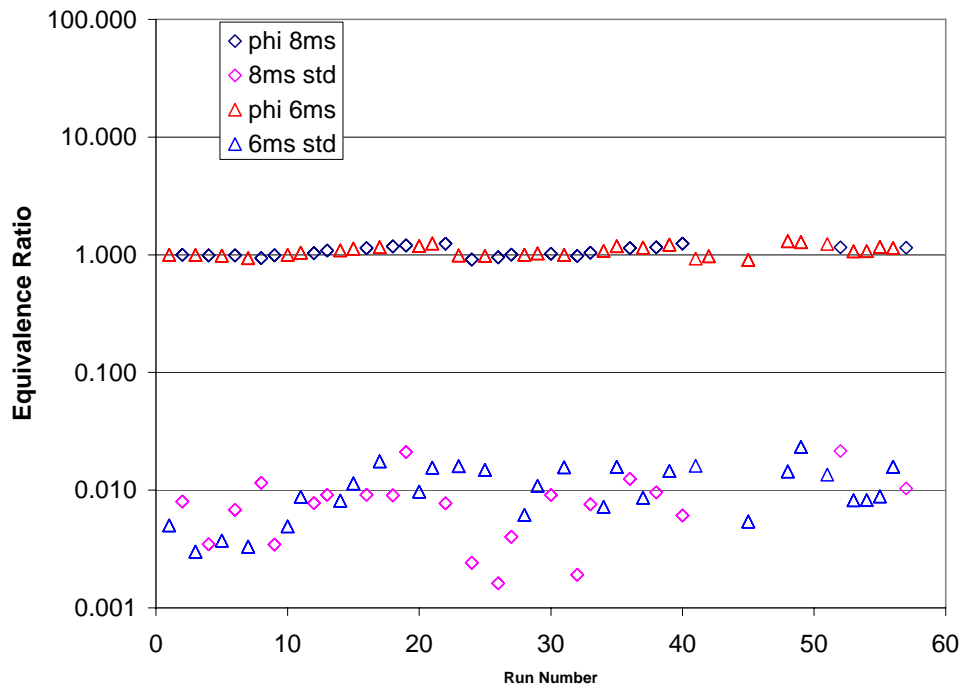
Figure D.6 n-Heptane fuel flow performance.
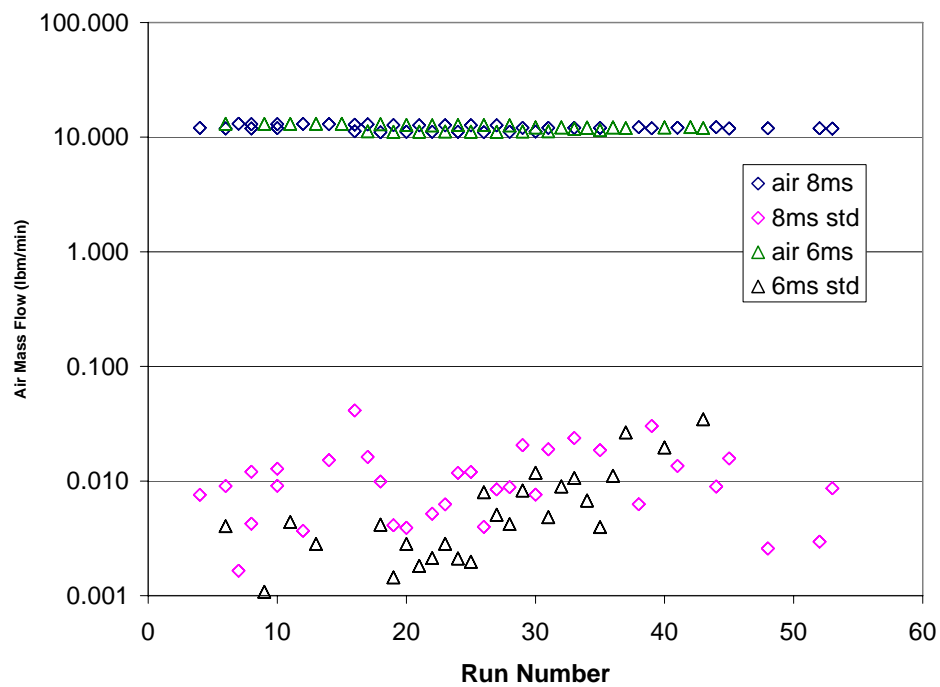
Figure D.7 JP-8 air flow performance.
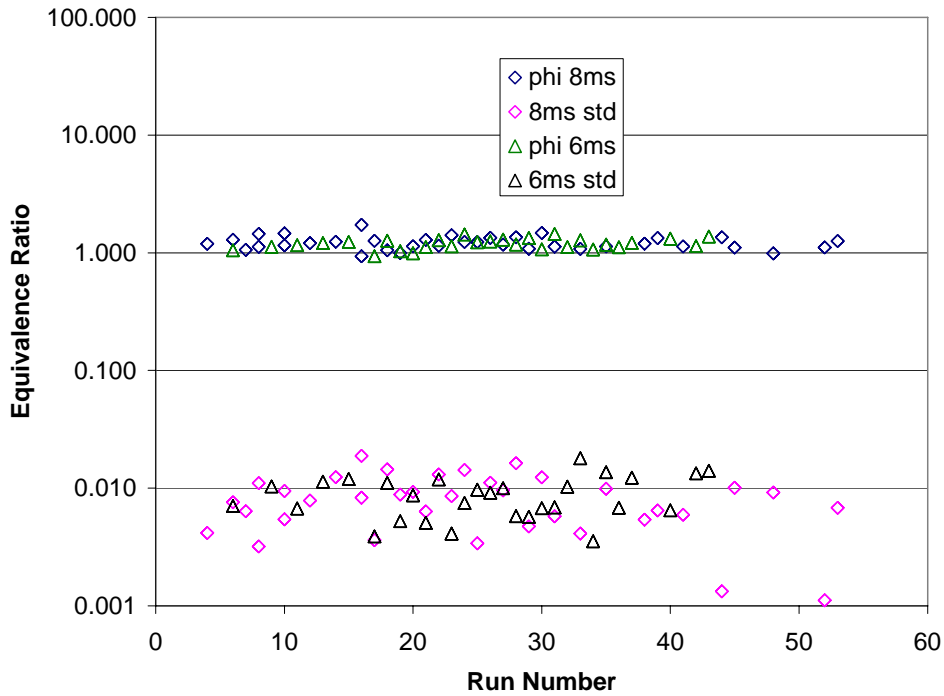
Figure D.8 JP-8 fuel flow performance.

Fuel Injection Temperature Variation

The following tables provide the actual temperatures during each data point taken during the test conditions. The far right column provides an average of how the values were changing during an individual run during the two seconds before and after the data point.

Table D.1 Aviation gasoline temperature variation.

Published fuel temperature (K)	Actual Average Temperature (K)	Average Standard Deviation Per Run
296.00	301 ± 3.9	0.651
430.00	435 ± 9.7	0.268
470.00	476 ± 5.8	0.537
500.00	522 ± 2.4	1.350

Table D.2 Isooctane gasoline temperature variation

Published fuel temperature (K)	Actual Average Temperature (K)	Average Standard Deviation Per Run
297	297 ± 1.7	0.267
430	428 ± 9.6	0.408
500	512 ± 12.4	1.600

Table D.3 n-Heptane fuel temperature variation.

Published fuel temperature (K)	Actual Average Temperature (K)	Average Standard Deviation Per Run
298	299 ± 2.8	0.479
430	434 ± 5.6	2.410
530	532 ± 11.0	9.270

Table D.4 JP-8 temperature variation.

Published fuel temperature (K)	Actual Average Temperature (K)	Average Standard Deviation Per Run
300	303 ± 3.0	0.401
473	469 ± 4.3	0.762
555	557 ± 5.5	0.651

Appendix E. Ion Probe Development

The ion probe is used to measure the detonation wave speed as a time of flight sensor. The arrival of a combustion wave is marked by the presence of ions due to the intermediate steps of chain branching during the chemical reactions occurring in the wave. The ion sensor described in this work is simply a spark plug used as a capacitor. Spark plugs are normally used as combustion initiators. During such an initiation process, a large voltage is applied to the center electrode of the spark plug, the energy potential reaches to the nearest ground and breaks down (ionizes) the gas between it to arc to the ground. In this application, a low voltage, low current source charges the gap of a spark plug. The voltage is insufficient to ionize the gas between the tip of the plug and ground, and the spark plug acts as a capacitor. After the capacitor is charged, no current flows through the circuit (neglecting leakage), and the output voltage remains constant at the source value. When a combustion wave, generating ions, flows across the sensor, the ions connect the circuit and discharge the capacitor. Now current is flowing in the circuit, and the voltage drops across the resistor to quickly recharge the spark plug gap. The circuit is represented in sketch in Fig E.1.
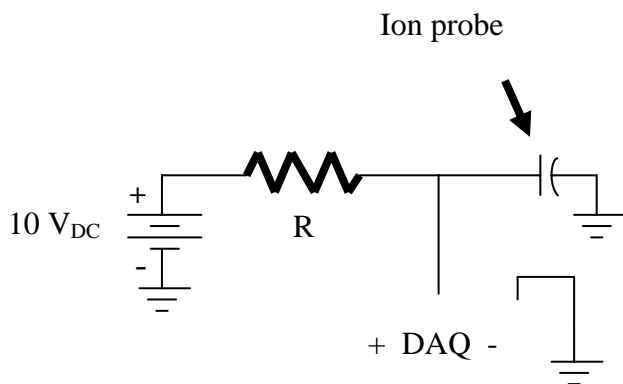
Figure E.1 Ion sensor circuit where DAQ is the data acquisition location.

Detonation Wave Environment

The conditions the sensors were to experience during the testing are based on the modeling provided by the CEA code.[34] The theoretical temperatures (Fig. E.2), pressures (Fig. E.3), and detonation wave speeds (Fig. E.4) are calculated for equivalence ratios varying from 0.8 to 1.4 and represent the harsh environment for a n-heptane and air mixture. The actual sensor average temperatures would be lower than the maximums shown in Fig. E.3 due to the convective cooling provided by the filling cycle and the purge cycles for this PDE described earlier in Appendix A. The strength of the leading shock of the detonation wave was also a concern. Von Neumann spikes were often observed experimentally at pressures exceeding two to three times the theoretical pressures provided in Fig. E.4. The time response of the sensors needed to be adequate to accurately capture the wave velocity with reasonable resolution within a 15 cm spacing.
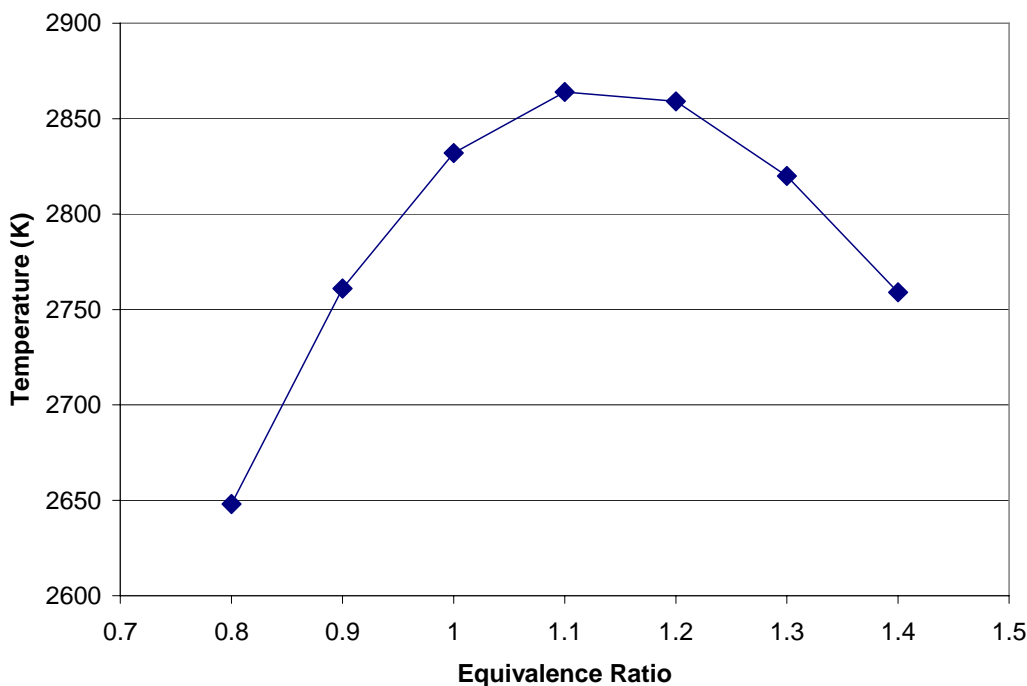
Figure E.2 Detonation wave temperatures for a n-C_7H_{16} and air mixture for varying equivalence ratios. Data from Ref. 34.
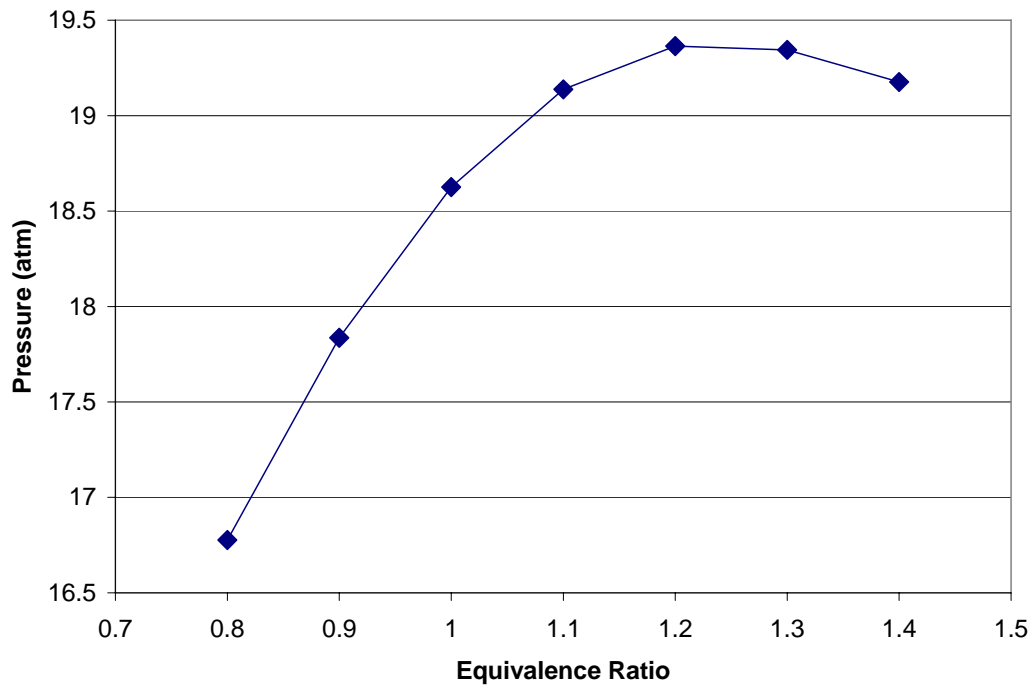
Figure E.3 Detonation wave pressures for a n-C_7H_{16} and air mixture for varying equivalence ratios. Data from Ref. 64.
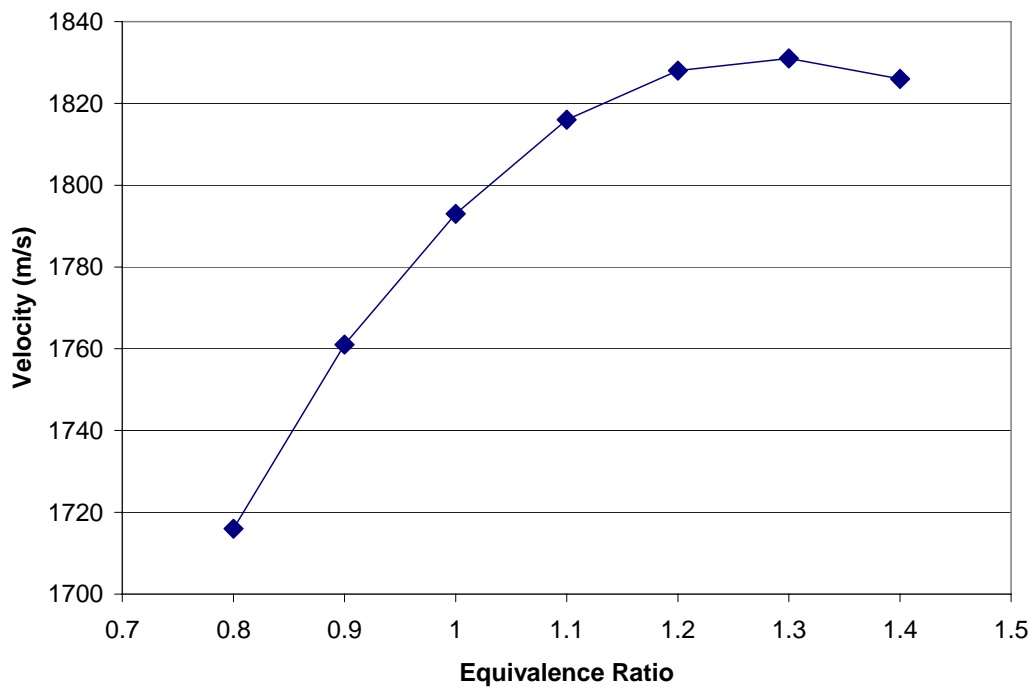
Figure E.4 Detonation wave pressures for a n-C_7H_{16} and air mixture for varying equivalence ratios. Data from Ref. 64.

Plug Iterations

The ion sensor was adapted to PDE testing for a variety of reasons. Most important is the durability of the sensor and the excellent detonation wave speed measurement capabilities. A series of plugs were studied to determine the best sensor. A brass and Teflon plug (Fig. E.5b) was used and showed very good response. Unfortunately, the Teflon plug began to melt at temperatures over 250 °C. Similar responsiveness and better temperature characteristics were seen with the ceramic model engine plug in Fig. E.5a. The plug had insufficient reach within the thrust tube and required expensive machining and resulted in a weakened structural casing. A third sensor was constructed from a drilled out bolt (Fig. E.5c), but the hardened ceramic mix used to insulate the device was fragile and was time consuming and thus expensive to make.
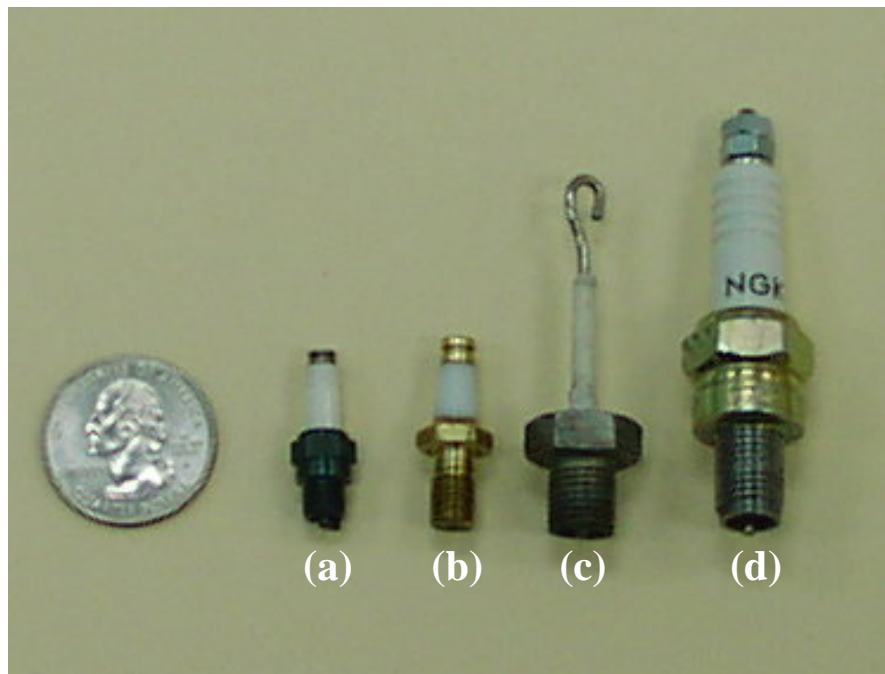
Figure E.5 Four ion sensors (a) ceramic model engine spark plug, (b) Teflon model engine spark plug, (c) 3/8 inch bolt with ceramic bonded wire, and (d) 10 mm NGK spark plug.

The final solution was the 10 mm, NGK C-9E plug (Fig. E.5d). This 10 mm plug was close to the 3/8 inch instrumentation ports on the thrust tubes, and the plug threads were cut with a 3/8 inch 24 thread count die to match the required size. Finding a robust method to attach the instrumentation wires to the plug and connecting to the circuit box was also a challenge. Early iterations used two nuts to hold a circular wire clip, but eventually the cycling and shaking during the tests caused the wire connector to fail. A basic spark plug harness and connector was adapted for the sensor. The end of the wire not attached to the spark plug was modified with a BNC connector and was attached to the ion circuit (Fig. E.1) and the data acquisition system.

The NGK C-9E spark plug is designed to be used in Kawasaki motorcycles and can handle the very high temperatures and pressures experienced in the PDE during continuous operation for thousands of cycles. For NGK plugs, the higher the designator number (in this case 9), the better the plug rejects heat from the combustion to stay cool. The higher number plugs have a shorter ceramic shroud length around the center electrode that is exposed to the combustion, and the plugs dissipate heat quickly from the spark plug. In the PDE application, it was desirable to reject heat quickly in order to increase the life of the sensor.

Spark Plug Sensor Performance

The spark plug handled the high heat loads well but eventually broke down over time due to thermal damage. During most runs, the walls surrounding the plugs reached 800 K after 2 minutes of run time. The primary failure point was the weld (Fig. E.6) that held the center electrode to the material that received the voltage. This would occur

within the ceramic insulation. After failure the $2 sensors were replaced. The highest tube wall temperatures were roughly 1100 K whereas the combustion waves supplied intermittent peak temperatures predicted at 2864 K.[64]
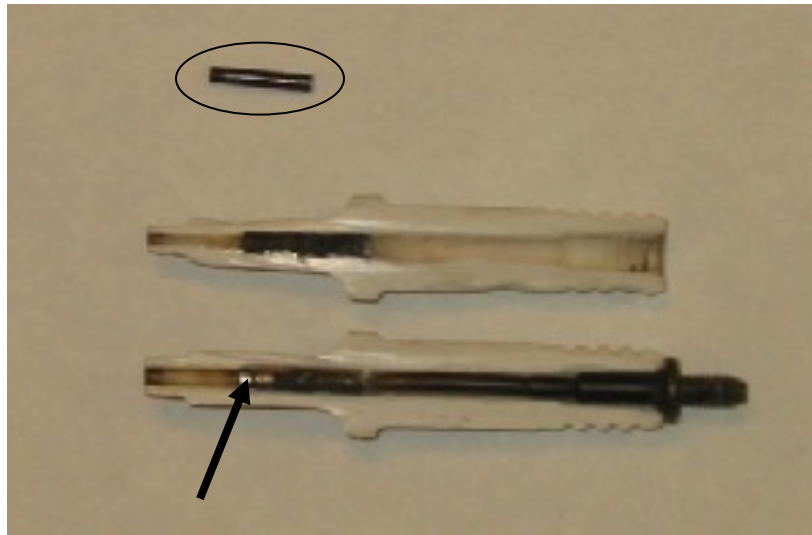
Figure E.6 Damage to center electrode of NGK spark plug. Circle denotes 1.17 cm long center electrode. Arrow is at point weld failed between two materials of center electrode.

Endurance tests or tests longer than 10 minutes were avoided with the sensors still attached to prevent complete sensor burnout. The photo in Fig. E.7 does not have ion probes on it but depicts the harsh environment to which the plugs were subjected.
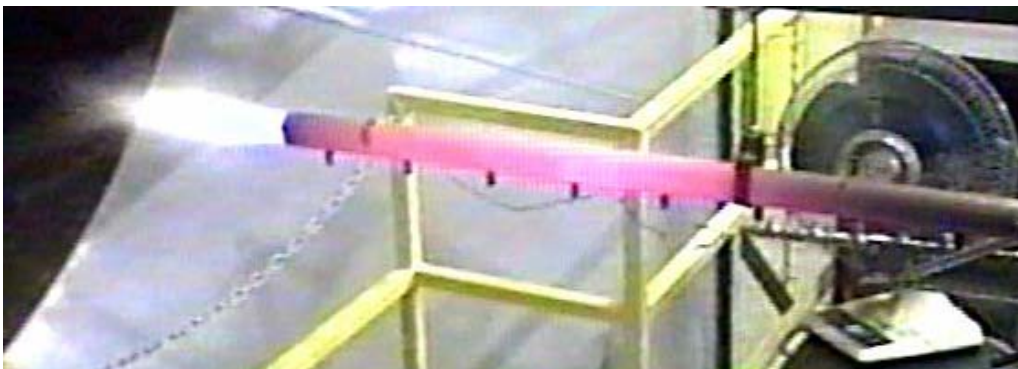
Figure E.7 Aviation gasoline and air at 15 Hz after a 10 minute heat soak.

Wave speeds are measured with two probes by noting the arrival time noted by the voltage drop at each sensor. Knowing the distance between the probes, the velocity can be determined. A sample output of ion probe is shown below in Fig. E.8.
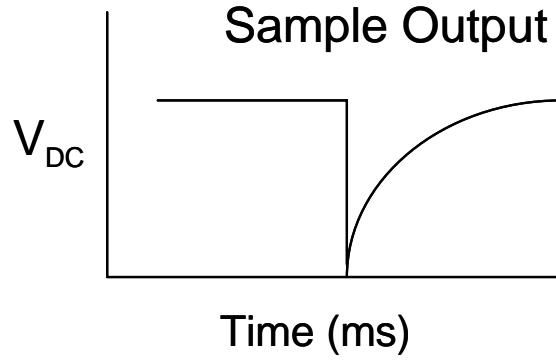
Figure E.8 Ion probe sample output.

The recharge time is defined as five times the characteristic time of the circuit. The time required to recharge the capacitor can be determined from the following relation

$$t_{RECHARGE} = 5RC \qquad (E.1)$$

where R is the resistance in Ohms and the C is the capacitance in Farads. The shape of the curve is determined by the function below, and the value of five is used because the result is 99.3% of the start and is considered sufficiently recharged.

$$V(t) = V_{IN}(1 - e^{\frac{-t}{RC}}) \qquad (E.2)$$

where t is time, R is the resistance in Ohms, C is the capacitance in Farads, and V_{IN} is the input voltage into the circuit.

Since the PDE is an unsteady device and detonation waves propagate past the sensors at regular intervals, the recharge time is important. The capacitance is inversely proportional to the space between the center electrode and the ground and is considered fixed. The resistor in the circuit can be varied to change the recharge time. The recharge

times can be lengthened considerably depending on the sensor location within the PDE thrust tube. For example, in a region of slower combustion such as the closed end (head), the probe will discharge slightly during the ignition event and again the detonation derived retonation waves arrive in the closed end of the tube.

Tests were performed to determine the ideal depth to place the sensors to adequately capture the detonation wave, minimize the recharge time, and not damage the probes. The probes were susceptible to the pressure waves generated by the detonations and several ceramic center electrodes were broken due to the detonation shock forces (Fig. E.9).
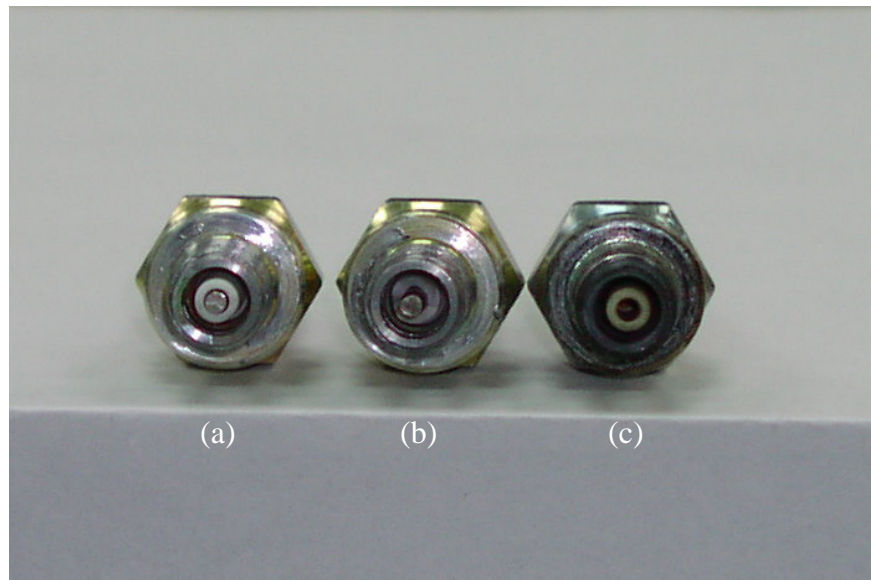
Figure E.9 Ion sensors (a) undamaged, (b) broken ceramic around center electrode, and (c) center electrode burned out.

It was determined that recessing the plug 2 mm out of the flow gave the best results. Sensor height was determined relative to the inside wall of the PDE thrust tube. Figure E.10 shows the spark plug below the wall with the center electrode out of the flow.
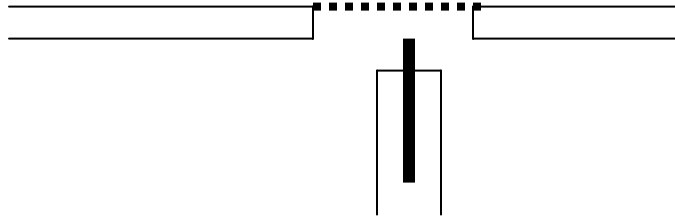
Figure E.10 Ion probe location recessed relative to the tube wall.

When the sensor was above the wall and in the flow by 1.65 mm, the following data was obtained (Fig. E.11). The recharge time is relatively long, due to the combustion products washing back and forth over the sensor. The remaining combustion ions continue to partially discharge the sensor.
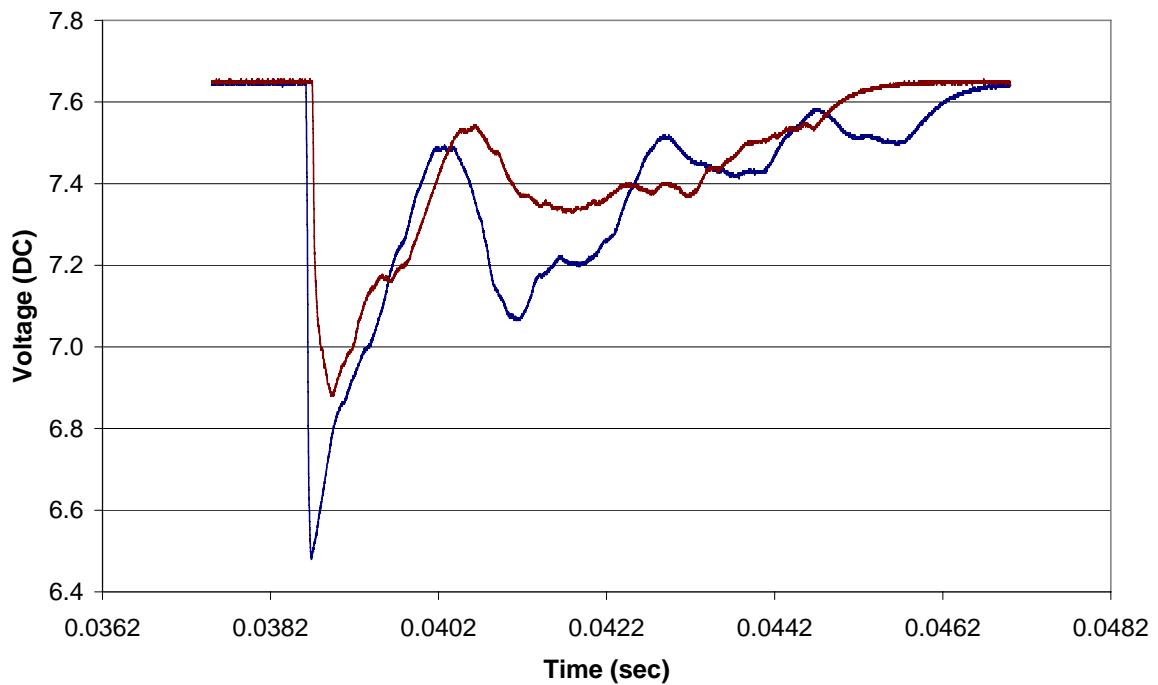
Figure E.11 Two ion probe traces when both sensors are 1.65 mm above the wall in the flow and 15 cm apart.

Recessing the ion probe slightly below the wall (2 mm) effectively shields the probe from the wash of the ions and protects the probe from the direct force of the

224

detonation wave and subsequent damage of the center electrode. The resulting signal is shown in Fig. E.12. The recharge time for the same (100 kΩ) resistor in the RC circuit is 3.5 times shorter due to being recessed out of the flow.
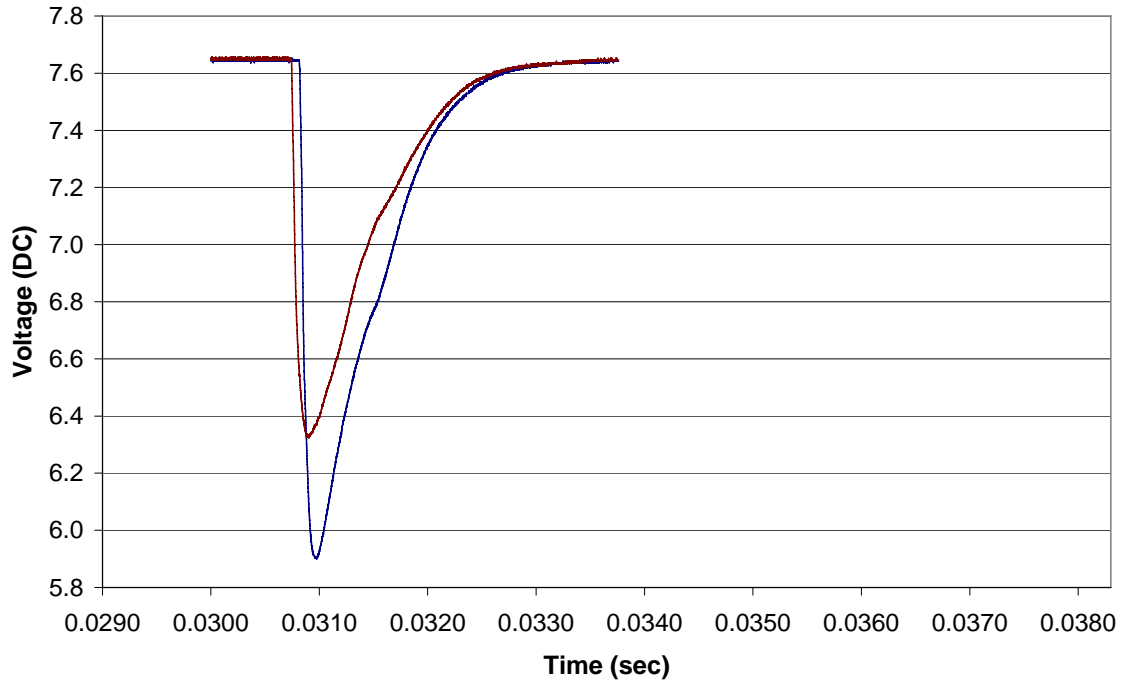
Figure E.12 Two ion probe traces when both sensors are 2.0 mm below the wall out of the flow and 15 cm apart.

The response time of the ion probes also showed excellent performance when compared to two other wave speed devices. Figure E.13 is a comparison of the three types of sensors located at the same axial location in a circular tube. The two top traces are ion probes, the two middle traces are dynamic pressure transducers, and the two bottom traces are photo diodes. A straight line can be drawn from the corner of the ion probe trace directly through the leading edge of the other two responses. The sensor output shows outstanding response time and agreement, and the measured wave speeds were within 1% of each other.
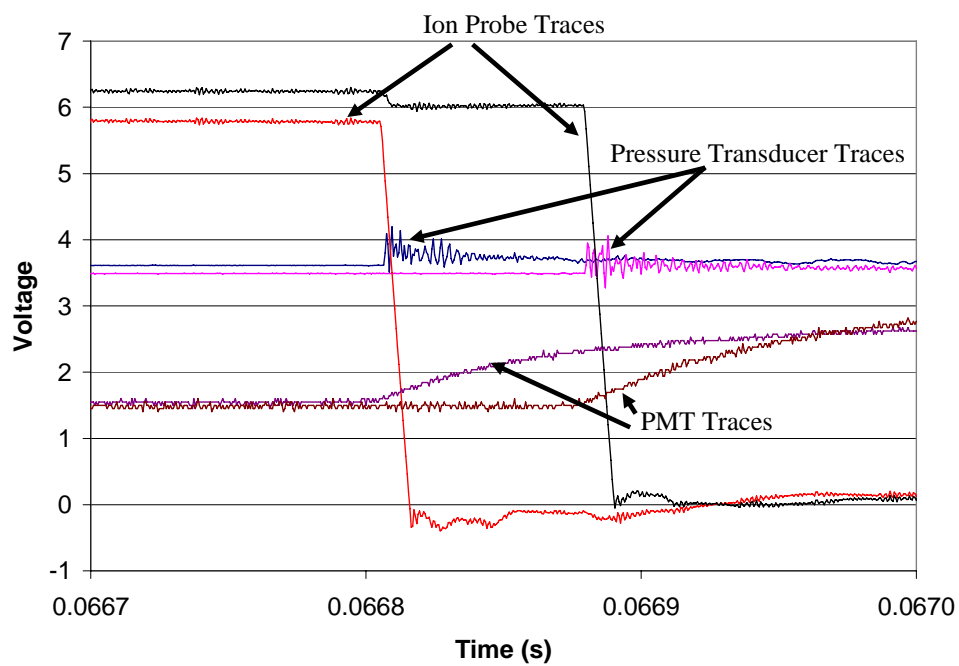
Figure E.13 Detonation wave sensor comparisons for stoichiometric hydrogen and air using ion probes, dynamic pressure transducers, and photo multiplier tubes.

References

1. Glassman, Irvin, *Combustion*, San Diego, Academic Press, 1996.

2. Kailasanath, K. "Review of Propulsion Applications of Detonation Waves," *AIAA Journal*, Vol. 38, No. 9, September 2000.

3. Goebel, G., "The V-1 Flying Bomb," Excerpt from an unpublished article, http://www.vectorsite.net/twcruz2.html., 1 Oct 2004

4. Schauer, F., Stutrud, J., and Bradley, R. "Detonation Initiation Studies and Performance Results for Pulsed Detonation Engine Applications," AIAA 2001-1129, 39th AIAA Aerospace Sciences Meeting & Exhibit, 8-11 January 2001, Reno, NV.

5. Roy, G. D., "Pulsed Detonation Phenomena for Air Breathing Propulsion," ISABE 1999-7127, 14th International Symposium of Air Breathing Engines, Florence Italy, 5-10 September, 1999.

6. Heiser, W. H. and Pratt, D. T. "Thermodynamic Cycle Analysis of Pulse Detonation Engines" *Journal of Propulsion and Power*, Vol. 18, No. 1, Jan-Feb 2002.

7. Povinelli, Louis A., "Impact of Dissociation and Sensible Heat Release on Pulse Detonation And Gas Turbine Engine Performance," ISABE 2001-1212, 15th International Symposium on Air Breathing Engines, Bangalore, India, September, 2001.

8. Shepherd, J. and Wintenberger, E., "Thermodynamic Analysis of Combustion Processes and Propulsive Systems," AIAA-2004-1033, 42nd AIAA Aerospace Sciences Meeting and Exhibit, Reno, Nevada, 5-8 January, 2004.

9. Kaneshige, M. and Shepherd, J.E. "Detonation Database," GALCIT Technical Report FM97-8, California Institute of Technology, Pasadena, CA, July 1997.

10. Kailasanath, K. "Resent Developments on the Research on Pulse Detonation Engines," *AIAA Journal*, Vol. 41, No. 2, February 2003.

11. Brophy, C. M., Netzer, D. W. and Sinibaldi, J., "Operation of a JP-10 / Air Pulse Detonation Engine," 36th AIAA/ASME/SAE/ASEE Joint Propulsion Conference, AIAA 2000-3591, 16-19 July 2000, Huntsville, AL.

12. Lefebvre, A. H., *Gas Turbine Combustion*, Taylor and Francis, 1999.

13. Hazlett, R. N., *Thermal Oxidation Stability of Aviation Turbine Fuels*, ASTM International, Philadelphia, PA, 1991.

14. Kay, I. W., Peschke, W. T., and Guile, R. N. "Hydrocarbon-Fueled Scramjet Combustor Investigation," *Journal of Propulsion and Power*, Vol. 8, No. 2, 1992 pp. 507-512.

15. Data supplied by Goodrich Turbine Fuel Technologies.

16. Lefebvre, A. H. Chapter 9, "Fuel Atomization, Droplet Evaporation, and Spray Combustion," *Fossil Fuel Combustion, A Source Book*, John Wiley and Sons, NY, 1991.

17. Zabetakis, M. G. "Flammability Characteristics of Combustible Gases and Vapors," Bulletin 627, Bureau of Mines, US Dept. of the Interior, 1965.

18. Kanury, A.M. *Introduction to Combustion Phenomena*, Gordon and Breach Science Publishers, Inc. Canada, 1975.

19. Lewis, B., and von Elbe, G., *Combustion Flames and Explosions of Gases, 2nd Edition*, Orlando, FL., Academic Press, 1987.

20. Balla, D. R. and Lefebvre, A. H., "Ignition and Flame Quenching of Quiescent Fuel Mists, "*Proceedings of the Royal Society London Ser. A*, Vol. 364, No. 1717, pp. 277-294, 1978.

21. Lefebvre, A. Freeman, W. and Cowell, L., "Spontaneous Ignition Delay Characteristics of Hydrocarbon Fuel/Air Mixtures," NASA CR 175064, February 1986.

22. Preusser, H., *Drop Size Distributions from the Breakup of Liquid Ligaments*, Master's Thesis, Queens University at Kingston, Canada, March 1997.

23. Kuo, Kenneth K., *Principles of Combustion*, New York: John Wiley & Sons, 1986.

24. Meyer, T.R. Hoke, J.L., Brown. M.S., Gord, J.R., and Schauer, F.R. "Experimental Study of Deflagration-To-Detonation Enhancement Techniques in a H_2/Air Pulsed Detonation Engine," AIAA 2002-3270, 38th AIAA/ASME/SAE/ASEE Joint Propulsion Conference, July 2002, Indianapolis, IN.

25. Lee, J.H.S., "On the Transition from Deflagration to Detonation," Dynamics of Explosions, Vol. 106: Progress in Astronautics and Aeronautics, AIAA, NY, 1986.

26. Cooper, M., Jackson, S., and Shepherd, J. E. "Effect of Deflagration-to-Detonaton Transition on Pulse Detonation Engine Impulse," GALCIT Technical Report FM00-3, California Institute of Technology, Pasadena, CA, May 2000.

27. Schauer, F., Stutrud, J., Bradley, R., Katta, V., and Hoke, J., "Detonation Initiation and Performance in Complex Hydrocarbon Fueled Pulsed Detonation Engines," 50th JANNAF Propulsion Meeting, Paper I-05, , Salt Lake City, UT, 11-13 July 2001.

28. Akbar, R, Thibault, P. A., Harris, P. G., Lussier, L.-S, Zhang. F., Murray, S. B., and Gerrard, K. "Detonation Properties of Unsensitized and Sensitized JP-10 and Jet-A Fuels in Air for Pulse Detonation Engines," AIAA 2000-3592, 36th AIAA/ASME/ASEE Joint Propulsion Conference and Exhibit 16-19 July 2000 Huntsville, Alabama.

29. Rolling, A. J., *Alternative Pulse Detonation Engine Ignition System Investigation Through Detonation Splitting*, Master's Thesis, Graduate School of Engineering and Management, Air Force Institute of Technology (AU), Wright-Patterson AFB OH, March 2002.

30. Rolling, A. J., King, P. I., and Schauer, F. R. "Propagation of Detonation Waves in Tubes Split from a PDE Thrust Tube," 38th AIAA/ASME/SAE/ASEE Joint Propulsion Conference and Exhibit, Indianapolis, Indiana, 7-10 July 2002.

31. Tucker, C., King, P., Schauer, F., and Hoke, J. "Branched Detonation in a Multi-Tube PDE," ISABE 2003-1218, 16th International Symposium on Air Breathing Engines, Cleveland, OH, September 2003.

32. Panzenhagen, K. L., King, P. I., Tucker, K. C., and Schauer, F. R., "Liquid Hydrocarbon Detonation Branching in a Pulse Detonation Engine," AIAA 2004-3401, 40th AIAA/ASME/ASEE Joint Propulsion Conference and Exhibit, Ft. Lauderdale, July 2004.

33. Turns, S.R. *An Introduction to Combustion*, McGraw-Hill, NY, 2000.

34. Gordon, S and McBride B. "Computer Program for Calculation of Complex Chemical Equilibrium Compositions and Applications," NASA RP 1311 I & II, October 1994 and June 1996.

35. Strehlow, Roger A. *Combustion Fundamentals* McGraw-Hill New York, 1984.

36. Katta, V. R., Chin, L. P. and Schauer, F.R. "Numerical Studies on Cellular Detonation Wave Subjected to Sudden Expansion," *Proceedings of the 17th International Colloquium on the Dynamics of Explosions and Reactive Systems*. Heidelberg, Germany, 1999.

37. "MSD Installation Instructions," Autotronic Controls Corporation, El Paso, Texas.

38. Holman, J. P., *Heat Transfer 5th Edition*, McGraw-Hill New York, 1981.

39. Schauer, F. R., *AIAA Short Course in Pulsed Detonation Engines*, Reno, NV, January 2003.

40. Coordinating Research Council, Inc. "Handbook of Aviation Fuel Properties," 2nd Printing, May 1984.

41. Zhang, F., Akbar, R., Thibault, P. A., and Murray, S. B., "Effects of Nitrates on Hydrocarbon-Air Flames and Detonations," *Shock Waves*, 2001, Vol. 10, 457-466.

42. Zeldovich, Y., Barenblatt, G., Librovich, V., Makhviladze, G., *The Mathematical Theory of Combustion and Explosions*, Consultants Bureau, New York, NY 1985.

43. Bar-Or, R., Sichel, M., and Nicholls, J. A. "The Reaction Zone Structure of Cylindrical Detonations in Monodisperse Sprays," Nineteenth Symposium (International) on Combustion, *The Combustion Institute*, pp. 665-673, 1982.

44. Lin, Z. C., Nicholls, J. A., Tang. M.J., Kauffman, C. W, and Sichel, M, "Vapor Pressure and Sensitization Effects in Detonation of a Decane Spray," Twentieth Symposium (International) on Combustion, *The Combustion Institute*, pp. 1709-1716, 1984.

45. Dabora, E. K., Ragland K. W., and Nicholls, J. A. "Droplet-Size Effects in Spray Detonations," Twelfth Symposium (International) on Combustion, *The Combustion Institute*, 1969.

46. Bar-Or, R., Sichel, M., and Nicholls, J. A. "The Propagation of Cylindrical Detonations in Monodisperse Sprays," Eighteenth Symposium (International) on Combustion, *The Combustion Institute*, pp. 1599-1606, 1981.

47. Frolov, S. M., Basevich, V. Ya., and Belyaev, A. A., "The Use of Fuel Blends and Distributed Injections for Active Detonability Control in a PDE," ICDERS 1999-252, International Colloquium on the Dynamics of Explosions and Reactive Systems, 1999.

48. Heywood, J. B., *Internal Combustion Engine Fundamentals*, McGraw-Hill, 1988.

49. Travis, G. "Octane Determination," *BMAA Microlight Flying*, July 1995. www.prime-mover.org /Engines/GArticles/octane.html.

50. Wu, P. C., and Hottel, H. C., "Appendix: Data on Fuel and Combustion Properties," *Fossil Fuel Combustion, A Source Book*, John Wiley and Sons, New York, NY, 1991.

51. Tucker, K. C, King, P. I. ,Bradley, R. P., and Schauer, F. R., "The Use of a Flash Vaporization System With Liquid Hydrocarbon Fuels in a Pulse Detonation Engine," AIAA 2004-0868, 42nd AIAA Aerospace Sciences Meeting and Exhibit, Reno, NV January, 2004.

52. ASTM D 2699-03a, "Standard Test Method for Research Octane Number of Spark-Ignition Engine Fuel," *ASTM International.*

53. ASTM D 2700-03a, "Standard Test Method for Motor Octane Number of Spark-Ignition Engine Fuel," *ASTM International.*

54. Stringer, F. W. Clarke, A. E. and Clarke, J. S., "The Spontaneous Ignition of Hydrocarbon Fuels in a Flowing System," Proc. Auto. Div., Institute of Mechanical Engineers, 1970.

55. Darrah, S. "Jet Fuel Deoxygenation," AF Wright Aeronautical Laboratories Interim Report for March 1987 - July 1988.

56. Ervin, J. S., Williams, T. F., and Hartman, G., "Effect of Test Period on the Rate of Fouling in a Complex Flowing System," *Structure of Jet Fuels V*, Boston, MA August 1998.

57. Rupprecht, S. D. and Faeth, G. M., "Investigation of Air Solubility in Jet A Fuel at High Pressures," NASA CR-3422, May 1981.

58. Heneghan, S. P., Martel, C. R., Williams, T. F. and Ballal, D. R., "Effects of Oxygen and Additives on the Thermal Stability of Jet Fuels," University of Dayton; Dayton, Ohio, 1992.

59. Yoon, E. M., Selvaraj, L., Eser, S., and Coleman, M.M. "High-Temperature Stabilizers for Jet Fuels and Similar Hydrocarbon Mixtures. 2. Kinetic Studies," *Energy and Fuels* Vol. 10, 1996, pp. 812-815.

60. Ward, T. A., Ervin, J. S., Striebich, R. C. and Zabarnick, S. "Simulations of Flowing Mildly-Cracked Normal Alkanes Incorporating Proportional Distributions," *Journal of Propulsion and Power*, Vol. 20, No. 3 2004.

61. Restek Corporation, Bellefonte, PA, 16823, 2003.

62. National Instruments Corporation "NI PCI-6110/6111 User Manual" Appendix A, NI.com.

63. McMillan, R. J., *Shock Tube Investigation of Pressure and Ion Sensors Used impulse Detonation Engine Research*, Master's Thesis, Graduate School of Engineering and Management, Air Force Institute of Technology (AU), Wright-Patterson AFB OH, March, 2004.

64. PCB Piezotronics. "Introduction to Piezoelectric Pressure Sensors." unpublished presentation, www.pcb.com/tech_pres.html March 2003.

65. Brown, Michael, Physicist, Innovative Scientific Solutions, Inc. (ISSI), AFRL/PRTC, Wright Patterson AFB, OH. Personal Interview. 30 August 04.

66. Ocean Optics, Inc. "Optical Fiber Specifications and Performance Characteristics," www.oceanoptics.com/products/fiberspecs.asp. Dunedin, FL 34698, 2004.

67. Minus, Donald, Research Chemist, AFRL/PRTG, Wright Patterson AFB, OH. Personal Interview. 25 March 2004.

68. Striebich, R. C. and Rubey, W. A. "Analytical Method for the Detection of Dissolved Oxygen," *Symposium on Distillate Fuel Auto-Oxidation Chemistry*, San Diego, CA, March 1994.

69. Panzenhagen, Kristin L. *Detonation Branching in a PDE with Liquid Hydrocarbon Fuel*. Master's Thesis, Graduate School of Engineering and Management, Air Force Institute of Technology (AU), Wright Patterson AFB OH, March, 2004.

70. Battino, R. et al. *Solubility Data Series, Nitrogen and Air*, Vol. 10, Pergamon Press, Elmsford, NY, 1982.

71. Mathur, T., et al. "Liquid JP-7 Combustion in a Scramjet Combustor," AIAA 2000-3581, 36th AIAA/ASME/SAE/ASEE Joint Propulsion Conference, Huntsville, AL, July 2000.

72. Parker, J. and Schauer, F. "Data Analysis and Compression Techniques for Megabyte-Data PDE Experiments," AIAA 2003-0892, 41st Aerospace Sciences Symposium, Reno, NV January 2003.

73. Beyer, W.H. CRC *Standard Mathematical Tables and Formulae, 29th Edition*, CRC Press 1981.

74. Zdenek, J. S. and Anthenien, R. A., "Ion Based Pressure Sensor for Pulse Detonation Engines," Submitted to *Review of Scientific Instruments*, 2004.

75. ICP Pressure Sensor, Model 102M232 specification sheet. PCB Piezotronics, Depew, NY, 14043.

76. Brophy C., Netzer, D., and Forster, D, "Detonation Studies of JP-10 with Oxygen and Air for Pulse Detonation Engine Development," AIAA 98-4003, 34th Joint Propulsion Conference, July 1998 Cleveland, OH.

77. Kanury, A.M. *Introduction to Combustion Phenomena*, Gordon and Breach Science Publishers, Inc. Canada, 1975.

78. Material Safety Data Sheet," Knovel Solvents - A Properties Database, ChemTec Publishing, 2000.

79. *Knovel Chemical Properties Handbook*, McGraw-Hill, 1999.

80. Lin, K.C., Cox-Stouffer, S., Kennedy, P. J., and Jackson, T. A. "Expansion of Supercritical Methane/Ethylene Jets in a Quiescent Subcritical Environment" AIAA 2003-0483, 41st Aerospace Sciences Symposium, Reno, NV January 2003.

81. Lemmon, E. W., McLinden, M. O. and Friend, D. G. "Thermophysical Properties of Fluid Systems", *NIST Chemistry WebBook, NIST Standard Reference Database Number 69*, Eds. P. J. Linstrom and W. G. Mallard, , National Institute of Standards and Technology, Gaithersburg MD, 20899, March 2003.

82. Edwards, T. "Liquid Fuels and Propellants for Aerospace Propulsion: 1903-2003*" Journal of Propulsion and Power*, Vol. 19, No. 6 Nov-Dec 2003.

83. Szetela, E. J. and TeVelde, J. A, "External Fuel Vaporization Study, Phase II Final Report," UTRC, NASA CR 165513, November 1981.

84. Sobel, D. R., and Spadaccini, L. J., "Hydrocarbon Fuel Cooling Technologies for Advanced Propulsion", *ASME Journal of Engineering for Gas Turbines and Power*, Vol. 119 pp 344-351 April 1997.

85. Peng, D. Y., and Robinson, D. B., "A New Two-Constant Equation of State," Ind. Eng. Chem., Fund., Vol. 15, No. 1, 1976.

86. Liberman, D. H., Parkin, K. L., and Shepherd, J. E. "Detonation Initiations by a Hot Turbulent Jet for Use in Pulse Detonation Engines," AIAA 2002-3909, 38th AIAA/ASME/SAE/ASEE Joint Propulsion Conference and Exhibit, Indianapolis, Indiana, July 7-10, 2002.

87. Edwards, J. T., and Striebich, R. C., AFRL/PRTG Fuels Branch, Personal Communication, 18 May 2004.

88. Katta, V, Tucker, C., Hoke, J., and Schauer, F., "Initiation of Detonation in a Large Tube," 19th International Colloquium on the Dynamics of Explosions and Reactive Systems, Hakone, Japan, July 2003.

89. White, F.M. *Viscous Fluid Flow*, McGraw-Hill, 1991.

90. Tannehill, J. C., Anderson, D. A., and Pletcher, R. H., *Computational Fluid Mechanics and Heat Transfer,* Hemisphere Publishing Company, Washington, D.C, pp.402-428, 1997.

91. Strange, G. *Introduction to Applied Mathematics*, Wellesley Cambridge Press, Cambridge, MA 1986.

92. Lindsey, W. F. and Daley, B. N. "Effects of Compressibility on the Flow Past a Two-Dimensional Bump," *Technical Note 2484, National Advisory Committee for Aeronautics,* Langley Aeronautical Laboratory, Langley Field, VA, 1952.

93. Clifford, T., *Fundamentals of Supercritical Fluids*, Oxford Univ. Press, NY, 1998.

94. Huber, M. L. "NIST Thermophysical Properties of Hydrocarbon Mixtures Database (SUPERTRAPP) Version 3.1 Users' Guide," U.S. Department of Commerce, Feb 2003.

95. Leland, T. W. and Chappelear, P. S. "The Corresponding States Principle" Applied Thermodynamics Symposium, Industrial and Engineering Chemistry, Vol. 60, No. 7, July 1968.

96. Fisher, G. D., and Leland, T. W., Jr, "Corresponding States Principle Using Shape Factors," *Ind. Eng. Chem. Fundam.*, Vol. 9, No. 4, pp. 537-544, 1970.

97. Ely, J. F. and Hanley, H. J. M. "Prediction of Transport Properties. 1. Viscosity of Fluids and Mixtures," *Ind. Eng. Chem. Fund.*, 20, 323-332, 1981.

98. Edwards, T, and Maurice, L. Q. "Surrogate Mixtures to Represent Complex Aviation and Rocket Fuels," *Journal of Propulsion and Power*, Vol. 17, No. 2, Mar-Apr 2001.

99. Shultz, W. D. "Oxidation Products of a Surrogate JP-8 Fuel" *Journal of Propulsion and Power*, Vol. 9, No. 1, pp 5-9, 1993.

100. Stouffer, Scott, Senior Research Engineer, Ph.D. University of Dayton Research Institute. Personal correspondence, 18 June 2004.

101. Faith, L. E., Ackerman, G. H., and Henderson, H. T., "Heat Sink Capabilities of Jet A Fuel: Heat Transfer and Coking Studies," NASA CR-72951, July 1971.

Vita

Kelly Colin Tucker is the son of an Army officer, the grandson of an Air Force officer, and the great-grandson of an Army officer. It was his great honor to accept a commission into the US Air Force after receiving his Batchelor of Science degree in Aerospace Engineering from Mississippi State University in May of 1994. Two weeks after graduation, he married his lovely wife. His first assignment on active duty was to attend the Air Force Institute of Technology (AFIT) at Wright Patterson Air Force Base in Ohio, where he graduated with a Master of Science degree in Aeronautical Engineering in December of 1995. Upon graduation, he assumed the job of Lead Engineer for Missile Engines, in the Propulsion Developmental System Office within the Aeronautical Systems Center under Air Force Material Command. Two years later, he accepted the job of Executive officer for the Director of Engineering, in the Engineering Directorate of the Aeronautical Systems Center. After serving the Director for one year, Colin competed for and received the opportunity to teach in the Aeronautics Department at the United States Air Force Academy. After three years of teaching, the Aeronautics Department saw fit to send Colin back to AFIT to earn his Doctorate in Aeronautical Engineering so that he would be able to return and teach at the Academy after an intervening tour. Upon graduation, Colin will serve as the Deputy Chief of the Energetic Materials Branch within the Munitions Directorate, in the Air Force Research Laboratory at Eglin Air Force Base in Florida.

1. REPORT DATE *(DD-MM-YYYY)*	2. REPORT TYPE	3. DATES COVERED *(From – To)*
00-06-2005	**Doctoral Dissertation**	Sep 2001 – Jun 2005

4. TITLE AND SUBTITLE	5a. CONTRACT NUMBER
A Flash Vaporization System for Detonation of Hydrocarbon Fuels in a Pulse Detonation Engine	5b. GRANT NUMBER
	5c. PROGRAM ELEMENT NUMBER

6. AUTHOR(S)	5d. PROJECT NUMBER
Tucker, Kelly C., Major, USAF	5e. TASK NUMBER
	5f. WORK UNIT NUMBER

7. PERFORMING ORGANIZATION NAMES(S) AND ADDRESS(S)	8. PERFORMING ORGANIZATION REPORT NUMBER
Air Force Institute of Technology Graduate School of Engineering and Management (AFIT/EN) 2950 P Street, Building 640 WPAFB OH 45433-7765	AFIT/DS/ENY/05-03

9. SPONSORING/MONITORING AGENCY NAME(S) AND ADDRESS(ES)	10. SPONSOR/MONITOR'S ACRONYM(S)
AFRL/PRTC Attn: Dr Fredrick Schauer 1790 Loop Road North DSN: 785-6462 WPAFB OH 45433 e-mail: frederick.schauer@wpafb.af.mil	11. SPONSOR/MONITOR'S REPORT NUMBER(S)

12. DISTRIBUTION/AVAILABILITY STATEMENT

APPROVED FOR PUBLIC RELEASE; DISTRIBUTION UNLIMITED.

13. SUPPLEMENTARY NOTES

14. ABSTRACT

Current research by the US Air Force and Navy is concentrating on obtaining detonations in a pulse detonation engine (PDE) with low vapor pressure, kerosene based jet fuels. These fuels have a low vapor pressure and the performance of a liquid hydrocarbon fueled PDE is significantly hindered by the presence of fuel droplets. A high pressure, fuel flash vaporization system (FVS) has been designed and built to reduce and eliminate the time required to evaporate the fuel droplets. Four fuels are tested: n-heptane, isooctane, aviation gasoline, and JP-8. The fuels vary in volatility and octane number and present a clear picture on the benefits of flash vaporization. Results show the FVS quickly provided a detonable mixture for all of the fuels tested without coking or clogging the fuel lines. Combustion results validated the model used to predict the fuel and air temperatures required to achieve gaseous mixtures with each fuel. The most significant achievement of the research was the detonation of flash vaporized JP-8 and air. The results show that the flash vaporized JP-8 used 20 percent less fuel to ignite the fuel air mixture twice as fast (8 ms from 16 ms) when compared to the unheated JP-8 combustion data.

15. SUBJECT TERMS

flash vaporization, pulse detonation engine, detonation waves, fuel systems, supercritical fuel, evaporation

16. SECURITY CLASSIFICATION OF:			17. LIMITATION OF ABSTRACT	18. NUMBER OF PAGES	19a. NAME OF RESPONSIBLE PERSON Paul I. King, (ENY)
a. REPORT	b. ABSTRACT	c. THIS PAGE	UU	260	19b. TELEPHONE NUMBER *(Include area code)* (937) 255-3636 ext 4628; e-mail: Paul.King@afit.edu
U	U	U			